

**NASA TECHNICAL
TRANSLATION**



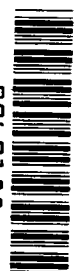
NASA TT F-655

2.1

NASA TT F-655

**LOAN COPY: RE
AFWL (DO
KIRTLAND AF**

0069188



TECH LIBRARY KAFB, NM

IONOSPHERIC RESEARCH

No. 18 - Collection of Articles

Edited by A. D. Danilov and L. A. Yudovich

Soviet Geophysical Committee

USSR Academy of Sciences

"Nauka" Press, Moscow, 1969



0069188

NASA T1 F-655

IONOSPHERIC RESEARCH

No. 18 - Collection of Articles

Edited by A. D. Danilov and L. A. Yudovich

**Translation of "Ionosfernyye Issledovaniya, No. 18, Sbornik Statey."
Soviet Geophysical Committee, USSR Academy of Sciences.
"Nauka" Press, Moscow, 1969**

NATIONAL AERONAUTICS AND SPACE ADMINISTRATION

For sale by the National Technical Information Service, Springfield, Virginia 22151

\$3.00

ANNOTATION

This collection contains articles based on the text of lectures given at the International Summer School on Physics of the Upper Ionosphere (Sochi, October 1966). The results of investigations on the basic parameters of the upper atmosphere (density, neutral and ion composition, electron concentration, temperature) were discussed. The most important elementary processes which control the behavior of the entire ionosphere as a whole and its individual parameters were examined. Methods were given for direct research on the neutral and charged particles in the atmosphere.

This collection is of interest to scientists studying plasma physics, for geophysicists and also for specialists in radio communication.

EDITORS-IN-CHIEF

Candidates of Physics and Mathematical Sciences

A. D. Danilov and L. A. Yudovich

FOREWORD

The present collection contains survey articles written from materials of the lectures read during the International School of Ionospheric Physics⁽¹⁾. /5 *
This school was organized by the Section on the Ionosphere, Interdepartmental Geophysics Committee and the Institute of Terrestrial Magnetism and Propagation of Radio Waves, Academy of Sciences, USSR in October and November 1966 in Sochi.

Nearly 100 scientists participated in the school; they came from the Soviet Union, Bulgaria, Hungary, The German Democratic Republic, Cuba, Czechoslovakia and Yugoslavia. The leading specialists on problems of theoretical and experimental research on atmospheric parameters in the region of the ionosphere were invited. Seminars were held during the operation of the school in which questions on the problems covered in each lecture were widely discussed. The results of this discussion, as well as artam materials which appeared at the end of 1966 and the beginning of 1967, are reflected in the articles contained in this collection.

At the present time, considerable attention is being paid to a study of the basic processes which determine the behavior of the ionosphere as a whole and its individual parameters in particular. Without an understanding of these processes (diffusion, photoionization, recombination, cohesion, etc.) it is impossible either to predict the behavior of the ionosphere or to interpret the experimental data correctly. In recent years numerous papers have been published, both Soviet and foreign, on these problems from different viewpoints. A. D. Danilov, V. M. Polyakov, J. Taubenheim, and K. H. Schmelovskiy discuss in their papers the current concepts as to the role and rates of the various processes which influence the distribution of charged particles both in space and in time in different regions of the ionosphere.

* Numbers in the margin indicate the pagination in the original foreign text.

(1) These materials were divided into two volumes during editing. The remaining articles can be found in the collection: Ionosfernyye Issledovaniya (Ionospheric Research) No. 19.

The specifics of rocket and satellite experiments, as well as the basic results and the prospects of the research, are described in the articles of V. V. Mikhnevich, G. L. Gdalevich and V. A. Misyura. A new method for studying charged particles above the maximum of the F2 region, i.e., the method of incoherent scattering of radio waves, and the basic results obtained using this method are discussed in another article by V. A. Misyura.

Unfortunately the review papers on the lectures of G. S. Ivanov-Kholodnyy, V. D. Gusev and Yu. V. Kushnerevskiy are not included in this collection.

/6

On the whole, the articles in this collection reflect the research on the basic questions of ionospheric physics based on the state-of-the-art at the end of 1966 quite well. Since study of the ionosphere at the present time is being developed at an extremely rapid pace, we should remember that upon publication of this collection new materials are appearing which are not contained herein. We should also remember that, although all the lectures are of a survey nature, in a number of cases the author's viewpoint on certain questions is reflected therein, and such a viewpoint is not necessarily that generally accepted today.

TABLE OF CONTENTS

	Pages
ANNOTATION -----	iii
FOREWORD -----	v
EXPERIMENTAL DATA ON THE DISTRIBUTION OF BASIC PARAMETERS AND RATES OF PHOTOCHEMICAL PROCESSES IN THE UPPER ATMOSPHERE ----- A. D. Danilov	1
AMBIPOLAR DIFFUSION OF ELECTRON-ION GAS AND STRATIFICATION OF THE F REGION OF THE IONOSPHERE ----- V. M. Polyakov	65
AERONOMIC PROBLEMS ARISING IN THE INTERPRETATION OF ELECTRON DENSITY PROFILES IN THE F REGION ----- J. Taubenheim	96
PRESSURE GAUGE MEASUREMENTS ON ROCKETS AND SATELLITES ----- V. V. Mikhnevich	114
RESULTS OF MULTI-YEAR OBSERVATIONS OF THE OUTER IONOSPHERE UTILIZING SIGNALS FROM SATELLITES ----- K. H. Schmelovsky	137
PROBE METHODS FOR STUDYING THE IONOSPHERE ----- G. L. Gdalevich	153
RADIOPHYSICS RESEARCH OF THE IONOSPHERE BASED ON THE PROPAGATION OF RADIO WAVES FROM ROCKETS AND SATELLITES ----- V. A. Misyura	195
IONOSPHERIC MEASUREMENTS USING THE METHOD OF INCOHERENT SCATTERING OF RADIO WAVES BY THE IONOSPHERE ----- V. A. Misyura, G. N. Tkachev, V. Ya. Bludov and Yu. G. Yerokhin	224

EXPERIMENTAL DATA ON THE DISTRIBUTION OF BASIC PARAMETERS AND RATES OF PHOTOCHEMICAL PROCESSES IN THE UPPER ATMOSPHERE

A. D. Danilov

This paper presents a brief survey of main achievements in the investigation of the most important atmospheric parameters in the earth's ionosphere with the aid of rockets and artificial satellites. A description is given of the results obtained in measuring atmospheric density, the results of determining the composition of neutral particles by mass spectrometric and optical methods are compared, and the main results of numerous measurements of the ion composition and electron concentration are shown. Present-day views on the ionization-recombination cycle of processes occurring in the atmosphere are expounded and the most reliable estimates are given of the effectiveness of basic processes, ionization rate, dissociative recombination, ionic-molecular reactions, processes where negative ions are involved, with emphasis being laid on the significance of the latter in the ionosphere. It is emphasized that in the ionosphere there exists a close relationship between processes where charged particles are involved and neutral reactions. A description is given of the problem of oxygen dissociation in the atmosphere, and the part that ionic reactions take in the formation of neutral components is discussed.

The purpose of the present paper is to describe the overall state of the / 7 art in research on the basic characteristics of the upper atmosphere (concentrations of both neutral and charged particles, temperature, short-wave solar radiation flux) and on the basic photochemical processes involving atmospheric components. Naturally, within the framework of a single paper such a survey must be very superficial, dealing only with the overall characteristics of the situation. For more detailed data, we refer the reader to the general works in [1 - 14] and to the monograph in [15].

[15].

RESULTS OF ROCKET RESEARCH ON THE PARAMETERS OF THE UPPER ATMOSPHERE

§ 1. Density, Temperature and Neutral Composition of the Atmosphere.

a. Altitude Range $H < 100$ km. At the present time it is a well-known fact that below approximately 100 to 120 km the earth's atmosphere is mixed, and therefore has an altitude-constant chemical composition if we are concerned with the basic components, i.e., nitrogen and oxygen molecules and argon atoms. As far as the so-called "minor impurities" are concerned — ozone, atomic oxygen, and nitric oxides — their absolute and relative concentrations undergo substantial variations both with altitude and with time of day, with the level of solar activity, etc. Altitude variation of the basic component concentrations is thus determined by the altitude drop in the overall atmospheric density, which in turn depends on the altitude of the uniform atmosphere at a given level, i.e., (at a constant mean molecular weight) on the temperature. Table 1 gives the basic atmospheric parameters in the altitude range from 30 to 100 km according to Nicolet [16]. It should be mentioned that at the present time practically nothing is known concerning variations in density and concentration of the basic atmospheric components below 100 km. We would expect, however, that such variations (if they do exist) are not high, and therefore the mean values of ρ , $[N_2]$ and $[O_2]$, shown in Table 1, must be valid at least within a factor of 2.

b. Altitude Range from 100 to 200 km. This altitude range at the present time has been studied the least from the viewpoint of research on atmospheric density and temperature. The reason for this is that above approximately 200 to 250 km the numerous determinations of density and other parameters are made on the basis of observations of the deceleration of artificial earth satellites. These observations give an extremely large amount of data which now permit a clarification of the very subtle effects of the behavior of atmospheric density at high altitudes (see below). At the

/8

TABLE 1

H, km	ρ , g/cm ³	[N ₂], cm ⁻³	[O ₂], cm ⁻³	T, °K
30	$1.79 \cdot 10^{-6}$	$2.90 \cdot 10^{17}$	$7.81 \cdot 10^{16}$	235.3
35	$8.34 \cdot 10^{-6}$	$1.35 \cdot 10^{17}$	$3.64 \cdot 10^{16}$	251.7
40	$4.08 \cdot 10^{-6}$	$6.53 \cdot 10^{16}$	$1.78 \cdot 10^{16}$	268.2
45	$2.09 \cdot 10^{-6}$	$3.40 \cdot 10^{16}$	$9.14 \cdot 10^{15}$	274.5
50	$1.13 \cdot 10^{-6}$	$1.84 \cdot 10^{16}$	$4.95 \cdot 10^{15}$	274.2
55	$6.17 \cdot 10^{-7}$	$9.98 \cdot 10^{15}$	$2.69 \cdot 10^{15}$	273.7
60	$3.52 \cdot 10^{-7}$	$5.70 \cdot 10^{15}$	$1.54 \cdot 10^{15}$	252.8
65	$1.92 \cdot 10^{-7}$	$3.11 \cdot 10^{15}$	$8.38 \cdot 10^{14}$	232.2
70	$9.90 \cdot 10^{-8}$	$1.61 \cdot 10^{15}$	$4.32 \cdot 10^{14}$	211.2
75	$4.57 \cdot 10^{-8}$	$7.42 \cdot 10^{14}$	$2.00 \cdot 10^{14}$	204.1
80	$2.06 \cdot 10^{-8}$	$3.34 \cdot 10^{14}$	$8.98 \cdot 10^{13}$	197.2
85	$9.00 \cdot 10^{-9}$	$1.46 \cdot 10^{14}$	$3.93 \cdot 10^{13}$	190.2
90	$3.68 \cdot 10^{-9}$	$5.96 \cdot 10^{13}$	$1.61 \cdot 10^{13}$	196.6
95	$1.55 \cdot 10^{-9}$	$2.51 \cdot 10^{13}$	$6.76 \cdot 10^{12}$	202.9
100	$6.70 \cdot 10^{-10}$	$1.09 \cdot 10^{13}$	$2.93 \cdot 10^{12}$	209.2

TABLE 2

H, km	ρ , g/cm ³	T, °K	H, km	ρ , g/cm ³	T, °K
100	$4.97 \cdot 10^{-10}$	205	140	$3.40 \cdot 10^{-12}$	666
110	$9.83 \cdot 10^{-11}$	250	160	$1.16 \cdot 10^{-12}$	935
120	$2.44 \cdot 10^{-11}$	332	180	$5.86 \cdot 10^{-13}$	1042
130	$7.59 \cdot 10^{-12}$	502	200	$3.32 \cdot 10^{-13}$	1100

same time, research atmospheric density in the 100-200 km range is /8
being conducted only during irregular rocket launchings in the very
short periods of time during which the rocket passes through this altitude
range, as a result of which the respective experimental data are quite limit-
ed. Table 2 gives the diurnal values of density in this altitude range
during the period of average solar activity (end of 1960) according to the
semiempirical model of Kallman and Sibley [17]. We should mention that the
numerous variations in atmospheric density, which are extremely pronounced
at high altitudes and about which we shall speak later, also exist at
altitudes of 160 to 240 km, although the amplitude of fluctuations in ρ
in this case is low. Thus, according to this same work [17], the nocturnal
atmospheric density at an altitude of 200 km is 1.5 times lower than the
value depicted in Table 2. It is clear from the survey paper of V. V.
Mikhnevich [9], that the daily variations in density have an amplitude on
the order of a factor of 2 only at an altitude of approximately 250 km.
Below this altitude, these variations are correspondingly lower. Density
variation during the cycle of solar activity is also manifested mainly
above 200 km; however, certain fluctuations in ρ do take place at lower
altitudes. According to the review [9], with variation in solar activity
from maximum to minimum, a variation by a factor of 1.8 takes place in the /9
noon and midnight densities at an altitude of 200 km.

Quite some time ago it became necessary to have knowledge of the
atmospheric composition above 100 km. As we have already mentioned, the atmos-
phere is mixed below 100-120 km and therefore the concentrations of the basic
components are known to us from measurements of the overall atmospheric
density, however the ratio among the basic components begins to vary above this
level. First of all, molecular oxygen dissociates quite effectively above
100 km under the influence of ultraviolet solar radiation. This results in
the relative concentration of O_2 molecules beginning to decrease with altitude
and the number of O atoms to grow. The O atoms are one of the major com-
ponents of the atmosphere above this level. Furthermore, beginning at
altitudes of 110 - 120 km, the diffusion-gravitational separation of gases
leads to a change in the chemical composition of the atmosphere with

TABLE 3

H, km	$[\bar{N}_2]$, cm^{-3}	$[\bar{O}_2]$, cm^{-3}	$[O]$, cm^{-3} according to [22]
100	$5.2 \cdot 10^{12}$	$1.7 \cdot 10^{12}$	$6 \cdot 10^{11}$
110	$1.2 \cdot 10^{12}$	$1.9 \cdot 10^{11}$	$1.8 \cdot 10^{11}$
120	$3.5 \cdot 10^{11}$	$3.2 \cdot 10^{10}$	$8 \cdot 10^{10}$
130	$1.1 \cdot 10^{11}$	$1.0 \cdot 10^{10}$	$5 \cdot 10^{10}$
140	$5.0 \cdot 10^{10}$	$4.8 \cdot 10^9$	$3 \cdot 10^{10}$
150	$3.5 \cdot 10^{10}$	$2.9 \cdot 10^9$	$1.9 \cdot 10^{10}$
160	$1.4 \cdot 10^{10}$	$1.4 \cdot 10^9$	$1.2 \cdot 10^{10}$
170	$8.7 \cdot 10^9$	$7.6 \cdot 10^8$	$8 \cdot 10^9$
180	$5.8 \cdot 10^9$	$4.4 \cdot 10^8$	$6 \cdot 10^9$
190	$4.9 \cdot 10^9$	$2.9 \cdot 10^8$	$4 \cdot 10^9$
200	$2.6 \cdot 10^9$	$1.9 \cdot 10^8$	$3.5 \cdot 10^9$

altitude. This is manifested in an increase in the number of light gases and a decrease in the relative concentrations of the heavy ones.

Until recently our knowledge on the chemical composition of the atmosphere above 100 km was derived basically from theoretical models after examining the diffusion-gravitational separation and dissociation of molecular oxygen under predetermined assumptions as to the temperature of the atmosphere, the intensity of ultraviolet solar radiation, etc. The overwhelming majority of these models led to the concept of a rapid drop with altitude in the relative amount of molecular nitrogen, thus implying the existence of a purely atomic atmosphere above approximately 150 - 160 km. However, recent years have provided experimental data on atmospheric composition in quantities sufficient to give an idea of the actual distribution of concentrations of the basic atmospheric components in the range from 100 - 200 km. These data were obtained as a result of experiments carried out by two theoretically different methods: optical and mass-spectrometric. Without dwelling here on the details, let us refer the reader to the survey articles mentioned above [11 - 13] where the experimental method is described in more detail. Now let us cite the basic results derived from comparing the data of various experiments

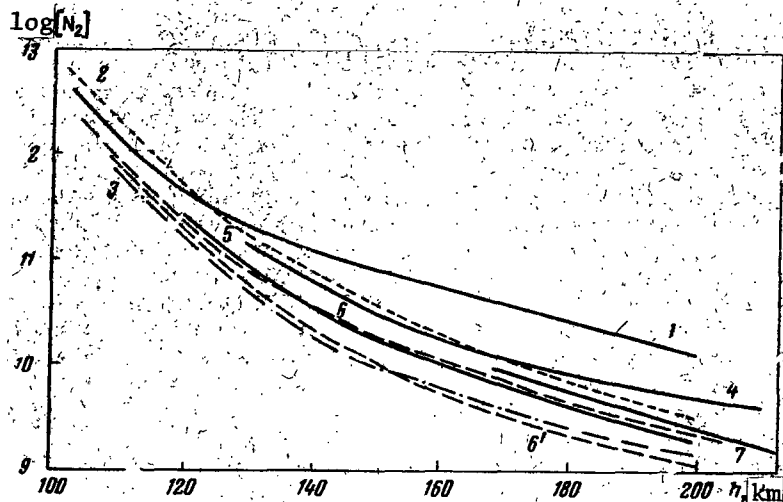


Figure 1. Altitude Variation in Molecular Nitrogen Concentration in the Atmosphere According to Various Experimental Data.

1. July, 1959, Morning [18]; 2. September 23, 1960, 0 hr. 56 min. [19]; 3. August 23, 1961, 10 hr. 03 min. [20]; 4. November 15, 1961, 16 hr. 00 min. [21]; 5. July 10, 1963, 10 hr. 00 min. [22]; 6 and 6'. June 6, 1963, 7 hr. 30 min. [23]; 7. Average for two launchings in 1962 [24].

according to Reference [11]. Table 3 gives a summary of the experiments. At the present time, there are already more than 20 experiments in existence on research of the neutral composition in the range of 100 - 200 km, conducted at different times of day and at different levels of solar activity. Figure 1 compares the values of $[N_2]$, obtained in these experiments. It is obvious from the figure that a large scatter is observed in the data, which reaches one order of magnitude in the range of 180 to 200 km. On the basis of these data it was not possible to find any dependence of nitrogen concentration on time of day, solar activity or season [11]. At the same time, if we discard the two curves representing the first experiment of A. A. Pokhunkov [18], where the values of $[N_2]$ were too high, and the first work of Hinteregger's group [20], where an unrealistically high concentration ratio of $[O]/[N_2]$ was obtained, the remaining curves on Figure 1 permit the selection of mean values

/10

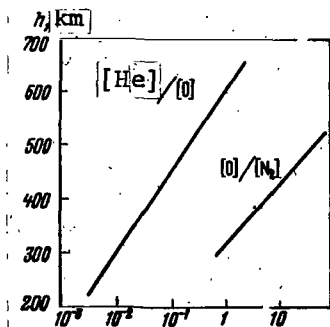


Figure 2. Altitude Variation in the Relative Concentrations $[\text{He}]/[\text{O}]$ and $[\text{O}]/[\text{N}_2]$ According to Measurements on the Satellite "Explorer XVII". Average Curves are Given that have been Obtained on the Basis of Experimental Points [28].

for the concentration of molecular nitrogen in the altitude range shown on Table 3. These mean values of $[\text{N}_2]$ differ from the other experimental data on Figure by a factor of no more than 1.6. Such a difference is fully allowable both from the viewpoint of possible measurement errors and from the viewpoint of possible variations in $[\text{N}_2]$ due to variation in the overall density, or to other as yet unknown reasons.

Mean values of the molecular oxygen concentrations obtained in rocket launchings can be similarly

selected. The mean values of $[\text{O}_2]$ are given in Table 3. As far as the O/N_2 concentration ratio is concerned, significantly different values are obtained in different experiments. Figure 2 depicts an attempt to compare the variation in the magnitude of $[\text{O}]/[\text{N}_2]$ at an altitude of 180 km with time of day. Along the horizontal axis on this figure we have plotted the absolute difference in times between the moment of observation and local noon. The data in Figure 2 show that a systematic variation is apparently observed in the concentrations of atomic oxygen and molecular nitrogen which leads to an increase in the ratio during the noon hours and a decrease in the evening and morning. Table 3 gives the concentrations of atomic oxygen in the range from 100 to 200 km according to the empirical model of Hinteregger et al. [22]. It should be borne in mind that this model pertains to daytime conditions. When we convert to 0 concentrations representing the morning, evening or nighttime conditions, Figure 2 should be borne in mind.

We find that substantial difficulty is encountered in researching the temperature of the atmosphere in the range of 100 - 200 km, where a transition occurs from the relatively low temperatures of the mesosphere

/11

TABLE 4

H, km	100	110	120	130	140	160	180	200
T, °K	205	250	332	502	666	935	1042	1100

(200 - 300° K) to the high temperatures of the thermopause (1000 - 2000° K). It is difficult to determine T on the basis of data on the altitude of the homogeneous atmosphere obtained from manometric density measurements because of the absence of reliable data (until quite recently) on the chemical composition

of the atmosphere, i.e. on the value of μ (molecular weight) necessary for finding the temperature. Methods have begun to be developed recently for determining the parameters of the atmosphere by actively influencing it (releasing metal vapors, nitric oxide and other reagents from rockets). However, for the present they give only the general character of the change in the value of T in this altitude range (see the article by Blamont [25]), without allowing for the complex variations in temperature which take place with change in time of day, solar activity, season, etc. Table 4 shows the temperature distribution in the range from 100 to 200 km according to the Kallman and Sibley model [17]. This model, as mentioned previously, pertains to the daytime conditions during the period of average solar activity (1960). It is essential to bear in mind that the temperatures cited in Table 4 are given only as an example of the possible distribution of T, and may differ substantially from the actual temperatures in the atmosphere.

c. Altitudes Above 200 km. Above 200 km, as mentioned above, investigation of the atmospheric density is conducted basically from observations of the deceleration of artificial satellites. The information accumulated for the past few years has permitted clarification of the significant variations in density at these altitudes. Two types of variations in ρ are apparently the most substantial: diurnal variations and those depending on solar activity. The diurnal variations are produced by

TABLE 5

H, km	1958	1959		1960	
200	$4,4 \cdot 10^{-13}$	$4,2 \cdot 10^{-13}$		$4,1 \cdot 10^{-13}$	
300	$4,6 \cdot 10^{-14}$	Day	Night	Day	Night
400	$1,4 \cdot 10^{-14}$	$3,9 \cdot 10^{-14}$	$5,6 \cdot 10^{-15}$	$3,6 \cdot 10^{-14}$	$3,3 \cdot 10^{-14}$
		$9,0 \cdot 10^{-15}$		$7,0 \cdot 10^{-15}$	$3,5 \cdot 10^{-15}$
500	$5,2 \cdot 10^{-15}$	$3,1 \cdot 10^{-15}$	$1,0 \cdot 10^{-15}$	$2,0 \cdot 10^{-15}$	$4,7 \cdot 10^{-16}$
600	$1,9 \cdot 10^{-15}$	$1,1 \cdot 10^{-15}$	$2,0 \cdot 10^{-16}$	$6,4 \cdot 10^{-16}$	$7,0 \cdot 10^{-17}$
700	$7,6 \cdot 10^{-16}$	$4,4 \cdot 10^{-16}$	$(5 \cdot 10^{-17})$	$2,0 \cdot 10^{-16}$	$1,4 \cdot 10^{-17}$
	1961		1962 (day)	1963-1964 (day)	1962-1964 (night)
	$4,0 \cdot 10^{-13}$			$2,7 \cdot 10^{-13}$	$1,8 \cdot 10^{-13}$
	Day	Night			
	$3,0 \cdot 10^{-14}$	$1,4 \cdot 10^{-14}$	$2,4 \cdot 10^{-14}$	$1,5 \cdot 10^{-14}$	$6,8 \cdot 10^{-15}$
	$4,4 \cdot 10^{-15}$	$1,5 \cdot 10^{-15}$	$3,0 \cdot 10^{-15}$	$2,1 \cdot 10^{-15}$	$7,6 \cdot 10^{-16}$
	$7,4 \cdot 10^{-16}$	$1,8 \cdot 10^{-16}$	$4,2 \cdot 10^{-16}$	$3,4 \cdot 10^{-16}$	$8,4 \cdot 10^{-17}$
	$1,6 \cdot 10^{-17}$	$3,2 \cdot 10^{-17}$	$7,0 \cdot 10^{-17}$	$6,0 \cdot 10^{-17}$	$1,8 \cdot 10^{-17}$
	$4,6 \cdot 10^{-18}$	$1,9 \cdot 10^{-17}$	$1,9 \cdot 10^{-17}$	$1,6 \cdot 10^{-17}$	$6,5 \cdot 10^{-18}$

* Translator's note: Commas represent decimal points.

changes during the day in the intensity of short-wave and corpuscular solar radiations, and consist of an increase in the atmospheric density at night as opposed to that during the day. As is obvious from Reference [9], the amplitude of the fluctuations in ρ grows with altitude, reaching almost one order of magnitude at an altitude of 600 km.

Variations in density from maximum to minimum solar activity take place with even greater amplitude. Table 5 shows the mean values of density obtained by King-Hele [7] on the basis of analyzing variations in the orbits of 45 satellites in 1958 - 1964. This table shows that the daytime values of ρ change by a factor of 30 - 50 from the period of minimum activity to the period of maximum activity at altitudes of 600 - 700 km. The nighttime values of the density vary from maximum to minimum activity even more strongly. /12

A variation in atmospheric density is observed over a period of 27 - 28 days (monthly effect). According to the work of V. V. Mikhnevich [9], this variation lies within a factor of 1.5 to 2 and must be greater

for higher altitudes. Variations in ρ are also noted with a semiannual period and a narrower latitude. In addition to the periodic variations in density it is possible to have variations in ρ which depend on spontaneous phenomena: geomagnetic perturbations, solar flares, etc.

Research on the neutral composition of the atmosphere above 200 km is extremely limited. During the launching of the geophysical rocket on November 15, 1961, A. A. Pokhunkov [21], using a radio-frequency mass-spectrometer, measured the concentrations of molecular nitrogen up to an altitude of 430 km. Comparison of these concentrations with the data on the atmospheric density showed that at a maximum altitude of 430 km molecular nitrogen comprises 30 to 60% of the total number of particles [21]. This latter indicates that the nitrogen molecule is a substantial component of the atmosphere up to significantly higher altitudes than was assumed previously (see, for example [20]).

These conclusions are also verified by the results of research on the neutral composition of the atmosphere on the "Explorer XVII" satellite [26, 27]. According to reference [26], atomic oxygen begins to prevail over molecular nitrogen at an altitude above 250 - 300 km. In individual instances, however, the level where the atomic and molecular concentrations are comparable ($[O] = [N_2]$) lies at significantly higher altitudes [28]. Figure 2 shows the values for the ratios of $[O]/[N_2]$ and $[He]/[O]$, obtained in these experiments by Reber [28].

The temperature of the thermosphere is very sensitive to change in solar activity. According to the work of Jacchia [8], the magnitude of T above the thermopause varies at night from 1400° K during the maximum activity (1958) to 700° K near the minimum (1963). The corresponding values for the daytime temperature [8] are 1800° K and 900° K; fluctuations in temperature during the day in the period of minimum solar activity are less than in the period of the maximum.

a. Altitude Range $H \leq 100$ km. The region of the ionosphere below 100 km (the so-called D region) has been studied less than the other ionospheric regions. The reason for this will be examined below. The electron concentrations in the lower ionosphere are distributed by several methods. Ionospheric cross-modulation and the method of oblique incidence of radio waves are among the surface methods used. Rocket experiments involve studying the propagation of radio waves transmitted from the rocket or measuring the parameters of the atmosphere directly around the rocket using various probes.

G. S. Ivanov-Kholodnyy [3] made a detailed survey of the results of measuring $[e]$ in the D region using these methods. He examined the magnitude of the electron concentrations measured in almost 40 rocket experiments, and found the existence of pronounced variations in $[e]$ from experiment to experiment. It was found that most of the investigations on electron concentration were done in period of disturbances (in the presence a sporadic E layer, polar blackouts, solar flares), when the magnitude of $[e]$ is greater than in the unperturbed D region. Nighttime values of the electron concentrations at altitudes of 60 - 100 km were found to be 1 - 1.5 orders lower than the daytime values. Comparison of the research results on $[e]$ using various methods shows [3] that the probe methods are greatly inferior, as concerns the reliability of the results, to the methods of radio wave propagation. Table 6 gives the mean values selected by G.S. Ivanov-Kholodnyy [3] for the electron concentration by day (under quiet conditions and in the perturbed ionosphere) and by night (the table gives $\log [e]$).

TABLE 6

Conditions	H, km								
	60	65	70	75	80	85	90	95	100
Day	1.6	1.9	2.2	2.6	2.9	3.3	3.8	4.5	4.8
Strongly perturbed ionosphere	2.7	3.2	3.5	3.6	3.8	4.1	4.5	4.9	5.1
Night	---	---	1	1.3	1.6	2.0	2.5	3.0	3.5

b. Altitudes Above 100 km. On the basis of analyzing the data obtained /14 in approximately 90 rocket experiments, T. V. Kazachevskaya and G. S. Ivanov-Kholodnyy [29] constructed an empirical model of the quiet ionosphere at altitudes of 100 - 300 km. Figure 3 shows the variation in [e] at various zenith angles of the sun in summer and in winter during low solar activity and in summer during high solar activity. This model at the present time is the most reliable and gives the magnitudes of the electron concentration with an error that does not exceed a factor of 2. Just as in Reference [3] for the D region, the authors of [29] came to the conclusion that the results of probe measurements of [e] are less reliable than the data obtained by other methods.

Figure 4, taken from the survey work of Bourdeau et al. [2], shows the variation in electron concentration above 200 km during the day (12 hr. 38 min., October 19, 1961) and during the night (2 hr. 27 min., March 29, 1962). It should be borne in mind that the curves on the drawing give only /15 the character of the variation in [e] above 200 km. The actual concentrations at each moment may differ from these values due to the existence of a different sort of variation in the electron concentration. According to the detailed investigation of Brace and Ready [30], at an altitude of 100 km the variation in [e] with latitude reaches a factor of 3 and decreases by approximately 2 times from day to night.

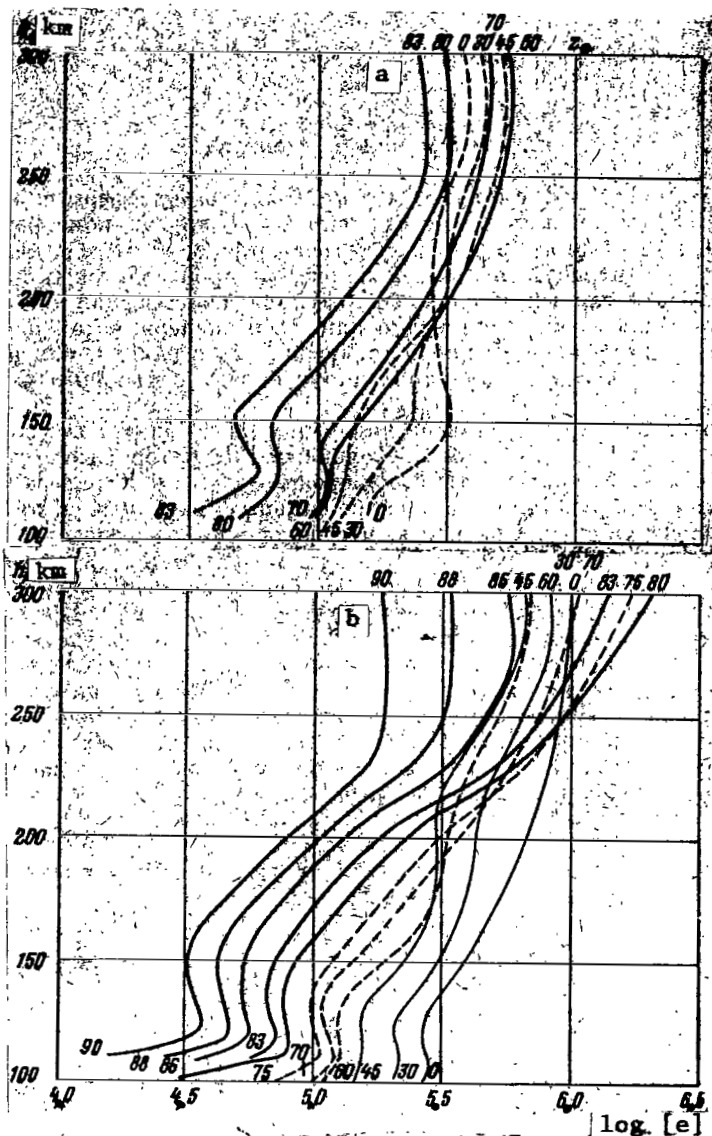


Figure 3. Altitude Variation in Electron Concentration of $[e]$ At Various Zenith Angles of the Sun According to the Model of G. S. Ivanov-Kholodnyy and T. V. Kazachevskaya [29].

a. In Summer during a Period of Low Activity. b and c. In Summer and Winter during a Period of High Solar Activity, Respectively.

(c, continued on next page)

§ 3. CONCENTRATIONS OF POSITIVE AND NEGATIVE IONS

a. The Range $H \leq 100$ km. At the present time experimental data on the ion composition of the atmosphere below 100 km are extremely limited. A series of experiments on studying the overall concentration of positive ions using probes was done by Sagalin and Smiddy [31] and by Smith [32]. The results show that the magnitudes of $[X^+]$ are almost constant at altitudes in

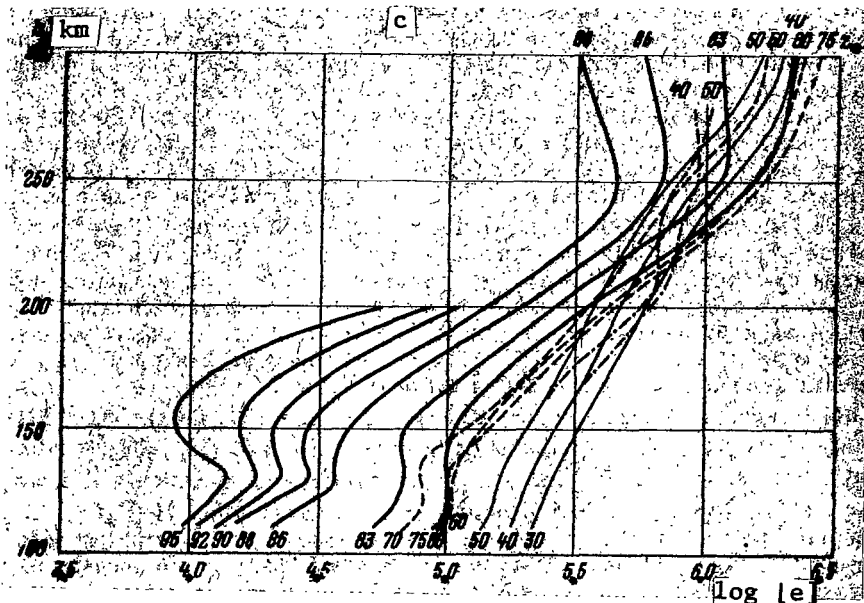


Figure 3. (Conclusion) Altitude Variation in Electron Concentration of $[e]$ At Various Zenith Angles of the Sun According to the Model of G. S. Ivanov-Kholodnyy and T. V. Kazachevskaya [29].

- a. In Summer during a Period of Low Activity. b and c. In Summer and Winter during a Period of High Solar Activity, Respectively.

the range from 60 to 100 km and are equal to $(23 - 10) \cdot 10^3 \text{ cm}^{-3}$. Comparison of these data with the most reliable measurements of the electron concentration in the D region was made by G. S. Ivanov-Kholodnyy [3] who concluded that during the day $[X^+] > [e]$ at altitudes below 75 - 80 km. This means that below this level a considerable contribution is made by the negative ions to the overall concentration of charged particles. The role of the negative ions in the D region and the level where $[X^-]/[e] = \lambda \approx 1$, will be discussed below. /16

The first investigations of the ion composition of the atmosphere below 100 km were made in the experiments of Johnson et al. [33]. It was estab-

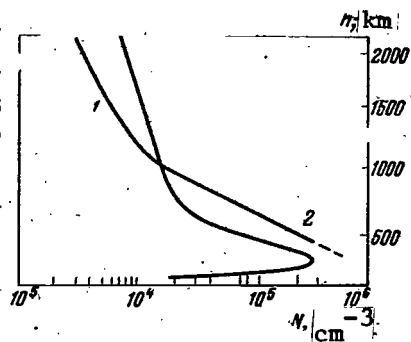


Figure 4. Variation Electron Concentration with Altitude During the Day (12 hr. 30 min., October 19, 1961, Curve 1) and at Night (2 hr. 27 min., March 29, 1962, Curve 2).

in 1963 - 1965. The accuracy of the concentrations is evaluated by the author [36] in the following manner: a factor of 4 for the absolute values and a factor of 2 for the relative values.

It is obvious from Figure 5 that in addition to the atmospheric ions N_2^+ (28^+), NO^+ (30^+) and O_2^+ (32^+), ions of H_2O (18^+), H_3O^+ (19^+) and H (H_2O) $_2^+$ (37^+) are also detected in the D region as well as ions with a high mass number (>45), which the authors identify as ion "bunches" of $H(H_2O)_3^+$ -type. It is natural to assume that the ions containing H_2O^+ are the result of contamination of the surrounding atmosphere by the rocket. However, computations show that even a very high degree of contamination cannot give the registered high concentrations of 19^+ , 37^+ and 45^+ ions; therefore, Narcisi [36] assumes that these ions are atmospheric.

b. Altitude Range from 100 to 200 km. At the present time the ion composition here has been investigated significantly better than in other regions of the atmosphere. The experiments were conducted at various times of day (at various zenith angles of the sun) and in various periods of solar activity (as an indicator, the radio emission flux at 10.7 cm wavelength

lished that at altitudes greater than 90 km O_2^+ and NO^+ ions were observed. Furthermore, during the flight a weak peak was observed for the negative ion with a mass of 46 amu (probably NO_2^-). Recently investigations of the ion composition of the D region were made by Narcisi and Bailey [34, 35]. Figure 5, taken from the survey work of Narcisi [36], shows the concentrations of positive ions at altitudes of 65 - 85 km according to three mass-spectrometric experiments conducted

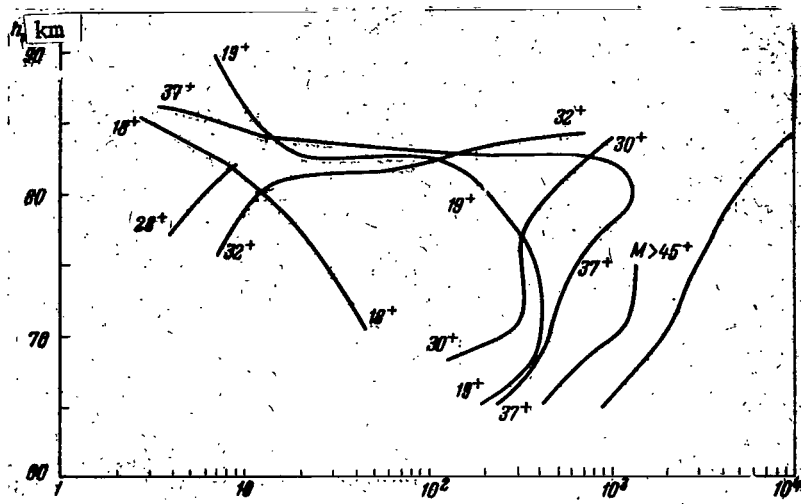


Figure 5. Concentration Distribution of Positive Ions in the Lower Part of the Ionosphere According to the Experimental Data of Narcisi [36].

/17

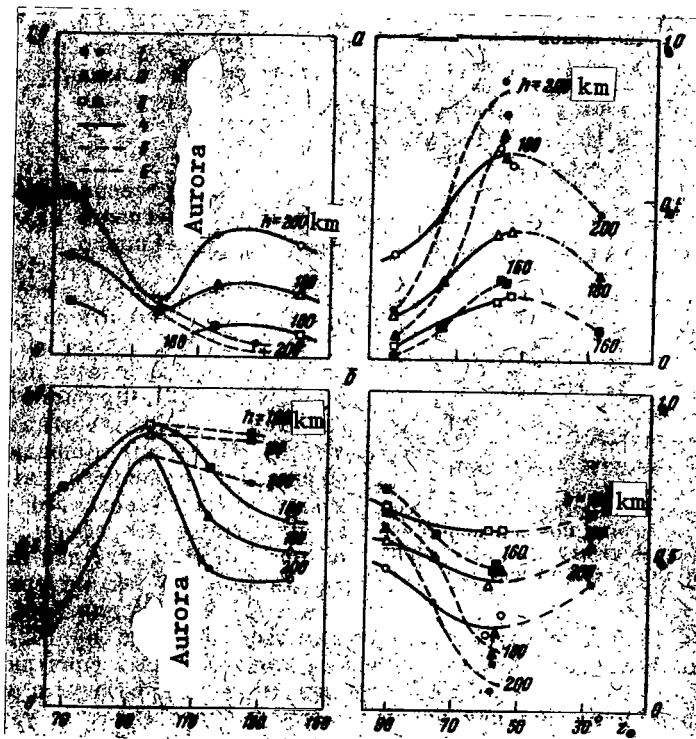


Figure 6. Variation in Relative Concentration of Ions at Various Altitudes as a Function of the Solar Zenith Angle z_0 .

a. For $O^+/[e]$; b. for $NO^+/[e]$; 1. 200 km; 2. 180 km; 3. 160 km; 4 and 5. High and Low Solar Activity, Respectively; 6. Nominal Variation in the Region $z_0 < 50^\circ$.

was used). This permits investigation of the variation in ion composition of the atmosphere with time of day and solar activity.

Figure 6 shows the experimental data on variation in ion composition at altitudes of 160, 180 and 200 km as a function of the solar zenith angle z during daylight hours. Let us point out the difference in the variations of $[O^+]/[e]$ (Figure 6a) is equal to approximately 0.40 for $z = 55^\circ$ during high activity and about 0.65 in the period near minimum solar activity. For these same periods the magnitude of $[O^+]/[e]$ when $z = 90^\circ$ is 0.15 and 0.08 respectively. Thus, analysis of the experimental data shows that the drop in relative concentration of the O^+ ions with an increase in z from 50° to 90° is more abrupt during low activity than during high activity. In this range of z the relative concentrations of NO^+ and O_2^+ ions vary approximately identically and specularly in comparison with the variation in the magnitude of $[O^+]/[e]$. In this regard, $[NO^+]/[e]$ also behaves differently with variation in z from 50° to 90° during periods of maximum and minimum solar activity.

c. Altitudes Greater than 200 km. A detailed investigation of the atmospheric ion composition in the range of 200 - 700 km was made by V. G. Istomin [37, 38] for the third Soviet satellite. With an increase in altitude, a rapid decrease was observed in concentrations of the molecular NO^+ and O_2^+ ions together with an increase in the relative concentrations of atomic O^+ and N^+ ions. It was found that at the maximum of the F2 region the ionosphere practically consists of electrons and ions of atomic oxygen with a small ($\sim 10\%$) addition of N^+ ions. The results of these investigations were found to be in good agreement with the data on ion composition obtained on rockets in the region $H < 200$ km. Figure 7, taken from the work of V. G. Istomin [39], shows the variation in relative ion concentrations at altitudes of 100-700 km. On this figure it is easy to see that rocket data for $[NO^+]/[O^+]$

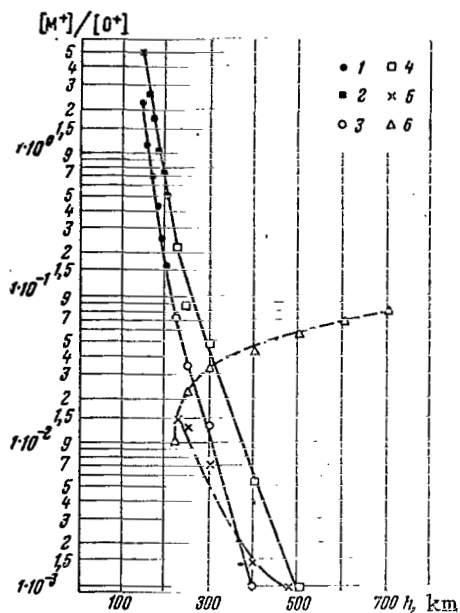


Figure 7. Variation in Ion Concentration Ratios.

On the Rocket (August, 1958, Daylight): 1. $[O_2^+]/[O^+]$; 2. $[NO^+]/[O^+]$; On the Third Artificial Earth Satellite (May 1958, Daylight): 3. $[O_2^+]/[O^+]$; 4. $[NO^+]/[O^+]$; 5. $[N_2^+]/[O^+]$; 6. $[N^+]/[O^+]$.

tions. It was emphasized in reference [40] that the conclusions concerning the basic parameter, i.e. the altitude of transition from the oxygen ionosphere to the proton ionosphere ($[O^+] = [H^+]$), differ considerably according to investigators using different experimental methods. The question of helium ions in the upper atmosphere will be examined below. Figure 8, taken from Reference [40], reflects the variation in ion composition with altitude according to the data from the satellite "Elektron".

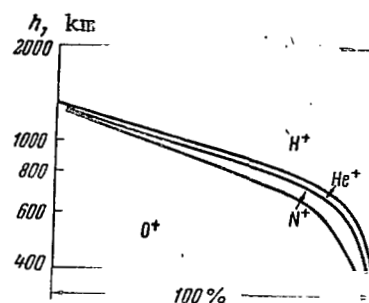


Figure 8. Variation in Altitude of the Relative Amount of Various Ions in the Ionosphere According to the Experiment of V. G. Istomin on the Satellite "Elektron" [40].

and $[O_2^+]/[O^+]$ agree well with the results from satellite research at high altitudes, giving smooth curves.

Investigations of the atmospheric ion composition above the maximum of the F2 region (300 km) involve a number of experimental difficulties and contradic-

§ 4. INTENSITY OF ULTRAVIOLET SOLAR RADIATION

The most complete investigations on the intensity of short-wave solar radiation have been rocket studies by U.S. researchers (Tousey [6], Friedman [41], Hinteregger [5], Hinteregger et al. [22], etc.). Below we shall cite data on the energy of solar ultraviolet and x-radiation outside the atmosphere taken from survey [5]. Table 7 gives the energy flux (in $\text{erg}/\text{cm}^2 \cdot \text{sec}$) within a range of $\Delta\lambda = \frac{\Delta\lambda}{\lambda}$ for the region $\lambda = 2625 - 1325 \text{ \AA}$ according to the measurements of Detwiler et al. [42]. Table 8 gives the radiation fluxes for separate spectral ranges in the region $\lambda < 1325 \text{ \AA}$. These data were obtained in Reference [22]. The quantity ΔI includes both the energy of the continuous spectrum and the energy of the basic emission lines in this region.

The radiation intensity in Table 8 refers to July 1963 [22] and the data in Table 7 to 1960 [42]. The question on variations in intensity of short-wave solar radiation with the cycle of the solar activity has not yet been adequately studied. According to [5] from August 1961 to December 1963 a decrease occurred in the intensity of the majority of the lines in the range from $1216 - 284 \text{ \AA}$ by 1.5 to 2 times. For lines with a high potential of excitation, such as $\text{FeXVI}(335.0 \text{ \AA})$ or $\text{FeXV}(284.2 \text{ \AA})$ this decrease was found to be slightly larger. It obviously follows that from maximum activity to minimum activity the intensity of the ultraviolet solar radiation with $\lambda < 1000 \text{ \AA}$ varies by 2 - 3 times. /19

Radiation in the Lyman - α line plays a major role in the upper atmosphere of the Earth. The intensity of this radiation was measured in several experiments. At the present time it is assumed that this intensity varies little with time and is $3 - 6 \text{ erg}/\text{cm}^2 \cdot \text{sec}$ [2]. On the basis of experimental data on ultraviolet solar radiation flux, the ionization rates and dissociation rates of the atmospheric components were computed

TABLE 7

/19

Region $\lambda, \text{\AA}$	$\Delta I, \frac{\text{ergs}}{\text{cm}^2 \cdot \text{sec}}$	Region $\lambda, \text{\AA}$	$\Delta I, \frac{\text{ergs}}{\text{cm}^2 \cdot \text{sec}}$	Region $\lambda, \text{\AA}$	$\Delta I, \frac{\text{ergs}}{\text{cm}^2 \cdot \text{sec}}$
2625-2575	700	2125-2075	145	1625-1575	3.2
2575-2525	560	2075-2025	90	1575-1525	1.7
2525-2475	380	2025-1975	70	1525-1475	0.95
2475-2425	390	1975-1925	55	1475-1425	0.50
2425-2375	340	1925-1875	41		
2375-2325	320	1875-1825	28	1425-1375	0.26
2325-2275	360	1825-1775	19	1375-1325	0.26
2275-2225	350	1775-1725	12		
2225-2175	310	1725-1675	8.2		
2175-2125	240	1675-1625	5.0		

TABLE 8

Region $\lambda, \text{\AA}$	ΔI		Region $\lambda, \text{\AA}$	ΔI	
	Photons $\times 10^{-9}$ $\frac{\text{cm}^2 \cdot \text{sec}}$	ergs $\frac{\text{cm}^2 \cdot \text{sec}}$		Photons $\times 10^{-9}$ $\frac{\text{cm}^2 \cdot \text{sec}}$	ergs $\frac{\text{cm}^2 \cdot \text{sec}}$
1775-1825	2700.0	32.0	460-370	2.0	0.088
1825-1875	350.0	5.7	370-280	9.2	0.58
1027-911	13.4	0.27	280-205	3.5	0.29
911-796	13.4	0.31	205-165	7.2	0.78
796-630	5.8	0.153	165-31	3.0	0.70
630-400	9.6	0.34	31-1	<0.01	<0.01

at various altitudes. The most complete data were obtained in the words of G. S. Ivanov-Kholodnyy [43, 44]. Figures 9 and 10, taken from these papers, show the total rate of ionization q as a function of the solar zenith angle and the ionization rate of the basic atmospheric components respectively, at altitudes of 100 - 300 km. It should be borne in mind that these data refer to low solar activity.

The profile of the rate of dissociation of molecular oxygen was obtained in Reference [22]. Figure 11, taken from this paper, shows the variation

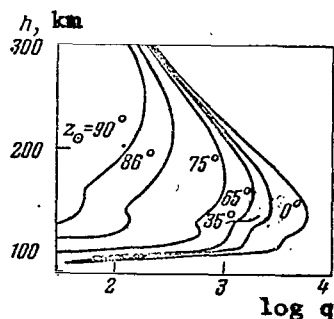


Figure 9. Altitude variation of the Overall Rate of Ion Formation in the Atmosphere at Various Solar Zenith Angles According to [43].

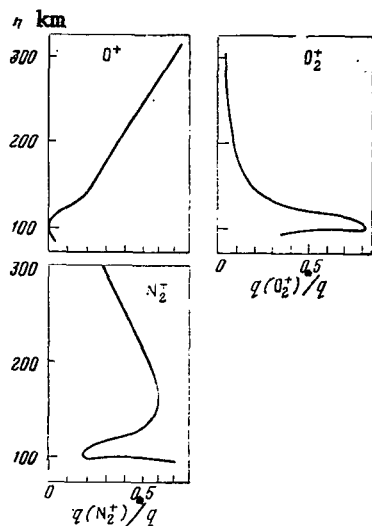


Figure 10. Altitude variation of the Relative Rate of Formation of Different Ions at Low Solar Activity According to [44].

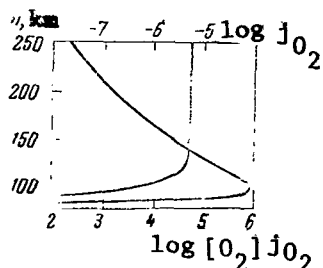


Figure 11. Coefficient of Dissociation j_{O_2} and Rate of Dissociation $j_{O_2} [O_2]$ of Molecular Oxygen in the Atmosphere According to Hinteregger et al. [22].

with altitude in the coefficient of dissociation j_{O_2} and the rate of dissociation $j_{O_2} [O_2]$ at altitudes of 100 - 200 km.

Thus, at the present time there are already sufficiently reliable experimental data on the distribution of the basic parameters in the upper atmosphere. The agenda includes the question of investigating those mechanisms which determine the distribution of these parameters with altitude, their variation with time of day, season, solar activity, etc. This in turn leads to the necessity of a detailed investigation of the basic processes in the upper atmosphere involve both neutral and charged particles. Let us examine the question as to what is known at the present time concerning the role and the effectiveness of these processes.

PROCESSES INVOLVING CHARGED PARTICLES

The influence of various hard radiations on the upper atmosphere of the Earth leads to ionization of the atmospheric components and to the formation of positive ions and electrons. In the role of ionizing agents we find ultraviolet solar radiation, x-radiation, cosmic rays and corpuscular streams. Each of these factors operates in a given altitude range and leads to pre-determined effects. The relative role of certain ionizing sources of radiation may vary as a function of time of day, solar activity or other factors (for example, ionization by x-radiation prevails during solar flares over ionization by radiation in the Lyman - α line; the corpuscular streams which have little effect during the day may determine the ionization of the nocturnal ionosphere, etc.).

The reactions of recombination of positive ions and electrons (in the lower part of the ionosphere it is the negative ions, about which we speak below in detail) are processes that are inverse to the ionization of neutral atmospheric particles. The problem of determining balanced concentrations of electrons formed under the influence of the processes of ionization and recombination was first studied in 1931 by Chapman [45]. He simplified the conditions of the problem: an atmosphere consisting of a single gas with an altitude-constant temperature, monochromatic radiation, and a two-dimensional layer. It is obvious that at the present time such a solution is inapplicable in the general case both because the atmosphere has a complex composition which, like the temperature, varies with altitude while the absorption coefficient varies strongly with the wavelength of the ionizing radiation, and because the positive ions and electrons formed as a result of direct photoionization may undergo a whole series of complex conversions before the inverse process of formation of neutral particles takes place with recombination of the charged particles, which leads to significantly more complicated laws governing recombination in the ionosphere than Chapman had assumed.

/21

a. Recombination of Electrons and Positive Ions. The processes of interaction between positive ions and electrons, leading to the formation of neutral particles, are called recombination processes. Since the energy expended on ionization of the neutral particle is released when the corresponding electron and positive ion combine, the question as to what happens to the resultant energy surplus becomes very significant.

The simplest mechanism for release of this energy is by radiation; the process of interaction between the positive ion and the electron, which leads to radiation of the energy surplus, is called radiative recombination:

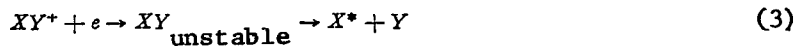


where X can designate either an atom or a molecule.

Another mechanism for release of the energy surplus may be by transmitting it to a third body (atom or molecule) which participates in the reaction:



where the symbol * shows that the particle M received an additional share of energy. Finally, when molecular ions interact with electrons, a process of dissociative recombination may take place in which the energy surplus goes to dissociation of the resultant short-lived complex and to excitation of the reaction products:



Now let us look at the effectiveness of recombination processes (1) - (3) and their role in the various regions of the ionosphere. A detailed survey of the present state of the art on research in recombination processes is

given in the work of Biondi [46].

The rate constants of the radiative recombination processes were computed theoretically on the basis of quantum theory for hydrogen ions. Theoretical computations of the radiative recombination rates of ions which are very important for atmospheric physics, i.e. ions of atomic oxygen and nitrogen, were made by Bates [47]. These computations show that the rate constants for radiative recombination are on the order of $10^{-12} \text{ cm}^3 \cdot \text{sec}^{-1}$.

Very little data exist on the effectiveness of the recombination process of ions and electrons with triple collisions. Massey and Burhop [48] found on the basis of theoretical arguments that the constant process of α_2 must be equal to $6 \cdot 10^{-27} \text{ cm}^6 \cdot \text{sec}^{-1}$ in air at a temperature of 300° K . At the present time, however, there are no experimental data on the magnitudes of α_2 which could be compared with these theoretical evaluations.

Dissociative recombination of molecular NO^+ , O_2^+ and N_2^+ ions is the basic process in practically the entire ionosphere leading to the loss of electrons and positive ions:



In recent years several papers have dealt with experimental and (partially) 22
theoretical investigations of these processes. Summaries of the basic attainments in this area have been published many times in recent years in survey papers [46, 49-55]. Theoretical computations of the constants of the dissociative recombination processes are extremely difficult due to the necessity of having precise knowledge of the potential curves of the molecule and the molecular ion, especially near the point of intersection of the curves for

the ion and the potential curves for the excited state of the molecule as well as the lifetime of the excited state. At the present time no such data are available.

Therefore, the conclusions of theoretical research are only qualitative at the present time. To obtain any reliable quantitative data on the magnitude of α^* it is necessary to carry out laboratory research on dissociative recombination and to use estimates of the rate of these processes obtained on the basis of ionospheric data.

Here we shall not cite a detailed survey of the laboratory research on the magnitude of α^* for atmospheric ions. Such a survey can be found in References [15, 51, 55]. We shall cite only the basic results of the combined analysis of laboratory and ionospheric data on α^* , given in References [55, 56].

At the present time the values of the constants $\alpha^*(N_2^+)$, $\alpha^*(O_2^+)$ and $\alpha^*(NO^+)$ for a temperature on the order of $300^\circ K$ are fairly reliably known and may be assumed equal to

$$\begin{aligned}\alpha^*(N_2^+) &= 3 \cdot 10^{-7} \text{ cm}^3 \cdot \text{sec}^{-1} \\ \alpha^*(O_2^+) &= 3 \cdot 10^{-7} \text{ cm}^3 \cdot \text{sec}^{-1} \\ \alpha^*(NO^+) &= 1.5 \cdot 10^{-7} \text{ cm}^3 \cdot \text{sec}^{-1}\end{aligned}\tag{7}$$

The error in these values of α^* should not exceed a factor of 1.5 for the N_2^+ and O_2^+ ions and a factor of 2 for the NO^+ ions.

The problem of the values of α^* at higher temperatures ($\sim 1000 - 2000^\circ K$), i.e. the temperature dependence of the constants (7), is more complicated. At the present time various authors accept different forms for the dependence of α^* on

T. We feel the most valid to be the viewpoint of G. S. Ivanov-Kholodnyy [56] who found on the basis of analyzing both laboratory and ionospheric data that the dissociative recombination constants depend on T in the following manner:

$$\left. \begin{aligned} \alpha^*(N_2^+) &\propto T^{-0.5}, \\ \alpha^*(O_2^+) &\propto T^{-1}, \\ \alpha^*(NO^+) &\propto T^{-1}. \end{aligned} \right\} \quad (8)$$

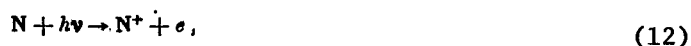
The problem of the temperature dependence of the constants α^* however is very complex. For example one of the problems is that the value of α^* must depend on the temperature of the charged particles (which in a number of cases may differ considerably from the temperature of the neutral atoms and molecules), and the laboratory data are "bound" to the temperature of the neutral component.

The evaluations given above for the rate of the various recombination processes allow us to judge the relative effectiveness of these processes in different regions of the ionosphere. Comparison of the rate of electron loss from the reaction of triple recombination (2) with the rate of the radiative recombination of electrons shows that when $\alpha_2 \approx 10^{-26} \text{ cm}^6 \cdot \text{sec}^{-1}$, we must have concentrations of neutral particles greater than 10^{14} cm^{-3} for the rate of process (2) to be greater than the rate of radiative recombination. Since the quantity [M] is much smaller than 10^{14} cm^{-3} , in a large part of the ionosphere (above approximately 110 km), reactions of triple recombination can be ignored in analyzing the ionospheric processes. /23

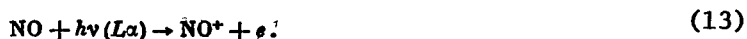
Thus, the basic "competing" processes of recombination in the upper atmosphere are the reactions of dissociative recombination of molecular ions (3) and radiative recombination of atomic ions (1). Since the values of α^* for the basic atmospheric ions are at least 4 orders higher than the constant of radiative recombination for the basic atmospheric atomic ions of

O^+ and N^+ , processes of dissociative recombination constitute the basic mechanism of electron loss in the ionosphere at altitudes of 100 - 500 km. Below 100 km, processes of dissociative recombination also constitute the basic process for interaction between positive ions and electrons. However, the overall rate of neutralization at these altitudes will depend on the processes of interaction between positive and negative ions (see below).

b. Ionization of Neutral Particles. Current opinion holds that the basic source of particle ionization in the upper atmosphere of the Earth is ultra-violet solar radiation. The ionization threshold of the basic atmospheric components, i.e. nitrogen and oxygen in atomic and molecular form, lies in the range of 800 - 1020 Å (see Table 9); therefore radiation on a shorter wavelength may lead to the formation of ions and electrons in the upper atmosphere. In addition to the direct photoionization of the basic atmospheric components by radiation at $\lambda = 800 - 1000$ Å:



in the lower atmosphere a substantial role may be played by the photoionization of nitric oxide molecules which have a low ionization potential of 9.25 eV [57] by radiation in the strong Lyman - α line of the solar spectrum:



If the quantum energy of the ionizing radiation is sufficiently high, dissociation (the process of dissociation ionization) may take place simultaneously with ionization of the molecules, which leads in the case of a diatomic

TABLE 9

Particles	O ₂	N ₂	O	N
Ionization threshold, Å (according to [57])	1020.4	796.0	911.6	852.7

molecule to the formation of an atomic ion and a neutral atom:



The quantum energy (or particle energy in the case of dissociative ionization by corpuscular fluxes) which is essential for dissociative ionization of molecular nitrogen, is approximately 25 eV ($\lambda = 495 \text{ Å}$), and of molecular oxygen, 19 eV ($\lambda = 650 \text{ Å}$). The relative effectiveness of the dissociative ionization process is low in comparison with direct ionization. According to the detailed research conducted by Weissler et al. [58], for example, the production cross section of N^+ ions with ionization of the N_2 molecule by radiation at $\lambda = 400 - 500 \text{ Å}$ is 1 - 2 orders smaller than the production cross section of N_2^+ ions. The same also applies to the production of O^+ ions with irradiation of the O_2 molecule. Since atomic oxygen exists in a large part of the ionosphere in greater amounts than does molecular oxygen, the role of O^+ production by process (15) can be ignored. /24

A different situation is observed with atomic nitrogen. Since the concentrations of atomic nitrogen at altitudes of 100 - 300 km are low and comprise approximately $10^{-2} - 10^{-3}$ of the N_2 molecule concentration, we cannot exclude the possibility that dissociative ionization of molecular nitrogen may be more effective in the formation of N^+ ions than direct ionization of N atoms, and the experimentally registered N^+ ions may be primarily the product

of reaction (14). Ionization rates for the basic atmospheric components above 100 km for minimum solar activity were, as shown above, obtained in the research of Hinteregger et al. [22] and G. S. Ivanov-Kholdnyy [43, 44]. However, it should be remembered that with variation in the level of solar activity the conditions in the atmosphere must also vary. In particular, with increase in solar activity, the intensity of ultra-violet solar radiation must increase, and the neutral composition of the atmosphere may vary. This means that the magnitude of the ionization rate in the atmosphere is a function of the level of solar activity and in principle we must have values of q for the various conditions.

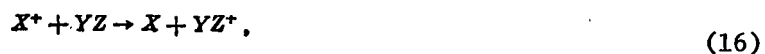
Analysis of the dependence of ionization rate on variations in density of the upper atmosphere is given in the work of G. S. Ivanov-Kholodnyy [59]. On the basis of experimental data for variations in density of the atmosphere with a change in the level of solar activity, Ivanov-Kholodnyy [59] computed the ionization rates at various solar zenith angles for the case of maximum and minimum atmospheric density. Table 10, obtained on the basis of the data in Reference [59], shows the ratio of the ionization rate for maximum values of ρ to the ionization rate for minimum density of the atmosphere at various altitudes for two solar zenith angles [$f(z_0)$ equals to 1 and 2 for the upper and lower lines of the table, respectively].

It is obvious from the table that the variation in ionization rate due to variations in atmospheric density increases with altitude. Below 300 km this effect may practically be ignored; however, at altitudes of 500 - 800 km the difference in q reaches a factor of 3-10. It should be borne in mind that these values of $\log \frac{q_{\max}}{q_{\min}}$ reflect only the variations in atmospheric density with variation in solar activity; the overall variation in ionization rate at each altitude with variation in activity will be determined both by variations in density and by variations in the intensity of radiation from the neutral composition of the atmosphere. As yet there are insufficient data concerning the dependence of these latter parameters on solar activity.

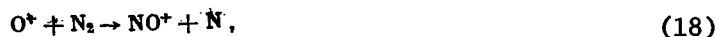
TABLE 10

H, km	100	150	200	250	300	400	500	600	800
$\lg \frac{q_{\max}}{q_{\min}}$	0	0	0.01	0.07	0.17	0.38	0.59	0.76	1.08
$\lg \frac{q_{\max}}{q_{\min}}$	0	0	0.08	0.02	0.13	0.35	0.58	0.76	1.08

c. Ion-Molecular Reactions. In 1949, Bates first mentioned the possible role in the upper atmosphere of reactions such as:



Later the role of processes (16) and (17) was studied in a number of papers which were discussed in detail in the surveys [15, 55, 60]. Here we shall give only a survey of the laboratory data on the effectiveness of the basic ion-molecular reactions in the ionosphere. The results of research on the two major ion-molecular reactions



which determine the ion loss of atomic oxygen in the atmosphere, are given in Table 11. As follows from the table, the situation with the laboratory investigations of the reaction constants that are of interest to us is extremely unsatisfactory. Even if we discard the high value

TABLE 11		
Authors	Reaction Constant	
	$O^+ + N_2 \rightarrow NO^+ + N(18)$	$O^+ + O_2 \rightarrow O_2^+ + O(19)$
Potter [62]	10^{-8}	—
Dickinson & Sayers [63]	—	$2.5 \cdot 10^{-11}$
Talrose et al. [64]	$< 8.7 \cdot 10^{-11}$	—
Langstroth & Hasted [65]	$4.7 \cdot 10^{-11}$	$1.8 \cdot 10^{-11}$
Fiet et al. [66]	—	$(1-10) \cdot 10^{-11}$
Volpe et al. [67] [sic]	$2.2 \cdot 10^{-11}$	—
Sayers & Smith [68]	$2.7 \cdot 10^{-11}$	$1.6 \cdot 10^{-11}$
Paulson [69]	$< 5 \cdot 10^{-11}$	—
Paulson et al. [70]	$2 \cdot 10^{-10}$	—
Fehsenfeld et al. [71, 72]	$3 \cdot 10^{-11}$	$4 \cdot 10^{-11}$

$\alpha_{18} = 2 \cdot 10^{-10} \text{ cm}^3 \cdot \text{sec}^{-1}$ found by Paulson et al. [70] (since it contradicts the value given in the review paper by Paulson himself [69] who found there that $\alpha_{18} \leq 5 \cdot 10^{-11} \text{ cm}^3 \cdot \text{sec}^{-1}$) and the high value $\alpha_{18} = 10^{-8} \text{ cm}^3 \cdot \text{sec}^{-1}$, which as repeatedly mentioned before, is obviously in error, a scatter is observed in the most reliable values of α_{18} by one order of magnitude and the high and the low values have been confirmed in two experiments. Formula (19) is slightly better for the reaction constant, but even here we must discard the data from the experiment of Langstroth and Hasten [65] (which yields a value of α_{18} that is allowable from the viewpoint of ionospheric data), in order that the other values of α_{19} might agree among themselves with an accuracy up to a factor of 2.

It is therefore of interest to look at the ionospheric data on the constants α_{18} and α_{19} . Table 12 (from Reference [61]) gives evaluations of the reaction constants (18) and (19) on the basis of ionospheric data.

As follows from the table these evaluations generally differ considerably among themselves. The most reliable values (lines 3 - 10) are found

TABLE 12		
Authors	Reaction Constant $O^+ + N_2 \rightarrow NO^+ + N$ (18)	Reaction Constant $O^+ + O_2 \rightarrow O_2^+ + O$ (19)
Bates & Nicolet [73]	$\alpha_{18} + 0,16$	$\alpha_{19} = 1,3 \cdot 10^{-13}$
Harteck & Reeves [74]	$< 10^{-13}$	$< 10^{-13}$
Norton et al. [75]	$1 \cdot 10^{-13}$	$5 \cdot 10^{-11}$
Danilov [76]	$(0,5-1) \cdot 10^{-13}$	$(0,5-1) \cdot 10^{-11}$
Whitten & Popoff [51]	$2 \cdot 10^{-13}$	$2 \cdot 10^{-11}$
Nisbet & Quinn [77]	$1,3 \cdot 10^{-13}$	$< 10^{-11}$
Nisbet, Sagalin & Smiddy [78]	$(1,6-3) \cdot 10^{-13}$	—
Danilov (according to α/α^* and α^* from [56])	$(1,5-3) \cdot 10^{-13}$	$(0,6-1,1) \cdot 10^{-11}$
Hall et al. [22] [sic]	$\alpha_{18} + 0,12$	$\alpha_{19} \approx 3 \cdot 10^{-13}$
Danilov & Yatsenko [79]	—	$\alpha_{18}/\alpha_{19} \lesssim 0,1$

TABLE 13						
Form- ula No.	Processes	Fite et al. [66]	Volpe et al. [67] [sic]	Paulson et al. [70]	Ferguson et al. [80]	Harteck [81]
(21)	$N^+ + O_2 \rightarrow NO^+ + O$	$5 \cdot 10^{-10}$	$1 \cdot 10^{-10}$	$3 \cdot 10^{-10}$	$5 \cdot 10^{-10}$	10^{-10}
(22)	$O_2^+ + N_2 \rightarrow NO^+ + NO$	—	$< 2,1 \cdot 10^{-13}$	$4 \cdot 10^{-11}$	10^{-13}	—
(23)	$N_2^+ + O_2 \rightarrow NO^+ + NO$	$2,1 \cdot 10^{-13}$	$< 2,1 \cdot 10^{-13}$	$4 \cdot 10^{-11}$	—	—
(24)	$N_2^+ + O_2 \rightarrow O_2^+ + N_2$	$2 \cdot 10^{-10}$	—	—	$1,0 \cdot 10^{-10}$	—
(25)	$N_2^+ + O \rightarrow NO^+ + N$	—	—	—	$2,5 \cdot 10^{-10}$	—
(26)	$N_2^+ + O \rightarrow N_2 + O^+$	—	—	—	$< 10^{-11}$	—
(27)	$N^+ + O_2 \rightarrow O_2^+ + N$	—	—	—	$(0,5-1) \cdot 10^{-9}$	—

to be in relative agreement and lead (with an accuracy up to a factor of 2 - 3) to the following values for the constants:

$$\begin{aligned} \alpha_{18} &= 2 \cdot 10^{-2} \text{ cm}^3 \cdot \text{sec}^{-1} \\ \alpha_{19} &= 2 \cdot 10^{-4} \text{ cm}^3 \cdot \text{sec}^{-1} \end{aligned} \quad (20)$$

Expression (20) is the best evaluation extant today for the constants of the basic ion-molecular reactions in the ionosphere, and is significantly more reliable than that which can be obtained on the basis of laboratory data.

The results of laboratory research of other ion-molecular reactions involving atmospheric ions are shown on Table 13. As is obvious from the table, for the majority of reactions, with the exception of (21), there are too few experiments to assume that the values of α are reliably known. However, these results give an order of magnitude of the constants of the various reactions and permit research on the question of the role of these reactions in the formation and loss of atmospheric ions. It should be mentioned that the question of the temperature dependence of the constants of ion-molecular reactions is still in a state of indeterminacy. Theory will not give the dependence of α on T , but the experiments of Sayers and Smith [68] result in $\alpha_{19} \propto T^{-1}$. At the same time, according to the experiments in [82] an increase is observed in the constant α_{18} with increase in temperature. This problem awaits experimental solution. /26

d. Ionization-Recombination Cycle of Processes in the Ionosphere.

Under conditions of photochemical balance when the role of the processes of diffusion, horizontal mass transport, mixing, etc. is small, the rates of formation and loss of charged particles per unit volume per unit of time are mutually equal:

$$q(h) = \alpha' [e]^2, \quad (28)*$$

where $q(h)$ is the total rate of ion formation at a given altitude. The quantity α' , in the right-hand side of expression (28) is called the effective coefficient of recombination and determines the rate of loss of the charged particles at the given altitude in the absence of an ionization source. The effective coefficient of recombination in the ionosphere has already been studied for some time using the methods of ionospheric radio probes. According to the variations in $[e]$ during a 24-hour period and during the time of the various perturbations it was found that the rate of electron loss in the E region is high and proportional to the square of the electron density, and in the F2 region this rate is substantially smaller and proportional to the first power of $[e]$. This phenomenon was first explained from the viewpoint of the basic processes taking place in the ionosphere by Ratcliffe and Weeks [83]. They suggested that the basic scheme of the ionization-recombination cycle of processes in the ionosphere is the following: as a result of photoionization only atomic ions $[A^+]$ are formed. As a result of interaction with molecules $[M]$ they are converted according to ion-molecular reactions such as (16) and (17) into molecular ions $[M^+]$, which in turn disappear as a result of the rapid processes of dissociative recombination. /27

Before we examine the conclusions which Ratcliffe and Weeks made in [83], let us see just how realistic are the assumptions that they made. As is obvious from Figure 10, the ionization rate of atomic oxygen, which of course leads to the formation of atomic O^+ ions, exceeds the ionization rate of N_2 and O_2 at altitudes above 130 - 150 km. Thus, the first assumption of Ratcliffe and Weeks is completely valid above 150 km. The basic mechanism of recombination of atomic ions with electrons is radiative recombination with a rate constant on the order of $10^{-12} \text{ cm}^3 \cdot \text{sec}^{-1}$. With

* Translator's Note: Reactions (21) - (27) are given in Table 13.

$[e] \approx 10^6 \text{ cm}^{-3}$ and rate constants of ion-molecular reactions of at least $10^{-12} \text{ cm}^3 \cdot \text{sec}^{-1}$, these reactions will be a significantly more effective mechanism of atomic ion loss than radiative recombination, at least up to altitudes where the concentration of neutral molecules drops to 10^6 cm^{-3} , which corresponds to $h \approx 500 \text{ km}$. Thus, the second assumption of Ratcliffe and Weeks [83] is fully valid for the basic part of the ionosphere. As far as the third assumption is concerned, i.e. that recombination is basically dissociative recombination of molecular ions, it is also valid for a large part of the ionosphere [15].

Thus, the scheme for the ionization-recombination cycle of the processes proposed by Ratcliffe and Weeks [83] is in fact a valid one. Let us look at the conclusions obtained in Reference [83]. In view of the assumptions made, we have

$$q(h) = \gamma [A^+] [M]; \quad (29)$$

$$q(h) = \alpha^* [M^+] [e]. \quad (30)$$

Above approximately 100 km where the role of the negative ions can be ignored the following formula for plasma neutrality is also valid,

$$[A^+] + [M^+] = [e] \quad (31)$$

Let us take the quantities $[A^+]$ and $[M^+]$ from (29) and (30), respectively, and after substituting them into (31) we find the expression for the ion formation rate:

$$q(h) = \frac{\gamma \alpha^* [M] [e]^2}{\gamma [M] + \alpha^* [e]}. \quad (32)$$

At altitudes where $\gamma [M] \gg \alpha^* [e]$ (the lower part of the ionosphere), the second term in the denominator of this latter equation can be ignored and

the expression for $q(h)$ assumes the form

$$q(h) = \alpha^* [e]^2 \quad (33)$$

In this case the recombination rate is proportional to $[e]$ (quadratic law of recombination) and, as is obvious from comparing (33) and (28), the effective coefficient of recombination is equal to the rate constant of the dissociative recombination. At altitudes where $\gamma [M] \ll \alpha^* [e]$, expression (32) /28 is written in the form

$$q(h) = \gamma [M] [e]. \quad (34)$$

In this case the recombination rate is proportional to the first power of the electron concentration, and the effective coefficient of recombination α' is itself found to be dependent on the electron concentration and equal to

$$\alpha' = \frac{\gamma [M]}{[e]}; \quad (35)$$

Therefore in the F2 region we use a linear coefficient of recombination β , equal to

$$\beta = \alpha' [e] = \gamma [M]. \quad (36)$$

We have looked at two different laws governing proportionality between $q(h)$ and $[e]$ from the viewpoint of the relationship between the terms $\gamma[M]$ and $\alpha^*[e]$ in expression (32). However, we can do the same from the viewpoint of variation in the ion composition of the atmosphere. In fact, from (28) and (32) we have

$$\alpha' = \alpha^* \frac{[M^*]}{[e]}; \quad (37)$$

Using (29) - (31) we can transform this expression:

$$\alpha' = \frac{\alpha^*}{1 + \frac{[A^+]}{[M^+]}} = \frac{\alpha^*}{1 + \frac{\alpha^* [e]}{\gamma [M]}} \quad (38)$$

In the lower part of the ionosphere where the concentration of molecular ions is much greater than the concentration of atomic ions this latter expression leads to $\alpha' = \alpha^*$. At higher altitudes where the atomic ions predominate, α' is much smaller than α^* and is equal to $\gamma [M]/[e]$, which leads to a linear law for the relationship between $q(h)$ and $[e]$:

$$q(h) = \alpha' [e]^2 = \gamma [M] [e] = \beta [e] \quad (39)$$

At the present time the existence of two different laws for recombination in the lower and upper parts of the ionosphere is an indisputable fact, established in a large number of experimental research projects. The fact that the theory, based on the system of basic processes, fully explains this phenomenon serves as proof of the validity of the system of processes selected.

Confirmation of the theoretical validity of the examined scheme of processes was obtained in recent years in a number of papers in which experimental data were analyzed on the ion composition of the atmosphere above 100 km. At the same time, appreciable refinements were made. For instance it was found that the dissociative recombination of N_2^+ ions becomes the basic mechanism for loss of these ions only above altitudes of 180 - 200 km, and below this point these ions disappear basically as a result of ion-molecular reactions; O_2^+ ions may be formed effectively at altitudes of $h \leq 150$ km also as a result of reaction (24), etc. Without pausing for a detailed analysis of these papers, we will cite here only those equations which according to present concepts determine the distribution of concentrations of the basic atmospheric ions under balanced conditions:

$$[O^+] = \frac{j_0 [O] + [N_2^+][O] \alpha_{26}}{[N_2] \alpha_{18} + [O_2] \alpha_{19}} \quad (40)$$

$$[N_2^+] = \frac{j_{N_2} [N_2]}{\alpha_{N_2}^* [e] + \alpha_{26} [O] + \alpha_{28} [O_2]} \quad (41)$$

$$[O_2^+] = \frac{[O_2]/\alpha_2 + [O^+][O_2] \alpha_{19} + [N^+][O_2] \alpha_{27}}{\alpha_{O_2}^* [e]} \quad (42)$$

$$[NO^+] = \frac{[O^+][N_2] \alpha_{18} + [N^+][O_2] \alpha_{21} + [N_2^+][O] \alpha_{25}}{\alpha_{NO^+}^* [e]} \quad (43)$$

$$[N^+] = \frac{[N] j_N + [N_2] j_{N_2}^{dis} + [N_2^+][N] \alpha}{[O_2] (\alpha_{21} + \alpha_{27})} \quad (44)$$

e. Ambipolar Diffusion and Distribution of Charged Particles in the Ionosphere. If the charged particles diffuse vertically at a rate of ω , then the equation of balance of ionization in the general case is written in the form:

$$\frac{d[e]}{dh} = q(h) - \alpha' [e]^2 - \frac{d([e] \omega)}{dh} \quad (45)$$

Here it is assumed that the vertical variations in electron concentration and diffusion rate are much greater than the corresponding quantities in the horizontal plane.

As is clear from equation (45) in the general case the equilibrium concentrations of electrons are determined by three factors rather than two: ionization, recombination and diffusion. In practice, however, either diffusion or photochemistry is found to be the predominant process at this altitude, which controls the distribution of charged particles. In fact, because of the

drop in atmospheric density, the ionization rate above approximately 150 - 180 km drops with altitude in proportion to the drop in concentration of the neutral particles. At the same time the diffusion rate increases with a reduction in atmospheric density, and consequently the diffusion term in equation (45) will increase with altitude. Thus, a level must exist in the ionosphere where the loss rates of the electrons due to chemical processes and to diffusion are comparable.

The question of the role of diffusion in determining the equilibrium concentrations of electrons in the ionosphere has been intensively studied for the past ten years. In the majority of these investigations to some degree the question was studied as to what altitude the equation of photochemical balance (28) is no longer valid, and it is necessary to study the role of diffusion. Ratcliffe et al. [84] made the first evaluation of the recombination and diffusion terms in Equation (45). They found that in the middle latitudes the rates of diffusion and of the chemical processes in the ionosphere are comparable at approximately an altitude of 300 km which coincides with the altitude of maximum electron concentration. It was shown (this was first done by Yonezawa [85]) that the formation of the ionization maximum in the F2 region at altitudes on the order of 300 km is associated with a shift in the mechanisms which determine the equilibrium concentrations of electrons, and that below this altitude photochemistry predominates and above it, diffusion predominates. In fact, at altitudes of the F region, the variation in ionization rate with altitude is determined only by the drop in the overall number of neutral particles. At the same time the recombination law at these altitudes is such that the linear coefficient of recombination β also drops with altitude due to the decrease in atmospheric density. Thus, the value of the electron concentration determined by equation (34) would have to either remain altitude-constant or increase slightly due to the slight decrease in the number of molecules M in the overall concentration of neutral particles. The fact that such an increase is observed in the 200 - 300 km range, where the intensity of the ionizing radiation is altitude-constant, shows that this mechanism does in fact exist in the

ionosphere. The decrease in electron concentration above the maximum of the F2 region indicates that another mechanism (diffusion) begins to function and leads to an exponential decrease in the electron concentration with altitude. /30

Detailed computations of the rates of photoionization, diffusion and recombination in the F region for the various atmospheric models were made by Rishbeth in Reference [86]. The author found that during daylight hours the relationship between the recombination and the diffusion terms in Equation (45) at the maximum of the F2 region varies, depending on the model used, from 0.76 to 3.5, thus indicating that the rates of electron loss due to diffusion and to recombination are near one another. This confirms the concept of the formation of a maximum of F2 distribution in the ionosphere due to a shift in the mechanisms which determine the distribution of charged particles. For nocturnal conditions Rishbeth found slightly lower values, on the order of 0.15 - 0.30, thus indicating an increase in the relative role of diffusion at night.

At the present time obviously we can assume that below 250 - 330 km (i.e. below the lowest altitude at which maximum concentration is observed) the behavior of the electron and ion concentrations is determined basically by photochemical processes. Therefore, the processes and the equations studied in this section pertain mainly to the region of the ionosphere below this altitude. Above the ionization maximum the distribution and behavior of the concentrations of charged particles are determined by laws of diffusion which are not dealt with in the present study.

f. Processes Involving Negative Ions. Below approximately 100 km in the ionosphere, due to the increase in density with decrease in altitude, the probability sharply increases for the formation of negative ions as a result of cohesion processes. Several such processes exist. Here we cannot describe them in detail but refer the reader to References [15, 51, 87]. Let us mention only that obviously the basic cohesion process under

the conditions of the upper atmosphere is the reaction



The rate constant α_{46} was investigated in the laboratory and was equal to $1.5 \cdot 10^{-30} \text{ cm}^6 \cdot \text{sec}^{-1}$ with $T = 300^\circ \text{ K}$.

The process of separation of the electron from the negative ion is called dissociation. Dissociation processes under the influence of radiation (photodissociation) play a basic role in the atmosphere:



and in the case of collision of a negative ion with a neutral particle:



Photodissociation from O_2^- ions was investigated in the laboratory [88], and the value of the coefficient of photodissociation ρ was found to equal 0.44 sec^{-1} . However, at the present time, this value is acknowledged as too high, and values of $0.1 - 0.2 \text{ sec}^{-1}$ are used for ρ . According to the laboratory experiments of Phelps and Pack [89], process (48) has a rate constant $\alpha_{48} = 4 \cdot 10^{-20} \text{ cm}^3 \cdot \text{sec}^{-1}$ for O_2^- ions when $T \approx 300^\circ \text{ K}$, O_2 molecules acting most effectively as the M particle. However, observations of the diurnal variation in absorption at the polar cap showed that dissociation in the nocturnal D region of the ionosphere takes place at a rate constant equal to $2 \cdot 10^{-17} \text{ cm}^3 \cdot \text{sec}^{-1}$. If O_2^- is the basic negative ion at the altitudes of the D region, then these latter two figures contradict one another. There are indications however, that the predominant role below 100 km is played not by O_2^- but rather by another ion with a high electron affinity on the order of 3 - 4 eV. The nature of this ion has yet to be established precisely; it is assumed that it may be NO_2^- or O_3^- . The formation of significant concentrations of negative ions of minor impurities (such

as NO_2 and O_3) as a result of direct cohesion is only slightly probable. /31
 The most probable means of their formation must be ion-molecular reactions of the type



Processes (49) and (51) have been investigated in the laboratory [90,91], and high rate constants were obtained for them on the order of $10^{-10} - 10^{-11} \text{ cm}^3 \cdot \text{sec}^{-1}$.

Loss of negative ions may take place also as a result of the mutual neutralization by positive ions which happens both with two-body collisions



and with triple collisions:



The laboratory investigations of these processes are rather limited and for the present give only the order of magnitude of the rate constants:

$$\alpha_{52} \approx 10^{-7} - 10^{-8} \text{ cm}^3 \cdot \text{sec}^{-1} \quad \alpha_{53} \approx 10^{-10} \text{ cm}^6 \cdot \text{sec}^{-1} \quad (54)$$

In the presence of a significant amount of negative ions the equation of ionization balance takes the form:

$$\frac{q}{(1+\lambda)} = (\alpha^* + \lambda \alpha_{\text{mut}}) [e]^2, \quad (55)$$

Here α_{mut} is the rate constant of mutual neutralization and $\lambda = [X^-]/[e]$ is the ratio of the concentration of negative ions to the concentration of electrons. The sum $(\alpha^* + \lambda\alpha_{\text{mut}}) = \alpha'$ acts as the effective coefficient of recombination in this case. The quantity λ is the most important, and at the same time the least known parameter of the lower ionosphere. The question of the altitude at which λ is equal to 1 (i.e. the level above which the negative ions can be ignored in describing the ionospheric processes), has as yet not been answered. Theoretical computations of λ involve difficulties in identifying the basic negative ion in the D region as well as uncertainty in knowledge of the constants of a number of processes. Attempts to estimate the number of negative ions by comparing the measured concentrations of electrons and positive ions involve problems of an experimental nature. Comparison of all data available today brings the author to the conclusion that the value of λ is equal to 1 at an altitude of 80 - 85 km; below this level the negative ions predominate over the electrons.

It should be emphasized that the problem of the chemistry of charged particles in the lower ionosphere at the present time is in a confused state. Besides the problems and contradictions associated with negative ions it is still necessary to explain the large number of ion bunches with the participation of molecules of water and hydroxyl ($(\text{H}_2\text{O})\text{H}^+$, $\text{H}(\text{H}_2\text{O})_2^+$, $\text{H}(\text{H}_2\text{O})_3^+$. . .), registered in the mass-spectrometric experiments of Narcisi [92]. The predominant role of such ions contradicts the previously existing concept as to the ionization mechanisms of the D region, according to which the basic positive ions must be NO^+ , O_2^+ and N_2^+ ions.

PROCESSES INVOLVING NEUTRAL PARTICLES IN THE IONOSPHERE

/32

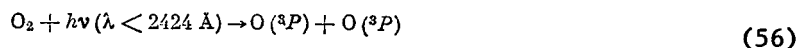
The close connection between neutral and charged particles in the Earth's ionosphere is presently becoming increasingly obvious. On the one hand, the formation and destruction of charged particles are directly connected with the neutral components of the atmosphere. The formation of atomic

and molecular ions, having completely different coefficients of recombination, depends at a given altitude first of all on the relationship between concentrations of atomic and molecular particles. The effectiveness of ion-molecular reactions, which play a very large role in the ionization-recombination cycle of the processes, is closely connected with the concentrations of neutral molecules. Ionization at altitudes of 70 - 80 km is caused apparently by the interaction of radiation in the Lyman - α line with NO molecules. The "minor components" of the atmosphere, NO_2 and O_3 may play an important role in the formation of negative ions in the lower ionosphere. All this indicates that a detailed investigation is essential for the processes which determine the behavior of the neutral components (both basic and "minor impurities") for a deep penetration into the chemistry of the charged particles in the ionosphere: dissociation of oxygen and nitrogen, formation of ozone, the reaction cycle involving nitric oxides, etc. On the other hand, an inverse relationship also exists between the processes involving neutral and charged components in the atmosphere. Thus, the formation of neutral atoms of nitrogen takes place basically as a result of ion-molecular reactions and dissociative recombination; above approximately 180 km the ion-molecular reactions make a substantial contribution to the dissociation of O_2 , etc.

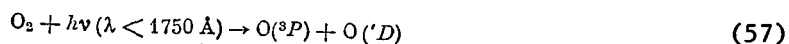
In the present section we are of course in no position to give a detailed survey of the research; therefore we shall confine ourselves only to enumeration of the major problems and the basic results attained.

a. Dissociation of Oxygen. Up to altitudes on the order of 100 km, oxygen in the Earth's atmosphere is found basically in a molecular state. The concentrations of O atoms comprise only a fraction of a percent of the overall concentration of particles. However, this small amount of oxygen atoms plays a major role in atmospheric chemistry, by leading to a whole cycle of processes involving ozone and nitric oxides. Let us look briefly at the basic reactions involving O atoms and O_3 molecules.

The destruction (dissociation) of O_2 molecules under the influence of solar radiation takes place in two spectral ranges:



(the so-called Hertzberg continuum) and



(the Schumann-Runge continuum). Since the cross section of radiation absorption by molecular oxygen in both continua is sharply different (for $\lambda = 2424 \text{ \AA}$ it comprises, for example, 10^{-24} cm^2 ; for $\lambda = 1750 \text{ \AA}$, 10^{-19} cm^2), there will also be a difference in depth of penetration of the radiation into the atmosphere in each of these spectral ranges, and consequently in the relative role of the Hertzberg and Schumann-Runge continua as well at various altitudes.

The oxygen atoms which form as a result of the photodissociation of O_2 must recombine among themselves, thus leading to an inverse process, i.e., the formation of oxygen molecules. Association of atoms is possible during triple collisions when the energy surplus released during formation of O_2 is removed by the third body M



and the radiative association which leads to radiation of the energy surplus,



Furthermore, the O atoms formed as a result of (56) and (57) may interact with the oxygen molecules following the reaction



which leads to the formation of ozone. This latter in turn may dissociate under the influence of solar radiation:



or interact with the atomic oxygen



Processes (56) - (62) determine the distribution of concentrations of atomic oxygen at altitudes below 100 km. Above 100 km it is necessary to study the role of the vertical diffusion of atoms and molecules of oxygen which becomes the basic process controlling the distribution of O and O₂ concentrations. Furthermore, in the E and F1 regions of the ionosphere the formation of atomic oxygen as a result of dissociative recombination of molecular O₂⁺ ions must be added to the formation of atoms as a result of direct photodissociation.

The rates of processes (56) - (62) have been measured in the laboratory and are known with sufficient reliability. One exception only is the reaction of radiative association (59), for which until recently no reliable determinations had been made of the quantity α . At the present time, ionospheric evaluations show that the magnitude of α must amount to several times units $10^{-17} \text{ cm}^3 \cdot \text{sec}^{-1}$ [15,93].

At altitudes less than 100 km, where processes (56) - (62) determine the behavior of the concentrations of atomic oxygen and ozone, the following equations are valid for the variation rates of O₂, O and O₃:

$$\frac{d[O_2]}{dt} = -\{[O_2]/O_2 + \alpha_6 [O] [O_2] [M]\} + \{\alpha_4 [O]^2 [M] + 2\alpha_8 [O] [O_3] + [O_3]/O_2 + [O]^2 \alpha_5\}, \quad (63)$$

$$\frac{d[O]}{dt} = -\{2\alpha_4 [O]^2 [M] + \alpha_6 [O_2] [O] [M] + \alpha_8 [O_3] [O] + 2\alpha_5 [O]^3\} + \\ + \{2[O_2] j_{O_2} + [O_3] j_{O_3}\}, \quad (64)$$

$$\frac{d[O_3]}{dt} = -\{[O_3] j_{O_3} + \alpha_8 [O] [O_3]\} + \alpha_6 [M] [O_2] [O]. \quad (65)$$

Under the conditions of photochemical equilibrium, the left-hand sides of equations (63) - (65) are equal to zero, and from (65) we can find the equilibrium ratio of concentrations

$$\frac{[O_3]}{[O]} = \frac{\alpha_6 [O_2] [M]}{j_{O_3} + [O] \alpha_8}. \quad (66)$$

Before we proceed to a discussion of the equilibrium conditions for concentrations of O and O₂, let us look at the effectiveness of the process of radiative association (59) and triple association (58):

$$\frac{\alpha_{58} [O]^2 [M]}{\alpha_{59} [O]^3} = [M] \frac{2.8 \cdot 10^{-22}}{\alpha_{59}} = [M] \cdot 3 \cdot 10^{-17} \quad (67)$$

As is clear from this relationship, with a value of $\alpha_{59} = 10^{-16} \text{ cm}^3 \cdot \text{sec}^{-1}$, process (59) becomes more effective than the reaction of triple collisions (58) above the level where $[M] = 3 \cdot 10^{16} \text{ cm}^{-3}$, i.e. above 50 km. Then /34 in the chemosphere we must assume reaction (59) to be the basic process of association of O into molecules. Since analysis of the rocket data on the distribution of concentrations of O and O₂ above 100 km leads to high values of $\alpha_{59} \approx 5 \cdot 10^{-7} \text{ cm}^3 \cdot \text{sec}^{-1}$ [93], we shall assume that in the chemosphere it is the reaction of radiative association (59) which predominates, and we can compare the rates of the other processes of annihilation of the atomic oxygen with the rate of this reaction:

$$\frac{2 [O]^2 \alpha_{59}}{[O] [O_2] [M] \alpha_{60}} = \frac{2 [O] \cdot 10^{-17}}{[O_2] [M] \cdot 2 \cdot 10^{-34}} = \frac{[O]}{[O_2]} \frac{10^{17}}{[M]} \quad (68)$$

$$\frac{2 [O]^2 \alpha_{59}}{[O_3] [O] \alpha_{62}} = \frac{2 [O] \cdot 10^{-17}}{[O_3] \cdot 2 \cdot 10^{-14}} = \frac{[O]}{[O_3]} \cdot 10^{-3} . \quad (69)$$

Comparison of the rates of radiative association (59) and triple reaction (60) shows (68) that process (60) can never be ignored in the entire chemosphere. At altitudes on the order of 70 km, expression (68) for $\alpha_{59} = 10^{-17} \text{ cm}^3 \cdot \text{sec}^{-1}$ becomes equal to 1, and below this level the rate of loss of the O atoms according to reaction (60) becomes greater than the rate of radiative association (59). It is necessary, however, to remember that reaction (60) will actually lead to association of atomic oxygen into molecular only if practically all the ozone forming as a result of this reaction then recombines with the atomic oxygen according to reaction (62), thus yielding two O_2 molecules. Since in an atmosphere irradiated by the sun this is not so:

$$\frac{[O_3] \dot{O}_3}{[O_3] [O] \alpha_{62}} = \frac{10^{-2}}{[O] \cdot 2 \cdot 10^{-14}} = \frac{5 \cdot 10^{11}}{[O]} \gg 1, \quad (70)$$

process (60) introduces a contribution to the association of O atoms into molecules only after sunset.

Comparison of the rates of O atom losses according to reactions (59) and (62) [equation (69)] shows that under nocturnal conditions when the concentrations of ozone are comparable in order of magnitude to the concentrations of atomic oxygen, the rate of interaction of O_3 and O is higher than the radiative association. During daylight hours when the concentrations of ozone at these altitudes are less than the value of [O], reaction (59) predominates over reaction (62) above approximately 75 km.

Thus, the balanced conditions for O during the day at altitudes greater than 75 km are written in the form

$$[O_2]/i_{O_2} = \alpha_{60} [O]^2. \quad (71)$$

This same equation is valid, as is easy to see, also for balanced daylight values of $[O_2]$, since we can ignore the corresponding slower terms in equation (63).

During the night, when $j_{O_3} = 0$, equation (66) is transformed into the equation

$$[O_3] = \alpha_{60}/\alpha_{62} [O_2] [M], \quad (72)$$

which permits us to obtain the distribution of O_3 concentration with the known ratio of constants α_{60}/α_{62} . Table 14 gives an example of such a computation for the value $\alpha_{60}/\alpha_{62} = 2.5 \cdot 10^{-20} \text{ cm}^3$, obtained experimentally [94]. As is clear from Table 14 the nocturnal concentrations of ozone increase rapidly with decrease in altitude, reaching at the boundary of the chemosphere (H \approx 60 km) values of $10^{11} - 10^{12} \text{ cm}^{-3}$.

During daylight hours, as is clear from expression (70), the rate of dissociation of ozone is determined by photodissociation; therefore (66) may be rewritten in the form

$$[O_3] = \frac{\alpha_{60} [O] [O_2] [M]}{i_{O_3}}. \quad (73)$$

As is obvious from this equation, the daylight values of the O_3 concentration depend on the concentrations of atomic oxygen. For a rough evaluation of the order of magnitude of the daylight concentrations of ozone let us assume that the quantity $[O]$ at altitudes of 70 - 100 km is constant and equal to approximately 10^{11} cm^{-3} . In this case when $j_{O_3} = 10^{-2} \text{ sec}^{-1}$ and $\alpha_{60} =$

TABLE 14				
H, km	M	O ₂	O ₃ (Night)	O ₃ (Day)
60	7.2·10 ¹⁵	1.5·10 ¹³	2.5·10 ¹¹	3.4·10 ⁹
70	2.0·10 ¹⁵	4.0·10 ¹⁴	2.0·10 ¹⁰	4.3·10 ⁸
80	4.2·10 ¹⁴	9.0·10 ¹³	9.5·10 ⁸	1.0·10 ⁸
90	7.5·10 ¹³	1.6·10 ¹³	3.0·10 ⁷	—
100	1.3·10 ¹³	2.9·10 ¹²	9.4·10 ⁶	—

$2 \cdot 10^{-34} \text{ cm}^6 \cdot \text{sec}^{-1}$ we have $[O_2] = 2 \cdot 10^{-21} [O_2] [M]$, (74)

If we compare this expression with (72) we find that the daylight concentration ^{/35} of ozone must be at least one order less than the nocturnal concentration. Since below 70 - 80 km the values of [O] are less than the assumed value of 10^{11} cm^{-3} , and since the nocturnal concentrations of ozone do not depend on the quantity [O], at these altitudes the difference between the day and night concentrations of O₃ must be greater. However, we must bear in mind that because of absorption in the atmosphere the value of j_{O_3} will decrease with altitude and beginning from altitudes on the order of 60 km this must be taken into account in evaluating the balanced O₃ concentrations during the day.

Table 14 gives the daytime concentrations of O₃ obtained as a result of averaging the values of [O₃] in rocket experiments. As is obvious from comparing the last two columns of this table, at altitudes of 100 - 80 km the nighttime values of [O₃] are approximately one order higher than the daylight values, just as theory predicted. Below approximately 70 km the difference in the day and night O₃ concentrations, for the reasons given above, is increased slightly. If we assume that process (59) is the basic process for the loss of O, we can carry out quantitative evaluations of the equilibrium values of O during the day.

$$[O]^e = \frac{j_{O_2} [O_2]}{\alpha_5} \quad (75)$$

Table 15 gives the computation for the equilibrium values of [O] on the basis of the dissociation rates j_{O_2} , taken with regard to the absorption of radiation in the atmosphere, and the value $\alpha_{49} = 10^{-16} \text{ cm}^3 \cdot \text{sec}^{-1}$.

TABLE 15				
H, km	j_{O_2}	$[O_2]$	$v_{diss} = [O_2]j_{O_2}$	$[O]$
70	$5 \cdot 10^{-10}$	$4,3 \cdot 10^{14}$	$2,1 \cdot 10^5$	$1,4 \cdot 10^{11}$
80	$1,5 \cdot 10^{-9}$	$9,0 \cdot 10^{13}$	$1,3 \cdot 10^6$	$1,2 \cdot 10^{11}$
90	$1,0 \cdot 10^{-8}$	$1,6 \cdot 10^{13}$	$1,6 \cdot 10^6$	$1,3 \cdot 10^{11}$
100	$5,9 \cdot 10^{-8}$	$2,9 \cdot 10^{12}$	$1,7 \cdot 10^6$	$1,3 \cdot 10^{11}$

Above 100 km the picture changes substantially. The lack of significant concentrations of ozone above 90 - 100 km permits us to exclude processes involving O_3 from our study of the upper atmosphere. At the same time the increase in ionization rate of the atmospheric components by ultraviolet solar radiation leads to the appearance of a new source of dissociation of molecular oxygen, i.e. the dissociative recombination of O_2^+ ions which may be found to be comparable in intensity to the decay rate of O_2 molecules as a result of photodissociation. On the other hand, the diffusion rate, which increases with altitude, poses the question concerning the maximal altitude above which it is no longer possible to assume satisfaction of the conditions of photochemical equilibrium, and it is necessary to study the diffusion equilibrium.

/36

The question as to the altitude at which the rates of the photochemical and diffusion processes with participation of O and O_2 become comparable has been repeatedly discussed in the literature. Nicolet and Mange [95], assuming that the basic mechanism of association of O atoms into the O_2 molecule is the reaction of triple collisions (58), concluded that diffusion plays the predominant role beginning from the level $H = 100$ km. At the present time, as shown above, there is a basis for assuming the basic mechanism of oxygen atom loss to be reaction (59) with a rate constant on the order of $10^{-17} \text{ cm}^3 \cdot \text{sec}^{-1}$. In this case the rates of the photochemical and diffusion processes become comparable at somewhat greater altitudes than found by Nicolet and Mange [95]. According to B.A. Mirtov [93], the level where the

rates of both processes become equal lies at an altitude on the order of 140 km. The evaluations of the author [15] give a somewhat smaller value: $H = 120 - 125$ km. In any case there is no doubt that at least above 140 - 150 km the concentration distribution of both atomic and molecular oxygen is controlled by the processes of vertical diffusion and obeys barometric law.

Now let us look at the role of the processes involving charged particles in the dissociation of molecular oxygen. The reaction of the dissociative recombination of O_2^+ ions:



just as the dissociation in the Schumann-Runge continuum leads to the formation of two O atoms in states 3P and 1D . The data available at the present time permit us to directly evaluate the rate of process (76) at the altitudes under study in the ionosphere; however, for purposes of clarity it is better to estimate the dissociation of molecular oxygen due to ionospheric processes in the following manner. Process (76) compensates, under equilibrium conditions, the formation of O_2^+ ions which takes place as a result of the direct ionization of O_2 molecules:



and as a result of ion-molecular reaction (19). The overall rate of formation of O_2^+ , equal to the loss rate of these ions according to reaction (76) and correspondingly to the rate of formation of O due to ionospheric processes, thus comprises.

$$V_{O_2}^I = [O_2] I_{O_2} + [O_2] [O^+] \alpha_{19} = [O_2] (I_{O_2} + [O^+] \alpha_{19}) \quad (78)$$

The quantity $(I_{O_2} + [O^+] \alpha_{19})$, which is the factor preceding $[O_2]$, may be

TABLE 16

/37

H, km	100	120	140	160	180	200
j_{O_2} , sec ⁻¹	$5 \cdot 10^{-7}$	$2.5 \cdot 10^{-6}$	$4.2 \cdot 10^{-6}$	$6 \cdot 10^{-6}$	$6 \cdot 10^{-6}$	$6 \cdot 10^{-6}$
$j_{O_2}^i$, sec ⁻¹	$9 \cdot 10^{-10}$	$1.4 \cdot 10^{-7}$	$8.4 \cdot 10^{-7}$	$2.0 \cdot 10^{-6}$	$4.5 \cdot 10^{-6}$	$5.3 \cdot 10^{-6}$

assumed as the effective coefficient of dissociation of molecular oxygen due to the ion reactions $j_{O_2}^i$.

Table 16 gives the values of $j_{O_2}^i$, computed on the basis of experimental data on the ionization rate of various components of the atmosphere, cited by Hinteregger et al. in [22].

The coefficients of direct photodissociation of molecular oxygen j_{O_2} , obtained in this same work [22], are given for comparison. As follows from the table, at altitudes below 140 km the ion reactions make a small contribution to the overall dissociation rate of molecular oxygen. At higher altitudes however the conversion of O_2 molecules into atoms takes place with identical intensity both as a result of direct photodissociation and as a result of ion reactions.

b. Dissociation of Nitrogen and the Processes Involving Nitric Oxides

The problem of dissociation of molecular nitrogen in the upper atmosphere is immeasurably more complex than the analogous problem for O_2 . Back in the 1930's Chapman gave a basically correct picture of the conversion from molecular oxygen to atomic oxygen at altitudes near 100 km, although the question of the formation and loss of atomic nitrogen in the upper atmosphere has been explained somewhat only in the past few years.

Until fairly recent times the very existence of atomic nitrogen in the atmosphere was under serious doubt. However, at the present time there does exist definite proof of the existence of N atoms in the upper layers of the atmosphere. Involved in this proof is the observation of radiation from emissions of atomic nitrogen (for example, 5200 \AA , 3466 \AA and 10.400 \AA) in the spectra of the nocturnal sky and the aurora, detection of N^+ ions in mass-spectrometric experiments, radiation observed from nitric oxide during rocket launches and that which takes place as a result of the interaction of NO and N, and other experimental facts.

Although we can no longer doubt the existence of significant concentrations of atomic nitrogen in the upper atmosphere, we are virtually ignorant of the precise amounts of the concentrations and their distribution with altitude. The mass-spectrometric and optical research presently available on the neutral composition of the atmosphere permit us only to obtain the upper limit of the amount of N in the range from 100 to 200 km: $[N] \leq 10^7 - 10^8 \text{ cm}^{-3}$. The theoretical computations available in the past involved considerable uncertainty since many factors that were necessary for determining the magnitude of $[N]$ were unknown and sometimes strongly contradicted one another. The existence of contradictory computations for the magnitudes of $[N]$ can be explained by the fact that for a long period of time no unified viewpoint existed as to the role of the various processes involved in the formation and loss of atomic nitrogen in the upper atmosphere.

At the present time it is generally accepted that direct dissociation of the N_2 molecule under the influence of solar radiation



is only a slightly effective process ($j_{N_2} \approx 10^{-12} \text{ sec}^{-1}$), and the basic source for the formation of N atoms in the upper atmosphere involves the processes of dissociative recombination of NO^+ and N_2^+ ions and ion-

molecular reaction (18). Thus, the overall rate of formation of N atoms due to the ion reactions may be written in the form

$$V_{\text{form}}^{\text{N}} = 2V_6 + V_4 + V_{18}. \quad (80)$$

Since processes (4) and (18) in the major part of the ionosphere are in equilibrium, $V_4 = V_{18}$ is valid. We can therefore rewrite (80) in the form

$$V_{\text{form}}^{\text{N}} = 2V_6 + 2V_4 = 2[e](\alpha_{\text{NO}^+}^* [\text{NO}^+] + \alpha_{\text{N}_2^+}^* [\text{N}_2^+]). \quad (81)$$

The relative role of the two recombination terms in the right-hand side of (81) may be different at different levels in the atmosphere. Thus, at altitudes on the order of 300 km, where the N_2^+ concentration is only slightly less than the NO^+ concentrations, the rate of formation of N according to reaction (6) may be of the same order or even greater than according to reaction (4). At the same time in the range 100 - 200 km, where $[\text{N}_2^+] < 10^{-2} [\text{NO}^+]$, the formation of N as a result of the dissociative recombination of N_2^+ ions can be ignored. With these computations it is assumed that the ratio of the constants $\alpha_{\text{N}_2^+}^* / \alpha_{\text{NO}^+}^*$ is equal to approximately 10.

In an oxygen-nitrogen mixture, which comprises the Earth's atmosphere, an interaction between the oxygen and nitrogen particles must of necessity take place, thus leading to the formation of "mixed" products, i.e., various nitrogen oxides. These latter in turn by possessing a high chemical activity will lead to the entire cycle of reactions with atomic and molecular oxygen, atomic nitrogen, etc. This entire group of such processes is often called the chemistry of the nitrogen-oxygen atmosphere.

Molecular nitrogen, as we know, is an inert gas and combines very poorly even with oxygen. Therefore, the effective formation of oxygen-nitrogen compounds and the further development of the reaction cycle involving nitric oxides is possible only in those regions of the atmosphere where atomic

nitrogen exists that is significantly more active than the N_2 . In the atmosphere above approximately 50 - 60 km, pronounced concentrations of nitrogen atoms exist produced by the dissociation of N_2 as a result of the various ion reactions. Thus, above 50 - 60 km in the Earth's atmosphere, the processes of formation of nitric oxides begin to actively function and as a result the rapid processes involving these oxides as well. The atmospheric range from 50 - 60 km up to approximately 160 km (above this level diffusion begins to predominate over the chemical processes), where the basic processes of the oxygen-nitrogen cycle also take place as well as the ozone-oxygen reactions and reactions of hydrogen compounds, is often called the "chemosphere".

The reactions which take place in a nitrogen-oxygen mixture and which lead to the formation and annihilation of the nitric oxides, are the basic mechanism for loss of nitrogen atoms in the atmosphere since the radiative association



similar to reaction (59), has a very low effectiveness ($\alpha_{82} \approx 10^{-20} \text{ cm}^3 \cdot \text{sec}^{-1}$). Without stopping for a detailed analysis of the entire nitrogen-oxygen reaction cycle and its effectiveness (we refer the reader to the survey papers [15, 96]), let us look first only at the major processes involved in the loss of atomic nitrogen. These are:



However, since in the major part of the ionosphere the ozone concentrations are small, process (85) makes little contribution to the N loss, and the

conditions of photochemical equilibrium for N are written in the form

$$2 [e] (\alpha_{NO}^* [NO^+] + \alpha_{N_2}^* [N_2^+]) = [N] [O_2] \alpha_{83} + [N] [NO] \alpha_{84}. \quad (86)$$

The author's computations made using this equation for [N] led in [15] to the value $[N] \sim 10^6 \text{ cm}^{-3}$ for $H = 100 - 160 \text{ km}$. This value of [N] is lower than the limit of sensitivity of the apparatus in the optical mass-spectrometric investigations of the composition, which give a figure of $[N] \leq 10^7 - 10^8 \text{ cm}^{-3}$, and therefore does not contradict the experimental data.

/39

The presence of nitrogen atoms in the atmosphere, as noted above, produces the formation of nitric oxide as a result of a series of reactions, the major ones of which are (83) and (85).

The nitric oxide molecules forming as a result of processes (83) and (85) will actively participate in reactions with O_3 molecules and with atoms of nitrogen and oxygen:



The NO_2 molecules forming as a result of reactions (87) - (89) will in turn react with the atomic oxygen and atomic nitrogen:



In the lower part of the chemosphere where ozone exists, the dissociation of NO_2 will also take place as a result of the reaction



The rate constants of the processes given above have been studied quite well in the laboratory (see [15, 96]). Knowledge of the rates of the

processes permits us to study their role at various levels in the atmosphere and to obtain equilibrium equations for the concentrations of nitric oxides.

The equations for photochemical equilibrium for $[\text{NO}_2]$ lead to the following relationship between the concentrations of NO and NO_2 :

$$\frac{[\text{NO}_2]}{[\text{NO}]} = \frac{[\text{O}] \alpha_{88} + [\text{O}_3] \alpha_{86}}{[\text{O}] \alpha_{89}} \quad (93)$$

Above approximately 90 km the second term in the numerator of (93) can be ignored because of the smallness of the magnitude of $[\text{O}_3]$, and the ratio $[\text{NO}_2]/[\text{NO}]$ becomes independent of $[\text{O}]$ and equal to $\alpha_{89}/\alpha_{90} \approx 10^{-4}$. Below approximately 70 km the formation of NO_2 is determined basically by process (87); therefore $[\text{NO}_2]/[\text{NO}]$ depends on the ratio $[\text{O}_3]/[\text{O}]$ and must vary strongly from day to night.

Study of the equilibrium conditions for $[\text{NO}]$ leads to the equation:

$$[\text{NO}] = \frac{[\text{O}_2] [\text{N}] \alpha_{83}}{I_{\text{NO}} + j_{\text{NO}} + [\text{N}] \alpha_{84}}, \quad (94)$$

where I_{NO} and j_{NO} are the coefficients of ionization and dissociation of the NO molecule, respectively. At altitudes above approximately 85 km where $[\text{N}]$ exceeds 10^5 cm^{-3} , process (84) becomes the basic mechanism of NO loss, and equation (93) is transformed into the expression

$$[\text{NO}] = \frac{\alpha_{83}}{\alpha_{84}} [\text{O}_2], \quad (95)$$

which indicates that $[\text{NO}]$ comprises a small fraction of the O_2 concentration, which depends only on temperature.

The question of the mechanisms which determine the concentrations of nitric oxide in the atmosphere however can never be ultimately resolved. In the recent optical experiments of Barth [97], NO concentrations were found at an altitude of 90 km comprising $4 \cdot 10^7 \text{ cm}^{-3}$ which exceeds the values of [NO] given by expression (5) by approximately two orders. Because of the great significance of nitric oxide for investigating ionization in the lower ionosphere, this question requires the most careful investigation. /40

REFERENCES

1. Bourdeau, R. E. Space Sci. Rev., No. 1, 1963, p. 683.
2. Bourdeau, R. E. et al. Kosmicheskiye Issledovaniya, No. 3, 1965, p. 42.
3. Ivanov-Kholodnyy, G. S. Geomagnetizm i Aeronomiya, No. 5, 1965, p. 417.
4. Gringauz, K. I. Geofizicheskiy Byulleten', No. 14, 1965, p. 110.
5. Hinteregger, H. E. Space Sci. Rev., No. 4, 1965, p. 461.
6. Tousey, R. Space Sci. Rev., No. 2, 1963, p. 3.
7. King-Hele, D. G. Space Res., No. 5, 1965, p. 1132.
8. Jacchia, L. Space Res., No. 5, 1965, p. 1152.
9. Mikhnevich, V. V. Iskusstvennyye Sputniki Zemli, No. 17, 1963, p. 31.
Also see this collection p. 70*.
10. Newton, P. Symposium D'Aeronomie, Paris, No. 4, 1966.
11. Danilov, A. D. Kosmicheskiye Issledovaniya, No. 4, 1966, p. 47.
12. Pokhunkov, A. A. Doklad na Konferentsii po Aeronomii, (Report on the Conference on Aeronomy), Boston, 1965.
13. Near, A. O. Symposium D'Aeronomie, Paris, No. 4, 1966.
14. Ivanov-Kholodnyy, G. S. and A. D. Danilov. Kosmicheskiye Issledovaniya, No. 4, 1966, p. 439.
15. Danilov, A. D. Khimiya Ionosfery, (Chemistry of the Ionosphere), State Scientific and Technical Hydrometeorological Publishing House (Gidrometeoizdat), Leningrad, 1967.
16. Nicolet, M. Aeronomiya (Aeronomy), Mir Press, 1964.
17. Kallman-Bijl, H. K. and W. Sibley. Planet. Space Sci., No. 11, 1963, p. 1379.
18. Pokhunkov, A. A. Iskusstvennyye Sputniki Zemli, No. 7, 1961, p. 89.
19. Pokhunkov, A. A. Iskusstvennyye Sputniki Zemli, No. 13, 1962, p. 110.

*Translator's Note: Material will be found on p. 114 of English translation.

20. Hinteregger, H. E. J. Atm. Sci., No. 19, 1962, p. 351.
21. Pokhunkov, A. A. Kosmicheskiye Issledovaniya, No. 1, 1963, p. 148.
22. Hinteregger, H. E. et al. Space Res., No. 5, 1965, p. 1175.
23. Near, A. O. et al. J. Geophys. Res., No. 69, 1964, p. 979.
24. Hall, L. A. et al. J. Geophys. Res., No. 68, 1963, p. 6913.
25. Blamont, J. E. and H. L. Chanin-Lory. Space Res., No. 5, 1965, p. 1137.
26. Spencer, N. W. et al. Doklad na 5 Simpoziume KOSPAR (Report on the Fifth Symposium of COSPAR), 1964.
27. Reber, C. and M. Nicolet. Planet. Space Sci., No. 13, 1965, p. 617.
28. Reber, C. et al. J. Geophys. Res., No. 69, 1964, p. 4681.
29. Kazachevskaya, T. V. and G. S. Ivanov-Kholodnyy. Geomagnetizm i Aeronomiya, No. 5, 1965, p. 1009.
30. Brace, L. H. et al. Doklad na V Simpoziume KOSPAR (Report on the Fifth Symposium of COSPAR), 1964.
31. Sagalin, R. C. and M. Smiddy. Space Res., No. 4, 1964, p. 371.
32. Smith, L. Progress Report, NASA-98, Geophys. Corp. Amer., 1961.
See also the Collection: Distribution of Electron Concentration in the Ionosphere, Mir Press, 1964.
33. Johnson, C. Y. et al. Ann. Geophys., No. 14, 1958, p. 475. /41
34. Narcisi, R. S. and A. D. Bailey. Space Res., No. 5, 1965, p. 753.
35. Narcisi, R. S. and A. D. Bailey. J. Geophys. Res., No. 70, 1965, p. 3687.
36. Narcisi, R. S. Symposium D'Aeronomie, Paris, No. 4, 1966.
37. Istomin, V. G. Iskusstvennyye Sputniki Zemli, No. 4, 1960, p. 171.
38. Istomin, V. G. Doklady AN SSSR, No. 129, 1959, p. 81
39. Istomin, V. G. Iskusstvennyye Sputniki Zemli, No. 7, 1961, p. 64.

40. Istomin, V. G. Sb: Issledovaniya Kosmicheskogo Prostranstva (Collection: Investigations in Outer Space), Nauka Press, 1965.
41. Friedman, H. Space Science, 1963, p. 549.
42. Detwiler, C. R. Ann. Geophys., No. 17, 1961, p. 9.
43. Ivanov-Kholodnyy, G. S. Geomagnetizm i Aeronomiya, No. 6, 1966, p. 382.
44. Ivanov-Kholodnyy, G. S. Doklady AN SSSR, No. 170, 1966, p. 831.
45. Chapman, S. Proc. Phys. Soc., No. 43, 1931, p. 433.
46. Biondi, M. Adv. Electronics and Electron Phys., No. 18, 1963, p. 67.
47. Bates, D. R. Planet. Space Sci., No. 9, 1962, p. 78.
48. Massey, H. S. and E. H. S. Burhop. Electronic and Ionic Impact Phenomena, New York - London, 1962.
49. Biondi, M. A. Chemical Reactions in Lower and Upper Atmosphere, Interscience, New York - London, 1961.
50. Biondi, M. A. Ann. Geophys., No. 20, 1964, p. 34.
51. Whitten, R. C. and I. G. Popoff. J. Atm. Sci., No. 21, 1964, p. 117.
52. McDaniel, E. W. Collision Phenomena in Ionized Gases, New York - London, 1964.
53. Stein, R. P. et al. Phys. Fluids, No. 7, 1964, p. 1641.
54. Mentzoni, M. H. J. Geophys. Res., No. 68, 1963, p. 4181.
55. Danilov, A. D. and G. S. Ivanov-Kholodnyy. Uspekhi Fizicheskikh Nauk (UFN), No. 85, 1965, p. 2569.
56. Ivanov-Kholodnyy, G. S. Geomagnetizm i Aeronomiya, Vol. 7, No. 1, 1967.
57. Weissler, J. L. J.O.S.A., No. 49, 1959, p. 4.
58. Weissler, J. L. et al. J.O.S.A., No. 49, 1960, p. 342.
59. Ivanov-Kholodnyy, G. S. Geomagnetizm i Aeronomiya, No. 2, 1962, p. 674.
60. Danilov, A. D. Iskusstvennyye Sputniki Zemli, No. 17, 1963, p. 19.

61. Danilov, A. D. Doklady AN SSSR, No. 169, 1966, p. 332.
62. Potter, R. F. J. Chem. Phys., No. 23, 1955, p. 2462.
63. Dickinson, P. H. D. and J. Sayers. Proc. Phys. Soc., No. 76, 1960, p. 137.
64. Talrose, V. L. et al. Disk. Far. Soc., No. 33, 1962, p. 257.
65. Langstroth, G. F. O. and J. Hasted. Disk. Far. Soc., No. 33, 1962, p. 298.
66. Fite, W. L. et al. Disk. Far. Soc., No. 33, 1962, p. 246.
67. Gall, A. et al. J. Chem. Phys., No. 39, 1963, p. 518.
68. Sayers, J. and D. Smith. Disk. Far. Soc., No. 37, 1964, p. 167.
69. Paulson, J. Ann. Geophys., No. 20, 1964, p. 75.
70. Paulson, J. F. et al. Proc. Nat. Acad. Sci. (India), No. A33, 1963, p. 522.
71. Fehsenfeld, F. C. et al. Planet. Space Sci., No. 13, 1965, p. 219.
72. Fehsenfeld, F. C. et al. Planet. Space Sci., No. 13, 1965, p. 579.
73. Bates, D. R. and M. Nicolet. J. Atm. Terr. Phys., No. 21, 1961, p. 286.
74. Harteck, P. and R. Reeves. Chem. Reaction in Lower and Upper Atmosphere, New York - London, 1961.
75. Norton, R. B. et al. Proc. Int. Conf. Ionosph., London, 1963.
76. Danilov, A. D. Kosmicheskiye Issledovaniya, No. 2, 1964, p. 856.
77. Nisbet, J. S. and T. P. Quinn. J. Geophys. Res., No. 70, 1965, p. 113.
78. Sagalin, R. C. and M. J. Smiddy. J. Geophys. Res., No. 69, 1964, p. 1809.
79. Danilov, A. D. and S. P. Yatsenko. Kosmicheskiye Issledovaniya, No. 2 1964, p. 276.
80. Ferguson, E. E. et al. J. Geophys. Res., No. 70, 1965, p. 4323.
81. Harteck, P. Disk. Far. Soc., No. 37, 1964, p. 224.

82. McGill, L. R. et al. Trans. Amer. Geophys. Union, No. 48, 1967, p. 65.
83. Ratcliffe, J. A. and K. Weeks. Physics of the Upper Atmosphere, Acad. Press, New York - London, 1960.
84. Ratcliffe, J. A. et al. Philos. Trans. Roy. Soc., No. A248, 1956, p. 621.
85. Yonezawa, T. Radio Res. Labor., No. 2, 1955, p. 281.
86. Rishbeth, H. J. Atm. Terr. Phys., No. 26, 1964, p. 657.
87. Branscomb, L. M. Khimicheskiye Protsessy v Zemnoy Ionosfere (Chemical Processes in the Earth's Ionosphere), Mir Press, 1968.
88. Branscomb, L. M. et al. Phys. Rev., No. 111, 1958, p. 504.
89. Phelps, A. V. and J. L. Pack. Phys. Rev. Letters, No. 6, 1961, p. 111.
90. Curren, R. K. Phys. Rev., No. 125, 1962, p. 910.
91. Fehsenfeld, F. C. et al. Planet Space Sci., No. 15, 1967, p. 373.
92. Narcisi, R. S. Symposium D'Aeronomie, Paris, No. 4, 1966.
93. Mirtov, B. A. Geomagnetizm i Aeronomiya, No. 6, 1966, p. 284.
94. Fuchen, A. and F. Patat. Z. Phys. Chem., No. 33, 1936, p. 459.
95. Nicolet, M. and P. Mange. J. Geophys. Res., No. 59, 1954, p. 15.
96. Shiff, I. G. Symposium D'Aeronomie, Paris, No. 2, 1964.
97. Barth, C. A. Space Res., No. 5, 1965, p. 767.

AMBIPOLAR DIFFUSION OF ELECTRON-ION GAS AND STRATIFICATION OF THE F REGION OF THE IONOSPHERE

V. M. Polyakov

The transfer of charged particles by diffusion and drift is one of the most important physical processes in the ionosphere. The transfer processes are especially important in the F region where the free path of charged particles and their lifetime rapidly increase as the altitude increases.

The vertical distribution of electron concentration determined by the effect of the incident diffusion flux is very similar to that of Chapman's layer as far as its shape is concerned.

The sources responsible for the diffusion flux are ionization-recombination processes.

Due to the effect of the intensive sources of electron-ionic gas, the level of photochemical equilibrium and zero diffusion is located lower than the maximum of the layer.

In the F region of the ionosphere, two levels exist near which a maximum in electron density may form. If these two levels are close to each other, then only the F2 layer is observed, as happens in winter at middle latitudes. In summer, when the maximum ion production drops down as the zenith distance of the sun decreases, F1 and F2 layers can be observed as separate layers.

This article examines the behavior of the F region of the ionosphere under the influence of three competing processes: ionization, neutralization and diffusion of electron-ion gas. The relative role of these processes differs at different levels of the F region. Even now we can speak with confidence about the predominance of diffusion in the upper ionosphere (above the maximum of the F2 layer), whereas the electron balance in the lower part (at the level of the F1 layer) is determined basically by the ionization-recombination processes. In the middle part, at the level of the F2 layer,

/42

the time constants of the ionization-recombination processes and diffusion are found to be of the same order. This fact does not allow us to differentiate between the effects associated with variation of electron concentration due to diffusion and those associated with the ionization-recombination processes. Therefore, near the maximum of the F2 layer, the balance of the number of electrons is described by an equation which allows for all three of these factors. This equation is usually written in the form

$$dN/dt = q - L - \operatorname{div}(Nv) \quad (1)$$

where N is the electron concentration; q is the intensity of ion formation; L is the rate of neutralization; and v is the rate of the ordered transfer of the electron-ion gas due to diffusion.

For the ionosphere which is uniform in the horizontal direction, we can examine only the vertical transfers; therefore $\operatorname{div}(Nv) = \partial(Nv)/\partial h$, where h is the altitude calculated in a linear scale from the earth's surface.

An expression for the vertical rate of diffusion of the electron-ion gas contained in the planetary atmosphere (in the central field of gravity) in the presence of a constant magnetic field, was obtained by Ferraro in Reference [1] and then discussed in detail in [2]. This expression has the form

$$v = -\frac{D}{N} \left(\frac{\partial N}{\partial h} + \frac{N}{H_i} \right) \sin^2 I, \quad (2)$$

where D is the coefficient of ambipolar diffusion; $H_i = 2kT/m_i g$ is the altitude of the uniform atmosphere for the electron-ion gas and I is the magnetic inclination. If the concentration of neutral gas varies according to the law

$$n = n_0 \exp \left(- \int_{h_0}^h \frac{dh}{H_m} \right), \quad (3)$$

the coefficient of diffusion then varies with altitude according to the formula

$$D = D_0 \exp \left(\int_{h_0}^h \frac{dh}{H_m} \right) \quad (4)$$

The altitude of the uniform atmosphere for the neutral gas H_m , just as for H_i , may also vary with altitude. It is useful to introduce into computation the ratio $\delta = H_m/H_i$ which, as shown in Reference [3], varies with altitude very little and may be considered constant with an accuracy that is sufficient for further computations.

If we introduce the dimensionless coordinate

$$z = \int_{h_0}^h \frac{dh}{H_m}, \quad (5)$$

we can write equation (2) in the form

$$v = - \frac{d}{N} (N' + \delta N), \quad (6)$$

where $d = \frac{D}{H_m^2} \sin^2 I$ and $N' = \frac{\partial N}{\partial z}$.

Several investigations are known in which equation (1) has been solved for the simplest models of the ionosphere under stationary conditions [4 - 6] and which take account of time variations [7,8]. These investigations show that the results are very sensitive to the values of the parameters which determine the rates of ionization, recombination and diffusion. All these solutions have been obtained in the form of series computed by numerical integration.

From the results obtained in such form, it is difficult to establish the common rules determining the structure of the diffusion flux and con-

sequently to evaluate the role of diffusion in the formation of the F2 layer maximum. In this respect it is useful to study the simple stationary conditions in the hydrodynamic aspect in which the ionization-recombination processes are assumed to be sources of the diffusion flux. Several useful results may be obtained by studying diffusion in the region without sources, and the effects for weak sources of diffusion flux [3,9].

VERTICAL DISTRIBUTION OF ELECTRON-ION GAS IN THE REGION WITHOUT SOURCES [3]

In this case equation (1) takes the form

$$\partial P / \partial z = 0, \quad (7)$$

where $P = N_v$ is the density of the diffusion flux which for the sake of brevity we shall call simply diffusion in the following discussion. Equation (7) with allowance for (6) is equivalent to the equation

$$N'' + (\delta + 1)N' + \delta N = 0, \quad (8)$$

and its solution with $\delta = \text{const}$ will have the form

$$N = C_1 e^{-\delta z} + C_2 e^{-z}.$$

The constants C_1 and C_2 may be determined from the boundary conditions. With $z = 0$, if we assume $N = 0$, we obtain

$$C_1 = -C_2.$$

The expression for the diffusion flux P from (6) may be written in the /44
form

$$P = d(N' + \delta N). \quad (9)$$

From (7) it follows that, in the absence of sources, under stationary conditions the diffusion flux must be constant. One of the particular values satisfying (7),

$$P = 0,$$

leads to the equation

$$N' + \delta N = 0.$$

In this case the solution to (8) assumes a simple form:

$$N = N_0 e^{-\delta z}, \quad (10)$$

which corresponds to the altitude distribution of the electron-ion gas on the assumption of hydrostatic equilibrium.

The solution to equation (8) is of special interest when $P = \text{const} \neq 0$. Such a distribution will be called quasiequilibrium. It takes place in the ionosphere under the influence of a diffusion flux that is constant in magnitude and directed downward (if $|N''| < \delta N$). The solution in this case may be written in the form

$$N = C_1 (e^{-\delta z} - e^{-z}). \quad (11)$$

We can show that for any value of $C_1 \neq 0$, distribution (11) has a maximum at $z = z_m$. In fact, from the condition

$$\partial N / \partial z = 0$$

we find that

$$\delta e^{-\delta z_m} = e^{-z_m}. \quad (12)$$

Since the maximal value is

$$N_m = C_1 (e^{-\delta z_m} - e^{-z_m}),$$

then (11) can be written in the form

$$N = N_m \varphi(z), \quad (13)$$

where

$$\varphi(z) = \frac{C_1}{N_m} (e^{-\delta z} - e^{-z}). \quad (14)$$

It is easy to see that $\phi(z) = 0$ when $z = 0$ and has a maximum when $z = z_m$, and when $z > z_m$ it decreases monotonically. From (12) and bearing in mind that $\phi(z_m) = \phi(z_m) = 1$, we find

$$\frac{C_1}{N_m} = \frac{\delta}{1-\delta} e^{\delta z_m} = \frac{1}{1-\delta} e^{z_m}, \quad (15)$$

If we substitute the respective values of C_1/N_m from (15) into (14), we find ultimately for $\phi(z)$ the expression

$$\varphi(z) = \frac{1}{1-\delta} \left[e^{-\delta(z-z_m)} - \delta e^{-(z-z_m)} \right] \quad (16)$$

or

$$N = \frac{N_m}{1-\delta} \left[e^{-\delta(z-z_m)} - \delta e^{-(z-z_m)} \right]. \quad (17)$$

The altitude of the maximum is determined from equation (15), whence it follows that

$$z_m = \frac{1}{1-\delta} \ln \frac{1}{\delta}$$

and z_m is figured from the level $z = 0$.

The form of the altitude distribution, described by equation (16), is shown on Figure 1. It is clear from the figure that this distribution in the upper part is near a simple exponent with the index $(-\delta z)$, that it has a maximum and that below this maximum it drops rapidly, vanishing when $z = 0$. Here it is useful to mention the following. In the present case of a magnitude-constant diffusion flux, from equation (8) which can be conveniently rewritten in the form

$$\varphi'' + (\delta + 1')\varphi' + \delta\varphi = 0, \quad (18)$$

we can exclude the sources and drains of the diffusion flux. Therefore when $z < 0$ the quantity $\phi(z)$ assumes negative values, which follows inescapably from the equation of continuity. The region in which $\phi(z) < 0$ corresponds to the efflux of electron-ion gas.

The conditions described by equations (9) and (18) are realized practically nowhere in the ionosphere since the ionization-recombination processes exert an influence there constantly. However these results show that under the influence of pure diffusion in the gravity field, the vertical distribution of the gas may take the form of (17), which has a clearly expressed maximum. For the formation of such a distribution we must have a diffusion current that is directed downward which, as we shall see later on, agrees fully with the ionospheric conditions.

We can show that the distribution, similar to the Chapman distribution,

$$\varphi_1(z) = \exp \left[\gamma \left(1 - \frac{h}{H} - e^{-h/H} \right) \right] \quad (19)$$

will be near the nondivergent distribution described by Formula (16) [3] for several values of the parameters γ and H .

In fact, in the upper part of the layer for sufficiently large values

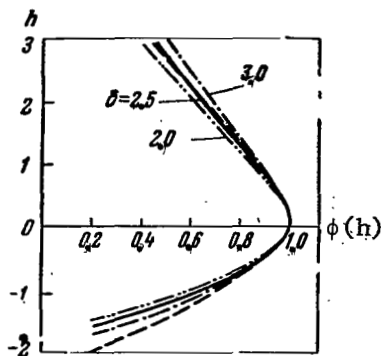


Figure 1. Comparison of the Vertical Distribution $\phi(h)$ for Various δ with Chapman Distribution (Broken Line).

of z and h/H formulas (16) and (19) are close to simple exponents.

If we equate the indices of these exponents we find the approximate relationship for the upper part of the F2 layer:

$$\delta z = \gamma \frac{h}{H},$$

and consequently:

$$H = \frac{\gamma}{\delta} H_m.$$

At the maximum of the layer, equation (18) takes the form

$$\varphi''(z_m) + \delta = 0, \quad (20)$$

and equation (19) will be the solution to this equation when $\gamma = \delta$ and $H = H_m$, which can be proved simply by direct substitution. Consequently, the Chapman distribution, described by formula (19), is near diffusion equilibrium when $\gamma = \delta$ and $H = H_m$ in the entire upper part, including the layer maximum.

/46

For illustration, Figure 1 shows comparison of the distribution described by formulas (16) and (19). The curves $\phi(z)$ are shown computed from formula (16) for three values of δ . The broken curve was plotted from formula (19) when $\gamma/\delta = 1$ and $\delta = 0.4$. It is clear from the graph that the broken curve is very near the solid one near the maximum in the upper part of the layer also. Pronounced divergences are observed only in the lower part when $z < -1$, i.e., where the diffusion ceases to be controlled by the spatial distribution of the electron-ion gas and where comparison of formulas (16) and (19) is of no interest.

STATIONARY DISTRIBUTION UNDER THE WEAK INFLUENCE OF SOURCES [9]

The vertical distribution of the electron concentration, which is determined by the joint effect of diffusion and ionization-recombination processes, will be described by the equation

$$N'' + (\delta + 1) N' + \delta N = \frac{1}{\alpha} [L(N, z) - p(z)]. \quad (21)$$

In equation (21), L is a function of N . If this function is linear, then (21) is reduced to the Bessel equation and its solution, with the assignment of parameters which determine the rates of ionization, neutralization and diffusion, may be obtained by numerical integration (see, for example, [4, 6]). The solution to (29) [sic] has not been analytically studied for a more complex dependence.

Let us look at the approximate solution to equation (21) for the case when the intensity of the diffusion flux sources is low. Under these conditions the function $\phi(z)$ will be only slightly distorted and in the region under study will have, as previously, one maximum. Then equation (21), on the basis of (13), can be rewritten:

$$\Psi'' + (\delta + 1) \Psi' + \delta \Psi = \frac{1}{\alpha N_m} [L(\Psi, z) - q(z)] \equiv \kappa(z), \quad (22)$$

where $\kappa(z)$ is the form-factor which determines the intensity of the sources. The form-factor κ is also a function of ϕ . However for weak sources this dependence can be ignored. Then, if we assume $\kappa(z)$ to be a known function of the coordinate z and if we ignore the dependence of κ on ϕ , we can write the solution to equation (21) in the form,

$$\varphi(z) = C_1 e^{-\delta z} + C_2 e^{-z} + \frac{1}{1-\delta} \left[e^{-\delta z} \int_c^z \kappa(z) e^{\delta z} dz - e^{-z} \int_c^z \kappa(z) e^z dz \right] \quad (23)$$

Let us assume, as previously, the lower boundary equation to be $\phi = 0$ when $z = 0$. Let us add the condition that $\kappa(z) = 0$ when $z \leq 0$. To avoid complicating computation of the integration constants, let us take the lower bound $c = -\infty$. Then when $z \leq 0$ the values of the integrals in the brackets vanish and as before

$$C_1 = -C_2,$$

whence

$$\varphi(z) = C_1 (e^{-\delta z} - e^{-z}) + \frac{1}{1-\delta} \left[e^{-\delta z} \int_{-\infty}^z \kappa(z) e^{\delta z} dz - e^{-z} \int_{-\infty}^z \kappa(z) e^z dz \right]. \quad (24)$$

Let us look only at the weak deviations from photochemical equilibrium which apparently are fully allowable for the F region of the ionosphere. In this case distribution (24) differs very little from the distribution which is established when $\kappa(z) = 0$. If the vertical distribution $\phi(z)$ when $z > 0$ is a slowly varying function having a maximum when $z = z_m$, then at the maximum

$$\varphi(z_m) = 1 \quad (25)$$

and

$$\frac{\partial \varphi(z_m)}{\partial z} = 0. \quad (26)$$

Conditionally, (25) gives

$$e^{-\delta z_m} \left[C_1 + \frac{1}{1-\delta} \int_{-\infty}^{z_m} \kappa(z) e^{\delta z} dz \right] - e^{-z_m} \left[C_1 + \frac{1}{1-\delta} \int_{-\infty}^{z_m} \kappa(z) e^z dz \right] = 1. \quad (27)$$

Let us introduce the definitions

$$\begin{aligned} \int_{-\infty}^{z_m} \kappa(z) e^z dz &= A(z_m); & \int_{-\infty}^z \kappa(z) e^z dz &= A(z); \\ \int_{-\infty}^{z_m} \kappa(z) e^{\delta z} dz &= B(z_m); & \int_{-\infty}^z \kappa(z) e^{\delta z} dz &= B(z). \end{aligned}$$

From (26) it follows that

$$\delta e^{-\delta z_m} \left[C_1 + \frac{1}{1-\delta} B(z_m) \right] = e^{-z_m} \left[C_1 + \frac{1}{1-\delta} A(z_m) \right], \quad (28)$$

whence

$$C_1 = \frac{1}{1-\delta} \left[\delta e^{z_m} - A(z_m) \right] = \frac{1}{1-\delta} \left[e^{\delta z_m} - B(z_m) \right]. \quad (29)$$

From (29) we find the equation

$$\delta e^{z_m} - e^{\delta z_m} = A(z_m) - B(z_m), \quad (30)$$

which determines the coordinate of the maximum of the z_m layer for a given function $\kappa(z)$.

After substituting the respective value of the constant C_1 from (29) into solution (24), we get

$$\varphi(z) = e^{-\delta z} \frac{1}{1-\delta} \left[e^{\delta z_m} + B(z) - B(z_m) \right] - \frac{e^{-z}}{1-\delta} \left[\delta e^{z_m} + A(z) - A(z_m) \right],$$

or

$$\varphi(z) = \frac{1}{1-\delta} \{ e^{-\delta(z-z_m)} - \delta e^{-(z-z_m)} + e^{-\delta z} [B(z) - B(z_m)] - e^{-z} [A(z) - A(z_m)] \}$$

Then, since

$$B(z) - B(z_m) = \int_{z_m}^z \kappa(z) e^{\delta z} dz$$

and

$$A(z) - A(z_m) = \int_{z_m}^z \kappa(z) e^z dz,$$

we can write the solution in the form

/48

$$\varphi(z) = \frac{1}{1-\delta} \{ e^{-\delta(z-z_m)} - \delta e^{-(z-z_m)} + e^{-\delta z} \int_{z_m}^z \kappa(z) e^{\delta z} dz - e^{-z} \int_{z_m}^z \kappa(z) e^z dz \}. \quad (31)$$

The last terms in formula (31) are determined by the form of function $\kappa(z)$. Generalized concepts as to the character of this function can be obtained from the altitude variation in the rate of ion formation $q(z)$ and neutralization $L(z)$. We know that above the maximum of ion formation, $L(z)$ drops more rapidly than $q(z)$. Therefore two cases are possible: either in the entire region under study $q(z) > L(z)$ or in this region there is a level where $q = L$. In the first case the stationary state is possible only under the condition that the ionization surplus is continually being removed due to diffusion downward and the maximum of the electron concentration must be created near the maximum of ion formation.

In the second case there exists a level at the altitude z_0 where $q = L$ and $(z_0)' = 0$. Let us call this level the level of photochemical equilibrium. In this case $\kappa(z)$ will be a slowly varying function that is negative when

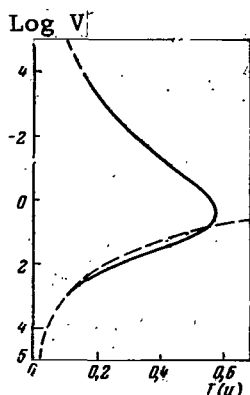


Figure 2. Graph of the Function $T(U)$, Computed by Bowhill. The Broken Line Shows the Conditions of Photochemical Equilibrium.

$z > z_0$, positive when $z < z_0$ and will vanish when $z = z_0$. Let us take advantage of this property of the function $\kappa(z)$ in solving (31). At the maximum $\phi(z)$, the values of the function ϕ and its derivative ϕ' , determined from formulas (16) and (31) coincide.

When $z = z_0$ the values of ϕ'' will also coincide. Thus, at the point z_0 both equations (18) and (22) themselves and their solutions (16) and (31) will also coincide. Hence it follows that the maxima of the electron concentration are found near the level of

photochemical equilibrium.

Bowhill [6] found the solution to equation (1) for stationary conditions. He chose fairly plausible values for the rate of the ionization-recombination processes and for diffusion. The result of the computations is shown on Figure 2. The values of the functions $T(U)$ are plotted along the horizontal axis and the logarithm of the dimensionless coordinate $U(\log U)$ is plotted along the vertical. The solid curve $T(U)$ changes into a broken curve in the upper part, representing pure diffusion. The broken line shows the position of the photochemical equilibrium level when diffusion can be ignored. This line (the condition $q = L$) lies above the curve $T(U)$, intersecting it near the maximum, but somewhat below it. This result indicates that with sufficiently intense sources the level of photochemical equilibrium lies slightly below the maximum of the layer. Computations show that the distance between these levels increases with increase in source intensity.

Consequently, the effect of the sources in a real daytime ionosphere leads to surplus ionization in the upper part of the F2 layer, which produces the phenomenon of diffusion flux. This flux transports the surplus ioniza- /49

tion from the upper part of the layer to the lower in such a manner that near the maximum of the layer the divergence of the flux changes sign and is therefore equal to zero.

NONSTATIONARY MODEL OF THE F2 LAYER

Under nonstationary conditions the equation of continuity for the electron gas can be written in the form

$$\frac{dN}{dt} = q_0 \psi(z, t) - \alpha [M^+] N + d[N^* + (\delta + 1)N' + \delta N], \quad (32)$$

where the concentration of molecular ions $[M^+]$ is determined by the equation [10]:

$$\frac{d[M^+]}{dt} = \gamma [M] (N - [M^+]) - \alpha [M^+] N. \quad (33)$$

Solution to the system of equations (32) and (33) requires knowledge of the kinetic coefficients α and γ (dimensionality — $\text{cm}^3 \cdot \text{sec}^{-1}$), $q_0 (\text{cm}^{-3})$ and structural parameters of the atmosphere $H_m = H_m(h)$ $[M] = f(h)$. Since these coefficients are unknown even in order of magnitude and since the solution is very sensitive to their values, there then remains the means of selecting these coefficients by one of the methods of trial-and-error. Since we do not have available a solution to this system in analytical form, the method of trial-and-error may give a sensible result only in the case where a rational method is found for obtaining a first approximation with a high degree of accuracy.

The method used is based on the fact that the kinetic coefficients are determined in this approximation for the layer maximum without allowing for diffusion.

It was shown earlier that with a weak effect from the sources of the diffusion flux the maximum of the diffusion layer (F2 layer) is found near the level of photochemical equilibrium. It is clear that the nearer the

maximum of the layer is to the level of photochemical equilibrium the less the diffusion will affect electron concentration at the layer maximum. At the limit, when the maximum coincides with the level of photochemical equilibrium, the divergence in the diffusion flux at the layer maximum will be equal to zero.

During the winter at middle latitudes when the altitude of the sun over the horizon is low, the maximum of the F2 layer must be near the level of photochemical equilibrium. Therefore we can assume that variations in electron concentration during the day in winter are distorted least by the effect of diffusion and that these variations may be used for determining the kinetic coefficients.

Under the presumed assumption equation (32) is simplified and can be written in the form

$$\frac{dN}{dt} = q_m \psi(t) - \alpha [M^+] N, \quad (34)$$

where q_m is the rate of formation at the layer maximum.

Equations (33) and (34) were modeled and investigated on an analog electronic computer (MN-7). The parameters α , γ and q_m were chosen so that the periodic solution $N(t)$ coincided best with the observed values of electron concentration in the entire time interval being studied. For this we used the diurnal variations in electron concentration at the maximum of the F2 layer obtained from ionospheric measurements.

Reference [10] describes in detail the technique used in determining the coefficients and the models used and the methods for computing the function $\psi(t)$. Variations in the atmospheric parameters were computed according to [12]. The values of α , γ and q_m found in this manner were used for further computations. The complete system of equations (32) and (33) was solved by a numerical method on a digital electronic computer. At the first stage of

150

the computations we assumed several simplifications. The atmospheric parameters in this operation were assumed to be constant for a period of twenty-four hours and were selected for the index of radio emission $S = 250$ and 1000 hours local time. A Chapman-type function $\psi(h, t)$ was taken in the form

$$\psi(h, t) = \exp \left(1 - \frac{280 - h}{H} - \frac{\sec \chi}{\sec \chi_0} e^{-\frac{280 - h}{H}} \right),$$

where we used the values of the zenith angle χ for December at the latitude of Irkutsk (χ_0 are noon values). The altitude of the maximum of ion formation is equal to 280 km. In the computations we took the following values:

$$\begin{aligned} D_0 &= 4.6 \cdot 10^9 \text{ cm}^2 \text{ sec}^{-1} \quad \gamma = 4 \cdot 10 \text{ cm}^3 \text{ sec}^{-1} \\ \alpha &= 1.1 \cdot 10^{-9} \text{ cm}^3 \text{ sec}^{-1}; \quad q_0 = 540 - 700 \text{ cm}^{-3} \cdot \text{sec}^{-1} \end{aligned}$$

We studied especially the question as to the influence of the boundary conditions on the solution near the maximum of the layer. The lower boundary conditions were the values $N = 0$ at an altitude of 100 km over the surface of the Earth. The upper boundary condition was given at an altitude of 700 km. In the first series of computations this value was chosen as constant and equal to 10^5 cm^{-3} . In the second series of computations the values of N varied as shown in Reference [11] according to the measurement data on the satellite "Alouette" for latitudes of $40 - 45^\circ$ in October - December 1962. With respect to the fact that the conditions of maximal solar activity were modeled with the index of radio emission $S = 250$, and the data pertain to the index $S = 70 - 100$, the values of N then were increased by three times.

The computation results were obtained in the form of a sequence of solutions with diurnal periodicity at various levels in the space coordinate h . The values $N(h, t)$; $(M^+) = f(h, t)$; $q(h, t)$; $L(h, t)$ and the value of diffusion $\partial(Nv)/\partial h = \phi(h, t)$ were introduced into the recording at hourly

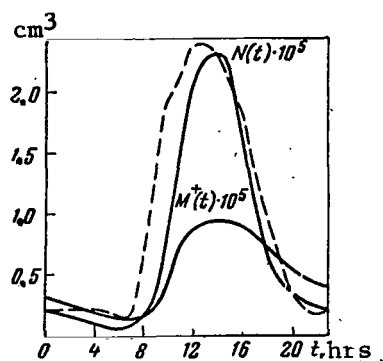


Figure 3. Diurnal Variations in N and $[M^+]$ at the Maximum of Vertical Distribution. The Broken Line Shows the Values of N at Irkutsk in December 1968.

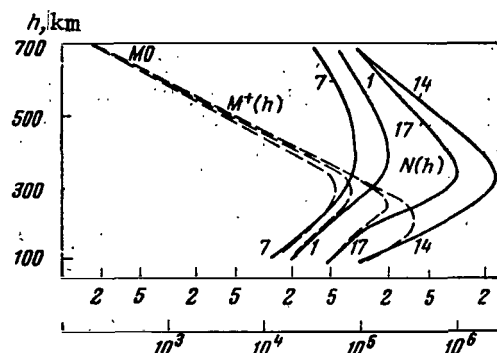


Figure 4. Profiles of the Vertical Distribution of $N(h)$ and $[M^+] = f(h)$ for 0100, 0700, 1400 and 1700 Hours Local Time.

intervals for the 21st and 41st values of the altitude coordinate h . Several results of the computations are shown below.

Figure 3 shows the diurnal variations in electron concentration and concentration of molecular ions at the maximum of the vertical distribution with variable upper boundary conditions.

Figure 4 shows the profiles of the vertical distribution $N(h)$ and $[M^+] = f(h)$ for 0100, 0700, 1400 and 1700 hours local time for variable boundary conditions.

Figure 5 shows the variations in altitude of the maxima of the electron and molecular ion concentration for variable boundary conditions.

From comparison of the results obtained for constant and variable boundary conditions it follows that the values of N at the maximum during daylight hours depend weakly on the boundary conditions. A pronounced difference is observed in the second half of the night and in the pre-morning hours.

Figure 6 shows the variations in the magnitude of the diffusion flux

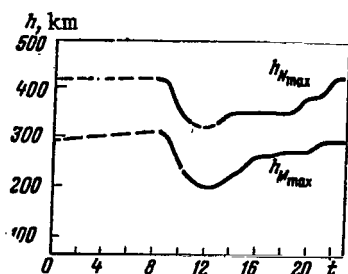


Figure 5. Altitude Variation in the Maxima of Electron and Molecular Ion Concentration.

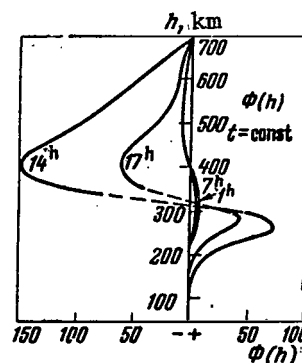


Figure 6. Value of the Magnitude of Diffusion $\phi(h)$.

along the vertical under variable boundary conditions. In all cases it is clear that the diffusion has large negative values above the maximum, high positive values below it and changes sign near the maximum, passing through zero.

It is characteristic that an intense influx of electron-ion gas is observed at levels on the order of $(1 - 2) H_m$ below the layer maximum. The maximum concentration of molecular ions lies near this level and ensures a high rate of electron recombination. Consequently the surplus concentration of electron-ion gas in the upper part of the layer "dips" downward and rapidly disappears by recombination. It is significant to mention that the recombination rate in this region, which depends on the concentration of M^+ , is controlled by the influx of electrons, and the maximum of the electron concentration is automatically established at an altitude with the corresponding value of the molecular component of the neutral atmosphere.

/51

Figure 3 shows also (the broken line) the observed values of N at the maximum of the F2 layer in December 1958 in Irkutsk. As is clear, the curves differ only in the morning and evening hours. This difference is explained by the fact that the Chapman function of ion formation is used in the computations and this becomes non-zero almost an hour later and vanishes earlier

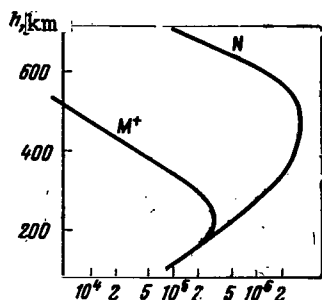


Figure 7. Vertical Distribution of the Concentration of Electrons and Molecular Ions Without Allowing for Diffusion.

than the more precise function which allows for diurnal variations in density of the neutral atmosphere and for the sphericity of the Earth.

We especially studied the solution of the system of equations (32) and (33) without a diffusion term. In this case the altitude of the layer maximum and the values of the electron concentration at the maximum were

measured throughout the entire time of the solution (in the present case two twenty-four hour periods) in such a manner that we were unable to obtain periodic stationary values of N and the altitude of the layer maximum. Figure 7 shows the vertical distribution $N(h)$ and $[M^+] = t(h)$ for noon of the second day. This result shows the impossibility of forming a layer maximum, similar /52 to that observed without diffusion of the electron-ion gas.

At the next stage we solved system (32) and (33) for the F region with varying atmospheric parameters taken from [12] for $S = 250$ and with various boundary conditions for $h = 700$ km. For this solution the space lattice was uniform with an interval of 20 km.

The function of ion formation $\psi(h, t)$ was computed with regard to the sphericity of the Earth for levels 200, 300, 400, 500, 600, 700 km; q_0 was given at noon at an altitude of 300 km. In the intermediate levels the rate of ion formation was found by linear interpolation.

In the first solution we assumed zero initial conditions in the entire region under study. The problem was solved up to finding a periodic stationary solution. In using the model of the neutral atmosphere [12] and the above-mentioned parameters the values of the electron concentration were

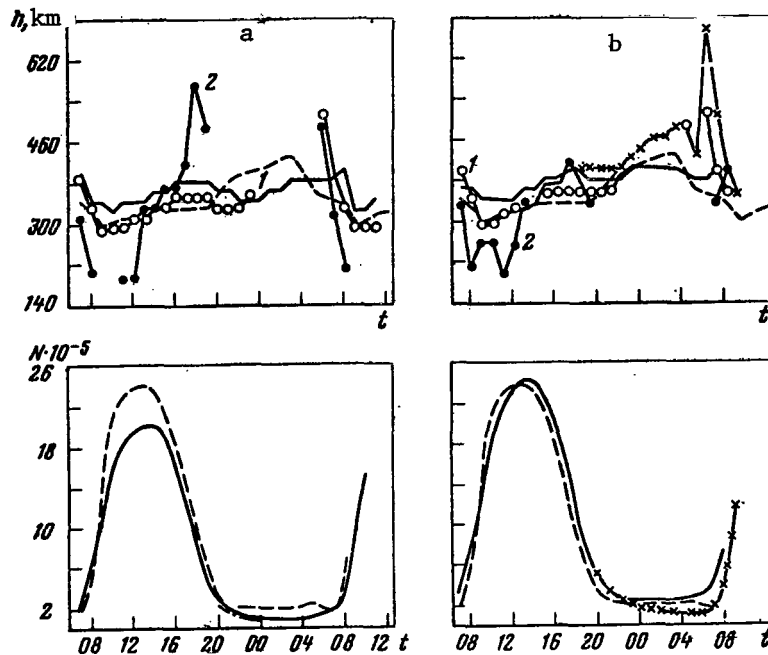


Figure 8. Diurnal Variations in Electron Concentration at the Layer Maximum, Layer Altitude and Level of Zero Diffusion and Photochemical Equilibrium.

The Solid Curve Shows the Results of Computations, The Broken Curve Shows the Observed Values in December 1958 in Irkutsk; 1. Level of Zero Diffusion; 2. Level of Photochemical Equilibrium.

established for the first six hours after the ionization function becomes effective. In subsequent solutions the initial conditions were taken from the results of the previous ones.

Figure 8a gives the results of solving the system of equations when $q_0 = 540 \text{ cm}^{-3}$ with the upper boundary conditions taken from [11] and increased by two times for all hours. The solid curves are the results of the solution and the broken curves are those of the observed values. In the upper part of the figure curve 1 shows the variable altitudes of the level of zero diffusion and curve 2 shows the variation in the level of photochemical equilibrium. The lower part shows the diurnal variations in electron concentration at the maximum.

Figure 8b shows the results of the solution for the case when $q_0 = 630 \text{ cm}^{-3}$ and the boundary conditions in comparison with Figure 8a increased by two times. From comparison of Figure 8a and 8b it is clear that the increase in boundary conditions by two times barely changes the electron concentration at the maximum during the day. Let us mention that the solution, when $q_0 = 540 \text{ cm}^{-3}$ and boundary conditions corresponding to the case of Figure 8b leads to noon values of N near those observed. If we compare the nighttime values of the electron concentration on Figure 8a and 8b we see that they differ from one another by approximately two times. It is also apparent that during the night the altitude of the maximum observed is greater than that computed. In connection with this we made computations for the atmospheric model in which the parameters varied during the day according to [12] and during the night remained constant for values corresponding to 1700 hours local mean time of the model in [12]. The results for this case are shown by the curve on Figure 8b (crosses).

To verify the influence of the upper boundary conditions we additionally obtained solutions for boundary conditions of N increased by 10 times in comparison with those used in [11] and also for the case when the flux P at the upper boundary is equal to zero. From the data obtained it follows that the value of the electron concentration at the layer maximum during the night is controlled by the boundary conditions, whereas during the day the sources of the diffusion flux are found basically below the upper boundary (700 km). We also found that the change in electron concentration at the maximum lags behind the corresponding variations at the upper boundary by approximately 1.5 - 2 hours. /53

The behavior of the level of zero diffusion is of interest, i.e. the level where $\phi(h) = 0$ (curve 1, Figure 8). During the day the level of the zero diffusion is found to be 20 - 40 km below the maximum of the electron concentration but during the morning and evening hours it coincides with the layer maximum or is above it. During the night there is diffusion flux on all levels.

The altitude of the level of photochemical equilibrium $q = L$ during the day undergoes large variations. It is obvious from Figure 8 (curve 2) that sometimes conditions are created under which the level of photochemical equilibrium ceases to exist. At all altitudes of the region studied in this case, $q > L$. When the ionization function is excluded, the level of the photochemical equilibrium travels upward and during the night, naturally, disappears. From comparison of the curves it is apparent that the level of photochemical equilibrium leads to a drift of the layer maximum. Only at the moment of time when $dN/dt = 0$ does the level of photochemical equilibrium coincide with the level of zero diffusion and is found to be approximately 20 km below the layer maximum.

FORMATION CONDITIONS OF THE F2 LAYER

The altitude profile of the F2 layer is formed under the influence of electron-ion gas diffusion. The diffusion flux at all levels of the layer is directed upwards from below. The sources of this flux are the regions which lie above the layer maximum. Investigations of the divergence of the diffusion flux show that the region of the efflux, where the diffusion flux disappears, is the region lying at 1 - 2 times the altitude of the uniform atmosphere below the layer maximum. Near the maximum of the equilibrium layer the divergence of the diffusion flux changes sign and therefore is near zero. Thus, the diffusion continuously transports the electron-ion gas from the upper part of the layer to the lower. /54

Under the influence of photoionization and recombination in the illuminated part of the day a tendency constantly exists to an increase in the electron concentration above the layer maximum. This tendency leads to a constant deviation of the altitude distribution of the electron concentration from the equilibrium value and continuously supports the existence of diffusion flux. Thus, in the altitude profile of the F2 layer we must distinguish two regions. In the first we have the upper part of the layer including the

maximum of electron density as well. The second contains the lower part of the layer and is found in the altitude range of $(1 - 2)H_m$ below the layer maximum.

In the first region we find the sources of the diffusion flux. Relatively high values of the coefficient of diffusion lead to a spatial distribution of the electron concentration in this region which deviates very little from the state of diffusion equilibrium. Therefore in a quiet ionosphere there are no intense local sources of the diffusion flux and this flux is formed in a wide altitude range above the maximum of the layer; each level introduces a given contribution to the creation of this flux.

The situation in the lower part of the layer is different. Here in a small altitude range the diffusion flux practically ceases to exist. This region is a reservoir to which the surplus ionization drains from the upper part of the layer. Under stationary conditions a dynamic equilibrium is established which guarantees the existence of a constant diffusion flux. The layer maximum is formed near the level of photochemical equilibrium where $q = L$. The altitude of this level varies during daylight and the altitude of the F2 layer maximum also varies correspondingly. The increase in q causes a lowering of this level, and a decrease in q causes it to be raised. This feature appears distinctly in the behavior of the F2 layer both during regular variations in the quiet ionosphere and during ionospheric perturbations. An increase in the altitude of the layer maximum is usually associated with a decrease in electron concentration and vice versa.

If there were no electron-ion gas, an increase would be observed for the greater part of the day in the electron concentration with a simultaneous increase in the altitude of the layer maximum. A similar picture, in somewhat distorted form, is observed near the magnetic equator. In the hypothetical case described, an increase in the altitude of the layer maximum must be accompanied by an increase in electron concentration. Usually

this decrease in electron concentration, observed at the middle latitudes with an increase in the altitude of the layer maximum and vice versa, is an indication of the diffusion mechanism in formation of the layer maximum.

Elevation of the diffusion layer is produced by a predominance of neutralization over photoionization near its maximum since the rate of neutralization drops with altitude more rapidly than does the rate of photoionization. Under these conditions the lower part of the layer is disrupted, producing the effect of moving the maximum upward. Here the electron concentration in the layer maximum must unavoidably be decreased, which in fact is observed.

The opposite picture must exist when the layer is lowered. Here photoionization predominates over recombination at the layer maximum. The deviation from diffusion equilibrium above the layer maximum is increased as is the diffusion influx, and the electron concentration maximum is lowered. Since in this case the influx of electrons increases the concentration at the lower levels, the lowering of the altitude of the layer maximum is accompanied by an increase in concentration.

Let us go on to describe several details of the diurnal variations in /55
electron concentration at the maximum of the F2 layer in the middle latitudes. During the winter and equinox seasons when ionizing radiation becomes effective, the number of molecular ions at the levels under study is small. The atomic oxygen ions which appear as a result of photoionization recombine slowly. Some time is required in order for these ions to be converted into molecular ions as a result of ion-molecular reactions.

The constant of this process is $\tau = 1/\gamma [M]$. This value grows rapidly with altitude. If we assume $\gamma = 4 \cdot 10^{-13} \text{ cm}^3 \cdot \text{sec}^{-1}$, and $[M]$ at the F2 layer maximum is on the order of $5 \cdot 10^8 \text{ cm}^{-3}$, then at this level $\tau \approx 1 - 1.5$ hours, and at an altitude of H_m above the maximum τ already amounts to several hours.

Therefore at the level of the maximum a rapid growth takes place in the electron concentration. This growth leads to an accumulation of electron concentration especially since during the morning the maximum of ion formation may also be found above the layer maximum for some time. The rapid increase in electron concentration at the upper levels sharply disturbs the stationary diffusion equilibrium at the end of the night and produces an acceleration of the diffusion flux which transports the electron-ion gas to the lower levels. It was mentioned above that in winter shortly after sunrise on the surface of the Earth, the level of the layer maximum drops by 30 - 40 km below the stable diurnal level and then slowly approaches this level near noon.

In the morning the value of $\gamma[M^+]$ assumes the least value, on the order of $10^{-5} \cdot \text{sec}^{-1}$. The quantity $\kappa(z) \cdot d$, which determines the magnitude of the diffusion, may also be of the same order or even greater during this time. Therefore during the early morning hours diffusion may fully compensate for recombination or even predominate over it. As a result the effective coefficient of recombination, which describes the total effect of neutralization and diffusion, is found to be in the morning hours of winter not only near zero but sometimes even negative, thus indicating the predominance of diffusion over neutralization.

A gradual approach to more or less stationary conditions then takes place. The maximum of the F2 layer occupies a stable position, which is determined by the dynamic equilibrium between ionization-recombination processes and diffusion. Further variation in electron concentration is controlled by photoionization and recombination.

At the moment of sunset when the maximum of ion formation shifts to the upper levels, it is again possible to have an increase in the diffusion flux which is accelerated by rapid cooling of electrons in spite of the masking effect of recombination processes. This effect may be detected if we examine the evening drop in electron concentration at a

constant level near the level of the maximal concentration during daylight hours. On all curves of this type the electron concentration from the time when ionizing radiation becomes effective and extending over a period of several hours drops almost linearly rather than exponentially as would be expected. This type of decline indicates an influx of electron-ion gas to the levels under study. This influx gradually weakens and then the linear drop changes to an exponential one.

In the evening following sunset the F2 layer for a period of several hours maintains its altitude in spite of intense neutralization. The rapid cooling of electrons, as shown in Reference [13], produces a disruption in the diffusion equilibrium.

The intense diffusion inhibits any increase in altitude of the layer during the first hours following cessation of photoionization. This increase begins somewhat later and continues during the first half of the night until neutralization at the level of the layer maximum no longer predominates over diffusion. Usually in the middle latitudes this sets in after midnight. In the first half of the night when recombination predominates over diffusion, the layer maximum is elevated. This elevation usually ends by 0000 - 0200 /56 hours local time when equilibrium sets in between recombination and diffusion. By this time the decrease in electron concentration at the layer maximum is also usually ended. After a certain "plateau" on the variation curve of the maximum altitude, under the effect of diffusion, the layer begins to be lowered and this lowering continues until sunrise.

Throughout the entire night the electron concentration at the maximum is maintained by diffusion of the electron-ion gas from upper regions of the ionosphere and the protonosphere which are reservoirs that hold the observed concentrations in the layer maximum. This is confirmed by the diurnal variations in electron concentration observed at altitudes on the order of 600 - 1000 km. For example, at an altitude of 800 km the electron concentration is decreased approximately by two times after 5 - 6 hours [11]. At these alti-

tudes only radiative recombination should exert any influence with a rate coefficient of $\alpha_2 = 10^{-12} \text{ cm}^3 \cdot \text{sec}^{-1}$. With such a low rate of recombination, about 10^3 hours are required for these variations in electron concentration. From these evaluations it is clear that an efflux of charged particles must take place from the upper ionosphere to the lower levels. During the night a gradual decrease takes place in the recombination rate that is associated with the decrease in electron concentration of molecular ions. With a stable diffusion flux, there will be a reduction in the level at which the influx due to diffusion is compensated for by neutralization.

Similar conditions are observed during the second half of the winter night at the middle latitudes when the layer drops slowly with an almost constant electron concentration at the maximum. The neutralization is compensated by the diffusion influx of electrons from the upper part of the layer.

Study of the kinetics of recombination processes shows that the value of the coefficient β (with linear approximation of the recombination term) undergoes a strong change during the course of the day, the mean values and the amplitude of the variations depending on the concentration of molecular components of the neutral gas. This property of the recombination term helps to explain several characteristics of the observed pattern of diurnal variations in electron density at the F2 layer maximum. The effect of this mechanism involves the fact that the shape and the amplitude of the variation in electron concentration during daylight hours depend on two factors: on the initial value of the concentration of molecular ions in the atmosphere (until the moment of sunrise) and on the concentration of the molecular component of the neutral gas. The initial conditions affect the rate of the morning increase in electron concentration, while the concentration of molecular gases determines the amplitude (noon) values of the recombination coefficient.

The recombination rate during the morning hours is determined by the residual concentration of molecular ions which is maintained at the level to

which the layer maximum descends by sunrise under the effect of diffusion. Since the maximum electron density at middle and low latitudes is at the lowest altitude, in the morning hours, we are dealing with a level which lies considerably below the altitude of the maximum of the nocturnal layer. From the data on the $N(h)$ -profile we know that the electron concentration (and consequently the concentration of molecular ions as well) at this level is found to be very low by the end of the night, and its values will depend on the duration of the nighttime hours. Therefore the initial morning values of the recombination coefficient β depend, in addition to other causes, also on the duration of the night.

The described picture is valid also during the equinox seasons with a slightly slower morning increase in electron concentration.

Summer conditions are characterized by a high concentration of molecular ions during the entire twenty-four hour period. This explains the slow growth in electron concentration in the morning and the small variations during the course of the day. In summer the maximum of ion formation drops at noon considerably below the layer maximum. Above the F2 layer maximum in summer the atmosphere is irradiated by the sun for the greater part of the day and at higher latitudes throughout the entire twenty-four hour period. Therefore in summer an intense diffusion flux exists continuously and the value of the diffusion at the maximum is a negative one. The basic mass of electron-ion gas which makes up the F2 layer is neutralized below the maximum, where the recombination rate is significantly higher. Where during the winter such conditions exist for a few hours around noon, in summer the steady state predominates for the greater part of the day. The lack of experimental data on the differences in composition of the summer and the winter atmosphere precludes any quantitative evaluations at the present time. However the factors given above are sufficient to explain two characteristic features of the summer picture, low values of electron concentration at the maximum of the F2 layer and small variations during the course of a day.

/57

CONCLUSIONS

1. A vertical distribution of the electron-ion gas concentration is established in the atmosphere under the influence of the central field of gravity with a stationary diffusion flux. This distribution has one maximum that is similar in form to the simple Chapman layer and is stable under steady-state conditions.

/58

This steady state is disturbed by ionization-recombination processes. When the influence of the electron-ion gas sources is weak, the maximum of the stationary distribution tends to the level of photochemical equilibrium, where $q = L$.

Under these conditions the divergence of the diffusion flux is negative above the maximum and positive below the maximum; it changes sign near the layer maximum, passing through zero (the region of zero diffusion). The diffusion transports the surplus concentration from the upper part of the layer to the lower, exerting no pronounced influence on the overall balance of electron-ion gas near the layer maximum.

2. Under the influence of intense electron-ion gas sources the level of photochemical equilibrium and zero diffusion is found below the layer maximum. In this case the diffusion at the layer maximum is negative. The efflux of electrons from the layer maximum is proportional to the electron concentration. The coefficient of proportionality (form-factor of the layer) depends on the intensity of the ionization-recombination processes.

3. In the F region of the ionosphere there exist two levels near which electron density maxima can form. The upper level coincides with the level of photochemical equilibrium. Near this level a basic (main) maximum of the electron density is formed — the F2 layer. This maximum is formed in the incident flux of electron-ion gas and is maintained by

sources located above the maximum. A lower maximum, identifiable with the F1 layer, is found near the greatest intensity of ion formation and therefore its behavior is similar to that of a simple layer. If these two levels are close, a single layer, the F2 layer, is observed, as happens during the winter at middle latitudes. In summer, when the maximum of ion formation descends with a decrease in the solar zenith distance, the F2 and F1 layers are observed separately.

REFERENCES

1. Ferraro, V. C. A. Terr. Magn. Atm. Electr., No. 50, 1945, p. 215.
2. Ferraro, V. C. A. J. Atm. Terr. Phys., No. 26, 1964, p. 913.
3. Polyadov, V. M. Geomagnetizm i aeronomiya, No. 6, 1966, p. 341.
4. Yonezawa, T. J. Atm. Terr. Phys., No. 15, 1959, p. 89.
5. Rishbeth, H. and D. W. Barron. J. Atm. Terr. Phys., No. 18, 1960, p. 234.
p. 234.
6. Bowhill, S. A. J. Atm. Terr. Phys., No. 24, 1962, p. 503.
7. Ferraro, V. C. A. and N. N. Ozdogan. J. Atm. Terr. Phys., No. 12, 1958,
p. 140.
8. Gliddon, J. E. and P. C. Kendall. J. Atm. Terr. Phys., No. 24, 1962,
p. 1073.
9. Polyakov, V. M. Sb. Ionosfernyye issledovaniya, (Collection: Ionos-
pheric Research) No. 16, Nauka Press, No. 16, 1966.
10. Polyakov, V. M. and T. B. Shchukina. Geomagnetizm i aeronomiya, Vol. 6,
No. 5, 1966.
11. Bauer, S. J. and L. J. Blumle. J. Geophys. Res., No. 17, 1964, p. 3613.
12. Harris, J. and W. Prister. Theoretical Models for the Solaroyde
Variation of the Upper Atmosphere, Greenbelt, Md., NASA Goddard
Space Flight Center, Theor. Division, N. Y., N. Y. Inst. Space
Studies, 1962.
13. Evans, J. W. J. Geophys. Res., Vol. 70, No. 5, 1965, p. 1175.

AERONOMIC PROBLEMS ARISING IN THE INTERPRETATION OF ELECTRON
DENSITY PROFILES IN THE F REGION

J. Taubenheim

In the F region the balance equation for electron density, including ionization, electron losses and transfer of charged particles, is mainly dependent on the balance of positive ions of atomic oxygen which are produced by photoionization, and are converted to O_2^+ and NO^+ by the charge exchange occurring before recombination. An explanation is given for the meaning of individual terms of this equation. Experimental laboratory and ionospheric investigations give quantitative estimates for ionization and electron losses. If these data are introduced into the balance equation and compared to the profiles of the electron density found by means of ionospheric sounding at middle latitudes, then considerable vertical movements of the ionospheric plasma in the F region must be assumed. These vertical movements vary during the day and especially during a solar eclipse. Diffusion alone is not sufficient to explain these phenomena.

The purpose of the theory is to physically explain not only the individual properties of electron density in the F region, but its behavior as a whole. It is very complicated to interpret the critical frequencies of the F2 layer since the formation of the electron concentration maximum depends on the interaction of many factors and the altitude of this maximum is not constant. Therefore it is difficult to properly evaluate the variations in aerodynamic conditions at the maximum of the F region. It is more convenient to first examine the variations in electron density at a constant altitude. Then explaining the behavior of the layer maximum is only a secondary step. /59

Let us look at the problem of the theoretical interpretation of the electron density profiles in the lower part of the F region obtained by

analyzing ionograms. At the present time there are already a number of vertical profiles for the electron density. For daylight hours these profiles represent data for the range of altitudes from approximately 160 to 250 km. The aeronomic conditions in this range seem to be especially complex. Let us discuss several of the problems which in my opinion have decisive significance for interpreting the profiles of electron density.

The bases of the F region theory have already been discussed in detail in the articles of A. D. Danilov and V. M. Polyakov⁽¹⁾ as well as in the lectures of G. S. Ivanov-Kholodnyy given at the International Summer School of Physics of the Upper Ionosphere (Sochi, 1966). Here it is shown that the greatest problems are concerned with determining the values of the coefficients of chemical reactions in the ionosphere and with explaining how great is the influence of the processes of electron transport. If we consider only diffusion as the transport process, then the observed variations in electron density can be explained only by selecting those values for the coefficients of the reactions which are significantly smaller than the laboratory data. On the other hand, if we wish to utilize the laboratory data, we must assume a strong vertical transport which can never be explained by diffusion [1 - 3].

The F region theory is usually verified by computing the theoretical profiles of the electron density by solving the equation of balance and comparing the results with the experimental data on variations in the electron density. We shall proceed along a different path, i.e. we shall consider both aeronomic and experimental data in the equation of balance in order to determine where the contradictions between theory and experimental data appear.

(1) See the present collection, pp. 11 - 61 and 62 - 95.

EQUATION OF ELECTRON BALANCE

The equation of electron balance in the ionosphere

/60

$$\frac{dN}{dt} = Q - L + D, \quad (1)$$

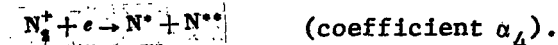
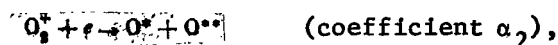
(where Q is the photionization rate, L is the electron loss rate and D is the transport velocity) can be feasibly transformed into such a form that would be suitable for comparing the aeronomic and ionospheric data. Atomic (O) and molecular oxygen (O_2) and molecular nitrogen (N_2) are the components of the air which are ionized in the F region. Then the overall photoionization rate Q is equal to

$$Q [\text{cm}^{-3} \cdot \text{sec}^{-1}] = q(O) + q(O_2) + q(N_2) \quad (2)$$

Ions of O^+ , O_2^+ and N_2^+ are found here in the atmosphere. The O^+ -ions may be converted into molecular ions as a result of the reactions



The molecular ions dissociate:



The direct recombination rate of atomic O^+ ions is so small in comparison with the ion molecular reactions that it can be ignored. The loss rate L in the equation of balance therefore is determined by the total electron recombination rate with various types of positive molecular ions.

This expression can be transformed by using the equation of balance of various positive ions. According to Ratcliffe, we can assume that photochemical equilibrium predominates for the positive ions and their transport can be ignored. Therefore the equations of balance for O^+ , NO^+ and N^+ can be written in simplified form:

$$L = (\alpha_1 [O_2] + \alpha_2 [NO^+] + \alpha_3 [N_2^+]) [e], \quad (3)$$

$$q(O_2) + \gamma_2 [O_2] [O^+] = \alpha_1 [O_2^+] [e], \quad (4)$$

$$\gamma_3 [N_2] [O^+] = \alpha_2 [NO^+] [e], \quad (5)$$

$$q(N_2) = \alpha_3 [N_2^+] [e], \quad (6)$$

The sum of the right-hand sides of the last three equations is equal to the expression given above for the loss rate L . In the same way L can be written in the form

$$L = (\gamma_2 [O_2] + \gamma_3 [N_2]) [O^+] + q(O_2) + q(N_2). \quad (7)$$

If this expression is substituted into the equation of electron balance (1) we then find the simple equation:

$$\frac{\partial [e]}{\partial t} = q(O) - (\gamma_2 [O_2] + \gamma_3 [N_2]) [O^+] - \text{div}([e]v_e). \quad (8)$$

Finally if we denote the expression in brackets by β'

$$\beta' = \gamma_2 [O_2] + \gamma_3 [N_2] \quad (9)$$

and introduce the notation

. /61

$$p = [O^+]/[e], \quad (10)$$

for the density ratio of O^+ ions to electrons, then for the equation of electron balance we find

$$\frac{\partial [e]}{\partial t} = q(0) - \beta' p [e] - \text{div}([e]_v). \quad (11)$$

In the same way, the variation in electron density is determined by three terms: (a) photoionization of atomic oxygen; (b) a loss term which contains the coefficient β' that depends on the model of the neutral composition of the atmosphere and on the coefficient p which characterizes the ion composition of the atmosphere; and (c) term which describes a electron transport.

If we solve the equations of balance (4), (5), (6) relative to the concentrations of molecular ions and substitute these concentrations in the condition of quasineutrality

$$[e] = [O^+] + [O_2^+] + [NO^+] + [N_2^+], \quad (12)$$

we find

$$[e] = \left\{ 1 + \frac{\gamma_2}{\alpha_2} \frac{[O_2]}{[e]} + \frac{\gamma_3}{\alpha_3} \frac{[N_2]}{[e]} \right\} [O^+] + \frac{q(O_2)}{\alpha_2 [e]} + \frac{q(N_2)}{\alpha_4 [e]}$$

Hence we find the expression for the coefficient p , i.e., the ratio of O^+ ion concentration to electron concentration:

$$p = \frac{1 - \frac{q(O_2)}{\alpha_2 [e]^2} - \frac{q(N_2)}{\alpha_4 [e]^2}}{1 + \frac{\gamma_2 [O_2]}{\alpha_2 [e]} + \frac{\gamma_3 [N_2]}{\alpha_3 [e]}} \quad (13)$$

We see that the ion composition at fixed altitudes of the F region is not constant since it depends on the electron concentrations and on

the variable densities of the neutral components and on the temperature dependence of the coefficients γ . Rough evaluation of the terms in the numerator of expression (13) shows that both values $q(O_2)/\alpha_2[e]^2$ and $q(N_2)/\alpha_4[e]^2$ are less than unity. Therefore with no great error the coefficient p may be written in the following form:

$$p = \left(1 + \frac{\delta}{[e]}\right)^{-1}, \quad (13')$$

where

$$\delta = \frac{\gamma_2}{\alpha_2} [O_2] + \frac{\gamma_4}{\alpha_4} [N_2]. \quad (14)$$

EXPERIMENTAL DATA

Photoionization. Hinteregger, Hall and Schmidtke [4] gave a considerable amount of reliable data relative to photoionization under conditions of low solar activity. The atmospheric model which these authors used corresponds approximately to the model proposed by Harris and Priester [5]. The values of the ionization rate computed by G. S. Ivanov-Kholodnyy [6] on the basis of the model from [5] agree very well with the data of these authors in the F region. Unfortunately the solar radiation fluxes during high solar activity are as yet known quite imprecisely. Therefore we shall confine ourselves to examining the conditions of low solar activity.

Ion Composition. The ion composition of the upper atmosphere has been known for some time from numerous direct measurements using mass-spectrometers on rockets and satellites. All these data can be found, for example, /62 in the work of G. S. Ivanov-Kholodnyy and A. D. Danilov [7]. New measurements during low solar activity were published by Johnson [8]. From these data we can choose the direct values for the coefficients p in the equation of electron balance (Table 1, first line). Besides, these data can be used to find certain information about reaction coefficients γ and α . If we compare the experimentally computed profile of the ratio

$p(h)$ with the measured profile of electron density $[e](h)$ from equation (13) we can determine the values of $\delta(h)$ for the various altitudes. Using the mass-spectrometric data and equation (8), we find the values of $\delta(h)$ given in the second line of Table 1 from the mean profiles of electron density for the equinox at middle latitudes during low solar activity (Slough, September, 1950). The values of $\delta(h)$ depend on the concentrations of neutral particles O_2 and N_2 and on the ratio (γ/α) . Furthermore, from the equation of balance

TABLE 1

	Altitude, km				
	160	180	200	220	240
$p = [O^+]/[e] [8]$	0.26	0.67	0.89	0.96	0.97
δ, cm^{-3}	5.3	1.3	0.44	0.24	$0.16 \cdot 10^5$
$\delta_{\text{comp}} \text{cm}^{-3}$	4.7	1.5	0.56	0.24	$0.11 \cdot 10^5$

(4) and (5) of positive ions it follows that in the F region where $q(O_2)$ is low in comparison with the other terms of equation (4), the ratio of NO^+ and O_2^+ ion concentrations is given by

$$\frac{[NO^+]}{[O_2^+]} \approx \frac{(\gamma_2/\alpha_2) [N_2]}{(\gamma_1/\alpha_1) [O_1]} \quad (15)$$

The ratio $[N^+]/[O_2^+]$, according to the measurements of Johnson [18], carried out with the aid of a mass-spectrometer in the frequency range from 160 to 240 km, is approximately constant and equal to 1.3 - 1.4. With the assistance of equations (14) and (15), from this value and the data for δ from Table 1 we can determine the quantities $(\gamma_2/\alpha_2) [O_2]$ and $(\gamma_3/\alpha_3) [N_2]$. The concentrations of neutral components (O_2) and (N_2) may without doubt be borrowed from the model of Harris - Priester [5], since the neutral composition of the air in this model corresponds well with direct measurements using a mass-spectrometer. By such a method we obtain the following ratio of the coefficients γ and α for an altitude of 200 km during low solar activity:

$$\gamma_2/\alpha_2 \approx 1 \cdot 10^{-4},$$

$$\gamma_3/\alpha_3 \approx 1.5 \cdot 10^{-4}.$$

If on the basis of these values we compute $\delta(h)$ for altitudes from 160 - 240 km, then data are obtained that are described in the third line of Table 1. From the satisfactory agreement with experimental values in the second line it follows that the data on the relationships (γ/α) vary insignificantly with altitude. This means that the temperature dependence of coefficients γ cannot differ strongly from the temperature dependence of coefficients α .

Laboratory Data on the Coefficients γ . In numerous laboratory experiments attempts were made to measure both the coefficients of ion-molecular reactions γ_2 and γ_3 and the values of the coefficients of dissociation α_2 and α_3 . These values were already given in the article by A. D. Danilov (see the present collection and Reference [1]). New data were published in [9 - 11]. Unfortunately all these data are quite contradictory. For example, the measurements of Ferguson's [sic] group [9, 10] gave the coefficients

/63

$$\gamma_2 = (4.0 \pm 1) \cdot 10^{-11} \text{ cm}^3 \cdot \text{sec}^{-1}, \gamma_3 = 3 \cdot 10^{-13} \text{ cm}^3 \cdot \text{sec}^{-1}$$

whereas on the basis of the measurements of Sayer's [sic] group [11], the following values were obtained

$$\alpha_2 = 1 \cdot 10^{-7} \text{ cm}^3 \cdot \text{sec}^{-1}, \alpha_3 = 7 \cdot 10^{-8} \text{ cm}^3 \cdot \text{sec}^{-1}.$$

The values of γ_3 here differ by a whole order of magnitude. We prefer to use the data of Ferguson's group since they represent the opinion of many

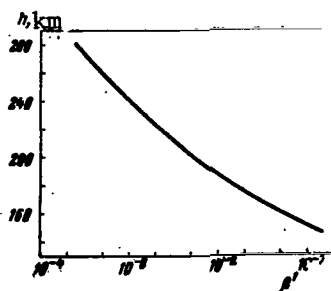


Figure 1. The Coefficient β' as a Function of Altitude.

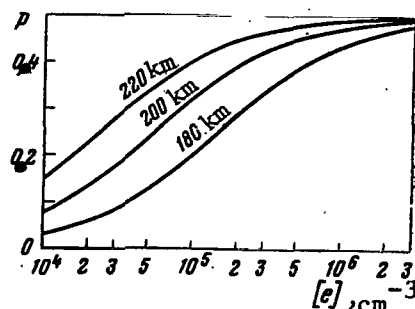


Figure 2. The Parameter p as a Function of Electron Concentration for Altitudes of 180, 200 and 220 km.

authors that the ratio γ_3/γ_2 must be equal to 0.1 (see for example [12]).

These laboratory measurements were made generally at a temperature of approximately 300° K. However the temperature in the F region is considerably higher. At an altitude of 200 km during low solar activity we must assume a temperature of approximately 900° K at noon. Unfortunately, the temperature dependence of the coefficients γ is very poorly known. The experimental data published in Reference [11] may be described by a dependence such as $T^{-0.7}$. It is possible that the temperature dependence is more pronounced.

It seems to be feasible to take the temperature dependence of the coefficients γ in the form T^{-1} for subsequent studies and to use for an altitude of 200 km (under conditions of low solar activity) the values

$$\gamma_1 = 1 \cdot 10^{-11} \text{ cm}^3 \cdot \text{sec}^{-1}, \gamma_2 = 1 \cdot 10^{-12} \text{ cm}^3 \cdot \text{sec}^{-1}$$

Then on the basis of the values given above of the ratios (γ/α) for the coefficients of dissociation we obtain

$$\alpha_1 = 1 \cdot 10^{-7} \text{ cm}^3 \cdot \text{sec}^{-1}, \alpha_2 = 7 \cdot 10^{-8} \text{ cm}^3 \cdot \text{sec}^{-1}$$

The agreement of these values with the laboratory data is satisfactory. Then with the assistance of these values of γ and the concentrations $[O_2]$ from the model of Harris - Priester [5] we find the coefficient for N_2 of the equation of electron balance at an altitude of 200 km:

$$\beta' = 5.4 \cdot 10^{-4} \text{ sec}^{-1}$$

The dependence of the coefficient β' on altitude is associated with the variation in density of the neutral molecules, as shown on Figure 1. These values are applicable during the noon hours at low solar activity (model No. 2 in Reference [5]). /64

Figure 2 shows the parameter $p = [O^+]/[e]$ as a function of the electron concentration for altitudes of 180, 200 and 220 km.

PROCESSES OF ELECTRON TRANSPORT

Now we can use the data of actually measured profiles of electron density to compute the value of the loss term $L' = \beta' p[e]$ in the equation of balance (11). In the noon hours the value of $\partial[e]/\partial t$ is always smaller than $q(0)$, so we can assume quasistationary conditions. In this case the difference between $q(0)$ and L must be equal to the value of the transport term

$$L' - q(0) = D = -\text{div}([e]v). \quad (16)$$

In order to avoid problems associated with the seasonal anomaly in the F region, let us first examine the $N(h)$ -profile for the equinox (The Slough station, September 1950) during low solar activity. Figure 3 shows the values of $q(0)$ and L' as a function of altitude for local noon. It is obvious that the difference $(L - q)$ varies quite strongly with altitude. Simultaneously this difference at fixed altitudes is confirmed by the strong diurnal variations as shown on Figure 4 (for an altitude of 200 km).

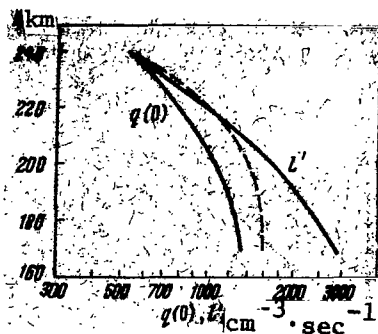


Figure 3. Altitude Variation of the Ionization Rate $q(0)$, Recombination Rate L' and Computed Value $q + D_{\text{comp}}$ (Broken Line) at the Slough Station in September 1950. Time 1200 hours.

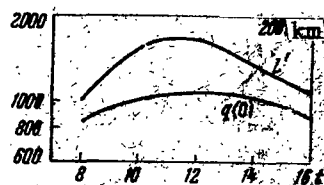


Figure 4. Ionization Rate $q(0)$ and Recombination Rate L as a Function of Local Time at the Slough Station, September 1950.

Such values for D , as we can see from Figures 3 and 4, can not be explained by the velocities which are due to diffusion. For altitudes above 200 km Rishbeth [13] could explain the analogous profile of electron density only by assuming very high diffusion rates. In a subsequent paper [14] Rishbeth attempted to find a more satisfactory explanation for this by assuming that the concentration of neutral molecules is significantly lower than in the Harris - Priester model [5]. In this way the coefficient β' as well as the values of L' are significantly lowered. As shown above, the neutral composition of the air in the Harris - Priester model [5] agrees rather well with the results of measurements using a mass-spectrometer. Therefore, Rishbeth's assumption must be rejected. Furthermore this assumption implies only the multiplication of L by a constant factor and this can never prevent the fact that at certain altitudes at certain moments of time the difference $(L' - q)$ still remains large. This is clearly evident in Figures 3 and 4 in logarithmic scale where this multiplication implies only a parallel shift in the curves L' . Therefore we come to the conclusion that the value of the difference $(L' - q)$ may be explained only by allowing for the dynamic processes in the plasma of the upper atmosphere.

/65

The movement of plasma in the F region may be caused not only by dif-

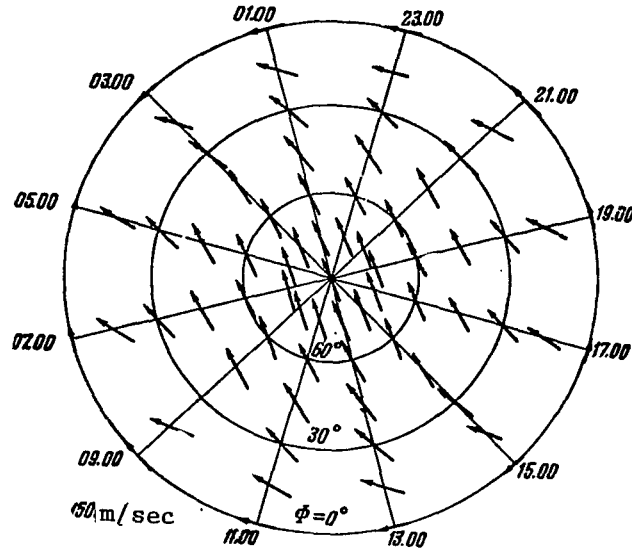


Figure 5. Geographic Distribution of Horizontal Velocity Vectors at an Altitude of 300 km in the Northern Hemisphere According to Kohl and King [15]. The North Pole is Located in the Center of the Figure, Local Time is Used Instead of Longitude, $N_{\max} = 3 \cdot 10^5 \text{ cm}^{-3}$.

fusion but also by the horizontal drift of the neutral gas. Since the ions and electrons may move only in the direction of the force lines of the Earth's magnetic field, the horizontal motion of the air creates a vertical component of the plasma motion. Let us denote the vector of the velocity of neutral air by \mathbf{u} , and the unit vector in the direction of the magnetic force lines by \mathbf{t} . Then the vector of the plasma rate \mathbf{V} , which is caused by the movement of the air, is equal to

$$\mathbf{V} = (\mathbf{u} \cdot \mathbf{t}) \mathbf{t}. \quad (17)$$

Let us choose a system of coordinates so that the coordinate x will be directed to the east, the coordinate y to the north and the coordinate z upward. Then the vertical component of the plasma velocity in the northern hemisphere, according to equation (17), will be equal to

$$V_z = -u_y \cdot \cos i \cdot \sin i,$$

where i denotes the geomagnetic inclination.

The horizontal drift of the neutral air is caused by the pressure gradients which set in as a result of the unbalanced heating of the Earth's atmosphere. This planetary distribution of the pressure was found on the basis of measuring the deceleration of artificial earth satellites. The model of the resulting planetary circulation of the upper atmosphere was computed by Kohl and King [15] by numerical solution of the equation of atmospheric motion:

$$\frac{\partial \mathbf{u}}{\partial t} - 2[\mathbf{u} \times \mathbf{w}] = -\frac{1}{\rho} \nabla p - M \frac{\partial^2 \mathbf{u}}{\partial h^2} - \frac{\nu_i N_i}{N_n} [\mathbf{u} - (\mathbf{u} \cdot \mathbf{t}) \mathbf{t}].$$

/66

The local variations in velocity and the Coriolis acceleration are given in the left-hand side of this equation and the pressure gradient and viscous deceleration are given in the left-hand side; by this latter term we imply the deceleration due to the collision between neutral molecules and ions (ν_i is the number of collisions, N_i and N_n are concentrations of ions and neutral molecules). It is clear that the deceleration is stronger as the ion concentration is higher. Therefore the daytime wind velocity during high solar activity and in winter will be lower than during low solar activity and in summer.

Kohl and King used only two very simple models of the ionosphere. For the entire northern hemisphere they assumed a constant profile for the Chapman electron density. One model has a maximal electron concentration of $3 \cdot 10^5 \text{ cm}^{-3}$ and the other, $1 \cdot 10^6 \text{ cm}^{-3}$. In both models the maximum of the Chapman layer lies at an altitude of 300 km. These models represent actual conditions poorly and therefore the computations of Kohl and King for the velocity field should be used only as a rough approximation.

The horizontal velocity vectors at an altitude of 300 km in the northern hemisphere, according to Kohl and King, at a maximal electron density of

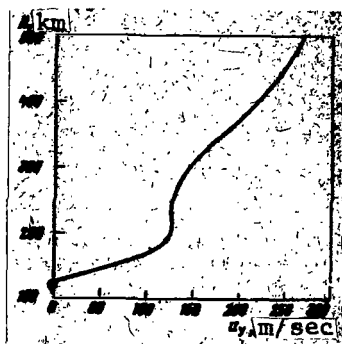


Figure 6. Altitude Profile of the Northern Component of the Velocity u_y at 1500 Hours Local Time for Latitude 45° .

$3 \cdot 10^5 \text{ cm}^{-3}$ are shown on Figure 5. (The North Pole lies in the center of the figure, the longitude is denoted in local time). The velocities of this model have a magnitude on the order of 150 m/sec. The component u_y , directed to the north, reaches a maximal value at 1500 hours local time in the middle latitudes. The corresponding altitude profile of the component u_y at 1500 hours local time for a latitude of 45°

is shown on Figure 6. Below an altitude of 200 km the velocity of u_y is lowered.

At a maximal electron density of $1 \cdot 10^6 \text{ cm}^{-3}$ the geographic distribution and the diurnal path of the velocity vectors are similar to that shown on Figure 5; however the magnitude of the velocities is only approximately 40 m/sec. Therefore the diurnal maximum of the plasma velocity is expected at approximately 1500 hours local time and the movement is directed downward. In the middle latitudes with an inclination of approximately $i = 60^\circ$ this maximal value of V_z at an altitude of about 200 km from these models is equal to

$$|V_z| = 56 \text{ m/sec when } [e]_{\text{max}} = 3 \cdot 10^6 \text{ cm}^{-3}$$

$$|V_z| = 15 \text{ m/sec when } [e]_{\text{max}} = 1 \cdot 10^6 \text{ cm}^{-3}$$

APPLICATION TO SOME PROFILES OF ELECTRON DENSITY

With the assistance of these data on the vertical velocities V_z of the 67 electrons and of the mean profile of $N(h)$ at midday in September 1950 (Slough), used on Figure 3, we can roughly estimate what values are assumed by the quantity $D = \text{div}([e]_v)$ at the various altitudes. Here we find that

D has a maximum at approximately an altitude of 190 km. On the basis of the values of D_{comp} and $q(0)$ thus computed, a sum is formed ($q + D_{\text{comp}}$) that is shown on Figure 3. This curve ($q + D_{\text{comp}}$) (h) according to Equation (16) must coincide with the curve L' (h). This requirement is well satisfied above 210 km. In the same manner we can explain the value of L' (h) which deviates from $q(h)$. However below 210 km the value of ($q + D_{\text{comp}}$) is still too small in comparison with L' . Let us assume that this divergence occurs because, in computing the profile of the electron density, erroneous assumptions were made relative to the electron density profile between the E and F layers. Because of these errors, below an altitude of approximately 200 km exaggerated values are generally obtained for the electron density and hence the computed values of the magnitude of L' become too high. Therefore it is very important to compute the possible errors in the calculation of the $N(h)$ -profiles before continuing on to an interpretation of these profiles from the physical point of view.

As a second example let us look at an analogous interpretation of a typical winter profile of electron concentration which was observed at noon of one quiet February day in 1961 in Bulgaria. Figure 7, just as Figure 3, shows the quantities $q(0)$ and L' as functions of altitude (in logarithmic scale). The difference ($L' - q$) here at all altitudes is very large. Without doubt, this takes place as a result of the large values of the electron density which occur as a result of the seasonal anomalies in the F2 region. From our viewpoint this anomaly may be explained by the fact that in winter the concentrations of molecular components of the atmosphere are slightly decreased in comparison with the Harris - Priester model [5], whereas the concentration of atomic oxygen is somewhat elevated. In this regard, the total atmospheric density should not vary strongly. If we assume that the concentration of (O_2) and (N_2) in winter reaches only 80% of the values of the model in [5], then the concentration of (O) must increase approximately up to 140%. Therefore the coefficient β' and also the quantity L' should be multiplied by 0.8 and the ionization rate $q(0)$ must be increased by 1.4 times. The values of $q(0)$ and L' , thus corrected, are plotted on Figure 7 as a function of altitude, depicted by the broken lines. The value of the electron transport term

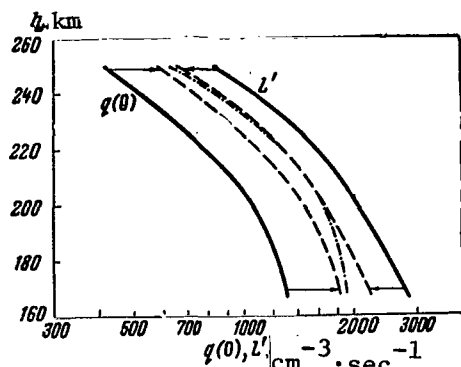


Figure 7. Ionization Rate $q(0)$ and Recombination Rate L' as a Function of Altitude.

The Broken Lines Denote the Values of $q(0)$ and L' , Corrected by Allowing for Variations in Chemical Composition of the Atmosphere. The Dot-Dash Line Denotes the Variation in the Computed Value of $1.2 \cdot q(0) + D_{\text{comp}}$.

D_{comp} was again computed from the data of Kohl and King. Since the maximal electron density reached a value of approximately $1 \cdot 10^6 \text{ cm}^{-3}$, we used the lower values of the velocity. The sum of the quantities $1.2 \cdot q(0)$ and D_{comp} is depicted on Figure 7 by the dot-dash line. The agreement of this curve and the curve $0.8 L'$ (the broken line) is very good for all altitudes above 200 km. This result supports the hypothesis expressed above to explain the seasonal anomaly. /68

Computation of the $N(h)$ -profiles in the F region during the total solar

eclipse on February 15, 1961 [16] shows that at the maximal phase of the eclipse the difference $(L - q)$ has very large values. This effect may be explained only by a strong increase in electron transport velocity during the eclipse. This increase in the transport velocity should in fact be expected on the basis of the Kohl - King theory since during the eclipse the electron concentration in the entire F region is lowered to a significant degree as a result of which an increase in the drift velocity begins.

In conclusion let us remember that the work of Kohl and King also makes possible an explanation of several features of the behavior of the critical frequencies of the F2 layer. For example, the decrease in the critical frequencies after noon in the summer is explained by the fact that the vertical component of the plasma velocity has a maximum at 1500 hours. Here the electron density maximum shifts downward to the region where the loss rate is higher than at higher altitudes.

CONCLUSION

1. The dynamic processes in the lower part of the F region produced by the overall system of atmospheric winds have an appreciable effect on electron distribution. This influence apparently is greater than the influence of diffusion. Even the rough evaluations of Kohl and King give the possibility of a better understanding of several features of the electron density profiles. A similar investigation on the dynamics of the upper atmosphere was also carried out by Geisler [17]. It is necessary to carry out further detailed computations of the system of winds corresponding to actual conditions.

2. Measurement of the ion composition offers not only important data for computing the electron loss rate in the F region, it also gives decisive criteria for the values of the coefficients of chemical reactions in the atmosphere. Therefore further study is necessary for the diurnal and seasonal variations in the ion composition by direct measurements, which should include measurements of the electron density profiles whenever possible.

3. It seems that even the quite small variations in the relative concentrations of neutral molecular and atomic components are sufficient for explaining the seasonal anomalies in the F region. Here the dynamic movements in the plasma of the F region play a secondary role.

4. Before we undertake a quantitative interpretation of the electron density profiles from the viewpoint of physics, we must investigate what errors may be allowable in the electron density values due to the assumptions on the distribution of electron concentration in the region between the E and F regions.

REFERENCES

/69

1. Danilov, A. D. and G. S. Ivanov-Kholodnyy. Uspekhi fizicheskikh nauk (UFN), No. 85, 1965, pp. 259-294.
2. Polyakov, V. M. and T. B. Shchukina. Geomagnetizm i aeronomiya, Vol. 6, 1966, pp. 858-868.
3. Taubenheim, J. Vortrag auf dem COSPAR-Symposium, (Report on the COSPAR Symposium), Vienna, 1966.
4. Hinteregger, H. E., L. A. Hall and G. Schmidtke. Space Res., No. 5, 1965, pp. 1175-1190.
5. Harris, I. and W. Priest. COSPAR International Reference Atmosphere (CIRA), Amsterdam, 1965.
6. Ivanov-Kholodnyy, G. S. Geomagnetizm i aeronomiya, No. 6, 1966, pp. 382-385.
7. Ivanov-Kholodnyy, G. S. and A. D. Danilov. Kosmicheskiye issledovaniya, No. 4, 1966, pp. 439-452.
8. Johnson, C. Y. J. Geophys. Res., No. 71, 1966, pp. 330-332.
9. Fehsenfeld, F. C. et al. Planet. Space Sci., No. 13, 1965, pp. 219-223.
10. Fehsenfeld, F. C. et al. Planet. Space Sci., No. 13, 1965, pp. 579-582.
11. Batey, P. H. et al. Planet. Space Sci., No. 13, 1965, pp. 911-917.
12. Danilov, A. D. and S. P. Yatsenko. Kosmicheskiye issledovaniya, No. 2, 1964, p. 276.
13. Rishbeth, H. J. Atm. Terr. Phys., No. 26, 1964, pp. 657-685.
14. Rishbeth, H. Persoenliche Mitteilung, (Personal Communication).
15. Kohl, H. and J. W. King. Atmospheric Winds Between 100 and 700 km and Their Effects on the Ionosphere, Rep. Radio and Space Res. Station Slough, 1966.
16. Serafimov, K. and J. Taubenheim. Kleinheubacher Ber., No. 9, 1964, pp. 65-68.
17. Geisler, J. E. J. Atm. Terr. Phys., No. 28, 1966, pp. 703-720.

PRESSURE GAUGE MEASUREMENTS ON ROCKETS AND SATELLITES

V. V. Mikhnevich

The paper presents a survey of techniques used for, and results obtained in, measuring the atmospheric density when employing rocket- and satellite-borne pressure gauges.

Experiments done with rockets present serious difficulties. Rockets travel at a tremendous velocity and are subjected to great accelerations and vibration in a wide range of frequencies when they are on their active path. The weight, size, and power requirements of rocket-borne instruments must of necessity be as small as possible. Owing to this, instruments intended for measuring pressure must be quick-response, have strong construction, light weight and small size, consume little power, and operate automatically.

In addition to measuring pressure (density) the pressure gauges provide for determining the atmospheric temperature as well.

One disadvantage of taking measurements with rocket-borne pressure gauges is that they cannot be used for determining the composition of the atmosphere, which results in measurement errors. Another disadvantage is that the measurement results may be distorted by gases escaping from a rocket or satellite. Under certain experimental conditions these errors can be reduced to an acceptable minimum by special measures.

Studies of the atmosphere (structural parameters) using pressure gauges /70 and mass-spectrometers installed in rockets and satellites presents difficult theoretical and experimental problem. The specifics of the experiment require studying a whole complex of phenomena. Let us look at some of these.

ATMOSPHERIC EQUILIBRIUM, BAROMETRIC FORMULA

The Earth's atmosphere is an uninsulated gas environment located in a gravity field. Its state, determined by the effect of various energy sources

including corpuscular and electromagnetic ones, varies with altitude and in time.

As a result of this there is no complete thermodynamic equilibrium in the Earth's atmosphere as a whole. At the same time there does exist a local thermodynamic equilibrium in the atmosphere. In this case the local properties of the gas (in a given volume) are described by ordinary laws of thermodynamic (statistical) equilibrium, including: the equation of state $p = nkT$ (p is the gas pressure, n is the concentration, T is the absolute temperature, k is the Boltzmann constant); the equation of hydrostatics (the barometric formula) $dp = -\rho g dz$ (ρ is the density, g is the acceleration of the force of gravity, z is the altitude); and the Maxwell law is satisfied for the velocity distribution of the particles:

$$dn(v_x) = \left(\frac{1}{2\pi mkT} \right)^{1/2} n e^{-\frac{mv_x^2}{2kT}} dv_x$$

($dn(v_x)$ is the number of particles whose velocity components along the x axis are given from v_x to $v_x + dv_x$; m is the mass of the particle).

With local equilibrium, the properties of the atmosphere may vary both in space and in time.

Furthermore, as happens much more frequently, a partial equilibrium in the atmosphere is observed for which statistically balanced distributions exist only for given kinds of particles in certain given intervals of time.

So, in the case of a partial local thermodynamic equilibrium, in particular for electrons, ions and molecules, balanced "electron", "ion" and "molecular" temperatures are established that are not equal to one another

/71

$$\frac{m_e v_e^2}{2} = \frac{3}{2} kT_e; \quad \frac{m_i v_i^2}{2} = \frac{3}{2} kT_i; \quad \frac{M v_m^2}{2} = \frac{3}{2} kT_m$$

where m_e , m_i , M , v_e , v_i , v_m are the masses and velocities of the electron, ion and molecule, respectively; T_e , T_i and T_m are their kinetic temperatures.

At high altitudes where the atmospheric density is low and the mean free path is long (Table 1), the gas is not a statistical continuum and as a result of this the barometric formula in the ordinary form given above does not describe the altitude distribution of the particles [1].

TABLE 1

h, km	p, torr	$l, \frac{\text{cm}}{p}$ ($l \approx \frac{3.4 \cdot 10^{-8}}{p}$)	ω, sec^{-1} ($\omega \approx v_{av}/l$)
0	760	$6.7 \cdot 10^{-8}$	$7 \cdot 10^6$
40	1	$3.4 \cdot 10^{-8}$	10^7
90	10^{-2}	3.4	10^4
200	10^{-3}	$3.4 \cdot 10^4$	50
500	10^{-5}	$3.4 \cdot 10^6$	10^{-2}

In this case the equation of hydrostatics has the following approximate form:

$$\frac{\partial}{\partial z} \left\{ p - 0.64e^3 \left[\frac{\partial^2 p}{\partial z^2} - \frac{1}{p} \left(\frac{\partial p}{\partial z} \right)^2 \right] \right\} = pg.$$

This equation is transformed into the ordinary barometric formula when the supplementary term for the absolute value is much smaller than the base term, i.e.,

$$0.64e^3 \left[\frac{\partial^2 p}{\partial z^2} - \frac{1}{p} \left(\frac{\partial p}{\partial z} \right)^2 \right] \ll p.$$

Computations show that up to an altitude of 300 - 500 km, depending on solar activity, we can use the ordinary barometric formula.

The altitude distribution of the particles and the photochemical reactions (ionization, dissociation, recombination, etc.) exert an appreciable influence on the temperature of the upper atmosphere. As a result of the

reactions which take place in the upper atmosphere under the influence of energy sources, the distribution of particles in the atmosphere, just as in the case where there is no continuum, is not described by the ordinary barometric formula.

Analysis of the system of hydrodynamic equations [2], which allows for the elastic processes in the atmosphere (ionization, dissociation, recombination, etc.) leads to the necessity of introducing into the barometric formula values of the effective temperature $T^* = T - A(Q/\rho^2)$, where Q is the difference between the absorbing radiation and that emitted as a result of the energy from the translational degrees of freedom of the molecules, ρ is the atmospheric density,

$$A = \frac{3}{16} \frac{m^2}{\sigma^2 \sqrt{\pi} \sqrt{kT/m}}$$

σ is the diameter of the molecule. From the computations it follows that, depending on the state of the atmosphere, the effective value of the temperature is equal to the usual value of the temperature up to altitudes of 400 - 600 km, and consequently, up to these altitudes the ordinary barometric formula is valid.

CONDITIONS OF FLOW AROUND A BODY

Since the atmospheric density differs at different altitudes, when an object moves in the atmosphere the character of the flow around it varies from the conditions of a dense atmosphere (continuum) to that of a free-molecular flow.

/72

Four regions of flows are differentiated in the modern theory of rarefied gases: a dense atmosphere when the mean free path is much shorter than the characteristic dimension of the body; a flow with glide when the mean free path is comparable with the characteristic dimension of the body; an intermediate region with the mean free path longer than the characteristic dimension of the body; when the mean free path is

much longer than the characteristic dimension of the body, the conditions of free-molecular flow are satisfied.

Under the conditions of a dense atmosphere, interaction of the atmospheric gas with the instrument installed on a moving object takes place through the boundary layer surrounding the body; with a free-molecular flow, the atmospheric gas is directly connected with the gas in the cavity of the instrument. The dimensions of the pronounced thin boundary layer in a dense atmosphere increase in proportion to the increase in the mean free path; in the free-molecular region the boundary layer disappears.

Before we examine what laws govern the interaction of gas in the atmosphere with the gas inside the instrument, let us pause to look at several special questions associated with the movement of a rocket (satellite), instrument in the upper atmosphere.

SPECIAL QUESTIONS

Gas Generation of a Rocket (Satellite), Sorption and Desorption of Walls. A rocket (satellite) lifts a large amount of gas into the upper atmosphere that forms a cloud around the rocket. This cloud dissipates with time. The time of such a degassing will depend upon the material from which the rocket is made and the air tightness of the unit. Furthermore, the degree to which the rocket gas liberation influences the instrument response will depend on the location of the instruments on the vehicle relative to the sources of the gas.

As a rule, pressure gauges and mass-spectrometers are not installed on the rocket itself, but in a container which is separated from the rocket at an assigned altitude.

The container or the satellite (external part) is made of good, vacuum-

pure materials with a low inherent vapor pressure and a high rate of degassing, such as, for example, metals and porcelain.

Under predetermined experimental conditions, this permits measuring such low values as 10^{-9} - 10^{-10} torr. But at these pressures the sorption and desorption of the structural units and the walls of the measuring instruments, preliminarily degassed, may influence the accuracy of the measurements. The pressure inside the instrument follows change in the atmospheric pressure. If the range of pressure variation for a certain time is very high, then the films which form on the walls of the structural units inside the measuring instruments will not be in equilibrium with the pressure inside the instrument.

Let us look at such an example.

A plate is placed in a nitrogen atmosphere with varying pressure. In the case of physical absorption the kinetics of the absorption is described by Langmuir's equation:

$$v_0 \frac{d\theta}{dt} = \alpha \mu (1 - \theta) - v\theta,$$

where $\mu = N_A p / \sqrt{2\pi M k T}$ is the number of molecules striking the surface per $1 \text{ cm}^2/\text{sec}$; $v = v_0 e^{-\Delta H/kT}$ is the number of molecules vaporizing per 1 sec per 1 cm^2 of surface, fully covered with adsorption molecules; v_0 is the number of gas molecules in the dense monomolecular layer per 1 cm^2 of surface; α is the coefficient of accommodation; θ is the amount of the surface covered with molecules at time t ; ΔH is the heat of adsorption; N_A is the Avogadro number; k is the Boltzmann constant.

/73

The recovery time for equilibrium between the film and the gas depends on the pressure, the kind of gas, and the temperature of the plate and the gas. At a pressure of $p = 10^{-4}$ torr equilibrium is established in 0.12 sec, $\theta = 1$; at a pressure of 10^{-7} torr equilibrium is established in 99.42 sec,

$\theta = 0.939$ (Table 2) (temperature of the plate and gas is equal to 300° K , coefficient of accommodation $\alpha = 1$). As is clear from the table, the state of the surface of the plate is constant for pressures of $10^{-4} - 10^{-7}$ torr ($\theta \approx 1$); therefore in this pressure range, the monomolecular film can not influence the accuracy of the pressure measurement. At lower pressures, especially at pressures less than 10^{-9} torr, the influence of the film on the accuracy of the measurements may be substantial and will depend on the design of the instrument and the trajectory of the unit.

TABLE 2

p, torr	t, sec	θ	p, torr	t, sec	θ
10^{-4}	0.12	1	10^{-7}	99.42	0.939
10^{-5}	1.2	0.999	10^{-8}	727.08	0.807
10^{-6}	12.345	0.993	10^{-9}	1532.99	0.184

Spontaneous Ionization of the Atmosphere. In the ionosphere the concentrations of ions and electrons may have values on the order of 10^6 cm^{-3} . If an object moves in the ionosphere at a velocity of 8 km/sec, a current of $\sim 10^{-7} \text{ A}$ may be induced in the measuring instrument installed on board, (with a diameter of the intake orifice of about 1 cm).

As a result of this, the measurement of neutral particle concentrations, whose equivalent currents may have values of 10^{-11} A , involves considerable difficulty.

"Impact" Ionization, Dissociation, Displacement of Atoms from a surface. Now let us look at the group of phenomena associated with studying the atmospheric properties on a moving body. As a result of the impacts of particles about the surface of the body, generally speaking they may dissociate and ionize and furthermore, the atoms may be displaced from the surface.

In rocket experiments the effectiveness of these processes is low. Comparison of the energy of the moving particles and the ionization poten-

tials shows that this energy is insufficient for ionization. (At a rate of speed of approximately 8 km/sec the energy of motion for nitrogen particles is about 10 eV and for atomic oxygen about 5.5 eV, and the ionization potentials of these gases are 15.51 eV and 13.55 eV, respectively) Although the energy of sublimation of the majority of metals (on the order of 3 - 4.5 eV) is less than the energy of motion of the particles at the velocity of the satellite, and consequently it is possible for the atoms to be expelled, research has shown that sublimation becomes significant only for energies of the particles striking the surface on the order of hundreds of electron volts.

Photoemission. Photocurrents are induced by direct ultraviolet solar radiation. The magnitude of the photocurrent per square centimeter of irradiated surface is approximately the same ($\sim 10^{-8}$ A) for all conducting surfaces in the region of the hard ultraviolet ($\lambda < 1500 \text{ \AA}$). /74

Thus, the entire series of processes, i.e. gas separation, spontaneous ionization and photoemission, must be taken into account in setting up experiments in the atmosphere. The design of the instruments and the units must be such that they will have no effect on the accuracy of the measurements.

So, in order to avoid errors in the measurements caused by the presence of ions and electrons in the atmosphere, at the inlet of the instrument a special trap-condenser is installed which prevents charged particles from entering the measuring cavity of the instrument.

BASIC INTERPRETATIONAL RELATIONSHIPS

At the present time the theory of the movement of gas and flow around a body has been developed for the region of a dense atmosphere and free-molecular flow. For the intermediate region only specific problems

have been solved. For the dense atmosphere and free-molecular flow, fairly strict expressions have been obtained which relate the characteristics of the atmosphere to those of the gas inside the measuring instrument. Let us look briefly at them.

Dense Atmosphere. The pressure and temperature on the surface of a streamlined body at a given point (p_e , T_e) in the case of nonadiabatic deceleration are related to the pressure and temperature of the unperturbed atmosphere (P_{atm} , T_{atm}) by the following expressions [3, 4]:

$$p_e = p_{atm} \left(1 + \frac{\gamma}{2} s M_{atm}^2 \right),$$

$$T_e = T_{atm} (1 + 0.2r M_{atm}^2),$$

where $s = \frac{p_e - p_{atm}}{1/2 \rho_{atm} u^2}$ is the coefficient of pressure recovery; $r = \frac{T_e - T_{atm}}{1/2 u^2 / c_p}$ is the thermal coefficient of restitution; u is the velocity of the body relative to the gaseous atmosphere at a given point; M_{atm} is the Mach number for the unperturbed atmosphere; $\gamma = \frac{c_p}{c_v}$ — is the relationship between heat capacity at a constant pressure (c_p) and constant volume (c_v). Between the pressure and the temperature on the surface and inside the instrument an equilibrium is established that can be written in the following form:

$$\frac{p_{pg}}{p_e} = \left(\frac{T_{pg}}{T_e} \right)^b$$

where

$$b = \frac{1.9 (l/a)^2}{1 + 3.5 (l/a) + 3.8 (l/a)^2}$$

(l is the mean free path inside a tube of radius a). Appropriate substitution leads to the basic equation:

$$p_{atm} = p_{pg} \left[\frac{T_{atm} (1 + 0.2r M_{atm}^2)}{T_{pg}} \right]^b \cdot \frac{1}{(1 + \gamma/2 \cdot s M_{atm}^2)}.$$

Based on the measured values of the pressure and temperature inside the instrument, if we use the barometric formula $dp_{\text{atm}} = -\rho g dz$, by the method of trial-and-error we can determine the values of the pressure and temperature of the atmosphere P_{atm} and T_{atm} .

Free-Molecular Flow ($U/R \gg 1$) [5]. Let us examine the simplest case: the cavity of the pressure gauge is connected with the atmosphere through a diaphragm with radius r (with no connection tube). Let us remember that the number of particles incident per unit area per unit of time from the oncoming flow will be

/75

$$n = \frac{Nv}{2\sqrt{\pi}} \chi(\beta),$$

where N is the number of particles per unit volume of the unperturbed atmosphere; v is the most probable velocity of thermal movement of the particle; m is its mass; $\beta = (u/v) \sin \theta$; $\chi(\beta) = e^{-\beta^2} + \sqrt{\pi}\beta [1 + \Phi(\beta)]$;

$$\Phi(\beta) = \frac{2}{\sqrt{\pi}} \int_0^\beta e^{-s^2} ds;$$

θ is the angle between the current vector and the plane of the diaphragm.

Let the satellite move at a velocity u in the atmosphere with concentration N , pressure p and temperature T . The characteristics of the gas in the cavity of the pressure gauge are designated by N_1 , P_1 , T_1 and v_1 . Change in pressure inside the pressure gauge W for the time dt , produced by the flow of particles into it $nsdt$, is equal to

$$\frac{kT_1}{W} nsdt = \frac{Nv}{2\sqrt{\pi}} \chi ds \frac{kT_1}{W}.$$

In this same period, the flow of particles from inside the pressure gauge $\frac{N_1 v_1}{2\sqrt{\pi}} s dt$ lowers the pressure in the pressure gauge by $\frac{N_1 v_1}{2\sqrt{\pi}} s dt \frac{kT_1}{W}$, where

s is the area of the pressure gauge orifice, and v_1 is the most probable velocity of the particles in the pressure gauge. At equilibrium these two currents are equal. And, consequently,

$$N = N_1 \frac{v_1}{v\chi} , \quad p = p_1 \frac{T_1 v_1}{T v} \frac{1}{\chi}$$

when $\beta \geq 1, 2$ $\chi(\beta) \approx 2 \sqrt{\pi} \beta$ $N = N_1 \sqrt{\frac{kT_1}{2\pi m}} \frac{1}{u \sin \theta}$,

$$p = p_1 \sqrt{\frac{k}{2\pi m}} \frac{T}{\sqrt{T_1} u \sin \theta} , \quad N = p_1 \sqrt{\frac{1}{2\pi m k}} \frac{T}{\sqrt{T_1} u \sin \theta} .$$

when $\theta = 0$, $\chi(\beta) = 1$ and $N_1 = N \sqrt{T_1/T}$, $p = p_1 \sqrt{T/T_1}$.

If the pressure gauge has a connecting tube, it is necessary to allow for the resistance of the tube to the input and output flows. The velocity of these flows will be different and consequently the computational formula must be changed [6]:

$$N = N_1 \frac{v_1}{v\chi(\beta)} \frac{k(0, l/r)}{k(\beta, l/r)}$$

where $k(\beta, l/r)$, $k(0, l/r)$ is the Clausing coefficient, which characterizes the conductivity of the tubes for a tube of length l and radius r in the presence and absence of a flow.

In these discussions we have assumed that the coefficient of accommodation of the gas in the pressure gauge is near unity and the coefficient of recombination is small. The gas inside the pressure gauge has one temperature (temperature of the wall of the pressure gauge) and the composition of the gas both inside the pressure gauge and in the atmosphere is the same. In the general case for high velocities of the instrument it is necessary to allow for the influence of recombination of atoms in the instrument, selection by masses and density gradient inside the instrument [7, 8].

In selecting a formula for the free-molecular flow we made the assumption /76 that the local velocity distribution of the molecules in the atmosphere obeys Maxwell law.

In a nonequilibrium atmosphere the local velocity distribution of the molecules can not be described by the Maxwell function and in this case the formula given can not be valid.

At the same time if the rate of motion of the instrument is much greater than the velocity of the thermal motion of the molecules, i.e., $\beta \geq 1.2$, then the density in the cavity of the instrument will not depend on the type of velocity distribution function of the molecules in the atmosphere.

If $\beta \sim 1$ or $\beta < 1$, then in the case of atmospheric nonequilibrium the interaction of the gas in the atmosphere with the gas in the instrument will have a different character and the above formula can not be used [9].

From these formulas it is clear that in determining the concentration or the density of the atmosphere with respect to the pressure and temperature of the gas, measured in one pressure gauge, we must make assumptions as to the temperature and composition of the atmosphere. Analysis of the dependence of these formulas on the values of the temperature and molecular weight of the atmosphere led to the following conclusion: the greater the velocity of movement of the instrument, the less will the results of the pressure gauge measurement depend on the temperature and composition of the atmosphere [10]. Thus, in the experiments on the satellites, as a result of the assumptions on temperature and composition of the atmosphere, we find an additional error in determining the density and concentration of particles of the atmosphere on the whole by several percent.

When two instruments (or one scanner) are installed on a vehicle, not only is the density determined but the temperature of the

atmosphere as well.

In the simplest case if one of the instruments is parallel to the flow ($\beta \geq 1.2$) and the other is in an effusion state, then as is obvious from the system of two equations:

$$N = p_1' \sqrt{\frac{1}{2\pi mk}} \frac{1}{\sqrt{T_1' u \sin \theta}} \quad (\beta \geq 1, 2) \text{ first instrument;}$$

$$N = N_1'' \sqrt{\frac{T_1''}{T}} \quad (\text{effusion}) \text{ second instrument;}$$

From the pressure, density and temperature measured in the pressure gauges we can determine both the concentration of particles in the atmosphere N and their temperature T . The characteristics of the atmosphere can be determined with slightly greater accuracy by using mass-spectrometers.

We have examined a number of questions involving interpretation of the readings of instruments installed on rockets and satellites. Let us look at the conditions of the experiments, equipment and their requirements.

EQUIPMENT

A rocket (satellite) moves at tremendous speed, undergoing in the propelled part of the flight high accelerations and vibrations in a wide frequency range. The weight, dimensions and power of the scientific equipment in the rocket experiment are always limited. Furthermore, rocket borne equipment used for measuring pressure must be of quick-response type, possess great stability, have small dimensions and operate automatically.

Since it is fundamentally impossible for any pressure gauge to provide measurements of pressure in the required wide range (for example, for the altitude range of 40 - 500 km, from 1 to 10^{-9} torr), a whole series of pressure gauges and the corresponding amplifier equipment was developed. We have

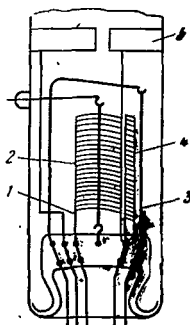


Figure 1. Ionization Pressure Gauge.

1. Accelerating Grid - Anode; 2. Collector; 3. Filament - Cathode;
4. Grid for Stabilization of Emission; 5. Trap.

used membrane, thermal, thermoionization and magnetic electrical discharge pressure gauges. In particular in the investigations on rockets up to altitudes of approximately 500 km in the 1958 experiments, thermoionization and magnetic electrical discharge pressure gauges were used with a measurement range of $2 \cdot 10^{-2}$ - $2 \cdot 10^{-6}$ torr and $1 \cdot 10^{-5}$ - $1 \cdot 10^{-9}$ torr, respectively. These pressure gauges differ substantially from their laboratory prototypes.

Let us briefly discuss the design of Soviet and foreign ionization pressure gauges used for investigation of the atmosphere above 100 km.

In the pressure gauge we have a filament, a cathode, a grid for stabilizing the current of emission, an anode and a collector (Figure 1). The anode is made in the form of a cylindrical grid, the collector in the form of a filament. With such a design the collector has a minimal irradiating surface, thus permitting a reduction in parasitic collector current. (This current is induced by photoemission from the collector produced by soft x-rays which arise when electrons emitted by the cathode are moderated by the grid material.) At a given pressure, the value of the ion current depends on the value of the emission current. To ensure no ambiguity in the measurements, the emission current is stabilized. In particular, the stabilization is accomplished using a supplementary grid located near the cathode in front of the anode. The grid has, with respect to the cathode, a small negative potential whose value is automatically regulated in the operating process of the instrument. Furthermore, the emission current during the experiment is registered.

At the input of the pressure gauge there is a special condenser by means of which the charged particles entering the pressure gauge from the atmosphere are removed from the discharge gap. The current of the pressure gauge at a fixed temperature is proportional to the number of particles per unit volume. We used direct current amplifiers to amplify the currents from the pressure gauges. The values of the output voltages from the amplifiers during the experiment are transmitted to Earth using radiotelemetry.

The pressure gauges are placed outside the unit, the amplifiers and the other equipment inside in an air tight compartment. They are electrically connected by a special hermetically sealed coupling. A special screen shields the electrode leads from charged particles. For the purpose of decreasing gassing in the experiments using rockets, the instruments were installed in containers which were separated from the rocket at the moment of the measurements; the external units, the design of the containers, the satellites on which the pressure gauges were installed were all made of materials possessing a good desorption rate and minimum vapor pressure. The pressure gauges were first degassed and evacuated. The pressure gauges were opened with the aid of separating equipment in the upper atmosphere at an assigned altitude.

To study the atmospheric properties up to an altitude of approximately 100 km, we used meteorological rockets; above this altitude we used geophysical rockets and satellites. The schematic of a standard meteorological rocket is shown on Figure 2. Thermal and membrane pressure gauges and resistance thermometers are placed in the spike. To allow for the effect of solar radiation incident on the open filaments of the resistance thermometers, bolometers were installed; auxiliary thermometers were installed for measuring the temperature on the walls of the pressure gauges. Behind the spike are three compartments of the nose cone of the rocket with measuring equipment. The nose cone of the rocket is recovered by use of a

/78

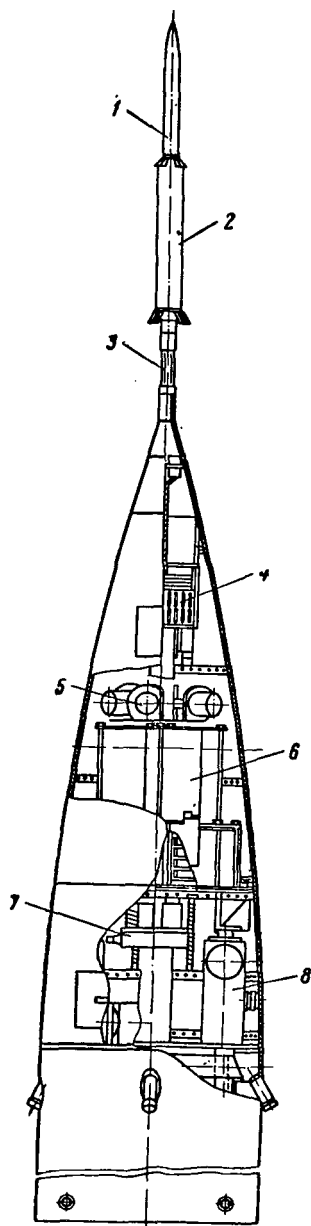


Figure 2. Schematic of a Meteorological Rocket.

1. Heat Pressure Gauge; 2. Resistance Thermometer; 3. Bolometer; 4. Commutator; 5. Membrane Pressure Gauge; 6. Accumulator Block; 7. Photo-equipment; 8. Transmitter.

parachute. The responses of these instruments are transmitted to Earth telemetrically.

The high-altitude geophysical automatic station, HAGAS, (Figure 3) is a hermetically sealed metal sphere with a diameter of about one meter in which a large complex of measuring equipment is installed (the weight of the HAGAS is about 360 kg) [10].

During ascent the station is located in the nose cone of the rocket and covered with two shielding half-cones. At an assigned altitude the half-cones open and the station is separated from the rocket. The movement of the station is stabilized according to three axes relative to the sun.

Figure 4 shows the schematic of an artificial earth satellite, in which equipment for measuring variations in density in the upper atmosphere was installed for the first time.

VARIATIONS IN ATMOSPHERIC DENSITY

In the past ten years the launching of a large number of rockets and

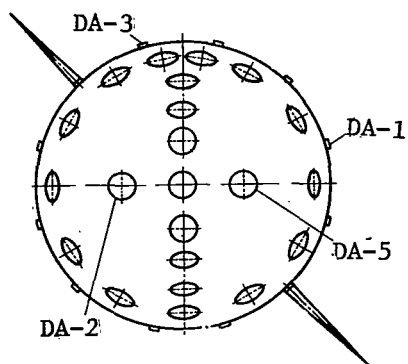


Figure 3. Schematic of the High-Altitude Geophysical Automatic Station, HAGAS.

DA-1, DA-2, DA-3, DA-5 are the Ionization and Magnetic Pressure Gauges.

/79

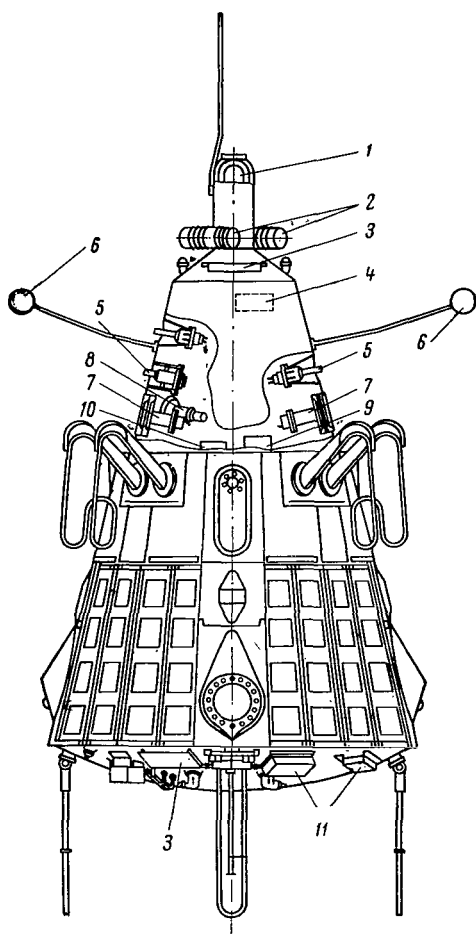


Figure 4. Schematic of the Third Soviet Artificial Earth Satellite.

1. Magnetometer; 2. Photomultiplier for Registering Corpuscular Radiation from the Sun; 3. Solar Batteries; 4. Instrument for Registering Photons; 5. Magnetic and Ionization Pressure Gauges; 6. Ion Traps; 7. Electrostatic Fluxmeters; 8. Mass-Spectrometers; 9. Instrument for Registering Heavy Nuclei in Cosmic Rays; 10. Instrument for Measuring the Intensity of Primary Cosmic Radiation; 11. Sensing Element for Registering Micrometeors.

satellites has permitted determination to be made of the atmospheric density at various altitudes, latitudes, at different times of the day, the year and at different levels of solar activity.

At altitudes below 150 km, the basic results were obtained from measurements using pressure gauges and by the method of falling spheres; above 150 km, by the deceleration of satellites. Analysis and comparison of the variations in atmospheric density above 150 km led to establishment of a correlation between density and solar and geomagnetic activity. Periodic variations were found in the density with a daily, monthly (27 - 28 days), semiannual, 11-year, etc. period. Besides the periodic variation there also exist non-periodic variations in density, depending on random perturbations on the sun. A latitude effect is observed [11].

With increase in solar activity (ultraviolet radiation) the atmospheric density is increased and the rate of increase in density grows with altitude. For example, with a two-fold increase in solar activity (it is customary to take solar radio emission on a wavelength in the range of 10 - 20 cm as the characteristic) the atmospheric density at an altitude of 200 km is increased by approximately two times and at an altitude of 500 km by approximately four times.

/82

In the course of a day the density undergoes very strong variations. At a given altitude with the same solar activity the density has the greatest value of 1600 hours. The amplitude of variation in density increases with altitude (Figure 5) [12]. According to the data obtained during years of maximal solar activity, at an altitude of 200 km the density varies from day to night by approximately 30%; at an altitude of 800 km, by one order. The diurnal effect during years of minimal solar activity up to an altitude of 500 km is slightly higher. At an altitude of 200 km during the day the density varies by approximately two times [13]. At the same time above 500 km the amplitude of the diurnal density variations is decreased and at an altitude of 1000 km is approximately equal to the diurnal variations at an altitude of 200 km. Of all periodic variations, the variations in density

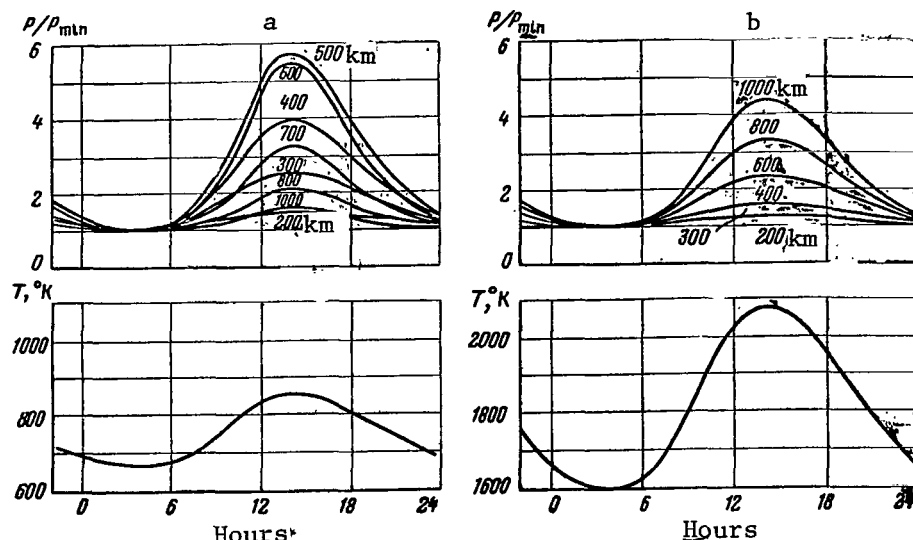


Figure 5. Diurnal Variations in Density at Various Altitudes and Temperature of the Exosphere during Low (a) and Very High Solar Activity (b).

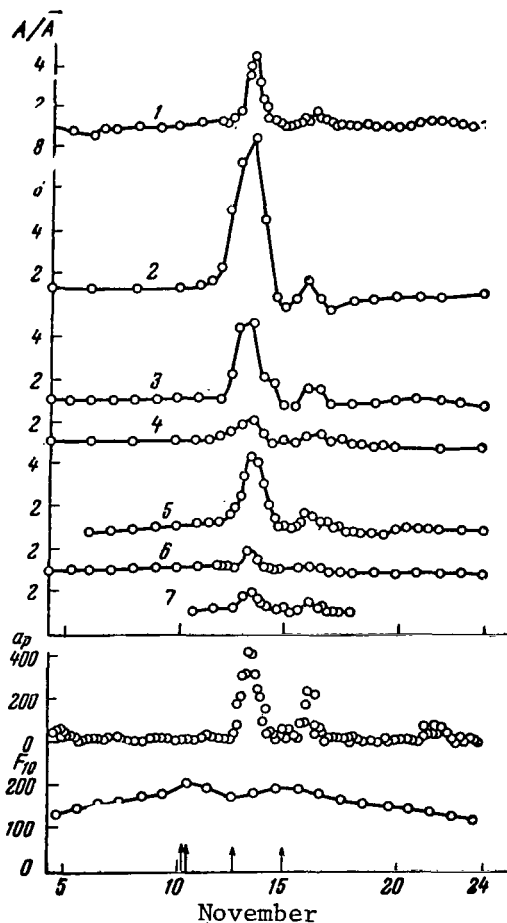


Figure 6. Variation in Deceleration of Satellites (Density) During Increased Geomagnetic Activity From 5 to 24 November, 1960.

Along the ordinate axis are plotted: The Ratio A/\bar{A} , where A are instantaneous accelerations; \bar{A} is the mean value; a_p is the index of the geomagnetic activity; F_{10} is the current of radio-emission at wavelength $\lambda = 10.7$ cm in units of $10^{-22} \text{ W} \cdot \text{m}^{-2} \cdot \text{Hz}^{-1} \cdot \text{sec}^{-1}$. The Arrows Denote Cases of the Observation of Class 3^+ Flares on the Sun. 1. 1121 km; 2. 650 km; 3. 564 km; 4. 528 km; 5. 415 km; 6. 350 km; 7. 205 km (Altitude of Perihelion).

during the day, and variation with solar activity, are the greatest in amplitude.

The variation in density correlated with the variation in geomagnetic activity may also be significant. For instance, according to the data in [14], with a strong increase in geomagnetic activity ($a_p \sim 400$) at an altitude of 650 km the density was increased by approximately 5 times (Figure 6).

Variations in temperature have the same character as do the variations in density, i.e. the variations in atmospheric temperature have a diurnal, monthly, semiannual 11-year periodicity and depend on solar activity, geomagnetic effect and on latitude. Figure 5 shows the diurnal variations in the temperature of the exosphere for the periods of minimum and maximum solar activity. The temperature of the exosphere increases with increase in solar activity (Figures 7, 8); by day its value is greater than by night [12, 15].

The results of several rocket experiments give a basis for assuming that apparently above 100 km the temperature (composition) does not vary monotonically but rather there is a temperature (composition) inversion [16] (Figure 9). This result requires additional study.

It is obvious even from a quite superficial discussion that the variations in density and temperature of the atmosphere have a complex character. As a result of this in setting up experiments for studying variations in structural parameters it is desirable to differentiate between these and other effects. For example, a satellite with a circular orbit reveals the diurnal variations of parameters at a given altitude to the best advantage. Rocket experiments permit us to obtain a vertical cross section of the atmosphere at a given geophysical point with constant values of the solar activity, time of day, etc. The widely used method of satellite deceleration gives averaged characteristics of the atmosphere in time and altitude (with an increase in the accuracy of determining the trajectory of the moving

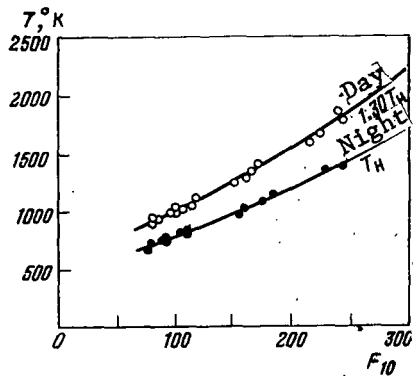


Figure 7. Temperature of the Exosphere (Night and Day) as a Function of the Flux of Solar Radio Emission F_{10} .

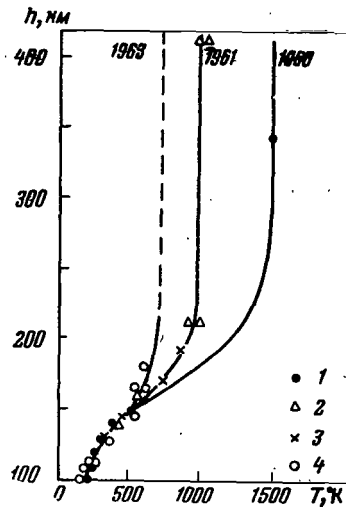


Figure 8. Temperature of the Atmosphere According to Experimental Data Obtained by Blamont and Lory Using Clouds of Sodium and Potassium.

1. March - December 1960; 2. September - December 1961; 3. June 1962; 4. May 1963.

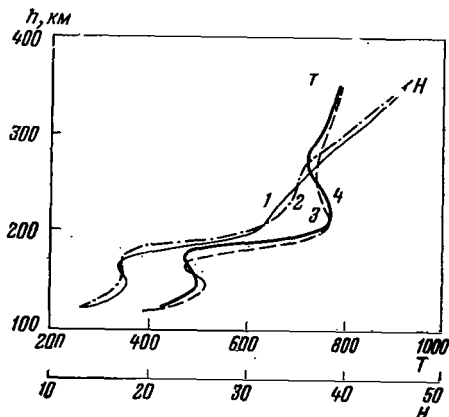


Figure 9. Altitude of the Uniform Atmosphere and Temperature of the Atmosphere June 18, 1963 (Pressure Gauges).

- 1, 3. First Approximation; 2, 4. Second Approximation.

satellite, the interval of averaging is decreased). On the other hand use of quick-response instruments -- pressure gauges and mass-spectrometers -- makes possible the study of the detailed structure of variations in atmospheric parameters. Only by using the most diverse methods of research can we obtain complete information on the properties of the upper atmosphere and their variations.

REFERENCES

1. Kokin, G. A. Trudy TsAO, (Reports of the Main Astronomical Observatory), No. 29, 1960, p. 74. /83
2. Ivanovskiy, A. I. Trudy TsAO, No. 40, 1962, p. 5.
3. Shvidkovskiy, Ye. G. Trudy TsAO, No. 29, 1960, p. 5.
4. Alekseyev, P. P. et al. Meteorologiya i gidrologiya, No. 8, 1957, p. 3.
5. Danilin, B. S. et al. UFN, Vol. 13, No. 1b, 1957, p. 205.
6. Ivanovskiy, A. I. V Sb: Issledovaniye kosmicheskogo prostranstva, (In: Research in Outer Space), Nauka Press, 1965, p. 56.
7. Ivanovskiy, A. I. and A. I. Repnev. V Sb: Issledovaniye kosmicheskogo prostranstva, (In: Research in Outer Space), Nauka Press, 1965, p. 51.
8. Repnev, A. I. Trudy TsAO, No. 29, 1960, p. 66.
9. Repnev, A. I. and A. I. Ivanovskiy. Trudy TsAO, No. 40, 1962, p. 67.
10. Mikhnevich, V. V., Ye. N. Golubev and Yu. N. Parfianovich. Kosmicheskiye issledovaniya, Vol. 3, No. 3, 1965, p. 457.
11. Mikhnevich, V. V. Iskusstvennyye sputniki Zemli, Press of the Academy of Sciences, USSR, No. 7, 1963, p. 31.
12. Jacchia, L. G. COSPAR International Reference. Atmosphere, Amsterdam, 1965.
13. King-Hele, D. G. Space Res., No. 7, 1967.
14. Jacchia, L. G. Space Res., No. 2, 1961, p. 747.
15. Blamont, J. E. and M. L. Lory. Space Res., No. 5, 1965, p. 1137.
16. Mikhnevich, V. V. V Sb: Issledovaniye kosmicheskogo prostranstva, (In: Research in Outer Space), Nauka Press, 1965.
17. Mikhnevich, V. V. and I. A. Khvostkov. Izvestiya AN SSSR, seriya geofiz., No. 11, 1957, p. 1394.

RESULTS OF MULTI-YEAR OBSERVATIONS OF THE OUTER IONOSPHERE
UTILIZING SIGNALS FROM SATELLITES

K. H. Schmelovsky

Regular observations of the signals coming from artificial satellites are carried out at the K  lungsborn observatory. These observations yield useful information on the behavior of, and changes in, the outer ionosphere. The paper presents a detailed description of techniques used for observing the signals and processing the results. The observed results reveal how the total number of electrons present in a column of the ionosphere depends on solar activity, they also help to investigate the latitude anomaly of N_e and the diurnal variations of N_e both during maximum and minimum activity. The analysis of experimental data also allows the electron temperature to be determined. It has been found that in case of low solar activity, T_e is 1.5 - 2 times as high as the temperature of neutral particles, whereas in case of high solar activity, T_e may reach 3000° K. A calculation has also been made of the mean rate of electron formation during the day time from the maximum period of solar activity to the minimum one. Similar calculations have been made for the flux of ionizing radiation as well.

Signals from satellites have been observed regularly at the K  lungsborn /84 observatory since the time that "Sputnik-3" was launched. The artificial earth satellite series "Kosmos" were used as well as the "Transit-4a" and "Explorer XXII" (S-66) .

Faraday fading of the signals from "Sputnik-3" was investigated at 20 MHz and from "Transit-4A" at 54 MHz. Faraday fading from the "Explorer-XXII" was registered at frequencies of 20, 40, and 41 MHz as well as the

phase shift (difference in Doppler frequency shift) between coherent frequencies of 20 and 40 MHz. Basically we investigated the total number of electrons

$$N_{\text{tot}} = \int_0^{h_s} N_e dh$$

(h_s is the orbital altitude of the satellite). Furthermore we have developed methods for determining other parameters of the electron density distribution. For this we used the differences in Faraday fading at various altitudes and compared the measurements of satellite signals with measurements from ionospheric probes.

Figure 1 shows an example of registering signals from the satellite "Explorer XXII".

For the registration we used a device with automatic frequency control which was necessary to compensate the Doppler frequency shift of the signals received. The width of the pass band of the receiver was 100 Hz. At the output of the receiver was a signal converted to a frequency of 80 Hz. This low frequency was registered directly. Furthermore, a signal from the 20 MHz channel was doubled and mixed with a signal from the 40 MHz channel. The difference between these two frequencies is shown on diagram 4 (Figure 1). A similar operation was carried out also with the 40 MHz signal shifted by 90° (diagram 5). The signals of the difference frequencies are a two-phase alternating current which is fed to a synchronous motor which drives a potentiometer. The voltage at the output of the potentiometer is a time integral of the Doppler differential. In addition to this the device gives a registration of the complete Doppler frequency shift of the signal received (Figure 2). This registration obviously is not adequate for a precise measurement of the trajectory; it may only be of help in the case when no other information sources are available concerning the precise elements of the trajectory.

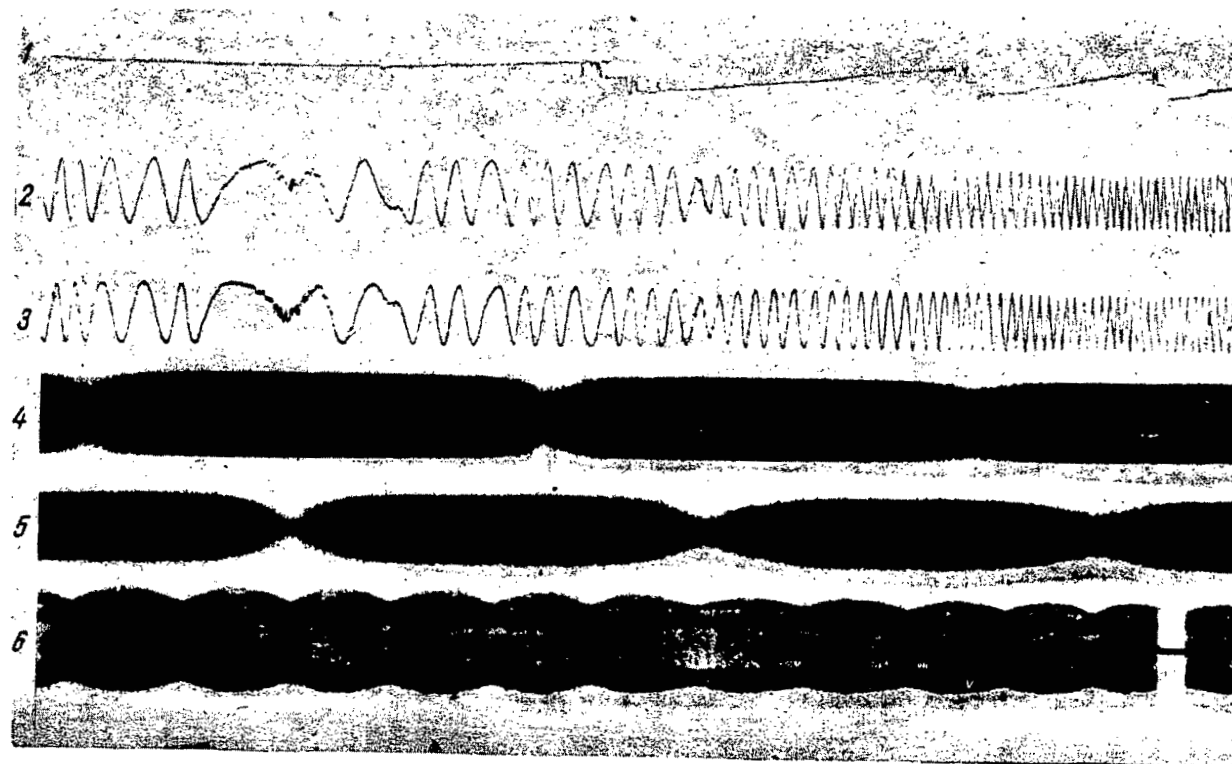


Figure 1. Examples of Registering Signals from the Satellite "Explorer XXII".
 1, 2 and 3. Faraday Fadings at Frequencies of 20, 40, 41 MHz, Respectively;
 4 and 5. Difference in Doppler Frequency Shifts Between Coherent Frequencies
 of 20 and 40 MHz; 6. Time Integral of the Difference in Doppler Frequency
 Shift.

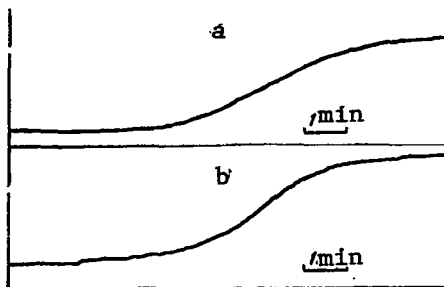


Figure 2. Example of Registering Complete Doppler Frequency Shift of the Signal Received on May 10, 1963 at a Frequency of 54 MHz.

a. Beginning 0845; b. Beginning 1136. Local Time.

If we compute the number of transitions through zero in differential Doppler registration, figured from the moment when the phase difference is minimal, and write the results in time, we obtain the curve $I(t)$ which gives the time behavior of the difference in phase paths between the coherent frequencies expressed in wavelengths. Under favorable conditions we can of course directly use the curve of registration shown on diagram 6 (Figure 1). But the difference in phase paths

can be determined only with an accuracy up to a constant term. Then we have

$$I(t) + C_D = N_{\text{tot}} G(t), \quad (1)$$

and

$$G(t) = \frac{40.3}{c f_1} n \left(1 - \frac{1}{n^2} \right) \sec \varphi.$$

Correspondingly, if we compute the number of minima in the registration of Faraday fading, we can obtain the time behavior of the Faraday rotation $K(t)$. The angle of rotation is in units of π . Then

$$K(t) + C_F = N_{\text{tot}}(t) \cdot F(t), \quad (1')$$

and

$$F(t) = \frac{2.26 \cdot 10^8}{c f^2} |L| \cos \theta \sec \varphi,$$

where f is the frequency, θ is the angle between the magnetic field of the

Earth and the direction of propagation, $|L|$ is the magnetic field strength, n is the ratio of coherent frequencies, t is the time figured from the moment of least distance of the satellite, ν is the angle between the vertical and the direction of propagation.

It is obvious that variation in N_{tot} with time does not reflect the true variation in the total number of electrons in time, but is determined mainly by the motion of the satellite.

Considerable difficulties in the interpretation are encountered in determining the constants C_D and C_F . If we assume only one registration, then one equation does not always suffice regardless of whether we proceed from the integral form according to equation (1) or (1') or directly use the fading frequency. This problem arises, for example, in analyzing the data from "Sputnik-3", "Transit-4A" and others. Thus, we must make additional assumptions. We use two different assumptions.

First Assumption. In a first approximation N_{tot} depends linearly on t . Thus,

$$N_{\text{tot}}(t) = N_{\text{tot}}(\bar{t}) + N'(\bar{t})(t - \bar{t}), \quad (2)$$

where \bar{t} is the moment of time corresponding to the middle of the registration to be computed. Then we find, for any three moments of time t_v , three equations such as

$$I(t_v) + C_D = F(t_v) N_{\text{tot}}(\bar{t}) + F(t_v)(t_v - \bar{t}) N'_{\text{tot}}(\bar{t}) \quad (2')$$

Second Assumption. The mean value of the total number of electrons in the course of the time under study is approximately equal to the total number of electrons at the moment of time \bar{t} . After transforming equation (1) and integrating with respect to time, we obtain the expression

/87

$$\bar{N}_{\text{tot}} = \frac{1}{t_2 - t_1} \int_{t_1}^{t_2} \frac{I(t) + C_D}{G(t)} dt. \quad (3)$$

If we denote

$$i_1 = \frac{1}{t_2 - t_1} \int_{t_1}^{t_2} \frac{I(t)}{G(t)} dt \quad \text{and} \quad i_2 = \frac{1}{t_2 - t_1} \int_{t_1}^{t_2} \frac{dt}{G(t)},$$

we find

$$\bar{N}_{\text{tot}} = i_1 + i_2 C_D. \quad (3')$$

If we use equation (1') one more time and substitute $t = \bar{t}$, we find

$$N_{\text{tot}}(t) = \frac{I(\bar{t}) + C_D}{G(\bar{t})}. \quad (4)$$

If we take these assumptions into consideration, we may assume the right-hand sides of equations (3) and (4) to be equal and find C_D . We obtain

$$C_D = \frac{i_1 G(\bar{t}) - I(\bar{t})}{1 - G(\bar{t}) i_2}. \quad (5)$$

A similar method can be used for computing the Faraday fading. After determining the additive constant we can of course very easily obtain the behavior of N_{tot} from equation (1) or (1').

To minimize errors resulting from these assumptions, the first method is used several times with different combinations of values of t_v and the highest and lowest values of the constant are discarded, after which the mean value of the remaining values is determined. In addition, the behavior of N_{tot} is determined independently by the second method. Depending on the results of the computations, it will be decided whether the mean value of N_{tot} from both values or from one value is to be used. All computations were carried out on a computer.

The best methods are chosen when there are several simultaneous registrations

(1) Let us assume registration of the Faraday fading at one frequency and registration of the differential Doppler shift at two frequencies. Since Equations (1) and (1') are linearly independent, then C_D and C_F may be jointly determined so as to give identical behavior of $N_{\text{tot}}(t)$ wherever possible.

According to the least squares method we find

$$\int_{t_1}^{t_2} \left[\frac{I(t) + C_D}{G(t)} - \frac{K(t) + C_F}{F(t)} \right]^2 dt = \text{Min}(C_D, C_F). \quad (6)$$

From this we have

$$A_{11}C_F + A_{12}C_D = B_1, \quad A_{21}C_F + A_{22}C_D = B_2,$$

where

$$\begin{aligned} B_1 &= \int_{t_1}^{t_2} \frac{1}{F} \left(\frac{I}{G} - \frac{K}{F} \right) dt; & B_2 &= \int_{t_1}^{t_2} \frac{1}{G} \left(\frac{I}{G} - \frac{K}{F} \right) dt, \\ A_{11} &= \int_{t_1}^{t_2} \frac{dt}{F^2}, & A_{22} &= \int_{t_1}^{t_2} \frac{dt}{G^2}; & A_{12} &= A_{21} = - \int_{t_1}^{t_2} \frac{dt}{F \cdot G}. \end{aligned} \quad (7)$$

(2) Let us assume registration of the Faraday fading on two close frequencies. In this case we can determine the difference in the angle of rotation accurate to integral multiples of π directly from the time shift in the minimum fading at both frequencies. Since the frequency dependence of the Faraday rotation is known theoretically, if we multiply the difference of the angles of rotation by a constant number, we then obtain directly the angle of rotation for a given moment. Because of ambiguity we find different solutions which may differ strongly if the difference in frequencies is small. In the majority of cases the proper solution may be found without fundamental difficulties.

/88

Furthermore, if we assume simultaneous registrations of the differential Doppler, then we can obtain a more reliable result, since a proper solution must also approximately correspond to the measured behavior of $I(t)$. In our method we nevertheless assume that the results from the Faraday fading must be multiplied by a factor of $\gamma \sim 1$, since for computation of the curves $F(t)$ we used values of the magnetic field at the surface of the Earth. This

factor is determined according to the method of least squares and gives an additional factor \bar{h} which is determined by the equation

$$\bar{h} = \frac{sh N_e dh}{s N_e dh} \quad (8)$$

and is related to γ by the equation

$$\bar{h} = R_0 (\sqrt[3]{V\gamma} - 1). \quad (9)$$

Finally we can still compare the Faraday fading at strongly differing frequencies (for example, 20 and 40 MHz) and obtain effects of a higher order. If we bear in mind the second order terms, the equation for the Faraday fading has the following form:

$$K(t) + C_F = F(t) N_{\text{tot}}(t) \left[1 + \frac{1}{2} x \left\{ s + (s-1) \tan V \left(\tan V - \frac{Z_1}{Z_L} \right) \right\} \right], \quad (10)$$

where Z_1 is the component of the magnetic field lying on the line of intersection between the plane of propagation and the plane perpendicular to the direction of propagation; Z_L is the component of the magnetic field in the direction of propagation:

$$x = 80.6 N_{\text{tot}} / f^2 h_e; \quad s = N^2 / N^2.$$

Since the individual terms depend differently on frequency, they can be determined independently.

RESULTS

The dependence of the total number of electrons on solar activity is shown on the example of diurnal variation during the equinox of 1958 - 1959 and in the fall of 1963 (Figure 3). Besides this, for both of these periods of time the mean values for the daylight periods are shown in the form of

individual columns. A significant drop is seen in the mean values of the total number of electrons by approximately 4.7 times.

To study the known seasonal anomaly, Figure 4 shows the diurnal variation of the total number of electrons for summer and winter during the periods of maximum and minimum solar spots. Besides this, the average value, during daylight hours, of the total number of electrons is again shown by the individual columns for 0600 - 1800 hours local time. It is clearly obvious that only with maximum solar spots is the total number of electrons during the daylight hours in winter greater than that during daylight hours in summer. The total number of electrons during minimum solar spots in winter is nevertheless /90 too high, if we take into account the low position of the sun. Thus, we can speak here about an insignificant seasonal anomaly.

Investigation of the variations with latitude became possible only by using differential Doppler measurements on the S-66 satellite. Figure 5 shows the isolines of the constant values of the total number of electrons as a function of latitude and time of day. Since the satellite had almost a precise circular orbit, at a higher altitude the variations in the total number of electrons during the time of transit may be explained only by geographic differences.

Here it was assumed that the difference in longitude plays a small role. In order to determine some effective latitude for each moment of time during transit, we proceeded from the fact that the greatest density of electrons is found at an altitude of 350 km. As the effective latitude we used the latitude at which the ray penetrated the 350 km level. As was expected, the isolines exhibited no unexpected features for sunspot minimum. The shift in the moments of sunrise and sunset with latitude may be clearly ascertained from the behavior of the isolines for N_{tot} . The lowering of the solar altitude with latitude also determines the decrease in the total number of electrons.

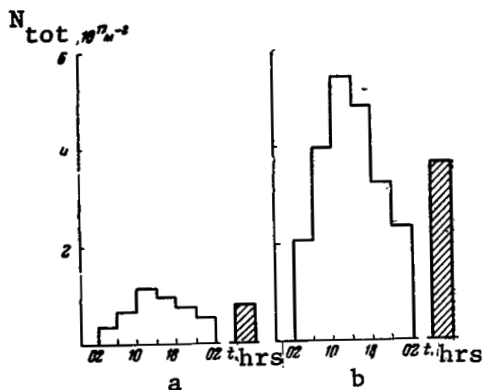


Figure 3. Total Number of Electrons in the Vertical Column of the Ionosphere N_{tot} as a Function of Local Time.

a. During High Solar Activity (1958 - 1959); b. During Low Solar Activity (Fall 1963); The Shaded Area Shows the Values Averaged for the Days.

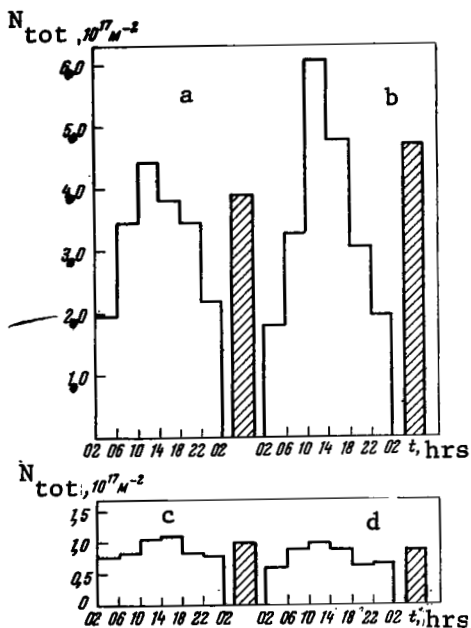


Figure 4. Total Number of Electrons in the Vertical Column of the Ionosphere N_{tot} as a Function of Local Time Average Values Between 0600 - 1800 hours shown by shaded area:

a. Summer, 1959; b. Winter 1958/1959; c. Summer, 1964; d. Winter 1963/1964.

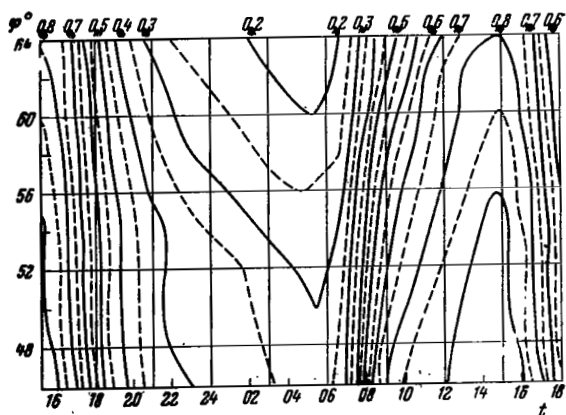


Figure 5. Isolines of the Constant Values of the Total Number of Electrons in the Coordinates, Latitude - Local Time.

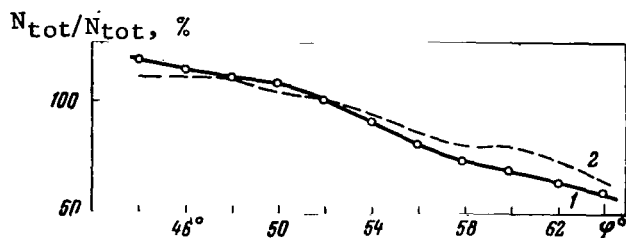


Figure 6. Variation in the Ratio $N_{\text{tot}}/\bar{N}_{\text{tot}}$ with Latitude. (Pertaining to an Altitude of 350 km).

1. Under Quiet Conditions; 2. Under Perturbed ($K_p \geq 2$) Conditions.

latitude of $58 - 64^\circ$ which corresponds to the position of the horns of the outer radiation belt at our longitude.

To interpret the results we took as a basis the diffusion theory of the F layer and proceeded from the following equation of balance:

$$d \frac{N_e}{dt} = q - \beta N_e - \frac{d}{dh} (\omega_D N_e), \quad (11)$$

where q is the rate of formation of electrons for the case of simple Chapman law; β is the coefficient of recombination which is proportional to the concentration of molecular particles of the neutral gas and thus decreases very rapidly with altitude.

The diffusion rate ω_D obeys the law

$$\omega_D = D \left(\frac{1}{N_e} \frac{dN_e}{dh} + \frac{\mu}{H} \right), \quad (12)$$

where H is the altitude of the uniform atmosphere; $\mu = T_i(T_e + T_i)$ (T_i is the ion temperature; T_e is the electron temperature). The equation for the diffusion coefficient is

Comparison of the nocturnal variations with latitude under perturbed and unperturbed conditions is shown on Figure 6. It is obvious that during perturbations the total number of electrons between 60 and 64° is slightly elevated. These phenomena are probably associated with the outer radiation belt. If we assume that the excess electrons are located mainly at an altitude of $150 - 200$ km rather than at 350 km, we then obtain a

$$D = \frac{k(T_e + T_i)}{v_i m_i}, \quad v_i = T_i^{1/2} n \quad (13) \quad \underline{/91}$$

(v_i is the frequency of ion collisions, n is the density of the neutral gas). Thus, the diffusion coefficient is inversely proportional to the density of neutral gas and, under the condition that the electron temperature is near that of the ions, is proportional to the square root of the temperature value. For very high electron temperatures, it increases linearly with T .

First of all we studied two cases: the equilibrium conditions and the nocturnal recombination ($q = 0$) with equilibrium as the initial state. Since a number of measured values exist for the reaction parameters, the composition of the atmosphere, and other required values, by using these data we could limit the range of individual parameters. The values varied within this range. Here it was found that the type of electron distribution depends on temperature more strongly than on the reaction parameters. In particular, above the F2 maximum the "plasma temperature" $T_p = 0.5 (T_e + T_i)$ was found to be the only decisive parameter for the form of the layer.

With this also is associated the fact that the normalized values are

$$Y = \int_{300 \text{ km}}^{1000 \text{ km}} \frac{N_e dh}{N_{e, \max}}$$

($N_{e, \max}$ is the electron concentration at the F2 maximum), and s depends almost only on the plasma temperature. This fact was used for determining the plasma temperature. In the "Sputnik-3" the value of Y was computed from the total number of electrons and from measurements of the ion probe and plotted as a function of altitude. Besides this the value of dY/dh could be determined from the time variations during transit by using the equation

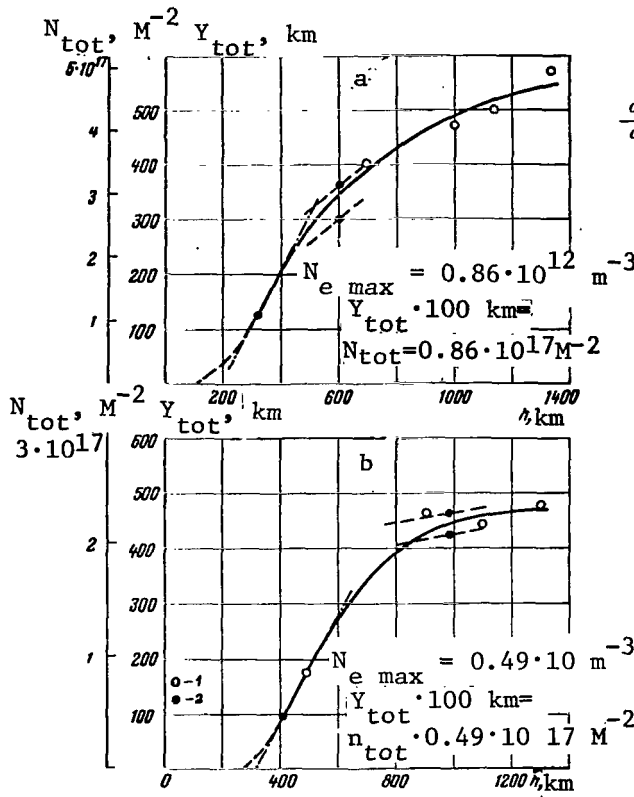


Figure 7. Path of the Curves $Y(h)$.

a. For Summer Days in 1958; b. For Nocturnal Conditions in 1958 - 1959; 1. Mean Values of $N_{\text{tot}}(h)$; 2. Mean Values of Y_{tot} for a Given Altitude Range.

$$\frac{dY}{dh} = \frac{1}{N_{e, \text{max}}} \frac{dN_{\text{tot}}}{dh} = \frac{1}{N_{e, \text{max}}} \frac{dN_{\text{tot}}}{dt} \frac{dt}{dh}, \quad (14)$$

Finally the value $\frac{dY}{dh} = 1$ is trivial for the altitude of the F2 maximum. Figure 7 a shows the type of curves $Y(h)$ for summer days in 1958 (the crosses represent the mean value of $Y(h)$, the broken line - the mean value of dY/dh for the given altitude range), and Figure 7 b shows the curves for the nocturnal values of 1958 - 1959.

For winter days it was impossible to directly plot the experimental curve $Y(h)$; therefore we plotted different theoretical curves and selected the suitable one. By differentiation we can obtain from these curves the distribution of electron density (Figure 8).

During sunspot minimum we had available only the satellites which had an almost circular trajectory. To determine the plasma temperature from the electron content, we could only use a comparison of experimentally determined values of Y for a given altitude with the theoretical values. But this method was found to be rather rough. Therefore we used the results of observations at several frequencies, and the plasma temperature was determined from comparison of the theoretical and measured values of s .

Whereas in winter, during the night and during sunspot minimum the

values of the plasma temperature do not exceed the temperature of the neutral gas by very much (1.2 - 1.5 times) in summer during sunspot maximum we find very high plasma temperatures (up to 3500° K). During geomagnetic perturbations the plasma temperature is also clearly elevated. Figure 9 shows for April 1959 the behavior of the number of electrons, the behavior of $f_0 F_2$, the index K_p and the plasma temperature computed using Y. Figure 10 shows for /92 fall of 1963 the dependence of Y_{tot} on the index of magnetic disturbance K_p .

In the course of several selected intervals of time, in addition to measurements of radio signals, telemetric information was also received from the "Explorer XXII" concerning probe measurements of local concentration. Here we are speaking of measurements by a plasma probe whose potential varied in a sawtooth manner with respect to the body of the satellite. The radio signal measurements during this time were processed with special care and from the values obtained we plotted the best theoretical profile for N_{tot} , s and \bar{h} . Here we assumed that during this time the electron temperature was 1.5 times greater than the temperature of the neutral gas. In equations (12) - (14) we considered only one type of ion, i.e. O^+ . Therefore at high altitudes the electron concentration should differ from this profile. Figure 11 shows a comparison of the theoretical profile with the results of direct measurements. If the theoretical profile, allowing for the helium ions, is changed such that it corresponds with the measurement results, we then obtain a mean molecular weight for the ionized particles of 8.5 atomic units at an altitude of 900 km. This agrees well with the results which were obtained by others using this satellite but an entirely different method.

The recombination coefficient β_0 at the altitude of the ion formation /93 maximum, as well as the reduced coefficient of diffusion $D \cdot n$, are significant for the rate at which the electron concentration drops following sunset. We used the following values: $\beta_0 = 2 \cdot 10^{-3} \text{ sec}^{-1}$; $n_0 = 1.5 \cdot 10^{10} \text{ cm}^{-3}$; $D \cdot n = 0.75 \cdot 10^{19} \text{ cm}^{-1}$. In this way, after 10 hours of recombination we find a drop in

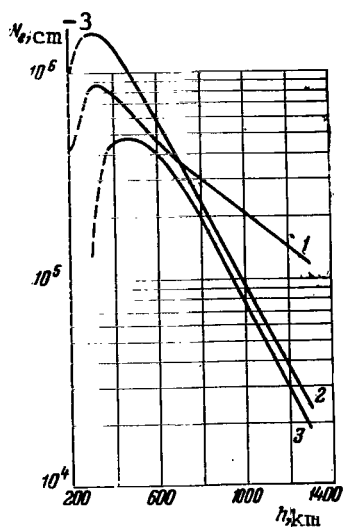


Figure 8. Distribution of Electron Concentrations with Altitude, Obtained by Differentiating the Data in Figure 7.

1. Summer Day; 2. Winter Day; 3. Night

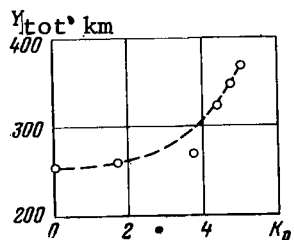


Figure 10. Mean Values of Y_{tot} as a Function of the Index K_p for Fall of 1963.

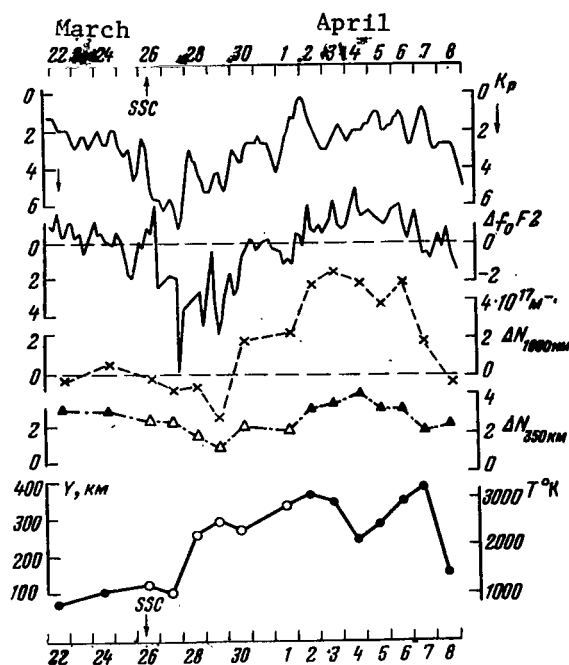


Figure 9. Variation in the Total Number of Electrons During March - April 1959 for Altitudes of 350 and 1000 km, Critical Frequencies f_oF2 , Index K_p and Plasma Temperature T .

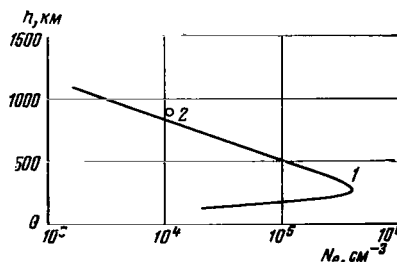


Figure 11. Electron Concentration as a Function of Altitude.

1. Theoretical Profile; 2. Measurement Results.

the number of electrons by 3.2 times. The experimental results for the ratio of N_{tot} at sunset to N_{tot} after 10 hours following sunset are found to be between 2.2 and 2.9. We detected no systematic variations with time of year or cycle of solar spots. Apparently, β_0 and the diffusion coefficient are smaller than had been assumed, and do not undergo significant variations. /94

Since the total number of electrons naturally depends on all the parameters, we made an attempt to find the variations in ionizing radiation with the cycle of solar activity using the most probable values from the literature as well as measurement data. Here we found the following results:

(1) The variation in the total number of electrons, averaged for the daylight periods, measured from $3.62 \cdot 10^{17} \text{ m}^{-2}$ at the equinox of 1958 - 1959 to $0.775 \cdot 10^{17} \text{ m}^{-2}$ in the fall of 1963;

(2) We computed the variation in the average rate of O^+ ion formation for the same time: from $3.53 \cdot 10^2 \text{ cm}^{-3}$;

(3) The flux of ionization radiation for the same period of variation consisted of values from $0.67 \cdot 10^{10}$ to $0.21 \cdot 10 \text{ cm}^{-2}$.

For computation of this latter we assumed that the altitude of the uniform atmosphere of neutral gas during sunspot maximum was 70 km, and during sunspot minimum was 50 km.

PROBE METHODS FOR STUDYING THE IONOSPHERE

G. L. Gdalevich

Probing is the main technique used for investigating a gas-discharge plasma (comparatively cold plasma with a rather low concentration and weak magnetic fields). Characteristics obtained from probing (dependences of probe current upon voltage applied to a probe) may, in the main, be used for determining all the basic parameters of a plasma, such as: electron and ion concentration, distribution of ions and electrons according to their energies and plasma potential in the area of the probe. Measurements carried out by means of probing allow the local parameters of the ionospheric plasma to be determined, the results of such measurements being independent of the condition of the medium between the probe and the Earth. In principle the advantage of measurements carried out by probing is that they may be used at any altitude. However, apart from difficulties encountered in the gas-discharge plasma, a number of difficulties which pertain particularly to the ionosphere may arise during measurements by means of probing.

Much information on the parameters of the ionosphere and their variations has been obtained with the help of measurements by means of probing. The comparison of measurement data obtained by different methods makes it possible to estimate the reliability of measurements and reveal methodological errors.

The methods of investigating the ionosphere using rockets and satellites /95 may be divided into two basic groups:

- (1) Study of radio wave propagation between the satellite or rocket and Earth (in certain instances based on reception on board the satellite of radio waves transmitted through the ionosphere);
- (2) Measurement of the ionospheric characteristics near the rocket or satellite using instruments installed on board.

The article of V. A. Misyura deals with the methods of the first group of tests. The basic disadvantage of this group of tests (from the viewpoint of studying local atmospheric parameters) is that the entire thickness of the atmosphere through which the radio waves pass affect the form of signals received.

The basic advantage of the methods in the second group is that the measurement results are completely independent of the characteristics of the atmospheric layers near the instruments on the satellite or rocket, and the processes which take place in it. In this case the instrument responses are completely determined by the small region near these instruments. However, the instrument responses are influenced by the perturbations created both by the instruments themselves and by the satellite or rocket.

These so-called probe methods began to be developed back in the 1920's by Langmuir and his associates for investigation of gas discharge plasma and at the present time are the basic methods used for measurements in a relatively cold plasma with relatively low concentration and in weak magnetic fields.

The ionosphere, as we shall see below, is an almost ideal medium for using the probe method. Investigations of the ionosphere have stimulated the development of probe methods. For measurements in the ionosphere, we have used both the methods developed earlier and specially created ones. In the present article we shall look briefly at the theory of probe measurements; let us examine the characteristics of measurements in the ionosphere; we shall discuss the methods used for ionospheric measurements; we shall cite theoretical and experimental information about the influence of perturbations, created by a moving satellite, on the measurement results using the probe method; in conclusion let us pay attention to the prospects of utilizing this method.

BRIEF DISCUSSION OF THE THEORY OF PROBE MEASUREMENTS AND ITS LIMITATIONS

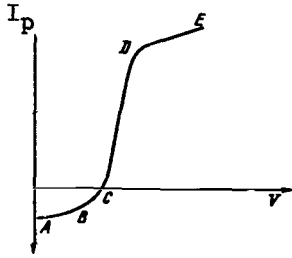


Figure 1. Volt-Ampere Curve of the Probe.

/96

The method of probes proposed by Langmuir in 1923 [1] involves an electrical probe, i.e. a small electrode of spherical, cylindrical or flat shape, being introduced into the gas discharge plasma and the probe

potential, given relative to the cathode or anode, being varied relative to the plasma potential at the site of the probe. The probe characteristic or the so-called volt-ampere characteristic, is the current on the probe versus the probe potential. Figure 1 shows a typical shape of the volt-ampere curve. It can be qualitatively explained in the following manner [2]: at high negative potentials of the probe the current on it is determined by the current of positive ions, since the thermal electrons may not overcome the retarding field of the probe (segment AB); with a decrease in the negative potential an electron current begins to affect the probe; this current initially determined by the fastest electrons. This explains the more rapid decrease in current on segment BC than on segment AB, and its subsequent change in sign (point C) with potentials on the probe even lower than the plasma potential at the site of the probe. After the current changes sign, it increases abruptly with a reduction in the negative potential (segment CD), reaching values in absolute magnitude that are approximately two orders greater than on the segment AB. Even in this region (CD) the electron current exceeds the ion current significantly. Near the potential of the probe, equal to the plasma potential (point D), the law governing the increase in current changes since the electrons are first held by the field of the probe and then begin to be accelerated. This change in the law governing increase in the probe current near the plasma potential appears as a more or less sharp bend in the volt-ampere curve.

In order to find the plasma parameters it is necessary to compute the shape of the volt-ampere curve from a certain simplified theoretical schematic and compare it with that observed.

To develop the theory of probes it is important to introduce Langmuir's concept for the layer of a space charge surrounding the probe. In fact, when the probe is injected into the plasma (just as when a rocket enters the ionosphere) it acquires a negative potential, since the electron velocity exceeds the velocity of the positive ions and consequently the electron current at the initial moment is greater than the current of positive ions. In the steady state the total current on the body is equal to zero. Consequently, the probe acquires the potential V , determined from the conditions of equality of the currents. For an isotropic plasma containing only electrons and positive ions, this condition is determined by the equation

$$\frac{en_+v_+}{4} = \frac{en_e v_e}{4} \exp\left(-\frac{eV}{kT_e}\right), \quad (1)$$

where e is the electron charge; n_+ , n_e are the concentrations of positive ions and electrons, respectively; v_+ , v_e are their mean (arithmetic) velocities with Maxwell distribution, which are related to the temperature T and the mass M by the formula $v = (8kT/\pi M)^{1/2}$; T_e is the electron temperature; k is the Boltzmann constant. From (1) it follows that any body in plasma (rocket or satellite in the ionosphere) when there are no other influences on the potential from other effects such as the photoeffect, secondary emission, currents of fast particles, etc., acquires a negative potential

$$V \simeq -\frac{5kT_e}{e}.$$

In this case a layer of a positive space charge is formed near the probe in which the electric field of the probe drops rapidly and the electron concentration is significantly less than the ion concentration. Introduction of the Langmuir concept of a space charge layer is important for the following reasons:

(1) The current on the probe is computed by computing the movement of the charged particles in the space charge layer on the assumption that no collisions occur;

(2) The limits of applicability of the theory become more distinct since the lack of collisions in the space charge layer means that the mean free path of the charged particles l will exceed the thickness of the space charge layer d significantly.

To find the shape of the volt-ampere curve we solve the Poisson equation for the distribution of the potential in the layer. Depending on the sign of the potential, the equation has the form [3]

$$\left. \begin{aligned} (\text{for } V > 0) \quad \nabla^2 V &= 4\pi e [n_+ \exp\left(-\frac{eV}{kT_+}\right) - n_-], \\ (\text{for } V < 0) \quad \nabla^2 V &= 4\pi e [n_- \exp\left(-\frac{eV}{kT_-}\right) - n_+]. \end{aligned} \right\} \quad (2)$$

The boundary conditions for solution of (2) are given on the surface of the probe and at a certain distance from it, where the field of the probe may be assumed either equal to zero or small. The solution of (2) with boundary conditions determines the distribution of the potential in the layer which also determines the movement of the particles taking into account the laws of conservation. For spherical and cylindrical probes, we examine the movement of the particles by allowing for the laws of conservation for the movement in a centrally-symmetric field (laws of conservation of energy and momentum). To compute the volt-ampere characteristics of a flat probe we use the law of conservation of energy and the equation of continuity of the particle flux. Such computations for spherical, cylindrical and flat probes were cited by Langmuir and his associates. Let us note that the computations of the electron branch were valid and at the present are used for interpreting the results of probe measurements. As far as the theory of the ion branch of the volt-ampere characteristics is concerned, they required further refining (following the research of Langmuir). Since, in making measurements of the ionosphere,

computations of the ion current flowing to the probe must be made by allowing for the characteristics of the measurements (see below) there is no sense in examining this question in detail. Let us give the basic formulas according to which the plasma parameters are determined in carrying out probe measurements. For the current of particles moving in a retarding field:

$$I_p = -\frac{env}{4} s \exp\left(-\frac{eV}{kT_e}\right), \quad (3)$$

where s is the surface of the probe. Formula (3) is valid regardless of the shape of the probe and consequently the semilogarithmic dependence $\log I_p = f(V)$ in this range of probe potentials is a straight line whose slope determines the temperature

$$T_e = \frac{5040}{d \lg I_e / dV} \quad (4) \quad \underline{/98}$$

The nature of this dependence may be explained by the fact that in the field of the repelling probe an equilibrium distribution must be established for the particles, i.e., the Boltzmann distribution.

For attracting probe potentials:

(a) For an Infinite Flat Probe.

$$I_p = I_e = \frac{en_e v_e}{4} s,$$

i.e.,

$$n_e = \frac{4.03 \cdot 10^{13}}{s \sqrt{T_e}} I_e, \quad (5)$$

where n_e is the electron concentration in cm^3 ; s is the surface of the probe in cm^2 ; I_e is the value of the electron current in amperes.

(b) For a Long Cylindrical Probe.

$$I = \frac{en_e v_e}{4} s \left\{ \Phi \left(\sqrt{\frac{eV_p}{kT_e} \left(\frac{r_{lay}^2}{r_p^2} - 1 \right)} \right) + \frac{r_p}{r_{lay}} \exp \frac{-eV_p}{kT_e} \times \right. \\ \left. \times \left[1 - \Phi \left(\sqrt{\frac{eV_p}{kT_e} \left(1 + \frac{1}{\left(\frac{r_{lay}^2}{r_p^2} - 1 \right)} \right)} \right) \right] \right\}, \quad (6)$$

where r_p , r_{lay} are the radii of the probe and the space charge layer;

$\Phi(x) = \frac{2}{\sqrt{\pi}} \int_0^x e^{-h^2} dh$ is the error function.

In computing the conditions $(eV_p/kT) > 1$ and $(r_{lay}^2/r_p^2) \gg 1$, Formula (6) is well approximated by the expression

$$I_e = 4 \sqrt{\pi} l r_s \frac{en_e v_e}{4} \left(1 + \frac{eV_p}{kT_e} \right)^{1/2} \quad (7)$$

where l is the length of the cylindrical probe. From (7) it follows that

$$n_e = 3.22 \cdot 10^{11} \frac{1}{s} \left(\frac{dI_e^2}{dV_p} \right)^{1/2}, \quad (8)$$

where s is the surface of the probe in cm^2 , I_e^2 is the square of the electron current in amperes and V_p is the voltage on the probe in volts. Proceeding from (8), Langmuir and Mott-Smith recommended a method for determining n_e from the function $I_e^2 = f(V)$ and the point on the volt-ampere curve at which the probe potential relative to the plasma is equal to zero, and from the intersection of the rectilinear part of the function $I_e^2 = f(V)$ with the axis $I_e = 0$. However, in practice this method is used rarely in a gas discharge plasma since it is rather complicated to satisfy the conditions of its use [4]. In 1961 this method was successfully used for measurements in a gas discharge plasma [5].

(c) For a Spherical Probe.

$$I_e = \frac{en_e v_e}{4} s \left[1 - \left(1 - \frac{r_p^2}{r_{lay}^2} \right) \exp \left(-\frac{eV}{kT_e \left(\frac{r_{lay}^2}{r_p^2} - 1 \right)} \right) \right] \quad (9)$$

Under the condition $(r_{\text{lay}}^2/r_p^2) \gg 1$, formula (9) is well approximated by the expression /99

$$I_e \simeq 4\pi r_p^2 \frac{en_e v_e}{4} \left(1 + \frac{eV}{kT_e} \right) \quad (10)$$

which represents the linear dependence of the current I_e on the voltage V on the probe.

In interpreting the volt-ampere characteristics of the probe we must first approximately determine the zero potential of the probe relative to the plasma (space potential at the site of the probe) based on the bend in the curve at point D (see Figure 1); the bending point is clearer on the semi-logarithmic curve). Then the ion branch of the curve (segment AB) must be extrapolated to the right of point B up to the point at which the probe potential is equal to the space potential and the ion current subtracted from the probe current to determine the electron branch. We then plot the functions $I_e = f(V)$, $\ln I_e = f(V)$, $I_e^2 = f(V)$ and determine T_e , n_e from the formulas. The value of the electron and ion concentrations based on the strength of the current at the point at which the probe has zero potential relative to the plasma is determined by (5). All these cited formulas are valid for a Maxwellian velocity distribution of charged particles. If there is no Maxwellian velocity distribution (which is determined by the presence or absence of a rectilinear part in the semilogarithmic curve), according to Dryvesteyn, the law governing electron energy distribution is determined from the value of the second derivative of the volt-ampere characteristic [4].

The practical utilization of probes is complicated by a number of factors such as perturbation of the plasma by the probe itself (change in the electric field inside the plasma, depletion of the plasma due to attraction of charged particles to the probe), photoemission and secondary emission from the surface of the probe, etc. Therefore, ever since the

probe method appeared, and still at the present time, many different refinements have been proposed. Unfortunately it is impossible to examine all these proposals in detail. Let us look only at the most important proposals and those which have direct application to measurements in the ionosphere. Even Langmuir himself began to use diode probes for separating the currents of particles of unlike sign [6]. In the 1950's Boyd used the diode probe for shielding plasma from the probe field [7], and N. I. Ionov proposed the use of a triode flat probe in which the potential difference between the two electrodes could be maintained constant. A substantial contribution was made to the method of probe methods by investigation of the probe operation under dynamic conditions, i.e., when, along with the slowly varying (usually in a sawtoothed manner) voltages, low amplitude harmonic signals were also fed to the probe [9 - 12]. This made it possible to obtain the derivatives of the volt-ampere characteristics. Finally we must mention the development of the theory of the double probe method in 1950 [13 - 15] which is used in a gas discharge plasma for the purpose of lowering the influence of the currents flowing to the probe or to the plasma being studied, or in electrodeless discharges.

MEASUREMENT CHARACTERISTICS IN THE IONOSPHERE

Ionospheric plasma, beginning from altitudes of ~ 100 km, is an almost ideal medium for using probe measurements since at these altitudes in the ionosphere the mean free path of the particles is significantly greater than the thickness of the space charge layer (i.e., the basic assumption concerning lack of collisions in the layer is valid). As an example, for the worst case (altitude of 100 km) we can cite the following numbers: mean free path $\lambda \simeq 10$ cm, thickness of the space charge layer d near the flat probe (when $V = 5kT_e/e$, $T_e = 600^\circ$ K and $n_e = 10^4 \text{ cm}^{-3}$) is equal to ~ 5 cm. Below this altitude use of the Langmuir probes is not theoretically justified, although attempts have been made to develop a theory of probe measurements for the cases of $d \gtrsim \lambda$ [16 - 18]. On the other hand the increase in the mean free path and the decrease in the concentration of charged

/100

particles in comparison with the corresponding parameters in the gas discharge plasma lead to a smoothing out of the bend in the volt-ampere curve near the space potential.

In making probe measurements in the ionosphere we should take into account the following factors.

(a) The probe potential varies relative to the body of the rocket or satellite. Thus, in making measurements in the ionosphere we must examine the operation of two probes (one of which is a reference probe). This follows from the fact that the total current on the entire system (probe-rocket or satellite body) as a whole must be equal to zero. Consequently, the increase in electron current in the circuit of the probe must be compensated by the increase in ion current on the surface of the rocket or satellite. Therefore the problem of compensating the current flowing to the probe is important in using the probe method. Computations show that the surface of the probe must be approximately three orders smaller than the conducting part of the surface of the body with respect to which the probe potential varies, so that the potential of the reference body remains practically constant with change in the probe potential [19, 20].

(b) Photoemission due to solar ultraviolet and X-radiation from the surface of the probe may influence the volt-ampere characteristics. The value of the photocurrent density from metal surfaces, according to the data of rocket and satellite tests, is equal to approximately $5 \cdot 10^{-9} \text{ A} \cdot \text{cm}^{-2}$ in the F region [21, 22]. This current density corresponds to the electron current density with a concentration of $n_e = 5 \cdot 10^3 \text{ cm}^{-3}$ and a temperature of $T_e \simeq 10^{30} \text{ K}$. Therefore, without using special measures to suppress the photoemission, measurements with a one-electrode probe are possible in the irradiated part of the ionosphere up to altitudes of about 1000 km. Besides this we must take into account the variation in potential of the rocket or satellite due to the photoeffect (and the possibility of probe measurement of the photocurrent flowing from the surface of the rocket

or satellite).

(c) The radio transmitters installed on the rocket or satellite may influence the probe measurements. This influence may appear either in the form of stray pickups by the probe circuit, or in variations in temperature or electron concentration near the probe, or in the excitation of fluctuations in the ionosphere, or in the change in potential of the reference body due to increase in the electron current on the antennas of the transmitter.

(d) The escape of gas from the rocket or satellite and desorption from their skin may decrease the concentration of charged particles near the probe. Therefore, in carrying out probe measurements in the ionosphere one must take special measures to decrease the desorption and gas separation. Removal of this effect in several experiments may be attained by separating (dumping) the equipment from the rocket or by separating the propellant assembly from the container with the equipment.

(e) The probes used to carry out the measurements are installed on vehicles moving at velocities either comparable to or exceeding the thermal velocity of the positive ions. This leads to a redistribution of the particle density around the rocket and satellite and changes the shape of the ion branch of the volt-ampere curve. The effect which atmospheric perturbations near the moving equipment have on measurements using the probe method will be examined below. The shape of the ion branches of the volt-ampere curves for a spherical probe, installed on board a satellite, was first computed by K. I. Gringauz, V. V. Bezrukikh and V. D. Ozerov in interpreting the measurements carried out on the third Soviet Earth satellite [23]. A /101
schematic representation of flow of an ion stream around a spherical trap is shown on Figure 2 a, from which it follows that the effective collecting surface of the trap varies as a function of the potential on the trap relative to the plasma. A schematic of the ion movement near the trap is shown on Figure 2 b, on the assumption that the ions move in the centrally-symmetric electric field of the trap. This assumption, strictly speaking, is not valid since a perturbed region is formed during the movement of the trap at a velocity which exceeds by approximately one order the

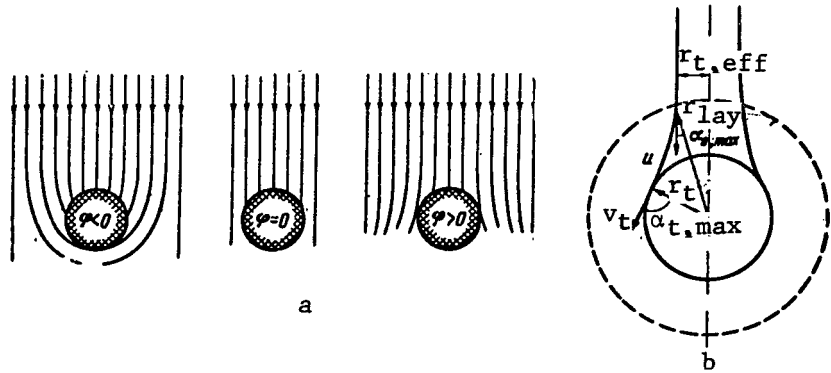


Figure 2. Movement of the Trap in Plasma

a. Schematic of the Flow of the Ion Flux Around a Spherical Trap (ϕ is the Trap Potential Relative to the Ionospheric Plasma); b. Schematic of the Movement of an Ion Near the Trap ($r_{t,eff}$ is the Radius of the Effective Cross Section of the Trap; $\alpha_{0,max}$ and $\alpha_{t,max}$ are the Maximal Angles Between the Direction of the Ion Velocity and its Radius-Vector, for Which the Ion is Incident on the Trap).

velocity of the ions behind the trap (in a direction counter to the velocity vector). Although study of this effect will be carried out below, let us mention here that the current on the spherical probe is created basically by ions incident on the front (in the direction of the velocity vector) of the trap. Therefore to prove the validity of the assumption on ion movement in a centrally-symmetric field, it is sufficient to show that the equipotential surfaces from the front of the trap have a spherical shape. As will be shown below, this is the case. If we use the law of conservation of momentum

$$u r_{lay} \sin \alpha_0 = v_t r_t \sin \alpha_t$$

[where u is the speed of the satellite, r_t is the radius of the trap (probe), v_t is the velocity of the ion at the surface of the trap, α_0 and α_t are the angles between the direction of the ion velocity and its radius-vector (see

Figure 2 b)]; and if we use the law of conservation of energy

$$\frac{m_i v_{\perp}^2}{2} = \frac{m_i u_0^2}{2} - e\phi$$

(where ϕ is the potential of the trap relative to the plasma), we find the equation for the ion branch of the volt-ampere curve:

$$I_p = \alpha n_+ e u \pi r_p^2 \left(1 - \frac{2e\phi}{m_i u} \right), \quad (11)$$

where α is the transmission coefficient of the trap, u is the speed of the satellite. Reference [23] gives the volt-ampere curves by allowing for the thermal velocities of the ions (Figure 3), although the expression for the current on the spherical probes allowing for the thermal velocities is not given. Such an expression was given later by Sagalyn and Smiddy [24] and /102 Medicus [25] and has the following form for the retarding potentials:

$$I_p(\eta) = c \{ e^{-\eta - \eta_0} [\alpha \alpha_0^{-1} \operatorname{sh}(2\alpha\alpha_0) + \operatorname{ch}(2\alpha\alpha_0)] + \alpha_0^{-1} \left(\frac{1}{2} + \eta_0 - \eta \right) E(\alpha - \alpha_0, \alpha + \alpha_0) \}, \quad (12)$$

where

$$c = \frac{en_+ v_+}{4} \pi r_p^2, \\ E(a, b) = \int_a^b e^{-x^2} dx; \quad \alpha_0 = \frac{4u}{v_+}; \quad \alpha = \sqrt{\frac{e\phi}{kT_+}}; \quad \eta_0 = \alpha_0^2; \quad \eta = \alpha^2.$$

The precise expression for the ion branch of the volt-ampere curve of a flat probe was given by Whipple [26]:

$$I_p = e n_+ s \left\{ \cos \left[\frac{1}{2} \theta + \frac{1}{2} \Phi(x) \right] + \frac{v_+}{2 u \cos \theta \sqrt{\pi}} e^{-x^2} \right\}, \quad (13)$$

where

$$x = \frac{4u \cos \theta}{v_+} - \left(\frac{e\phi}{kT} \right)^{1/2},$$

θ is the angle between the velocity vector and the normal to the probe

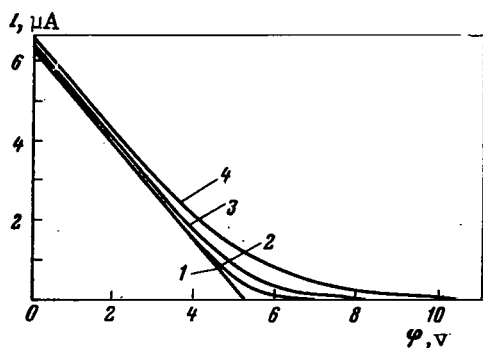


Figure 3. View of the Ion Branches of the Volt-Ampere Curve, Computed for the Case of O^+ Ions with the Concentration $n_+ = 10^6 \text{ cm}^{-3}$ at a Satellite Velocity of $u = 8 \cdot 10^5 \text{ cm} \cdot \text{sec}^{-1}$.

1. $T = 0^\circ \text{ K}$; 2. $T = 500^\circ \text{ K}$; 3. $T = 1800^\circ \text{ K}$; 4. $T = 5000^\circ \text{ K}$.

surface, $\phi(x)$ is the error function. From (13) it follows that the current on the segment of the infinite plane does not depend on the potential of this segment relative to the plasma (in the region of attracting potentials).

(f) The volt-ampere curves are plotted in the presence of the Earth's magnetic field. Besides this, the volt-ampere curves may also be influenced by the magnetic fields created by the rockets or satellites themselves. There is no overall theory for the operation of probes in the presence of a magnetic field.

However, in a gas discharge plasma for magnetic fields in which the cyclotron radius of the electron becomes smaller than the characteristic dimensions of the probe and the Debye radius, based on Baum's assumption, the ion branch is utilized for carrying out measurements involving probes. In this case we proceed from the following arguments. If the cyclotron radius of the particles is greater than the Debye radius and the characteristic dimension of the probe, then the movement of the particles in the space charge layer may be studied just as in the absence of a magnetic field. Thus, it is assumed that in the presence of a magnetic field, instead of the mean free path of the particles we should bear in mind the cyclotron radius of the particle. The research of G. V. Spivak and E. M. Reykhrudel' showed that for a cylindrical probe the base radius is less than the cyclotron radius, and the magnetic field has practically no influence on the measurements of temperature and concentration of electrons [27]. Smith notes in the methodology handbook of COSPAR (International Committee on Research in Outer Space) that in the unpublished lectures of F. F. Chen, the lack of any influence from the magnetic field on the mea-

surements of electron temperature was established even in the case where the cyclotron radius of the ion is greater than the radius of the probe and the Debye radius [20]. However in this latter case the value of the electron current flowing to the probe is decreased.

PROBE MEASUREMENTS IN THE IONOSPHERE

To investigate the ionosphere, probe methods began to be used in 1946 during the time of the first V-2 rocket launches in the USA. In 1946 - 1947 three experiments were carried out with a Langmuir probe used as the front of the rocket (truncated cone) insulated from the remaining part of the rocket. The probe potential relative to the body of the rocket varied linearly from -22.5 V to 22.5 V for a period of 0.5 sec. The volt-ampere characteristics of the probe were transmitted on telemetric lines. Since the areas of the probe and the rocket body in these experiments were comparable, a double probe was in fact used, the theory of which began to be developed only during the 1950's. Therefore a detailed description of the experiments by Hock, Spenser and Dow was done only in 1953 [28]. Because of the complex shape of the probe, no complete computation of the volt-ampere characteristics could be done and the data on the concentration of charged particles obtained in these experiments are apparently incorrect. In spite of the unsuccessful determination of the parameters, these experiments showed that by allowing for the characteristics of the measurements the probe method is applicable for investigations in the ionosphere.

The first reliable results using the probe method were obtained by K. I. Gringauz, V. V. Bezrukikh and V. D. Ozerov in 1958 on the third Soviet satellite when the characteristics of the measurements in the ionosphere were taken into account [19, 23]. The ion branch of the volt-ampere curve was used for the measurements so that the magnetic field could be disregarded. For the purpose of decreasing the influence of orientation on the measurements, a spherically shaped probe was used. The effect of

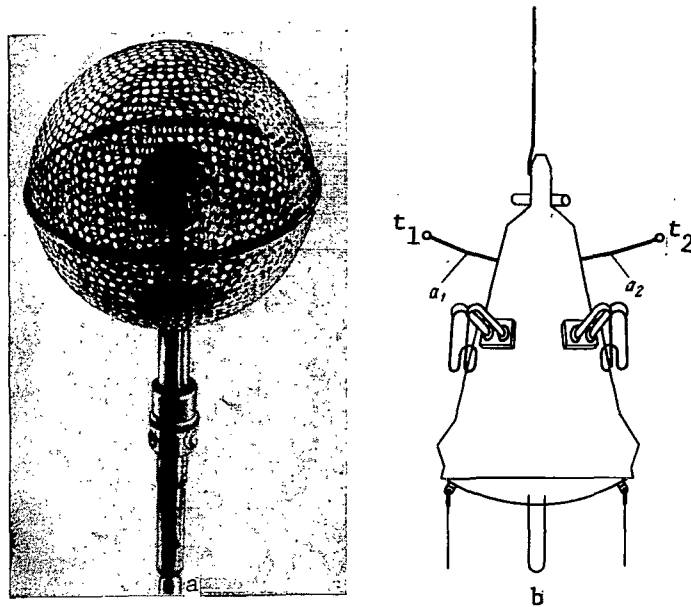


Figure 4. Spherical Ion Trap.

Position of the Spherical Trap on the Satellite: t_1 , t_2 are the traps; a_1 , a_2 are the Adjusting Rods.

photocurrent was reduced by determining the accumulation of ions from the potential and the dimensions of the mesh enclosure (10 cm diameter), but the photocurrent which could exert an influence on the measurements was determined by an internal collector (3 cm diameter). The outside diameter of the spherical ion trap is shown on Figure 4 a. The accumulation of all the ions passing through the inner grid was attained by having a negative voltage of - 150 V, with reference to the satellite body, fed to the collector. Thus, the electric field inside the trap collected all the positive ions and prevented electrons with an energy less than 150 eV from reaching the collector. In order to exclude measurements during those moments of time when the ion trap enters the perturbed region behind the shadow of the satellite (with respect to the velocity vector) and along with this to obtain the results directly, two spherical ion traps were installed over

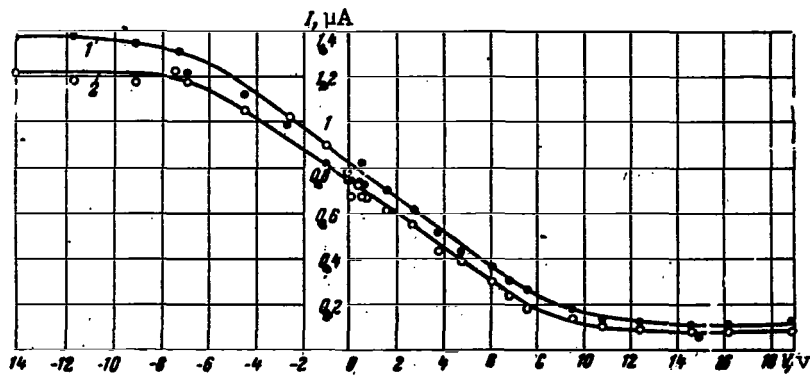


Figure 5. Example of the Ion Volt-Ampere Curves.

1. For the Trap t_1 ; 2. For the Trap t_2 .

diametrically opposed segments of the satellite on thin rods 65 cm long (Figure 4 b). Bipolar pulses relative to the satellite hull were applied periodically (once every 2 sec) to the mesh enclosures of the traps: a positive pulse with an amplitude of 25 V and duration of 0.13 sec and a negative pulse with an amplitude of 15 V and a duration of 0.07 sec. Figure 5 shows an example of the ion volt-ampere characteristics obtained. Computation of the concentration of charged ions was done according to formula (11). As a result of this experiment, the following results were obtained on the third Soviet satellite on measuring the concentration of positive ions:

(a) The region of the ionosphere first investigated was at altitudes of 600 - 1000 km;

(b) It was established that at the altitude at which the satellite flew /104 the electron concentration is equal to the concentration of positive ions;

(c) The decrease in concentration of charged particles with increase in altitude in the outer ionosphere during the period of maximum solar activity (1958) takes place more slowly than does its increase with increase in altitude in the region lying below the layer maximum; at an altitude of 1000 km the concentration of charged particles reaches $\sim 6 \cdot 10^4 \text{ cm}^{-3}$.

Triode ion traps [29] were installed on three Soviet lunar rockets in 1959. Figure 6 a shows the position of the traps on the rocket "Luna-2". Figure 6 b shows the schematic of the triode traps. In these experiments, designed to investigate outer space, K. I. Gringauz, V. V. Bezrukikh, V. D. Ozerov and R. Ye. Rybchinskiy first used a special grid with a negative potential relative to the collector for suppressing photoemission. Later this method for suppressing photocurrent interference began to be used quite widely both in Soviet instruments and in foreign ones. This made it possible to decrease the value of the photocurrent and thus measure small ion currents and establish that the ionized gas mantle of the Earth stretches out in the equatorial plane to an altitude of approximately 20,000 km above the surface of the Earth. The concentration of charged particles at these altitudes is 10^2 cm^{-3} and above this level it is less than 10 cm^{-3} . In these experiments various constant voltages from -10 eV to + 15 V relative to the container body were fed to the mesh enclosures of the traps (with the exception of the test on the rocket "Luna-3"). This also made it possible to distinguish the thermal plasma (with an energy of $\sim 1 \text{ eV}$) since no voltage appeared on the external grids at frequencies having an energy greater than 15 eV. Computation of the ion concentration was made according to the value of the collector current in the trap with zero potential on the mesh enclosure from formula (13), i.e. on the assumption that the trap is a segment of the infinite plane.

The successful completion of the experiment on the third Soviet satellite /105 served as the beginning of the use of the probe method for measurements in the ionosphere in different countries. We shall confine ourselves only to an examination of the tests which are either of methodological interest or which introduce substantially new concepts concerning the ionosphere.

A group of U.S. scientists, beginning with November 1958 and continuing until the present, has used a double probe for investigating the ionosphere; this probe is separated from the rocket during the ascending

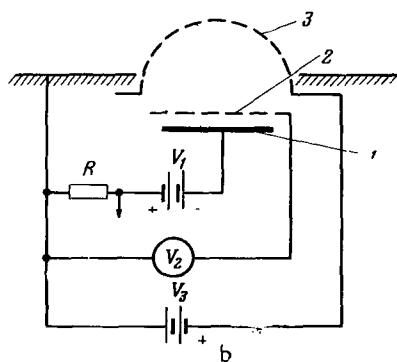
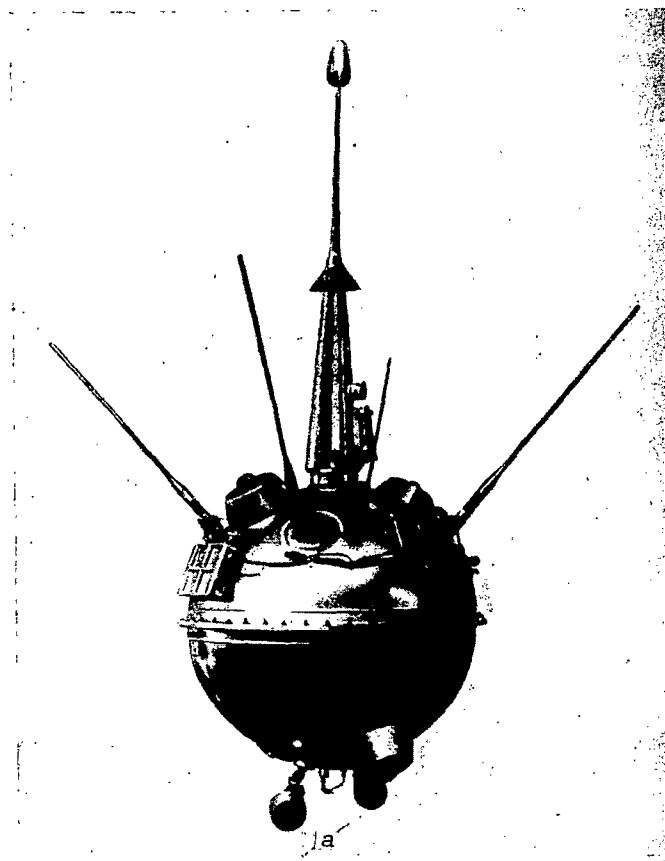


Figure 6. Container with Scientific Equipment, Installed on Board the Rocket "Luna-2".

a. Position of the Triode Ion Trap; b. Schematic of the Trap; 1. Collector; 2. Anti-photelectron Grid; 3. Enclosing Mesh; V_1 , V_2 , V_3 are the Voltages on the Electrodes, Given Relative to the Body of the Container.

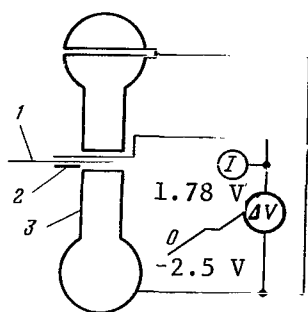


Figure 7. Schematic of an Instrument for Investigating the Ionosphere.

1. Cylindrical Langmuir Probe; 2. Guard Rings; 3. Double Probe.

the surrounding gas (T_g) in the ionosphere [31].

In 1960 - 1961 in Japan during rocket launches a probe was used with a small characteristic surface [34]. The probe consisted of two crossed wire rings at an angle of 90° . The wire diameter was 0.1 mm and the ring diameter was 4 mm. A voltage of 100 V was supplied to the rings and the ion current was measured. In carrying out the experiments it was assumed that the probe operates as a compact spherical probe. The value of the photocurrent in such a probe is low. To obtain data on the concentration of positive ions utilizing such a probe, it is necessary to carry out experiments in a gas discharge tube for the purpose of establishing an empirical dependence between the current on the probe and the ion concentration.

An interesting measurement program utilizing the probe method was done on the American satellite "Explorer VIII" [35]. Flat diode and triode traps of charged particles were installed on board. It was found for the first time that in the diurnal variation of the electron temperature there is a maximum during sunrise.

On the satellite "Kosmos-2", launched April 6, 1962, flat and spherical

branch of its trajectory after the engine is turned off [30 - 33]. The design of the probe varied slightly in order to measure a large number of parameters. Figure 7 shows the design of one such probe. Separation of the probe from rocket permitted decreasing the perturbations created near the surface of the rocket. We should mention that the experiments with such a probe were the first to establish the inequality between the electron temperature (T_e) and the temperature of

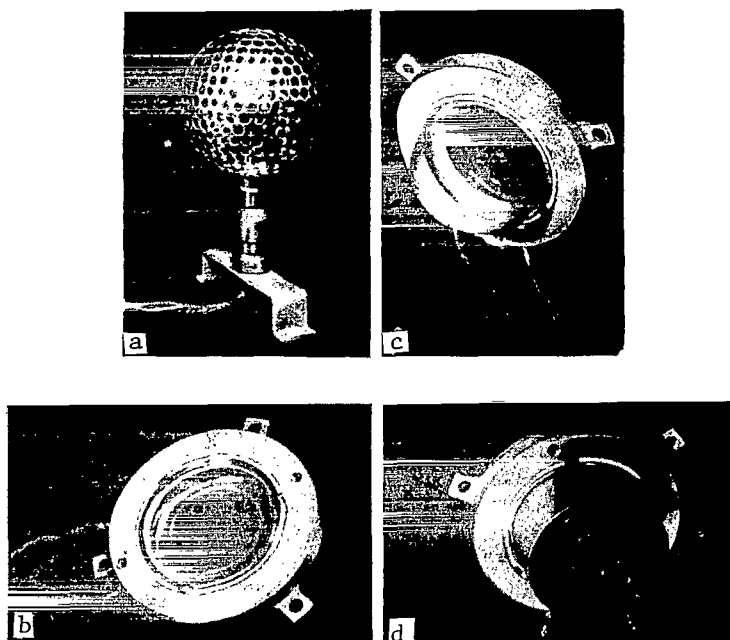


Figure 8. Traps Used in the Experiments on Board the Satellite "Kosmos-2".

a. Spherical; b. Flat; c. Hemispherical; d. Honeycomb.

triode traps were installed to measure n_i , cylindrical Langmuir probes were installed to measure n_e and T_e , and for the first time an ion trap was used with a "honeycomb" adapter to measure T_i (Figure 8) [36 - 38]. The ion trap with the honeycomb adapter is a triode device consisting of a collector and an antiphotoelectron grid serving to suppress the photocurrent from the collector and an external honeycomb adapter connected to the satellite body. The honeycomb adapter consists of a set of tubes adjoining one another, i.e., the "honeycombs". It is obvious that the directional properties of such a trap remain the same as in a single tube, but the collector current increases in proportion to the number of tubes. With the given shape of the tube the form of the dependence of the collector current relative to the vector of the incoming current is determined by the ion temperature (T_i) and the ion

/107

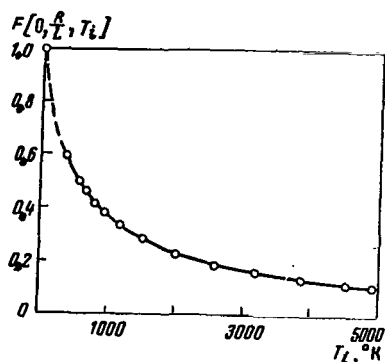


Figure 9. Computed Dependence of the Function F on Temperature T_i for $\psi = 0$ and for $R/L = 0.1057$, O^+ ions, Velocity of Satellite $u = 7.5$ km/sec.

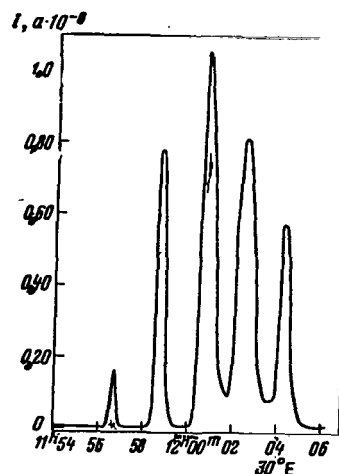


Figure 10. Example of Experimental Recording of the Collector Current from a Honeycomb Trap, Obtained on the Satellite "Kosmos-2".

mass. The collector current in such a trap is determined by the expression

$$I_C = e s u n_+ F\left(\psi, \frac{R}{L}, T_i\right), \quad (14)$$

where $e s u n_+$ is the current in the trap when $T = 0$ and the velocity vector coincides with the axis of the cross sections of all the traps; u is the speed of the satellite; s is the sum of cross sections of all the tubes; F is a function which determines the dependence of collector current on orientation and temperature; R/L is the ratio of the cross section of the tube to the length; ψ is the angle between the axis of the trap and the velocity vector of the satellite. The function F when $T_i \neq 0$ is a quintuple integral which is not expressed in analytical form and must be computed on an electronic computer. The results of the computation for the trap installed on board the satellite "Kosmos-2", for $\psi = 0$ are shown on Figure 9 [37], from which it is clear that the maximally possible current in the trap (with coincidence of the axes of the tubes with the velocity vector of the satellite) depends strongly on the temperature of the particles. Let us mention that the relationship with orientation (ψ) also depends on T_i . Such a de-

/108

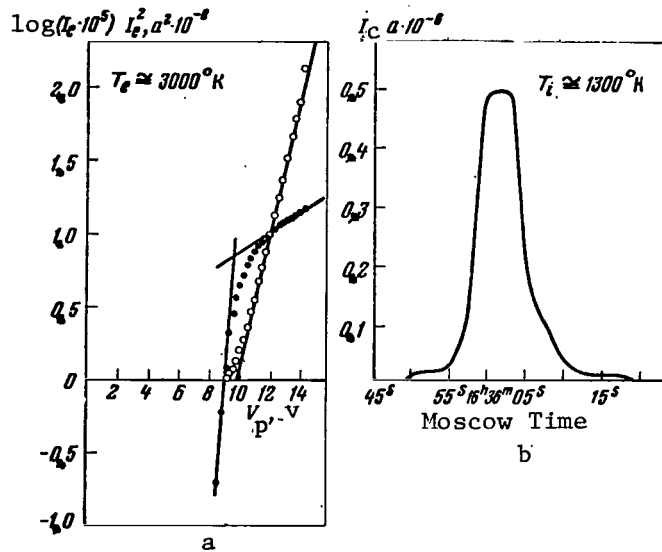


Figure 11. Simultaneous Recordings of Currents from the Langmuir Probe and the Ion Trap on the Satellite "Kosmos-2".

- a. Semilogarithmic Curve (Points) and the Function $I_e^2 = f(V)$ (Lines);
- b. Time Dependence of the Collector Current in a "Honeycomb" Ion Trap.

pendence of the collector current, in a "honeycomb" ion trap on T_i permits determining the temperature of the ions with sufficiently good accuracy. An example of an experimental recording of the collector current from the honeycomb-type trap obtained during the flight of the satellite "Kosmos-2" is shown on Figure 10. Figure 11 shows the characteristics of the cylindrical Langmuir probe measured during the flight of the satellite "Kosmos-2" simultaneously with the dependence of the collector current from the honeycomb-type ion trap. The results of the computations for these characteristics give an electron temperature which exceeds by more than two times the values of the ion temperature [38]. This indicates an absence of thermal equilibrium in the ionosphere at altitudes of the F2 layer. From the methodological point of view it is of interest to look at the expression shown on Figure 11: $I_e^2 = f(V_p)$. In fact, the correlation of the values of n_e and T_e computed by two methods according to (4), (5) and (8) shows that

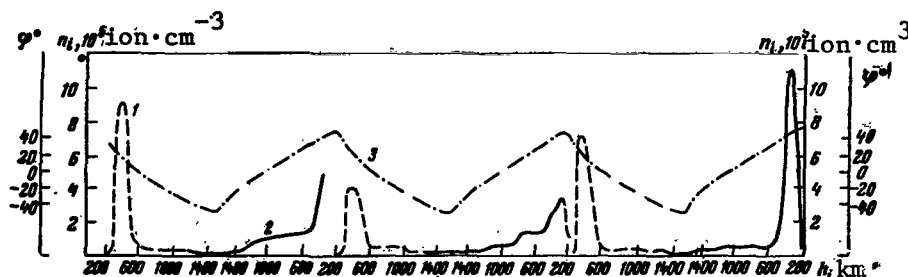


Figure 12. Altitude Dependence of the Concentration of Positive Ions (Measured along the Orbit of the Satellite).

1. Unilluminated Segments of the Orbit; 2. Illuminated Segments;
3. Latitude. Moscow Time. Change in Altitude from Left to Right.

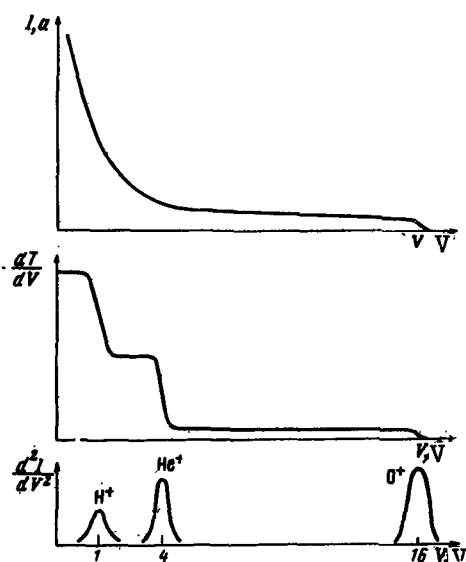


Figure 13. Theoretical Form of the Volt-Ampere Curve of the Spherical Ion Trap in the Case of Recording Ions with Different Masses, and its Derivatives.

in measurements of ionospheric plasma the conditions for utilizing (8) can be easily satisfied.

Figure 12 shows graphs of the variations in positive ion concentration along the orbit of the satellite "Kosmos-2", plotted in the form of a function of altitude above the Earth. The value of n_+ was obtained according to data from the system of flat traps installed on board the satellite [39].

Analysis of the volt-ampere characteristics of the spherical ion traps, installed on board the satellite "Kosmos-2", permitted investigation of the altitude distribution of ions at altitudes of 500 - 700 km. K. I. Gringauz and M. Kh. Zelikman [19] first showed the mass-spectrometric possibilities of ion traps on board a satellite. Such a possibility follows from (11). Figure 13 shows the type of volt-ampere characteristic of the spherical ion trap in the case of ions being present in the ionosphere with different masses.

This same figure shows the first and second derivative of the current with respect to voltage. Thus, the ion trap on board the satellite is the simplest mass-spectrometer with a low resolving power. However the ions of oxygen, helium and hydrogen, the basic ions at altitudes above 300 km, may be different in the case of significant relative concentrations. Graphic differentiation of the volt-ampere characteristic from the ion trap yields significant errors. On the Anglo-American satellite "Ariel I" launched April 26, 1962, the differentiation of volt-ampere characteristics was done by superposing two low-amplitude harmonic signals ($b_1 \sin \omega_1 t + b_2 \sin \omega_2 t$) onto a sawtooth-varying voltage. When the low-amplitude harmonic signal is superposed onto the slowly varying voltage, the volt-ampere characteristic $i = f(V)$ may, for any given voltage on the probe V_0 , be expanded in a Taylor series:

$$i = f(V_0) + (b_1 \sin \omega_1 t + b_2 \sin \omega_2 t) f'(V_0) + \frac{(b_1 \sin \omega_1 t + b_2 \sin \omega_2 t)^2}{2} f''(V_0) + \dots \quad (15)$$

From (15) it is clear that the first derivative of the volt-ampere characteristic is proportional to the frequencies ω_1 and ω_2 , and the second derivative (after transformation) is proportional to the term containing $\omega_2 \pm \omega_1$. Thus, if we make the measurement of current at frequencies of ω_1 or ω_2 ; $\omega_2 + \omega_1$ or $\omega_2 - \omega_1$, we can find the first and second derivative of the volt-ampere characteristic with respect to voltage. /110

To measure the ion composition and temperature we used a spherical diode trap with mesh enclosure diameter of 10 cm and collector diameter of 9 cm [40]. To measure the electron temperature we used two flat probes with a guard ring, one of which was installed on a rod (about 1 m long) and the other directly on the surface of the satellite [41]. The amplitude of the harmonic signals was 35 and 54 mV, respectively, for frequencies of 500 and 3000 Hz. The form of the second derivatives of the ion branch of the volt-ampere characteristic obtained on the "Ariel I" is shown on Figure 14. From this figure it is clear that O^+ , H^+ and He^+ ions can be easily distinguished. We should mention that the half-width of the peaks on Figure 14 is determined by the ion temperature so that the second derivative of the ion

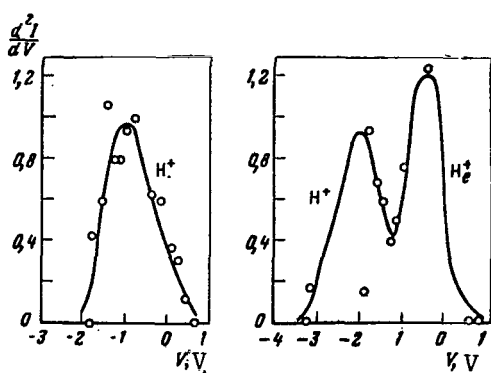


Figure 14. Experimental Recording of the Second Derivative of the Ion Branch of the Volt-Ampere Curve of the Spherical Trap, Obtained During the Flight of the Satellite "Ariel I".

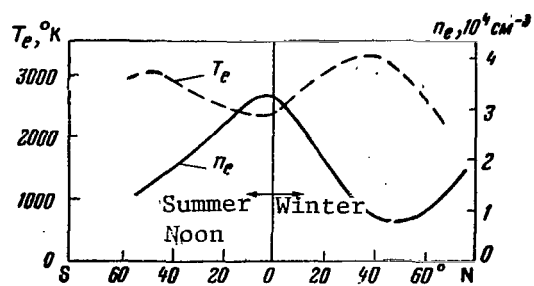


Figure 15. Latitude Dependences of Concentration and Temperature of Electrons at an Altitude of 1000 km from the Data of the Cylindrical Langmuir Probe Installed on the Satellite "Explorer XXII".

branch of the volt-ampere curve of the probe, installed on board the satellite, permits measuring T_i [42]. To study the mass composition of the ions we can also use the flat ion trap as was shown in the experiment on the satellite "Explorer VIII" [35].

A spherical trap was used on board rockets and satellites for measuring the temperature and concentration of electrons [24, 43].

Cylindrical Langmuir probes were successfully used for measuring the ion concentration and electron temperature on board the satellites "Explorer XVII" and "Explorer XXII" [44, 45]. As an example, Figure 15 shows the results of measuring the concentration and temperature of electrons obtained using the cylindrical Langmuir probe on board the satellite "Explorer XXII".

To decrease the influence of photocurrents on the results of the probe measurements, which is especially important for experiments conducted at altitudes above 1000 km, we can use modulation traps in which the input

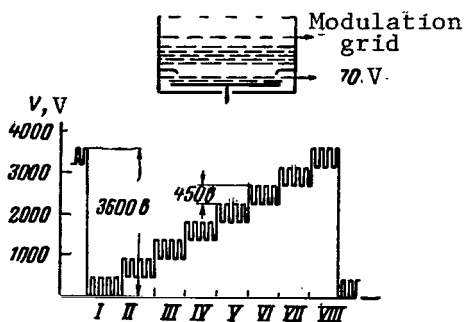


Figure 16. Modulation Trap for Studying Solar Corpuscular Streams.

current is modulated using voltages supplied on one of the trap grids, and the photocurrent from the collector remains constant. Figure 16 shows the modulation trap used for studying solar corpuscular streams (solar wind) on board Soviet space ships [46, 47]. The modulation trap permits decreasing the influence of the photocurrent by approximately 10^6 times.

Let us look briefly at the high-frequency probes which are widely used for measurements in the ionosphere. Included in this group of probes are instruments in which the ionospheric plasma influences the circuits which carry the high frequency. The terminology has not been established for this group of probes as yet. The high-frequency probe methods of measurements basically can be divided into two groups: the method of the resonance probe (or high-frequency probe with a floating potential) and the methods of impedance probes (antenna, capacitor and radio-frequency probes). /111

The resonance probe method is based on the fact that when a high-frequency voltage is fed to the probe an increase takes place in the constant component of the probe current and, when the frequency approaches the plasma frequency a resonance increase in the direct current occurs. If the frequency of the high-frequency voltage is less than 10% of the plasma frequency then the increment in direct current is independent of frequency and is determined by the expression [48].

$$\Delta i = i_0 I_0 \left(\frac{eA}{kT_e} \right), \quad (16)$$

where i_0 is the current of the probe in the absence of a high-frequency voltage, I_0 is a modified Bessel function of zero order, A is the amplitude of the applied voltage, e is the electron charge and k is the Boltzmann constant.

From (16) it follows that the ratio of increases in the probe current for two different amplitudes of the high-frequency voltage A_1 and A_2 is determined (for known A_1 and A_2) only by the temperature of the electrons T_e . In using this method of measuring T_e it should be borne in mind that the probe must have a negative potential relative to the plasma. Otherwise expression (16) can not be used.

The discovery of a resonance increase in the probe current by Japanese scientists when the frequency of the high-frequency voltage approaches the plasma frequency caused considerable interest throughout the world. With the initial interpretation of this phenomenon it was assumed that the resonance increase takes place at a frequency which coincides with the plasma frequency and therefore this method gives a very simple and reliable method for measuring the concentration of electrons. However, development of the theory [49 - 54] showed that the resonance takes place at a frequency ω_{res} which differs from the plasma frequency ω_{pl} and is determined (without allowing for the influence of the magnetic field and the collisions) by the expression

$$\omega_{res} = \frac{\omega_{pl}}{\sqrt{1 + (r_p/k r_D)^2}}, \quad (17)$$

where r_p is the radius of the probe, r_D is the Debye radius, k is an empirical constant which expresses the thickness of the space charge layer near the probe in Debye radii.

Allowance for the collisions leads to a smoothing out of the resonance effect. The influence of collisions on the resonance frequency and the value of the probe current (at this frequency) can be ignored under the condition $\omega_{res}^2 \gg \nu^2$ (ν is the frequency of collisions). Allowance for influence of the magnetic field leads to a change in ω_{res} [52].

Expression (17) is applicable only under the condition $\omega_H^2 \ll \omega_{pl}^2$ (ω_H is the cyclotron part of the electron). If this condition is not satisfied then we must have knowledge of ω_H .

By the middle of 1966 this method had been attempted several times in the laboratory and in the ionospheric plasma [52, 55]. The results of these experiments confirmed that the resonance does not occur at the plasma frequency, but that ω_{res} is determined by the approximate expression (16).

The various so-called impedance methods are based on measuring variations in capacitance, input impedance, or emission impedance of a probe to which high frequency is applied. In several experiments, transmitter antennas were used as the probes and were installed on board rockets or satellites for communication or other purposes, and in several experiments specially designed probes were used. The measurements are made both at frequencies above the plasma frequency and at lower frequencies including the cyclotron frequencies of electrons and ions. The use of measurements at cyclotron frequencies began after the discovery (in the experiments with the ionospheric station on the satellites "Alouette I" and "Explorer XX") of reflections on these frequencies and on the hybrid frequency $f_h (f_h = \sqrt{f_H^2 + f_{p1}^2})$, where f_H is the cyclotron frequency and f_{p1} is the plasma frequency.

Figure 17 shows the equivalent circuit of an impedance probe used in experiments on board satellites and rockets, and called a standing wave impedance probe from the way that measurements are made [56]. In this case, if the influence from the magnetic field and the collisions can be ignored, for the electron concentration we find the expression

$$n_e = \frac{f^2 (\text{MHz})}{80.6} \frac{C_0}{C_2} \frac{\Delta x}{\Delta x + (1/\omega C_0)} \quad (18)$$

where C_2 is the capacitance of the antenna in free space, $C_0 = C_1 + C_2$, C_1 is the capacitance of the circuit which bypasses the capacitance of the antenna, Δx is the variation in the reactive component of the antenna impedance.

In measurements with high-frequency probes in the ionosphere it should /113

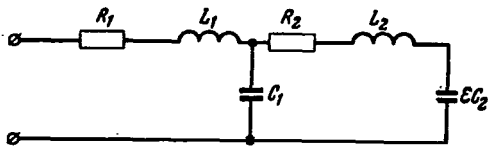


Figure 17. Equivalent Circuit of a Standing Wave Impedance Probe.

C_1 is the Capacitance of the Circuit Which Bypasses the Antenna Capacitance; C_2 is the Antenna Capacitance in Free Space; ϵ is the Dielectric Constant of the Medium; R_1 is the Resistance of the Circuit; R_2 is the Active Resistance Combined with the Radiation Resistance of the Antenna; L_1 is the Inductance Introduced for Matching the Antenna with the Transmission Line; L_2 is the Inductance of the Antenna Itself.

be borne in mind that the high-frequency field exerts pressure on the plasma near the probe (as a result the electron concentration (n_e) may be lowered [57]) and that the measurements are made in the space charge layer which surrounds the probe in the plasma (see above), in which n_e differs from n_e in the unperturbed ionosphere. For the purpose of removing the influence of pressure created by the high-frequency field, the amplitude of this latter should be lowered. Allowing for influence of the space charge layer may be done by the method of successive approximations (n_e is first determined without allowing for the space charge layer and then the thickness of the space charge

layer is computed under the condition that the probe potential is known, after which n_e is again computed, etc.). It is possible to eliminate the influence of the space charge layer by varying the probe potential, but in this case it is necessary to measure the zero potential of the probe relative to the plasma, i.e. measurements similar to the method of the Langmuir probe.

We should mention that the influence of the space charge layer on measurements using high-frequency probes may to some degree be taken into account by using several frequencies and that this influence is practically absent if we use effects on cyclotron and hybrid frequencies; however in this latter case we must have knowledge of the magnetic field strength.

The most interesting results using the impedance methods are those ob-

/114

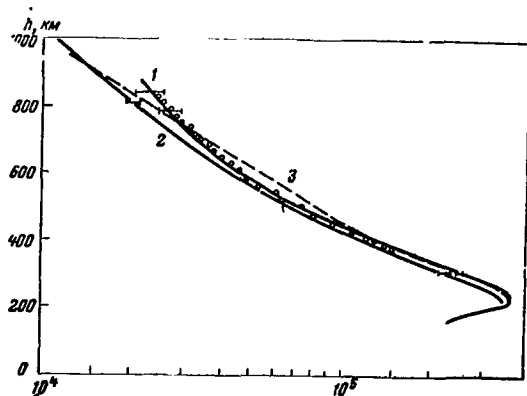


Figure 18. Simultaneously Measured Altitude Distributions of the Concentration of Charged Particles from the Data of Different Methods.

1. Dispersion Interferometer and Ion Trap (Points); 2. Ionospheric Station on the Satellite "Alouette I"; 3. Station of Incoherent Scattering.

tained on Soviet rockets [58], American rockets and satellites [59] and the Anglo-American Satellite "Ariel I" [60].

The large variety of probes used in the ionospheric experiments is due to the fact that better methods are being sought both from the viewpoint of accuracy of the measurements and simplicity of the equipment and interpretation of the measurement results. In many of the experiments, the results of the measurements obtained by the different methods are compared for the purpose of evaluating their reliability.

Figure 18 shows the results of charged particle concentration measurements carried out simultaneously using a dispersion interferometer and ion trap installed on a rocket, the ionospheric station on board the satellite "Alouette I", and on the station of incoherent scattering [61]. From Figure 18 it follows that the altitude distributions of the charged particle concentration obtained by the various methods coincide within measurement error.

Simultaneous measurements were made on the American rockets using the various high-frequency methods and spherical and cylindrical Langmuir probes [55]. These measurements confirm the conclusions on the high-frequency methods given above.

Simultaneous measurements were carried out on Soviet geophysical rockets for electron concentration both by the method of a dispersion

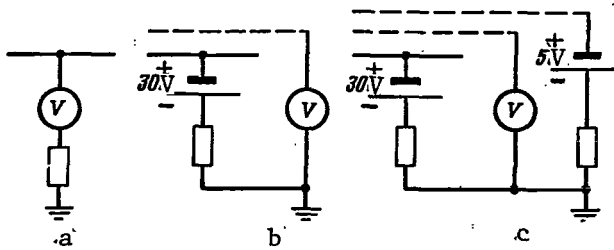


Figure 19. Schematic of the Measurements.

- a. Langmuir Probe; b. Diode Trap;
c. Triode Trap.

interferometer and the method of probes, and for electron temperature using various probe methods [62]. The measurement results show that the altitude distributions

of n_e are symbatic although the values of n_e from the probe data are less than the values of n_e from the dispersion interferometer data.

Figure 19 shows the schematic of the measurements using a flat Langmuir

probe and flat diode and triode traps; Figure 20 shows their semilogarithmic characteristics [63]. From Figure 20 it follows that the results of measuring T_e using various probes agree within measurement errors if there are no deviations from the Maxwellian velocity distribution.

THEORETICAL COMPUTATIONS AND EXPERIMENTAL DATA ON THE INFLUENCE OF PERTURBATIONS, CREATED BY A MOVING SATELLITE, ON THE MEASUREMENT RESULTS

It was noted above that one of the singularities of measurements using ionospheric probes is measurements on board a satellite whose orbital velocity exceeds the thermal velocity of the ions by approximately one order. This leads to the formation of a perturbed region behind the satellite (with respect to the velocity vector) where the ion concentration differs substantially from the ion concentration in the unperturbed ionosphere [19]. For the measurements using the probe method it is of interest to examine two problems:

/115

(1) Whether the parameters of the ionospheric plasma vary near the satellite outside this region;

(2) The distribution of the equipotential surfaces near the satellite or spherical ion trap.

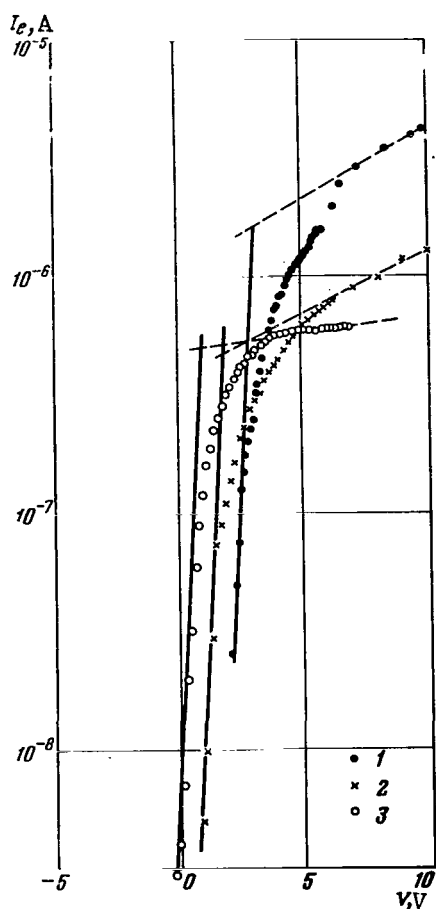


Figure 20. Semilogarithmic Characteristics.

1. Langmuir Probe, $T_e = 2400^\circ \text{ K}$;
2. Diode Trap, $T_e = 2500^\circ \text{ K}$;
3. Triode Trap, $T_e = 2300^\circ \text{ K}$.

$(R/r_D) \ll 1$ under the given assumptions as to the smallness of the relative value of the potential; therefore for computation of the structure of the region near the satellite we use computational methods. /116

Evaluation of the effects of ionization and heating of the gas due to particles reflected from the satellite shows that for the real parameters of the ionosphere and the dimensions of the satellites these effects can be ignored [64].

Without pausing for a detailed examination of the various theoretical computations of the structure of the perturbed region near a rapidly moving satellite [64, 65], let us note that for the theoretical computations we use dimensionless parameters, i.e. the ratio of the characteristic dimension of the satellite R to the Debye radius r_D , and the relative value of the satellite potential, which characterizes the ratio of the energy eV acquired by the particle in the satellite's field to the thermal energy of the particle kT . At the present time we have been able to analytically obtain the asymptotic distribution of the basic physical values at large distances from the satellite for $(R/r_D) \ll 1$ and for

Figure 21 shows the lines of equal potential close to a metal sphere which

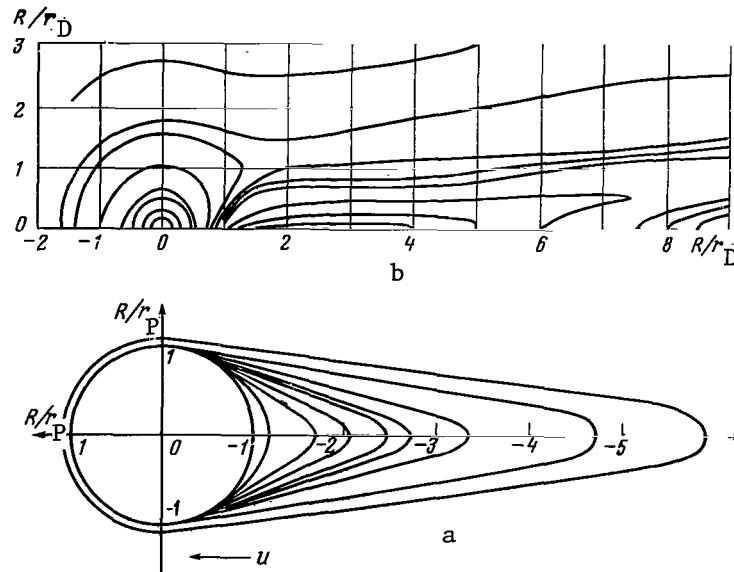


Figure 21. Equipotential Surfaces Near a Metal Sphere Which Absorbs the Particles Incident on It.

a. $R/r_D \gg 1$; b. $R/r_D \ll 1$.

absorbs the particles incident on it, for the cases $(R/r_D) \gg 1$ [64] and $(R/r_D) \ll 1$ [65]. On the drawing it is clear that the equipotentials have a spherical shape on the front (with respect to the velocity vector) of the satellite. Thus, the theoretical computations give a basis for assumptions concerning the movement of ions in a spherically symmetric field near the ion trap, which was done in deriving expression (11), since the ions are basically incident on the front of the ion trap.

The experimental results on studying the distribution of ion concentration near the satellite agree qualitatively with the results of the theory [23, 35]. As far as the distribution of electron concentration near the satellite is concerned, the following should be mentioned. Since the thermal velocity of the electrons is approximately one order greater than the rate of movement of the satellite, this latter can not change the distribution of the electrons. However, from theoretical arguments it follows that

because of the electrostatic forces the electron concentration distribution (n_e) in the perturbed region to the rear of the satellite must agree with the distribution of the positive ion concentration [64]. The experimental data on this question are contradictory: some results show zero n_e behind the satellite [41], and some results show that the n_e behind the satellite is lowered in comparison with the unperturbed ionosphere by a factor of no more than 2 [38].

From the data given in this section it follows that in setting up the probe measurements on board satellites it is necessary to take into account the possibility that the probes will enter the perturbed region behind the satellite and that the data obtained in such cases pertain to this region rather than to the ionospheric plasma.

PROSPECTS FOR USING THE PROBE METHOD FOR IONOSPHERIC RESEARCH

The fact that probe measurement results are completely independent of the characteristics of the ionospheric region far from the probes, as already mentioned above, makes these methods quite promising for investigating the ionospheric structure. It especially should be mentioned that it is possible to investigate the inhomogeneities and nonstationary phenomena using probes. The choice of one or another type of probe will depend on the characteristics of the bodies on which the experiments are carried out. The complexity of interpreting the probe measurements and the large amount of primary data obtained in the experiments on board the satellites and rockets, requires a careful use of the methods involved and the creation of methods for interpreting the primary results of the measurements directly on board the satellite or rocket, as well as developing programs for computer processing. Here it is necessary to bear in mind that in studying new phenomena or properties which had previously been unknown, using the method with an a priori given system of interpreting the results may prevent these investigations from being carried out.

Developing methods for investigating the ionosphere will require preliminary testing and since the ionospheric plasma is an ideal medium for using the probe method, in certain instances testing under laboratory conditions is not sufficient and it is necessary to conduct methodological experiments directly under ionospheric conditions. Such treatment will permit obtaining reliable methods for use, not only in the ionosphere, but also in laboratory plasma.

The fact that the form of the electron branch of the volt-ampere curve in the case of retarding potentials is independent of the configuration of the probe permits a probe of any shape to be used for measuring the concentration and temperature of electrons. However the possibility of using a part /117 of the volt-ampere curve with attracting potentials and the influence of the magnetic field give a basis for selecting the Langmuir probe with a cylindrical shape. In fact the use of a flat probe does not permit utilization of the region of attracting potentials to obtain information. The use of a spherical probe involves certain difficulties caused by the fact that, to decrease the influence of the magnetic field on the shape of the volt-ampere curve, the radius of the sphere must be less than the cyclotron radius (which at altitudes of about 300 km is on the order of 3 cm). The surface of a spherical probe which satisfies this condition is small; furthermore, the spherical probe should be set up on a rod which, with the small radius of the probe, must disturb the structure of the electric field.

A long cylindrical probe may have a large collecting surface with a small radius; the cylindrical rod in this case will not disturb the symmetry of the electric field, but on the contrary will serve as a protective electrode. It is feasible to increase the distance between the probe and the body of the satellite (or rocket) to make the measurements outside the space charge layer which surrounds the satellite (or rocket). However for determination of the electron concentration using such a probe, it is necessary that it be oriented in a direction near to perpendicular with respect to the force lines

of the geomagnetic field. Failure to satisfy these conditions will have no effect on determining the electron temperature.

The use of Langmuir probes, which is desirable because of their simplicity and the theoretical possibility which they give for obtaining (from one volt-ampere curve) information on the particle concentration with charges of both signs and about both energy distributions, should be confined during daylight hours to those regions of the ionosphere in which the flows of charged particles to the probe exceed the flows of photoelectrons emitted by the probe. For a valid evaluation of the degree of reliability of determining the electron concentration using the probes we must make additional theoretical and experimental investigations, since from the results of comparison with other methods it follows that the probe measurements give smaller values than do the results of other methods.

The Langmuir probes and the probe methods based on analysis of the volt-ampere characteristics should be used with care in studying the regions of the ionosphere below 100 km, since the mean free path of the particles in these regions is small; it is true that there are individual theoretical attempts to justify operation of the probes under diffusion conditions (see [16 - 18]). In these regions the high-frequency methods have the advantage, since at altitudes below 100 km the probe potential can not be high and the thickness of the space charge layer plays a small role.

At high altitudes with small concentrations the use of high-frequency methods is complicated by the space charge layers. In these regions the charged particle traps including modulation traps, are advantageous for research.

To investigate the ion temperature it is feasible to use "honeycomb"-type traps, similar to the trap used on board the "Kosmos-2". Here it should be remembered that the accuracy of determining the ion temperature will de-

pend on determination of the variations in orientation of the trap relative to the velocity vector of the oncoming flow.

REFERENCES

1. Langmuir, I. Gen. Electr. Rev., No. 26, 1923, p. 731. /118
2. Kagan, Yu. M. and V. I. Perel'. Uspekhi fizicheskikh nauk (UFN), No. 31, 1963, p. 409.
3. Rusanov, V. D. Sovremennyye metody issledovaniya plazmy (Contemporary Methods of Plasma Research), 1962.
4. Granovskiy, V. L. Elektricheskiy tok v gaze. T. 1. (Electric Current in a Gas. Vol. 1), State Technical and Theoretical Press, (GITTL), 1952.
5. Verwey, W. Philos. Res. Repts. Suppl., No. 2, 1961.
6. Tonks, L., H. Mott-Smith and I. Langmuir. Phys. Rev., No. 28, 1926, p. 104.
7. Boyd, R. L. F. Proc. Roy. Soc., No. 201, 1950, p. 329.
8. Ionov, N. I. Dokl. AN SSR, No. 85, 1952, p. 753.
9. Sloane, R. H. and E. McGregor. Philos. Mag., Vol. 7, No. 18, 1954, p. 193.
10. Kulakov, Yu. M. and A. A. Zaytsev. Vestnik MGU, No. 3, 1949, p. 101.
11. Holle, F. Ann. Phys., No. 18, 1956, p. 328.
12. Boyd, R. and N. Twiddy. Proc. Roy. Soc., No. A250, 1959, p. 53.
13. Johnson, E. and L. Malter. Phys. Rev., No. 80, 1950, p. 59.
14. Kojima, S. and K. Takayama. J. Phys. Soc. Japan, No. 5, 1950, p. 357.
15. Biberman, L. M. and B. Panin. Journal of Technical Physics (ZhTF), No. 21, 1951, p. 2.
16. Davydov, B. I. and L. I. Zmanovskaya. ZhTF, No. 6, 1936, p. 1244.
17. Body, R. Proc. Phys. Soc., No. B64, 1951, p. 795.
18. Hault, D. P. J. Geophys. Res., No. 70, 1965, p. 3188.

19. Gringauz, K. I. and M. Kh. Zelikman. UFN, No. 13, 1957, p. 239.
20. Smith, L. J. Technique Manual on Electron Density and Temperature Measurements in the Ionosphere, ed. Maeda, COSPAR Information Bulletin, No. 17, 1964, p. 37.
21. Hinteregger, H. E., K. Damon and L. A. Hall. J. Geophys. Res., No. 64, 1959, p. 961.
22. Gringauz, K. I., B. N. Gorozhankin, N. M. Shutte and G. L. Gdalevich. Preprint Paper, Prepared for the 14th Intern. Astronautical Congress, Paris, 1963.
23. Gringauz, K. I., V. V. Bezrukikh and V. D. Ozerov. Iskusstvennyye sputniki Zemli, No. 6, 1961, p. 63.
24. Sagalyn, R. C., M. Smiddy and J. Wisnia. J. Geophys. Res., No. 68, 1963, p. 199.
25. Medicus, G. J. Appl. Phys., No. 33, 1962, p. 3094.
26. Whipple, E. C. Proc. IRE, No. 47, 1959, p. 2023.
27. Spivak, G. V. and E. M. Reykhrudel'. Journal of Experimental and Theoretical Physics (ZhETF), No. 6, 1936, p. 816; Izv. AN SSR, seriya fizich., No. 4, 1938, p. 479; Techn. Phys. USSR, No. 5, 1938, p. 715.
28. Hock, G., N. W. Spenser and W. G. Dow. J. Geophys. Res., No. 58, 1953, p. 235.
29. Gringauz, K. I., V. V. Bezrukikh, V. D. Ozerov and R. Ye. Rybchinskiy. Dokl. AN SSSR, No. 131, 1960, p. 1301.
30. Boggess, R. L., L. H. Brace and N. W. Spenser. J. Geophys. Res., No. 64, 1959, p. 1627.
31. Spenser, N. W., L. H. Brace and G. R. Carignan. J. Geophys. Res., No. 67, 119 1962, p. 157.
32. Brace, L. H., N. W. Spenser and G. R. Carignan. J. Geophys. Res., No. 68, 1963, p. 5397.
33. Nagy, A. F. and A. Z. Faruqui. J. Geophys. Res., No. 70, 1965, p. 4847.
34. Ichmimija, T., K. Takayama and Y. Aono. Space Res., 1960, p. 397.
35. Bourdeau, R. E. and J. L. Donley. Proc. Roy. Soc., No. 281, 1964, p. 481.
36. Gringauz, K. I., B. N. Gorozhankin, N. M. Shutte and G. L. Gdalevich. Space Res., No. 4, 1964, p. 473.

37. Afonin, V. V., T. K. Breus, G. L. Gdalevich, B. N. Gorozhankin, K. I. Gringauz, R. Ye. Rybchinskiy and N. M. Shutte. Sb. "Issledovaniya kosmicheskogo prostranstva" (Collection "Outer Space Research"), Nauka Press, 1965.
38. Gringauz, K. I., B. N. Gorozhankin, G. L. Gdalevich, V. V. Afonin, R. Ye. Rybchinskiy and N. M. Shutte. Space Res., No. 5, 1965, p. 733.
39. Gringauz, K. I., B. N. Gorozhankin, N. M. Shutte and G. L. Gdalevich. Dokl. AN SSSR, No. 151, 1963, p. 560.
40. Bowen, P. J., R. L. F. Boyd, W. J. Raitt and A. P. Willmore. Proc. Roy. Soc., No. 282, 1964, p. 504.
41. Bowen, P. J., R. L. F. Boyd, G. L. Henderson, W. J. Raitt and A. P. Willmore. Proc. Roy. Soc., No. 281, 1964, p. 514.
42. Boyd, R. L. F. and W. J. Raitt. Space Res., No. 5, 1965, p. 207.
43. Sagalyn, R. C., M. Smiddy and J. N. Bhargava. Space Res., No. 5, 1965, p. 189.
44. Brace, L. H., N. W. Spenser and A. Dalgarno. Planet. Space Sci., No. 13, 1965, p. 647.
45. Brace, L. H. and B. M. Reddy. J. Geophys. Res., No. 70, 1965, p. 5783.
46. Gringauz, K. I., V. V. Bezrukikh and L. S. Musatov. Preprint Paper Prepared for the Inter-Union Symposium on Solar-Terrestrial Physics, Belgrade, August, 1966.
47. Bezrukikh, V. V., K. I. Gringauz, R. Ye. Rybchinskiy, L. S. Musatov and M. Z. Kokhlov. Dokl. AN SSSR, No. 163, 1965, p. 4.
48. Takayama, K., H. Ikegami and Hiizaky. Phys. Rev. Lett., No. 5, 1960, p. 238.
49. Levitskiy, S. M. and I. P. Shashurin. ZhETF, No. 31, 1961, p. 436.
50. Crawford, E. W. and R. F. Mlodnosky. J. Geophys. Res., No. 69, 1964, p. 2765.
51. Harp, R. S. and E. W. Crawford. J. Appl. Phys., No. 35, 1964, p. 12.
52. Crawford, E. W. and R. S. Harp. J. Geophys. Res., No. 70, 1965, p. 587.
53. Samokhin, M. V. Geomagnetizm i aeronomiya, No. 6, 1966, p. 754.
54. Harp, R. S., G. S. Kino and J. Pavkovich. Phys. Rev. Lett., No. 11, 1963, p. 310.

55. Heikkila, W. J., J. A. Fejer, J. Hugill and W. Calvert. Preprint Paper Prepared for VII COSPAR, Vienna, Austria, 1966.
56. Ulvick, J. C., W. Pfister, O. C. Haycock and K. D. Baker. Technique Manual on Electron Density and Temperature Measurements of the Ionosphere, ed. K. Maeda, COSPAR Information Bulletin, No. 17, 1964, p. 117.
57. Getmantsev, G. and N. G. Denisov. Geomagnetizm i aeronomiya, No. 2, 1963, p. 691.
58. Krasnushkin, P. Ye. and N. L. Kolesnikov. Dokl. AN SSR, No. 146, 1963, p. 596.
59. Ulvick, J. C. and W. Pfister. Space Res., No. 3, 1964, p. 194.
60. Rothwell, P., J. Sayers and J. Wager. J. Geophys. Res., No. 67, 1962, p. 921.
61. Bauer, S. I., J. Blumle, J. L. Donley, R. J. Fitzenreiter and J. E. Jackson. J. Geophys. Res., No. 69, 1964, p. 186.
62. Gringauz, K. I., G. L. Gdalevich, V. F. Gubskiy, I. A. Knorin, V. A. Rudakov and N. M. Shutte. Preprint Paper Prepared for VII COSPAR, Vienna, 1966.
63. Gdalevich, G. L., V. F. Gubskiy and I. D. Dmitriyeva. Preprint Paper Prepared for the Inter-Union Symposium on Solar-Terrestrial Physics, Belgrade, August, 1966.
64. Al'pert, R. L., A. V. Gurevich and L. P. Pitayevskiy. Iskusstvennyye sputniki v razrezhennoy plazme (Artificial Satellites in Rarefied Plasma), Nauka Press, 1964.
65. Zhukov, V. V., M. G. Kuz'mina, M. V. Maslennikov and Yu. S. Sigov. Tezisy dokladay na 5 Rizhskom soveshchanii po magnitnoy gidrodinamike (Abstract of the Report at the Fifth Riga Conference on Magnetic Hydrodynamics), June 20 - 25, 1966.

RADIOPHYSICS RESEARCH OF THE IONOSPHERE BASED ON THE
PROPAGATION OF RADIO WAVES FROM ROCKETS
AND SATELLITES⁽¹⁾

V. A. Misyura

ABSTRACT. Radio-physical ionospheric investigations can be used for direct measurement of effects arising in propagation of radio waves. These are: Faraday effect (angle ϕ and "frequency" ω of rotation of the plane of polarization), the environmental correction to the Doppler shift, a correction to the phase and group path (phase $|\Delta L|$ and group $|\Delta R|$ "lag"), refraction, incoherent scattering of radio waves and some other effects. Then the required parameters of the ionosphere are found according to the measured effects and to the data on the position and movement of the beam (a reverse problem). These effects are also interesting for investigation of their own properties.

The paper presents a brief analysis of basic radio-physical methods for ionospheric investigations with the help of artificial satellites and rockets and of the most important data on ionospheric parameters (mainly of the outer ionosphere) obtained by means of them.

Radiophysics research of the ionosphere includes, as we know, the direct measurement of certain effects which set in during the propagation (or re-emission) of radio waves from objects in space⁽²⁾. Then, based on the measured effects and the data on movement and position of the object in

(1) The present article reflects the viewpoint of the author, which is not the generally accepted one. An alternative viewpoint is reflected in the works of K. I. Gringauz et al., "Geomagnetizm i aeronomiya", Vol. 5, No. 4, 1965, p. 762; Vol. 6, No. 3, 1966, p. 568; W. T. Ross et al., J. Geophys. Res. (Preprint), October, 1967.

(2) By objects in space we shall imply in general satellites, rockets and spacecraft, planets, masses of plasma, astronomical sources of radio waves, and other natural and artificial formations in the ionosphere and above, which emit or re-emit radio waves.

space, these or other physical parameters of the ionosphere (inverse problem) or other effects are determined which can not be measured in any manner directly. These effects may be of independent practical⁽³⁾ and scientific interest.

So, sometimes (for example, in radiophysics and in the process of radio measurements), we may find it convenient to look at these effects themselves and certain generalized physical characteristics of the ionosphere and the radio signal rather than proceeding to the electron concentration or to other generally accepted ionospheric parameters. This is especially the case since the transition, associated usually with solving the "inverse" problem, may involve considerable difficulty

Basic among effects measured directly are: the Faraday effect (the angle Φ_ϕ and the "frequency" $\dot{\Phi}_\phi$ of rotation of the polarization plane), corrections for the Doppler frequency shift due to the atmosphere in comparison with a vacuum, for the phase and group path of the radio waves (phase (ΔL) and group (ΔR) radio wave lag; refraction, distortion of the signal shape, radio wave scattering and other effects.

The basic parameter of the ionosphere (especially for radiophysics), obtained from further interpretation, as we know, is the electron concentration of the ionosphere $N^{(4)}$. Instead of N (or in addition to N) we often use a parameter which is dependent on the distribution of N in space, i.e. the total (integral) electron content N_0 in the vertical column or in the

(3) For example, in the practical problems of radio communication, radio navigation, radar and radio measurements associated with the flights of objects in space.

(4) Or the "effective" electron concentration which takes into account the influence not only of electrons but also of ions on the refractive index of the ionosphere for the radio waves.

column inclined along the line of sight N_{OL} of the ionosphere of a unit cross section extending from the observation point to the object in space. Among the other parameters which might be determined for the ionosphere, are the kinetic temperatures of the electrons T_e and ions T_i and their gyrofrequencies, number of collisions ν of electrons with heavy particles of the ionosphere, its ion composition and also several derived parameters and /121 effects; parameters of neutral particles etc.

The atmospheric parameters, just as the effects which take place with the propagation of radio waves, may contain both a regular and an irregular component.

The advantage of radiophysics measurements on the propagation of radio waves from satellites is the possibility of obtaining the dependences of the measured values on latitude and longitude over large areas of the Earth's surface.

On the other hand when using geophysics rockets with a vertical trajectory we can make the measurements over the entire thickness of the ionosphere up to the altitude of rocket ascent for a brief time in one set of observations, but at limited distances from the site of the rocket launch. Furthermore, each test using the geophysics rockets is significantly more expensive than the experiment using artificial Earth satellites (AES).

Let us pay the greatest attention to the method of coherent frequencies and the method of the Faraday effect as the ones most widely used at the present time.⁽⁵⁾ To a lesser degree we shall touch upon the methods based on the use of group lag, ionospheric refraction of radio waves, etc.

(5) For measuring the parameters of the ionosphere we use the methods of probing the ionosphere above the satellite and the method of incoherent scattering of radiowaves of the ionosphere; they are the most promising, but are as yet insufficiently used.

METHODS BASED ON THE USE OF THE FARADAY EFFECT, THE DOPPLER EFFECT AND THE PHASE LAG OF RADIO WAVES AT COHERENT FREQUENCIES

The methods studied are based on measuring the Faraday effect ($\dot{\Phi}_\phi$ and Φ_ϕ) and the so-called normalized difference in the Doppler frequency shift of coherent waves and the corresponding normalized phase difference Φ , proportional, respectively, to the rate of change in the phase lag and the lag itself ($\dot{\Phi} \sim \frac{d\Delta L}{dt}$, $\Phi \sim \Delta L$) of the coherent radio waves, propagating from objects in space. The method using the Faraday effect began to be used for determining the neutral electron content in the entire ionosphere of the Earth even before launching of satellites with lunar radar measurements (Brown, Evans et al. [1, 2, 3]). After geophysics rockets and especially satellites began to be launched, this method found widespread usage, and based on measurements of $\dot{\Phi}$ and Φ it appeared to be a more precise, although more complex, method. This so-called method of the "difference" Doppler effect of coherent frequencies is based on the familiar method of "dispersion interferometer" which was proposed back in the 1930's by L. I. Mandel'shtam and N. D. Papaleksi [4] and then used by Ya. L. Al'pert, V. V. Migulin, P. A. Razin and others for measuring the phase velocity of radio waves at the surface of the Earth with a high degree of accuracy. This method was used for ionospheric measurements with the assistance of rockets abroad [5, 6] and in the Soviet Union (K. I. Gringauz, V. A. Rudakov [7, 8]) and with the assistance of satellites (Ya. L. Al'pert et al., [9 - 15]). In the foreign literature we can see a modification of this method as evidenced by the method used by Seddon-Jackson [3, 5, 6].

The initial expressions for both methods for the case of dependence of the refractive index of the ionosphere n on the three coordinates $x_{1,2,3}$ and time can be represented approximately with an accuracy up to small

values on the order of $\alpha^2 ([\alpha] \ll 1, n = \sqrt{1+\alpha} \cong 1 + \frac{\alpha}{2}, \alpha = -kNf^{-2})$ (6)

$$\Phi_{\Phi} \sim \bar{b}_L \Delta L + C_1, \quad \Phi \sim \Delta L + C_2, \quad (1) \quad \underline{/122}$$

$$\Delta L = -0.5 k f^{-2} N_{0L}, \quad N_0 = N_{0L} \overline{\sin \beta'}, \quad (2)$$

$$N_{0L} = \int_0^R N dx_1, \quad N_0 = \int_0^{z_B} N dz, \quad (3)$$

$$\overline{\sin \beta'} = N_0 \left(\int_0^{z_B} N \sin \beta'^{-1} \right)^{-1}, \quad r \cos \beta' = r_A \cos \beta_A, \quad (4)$$

$$\bar{b}_L = \left(\int_0^R N b_L dx_1 \right) N_{0L}^{-1}, \quad b_L = f^{-1} f_L, \quad (5)$$

$$\Phi \sim \alpha_B V_R + V_{\tau B} I + I_t, \quad (6)$$

$$\Phi_{\Phi} \sim \alpha_B b_{LB} V_R + V_{\tau B} I' + I'_t + \delta, \quad (7)$$

$$I = R^{-1} \int_0^R x_1 \nabla_{\tau} x dx_1, \quad (8)$$

$$V_{\tau B} I = V_{\beta} I_{\beta} + V_{\epsilon} I_{\epsilon}, \quad (9)$$

(6) We use the expressions and definitions given in [11, 12, (p. 138)] and [16].

$$I_{\beta, \varepsilon} = R^{-1} \int_0^R x_1 \frac{\partial \alpha}{\partial x_{2,3}} dx_1, \quad I_t = \int_0^R \frac{\partial \alpha}{\partial t} dx_1 \sim \frac{\partial N_{eL}}{\partial t}. \quad (10)$$

Definitions in these formulas are the following: f is the effective frequency; k is a known constant; r_A , r represent the distance from the center of the Earth to the observation point A and to the instantaneous point of the beam, respectively; z_B , z represent the altitude of the radiator B and the instantaneous point of the beam over the surface of the Earth; R is the distance from A to B; β' , β_A represent the angle of elevation of the beam at the instantaneous point and at point A, formed with the plane of the horizon at the respective point; f_L is the projection of the gyrofrequency on the beam at the instantaneous point; C_1 , C_2 represent the constants of integration; $V_{\tau B}$ is the velocity component of the radiator transverse to the beam; V_β , V_ε are the components of $V_{\tau B}$ in the vertical plane, passing through points A and B, and in the plane perpendicular to it and passing through A and B (i.e., $V_{\beta, \varepsilon}$ are the components of $V_{\tau B}$ along the axes x_2 and x_3 , respectively, transverse to the beam); the integrals I' and I'_t are found respectively from I and I_t in (8) - (11) by substituting α_{bL} for α . The variable components I_t and I'_t in formulas (6), (7) can usually be ignored for measurements on board satellites up to altitudes $\sim 2000 - 3000$ km [16], and in measurements with the assistance of rockets, up to altitudes less than the altitude of the vertical ascent of the rocket⁽⁷⁾.

With movement of the radiator along the beam (along R) we can probably measure the electron concentration N_B along the trajectory of the object [in the right hand side of expressions (6), (7) we need take into account only the first term] with a high degree of accuracy if we use the

(7) At this point it is possible to measure the ionospheric variables I_t , I'_t .

independent measurements of $\dot{\Phi}$ or $\dot{\Phi}_\phi$; the combined use of $\dot{\Phi}$ and $\dot{\Phi}_\phi$ reveals in this case the theoretical potentialities of an independent measurement of the geomagnetic field (parameter b_{LB}) along the trajectory of the object. This situation exists in particular in observations at the site of vertical launching of geophysical rockets. Apparently the first correct and most accurate measurements of the vertical profiles N of the outer ionosphere were obtained mainly in this manner by using $\dot{\Phi}$ [7, 8, 3].

/124

In all the works published prior to 1960 where the electron concentration N_B was measured from the registrations of $\dot{\Phi}$ and $\dot{\Phi}_\phi$ from the AES signals, the value of N_B was determined approximately at one point or on a small segment of the AES orbit where all terms except the first could be ignored in the right-hand side of expressions (6) and (7).

The method of chains of equations proposed by Ya. L. Al'pert [17] and developed and investigated in [11, 16], is interesting in that it permits an approximate determination of the electron density N_B along the AES orbit on a significant segment of it.

This method, as we know from [11, 16, 17] involves the fact that if we neglect the change in α and I in equation (6) or (7) ($\Delta\alpha = \alpha_2 - \alpha_1 \simeq 0$, $\Delta I = I_2 - I_1 = 0$) and take into account the change in V_R and V_{TB} ($\Delta V_R = V_{R_2} - V_{R_1} \neq 0$, $\Delta V_{TB} = V_{TB_2} - V_{TB_1} \neq 0$) known from orbital data for a certain interval of time $\Delta t = t_2 - t_1$, equation (6) [or (7)] is formulated for two moments of time t_1 and t_2 ; as a result we find a system of two equations relative to the values of the two unknowns α and I for the interval Δt . The lack of sufficient analysis of the accuracy of the method stimulated a more detailed investigation and development of the method [11, 16, 19, 20] as well as the criticism [18].

The sufficient conditions for applicability of the method of the "chain" were cited in [11] and the necessary and sufficient conditions in [16, 18, 20]. Reference [16] investigates the theoretical and experimental possibi-

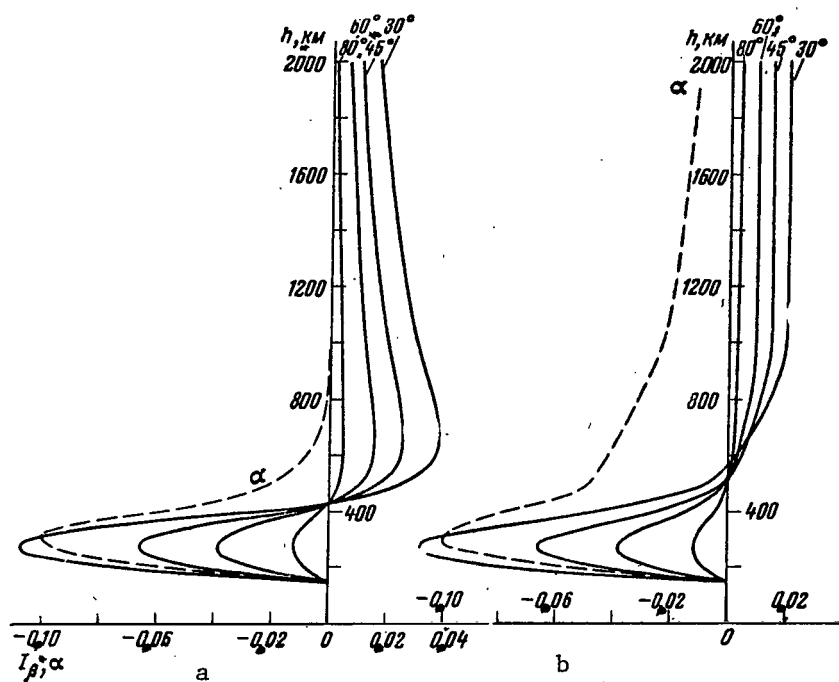


Figure 1. Dependence of the Quantity $I_{\beta} \cdot \alpha^{-1}$ on Altitude h for Different Angles of Elevation $\beta_B = \text{const}$ (80, 60, 45 and 30°) for a Parabolic-Exponential Model with the Parameters: $z_0 = 150$ km, $z_m = 300$ km, $b^2 = f_0^2 f^{-2} = 0.1$, Where f_0 is the Critical Frequency for Various Values of the Ionosphere Altitude.

a. $H = 100$ km; b. $H = 250$ km.

lities of realizing these conditions for the practically attainable values of the error in determining N_B . It was established that the "chain" method permits determination of N_B along the satellite's orbit with an error which usually does not exceed 20 - 30% of the wide range of AES orbital types and states of the ionosphere.

In the various methods of interpreting registrations of the Doppler and Faraday effects by using expressions (6) and (7), a substantial role (especially in the "chain" method) is played by the relationship in (6)

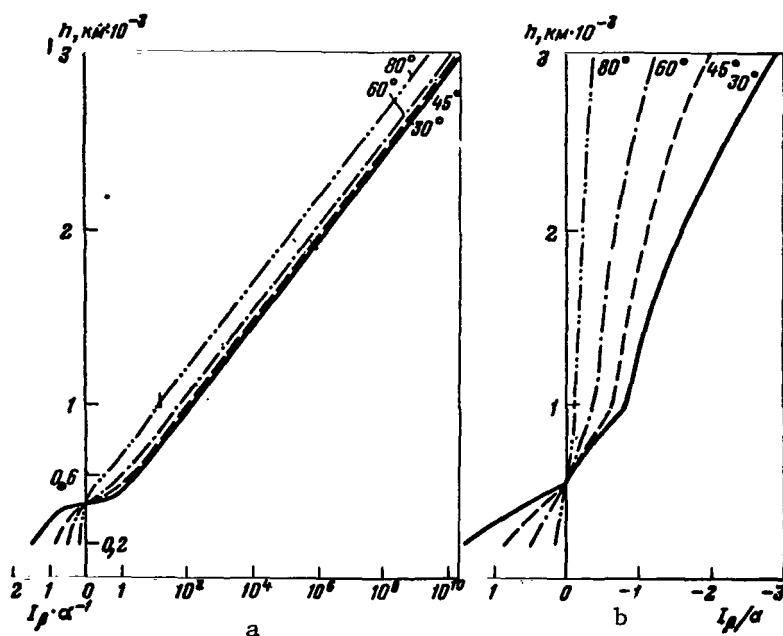


Figure 2. Computed Function $I_{\beta} \cdot \alpha^{-1}$ for the Model.

a. $H = 100$ km; b. $H = 250$ km.

between I_{β} and α_B (Figures 1 - 3) [27] or in (7) between I_{β}' and $\alpha_{B_{LB}}^{b(8)}$. The smaller the ratio $I_{\beta} / \alpha_B^{(9)}$, then the smaller is the error of the "chain" method [16] under stable equal conditions. The dependences of I_{β} , α_B and

(8) In the case of a stratified atmosphere or when the horizontal gradient component along the x_3 axis can be ignored, as well as in the tests on rockets in the general case $I_{\epsilon} = 0$ and $I = I_{\beta}$. The dependence of I_{ϵ} on the coordinates ($I_{\epsilon} \neq 0$ in the presence of horizontal gradients N) is analyzed in [16].

(9) It is obvious that when this ratio is sufficiently small, then N_B is determined from (6) or (7) automatically, since in these expressions only the first term which contains N_B can be left.

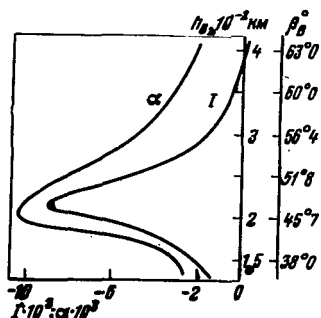


Figure 3. Experimental Dependence of I and α_B on h and β_B , Obtained from the Spaced Observation of Signals from Geophysical Rockets [19, 20].

$I \alpha_B^{-1}$ on altitude z , computed (Figure 2) [21] and experimentally obtained from the spaced reception of signals from the geophysics rockets [11, 16, 22, 23], for the various values of the angle of elevation β_B illustrate a fact that is essential for accuracy of the "chain" method that for the real ionosphere with an altitude-variable value of the normalized altitude H (Figure 1 b, Figure 2 b) the ratio $\alpha_B I \alpha_B^{-1}$ remains significant up to high altitudes ($\sim 2000 - 3000$ km) and rapidly drops with decrease in β_B . This fact also ensures the allowable ($< 30\%$) error in the "chain" method (Figure 4). Figure 4 shows the values of α_B along the orbit of the "Elektron-1" corresponding to the given model (Figure 1) and computed from the "chain" method (for the given model using (6) the values of I_B and ϕ are computed and then from them by using the "chain" method, the value of α was again determined and compared with the value of α in the given model).

Similar investigations showed the applicability of the "chain" method to expression (7) for the Faraday effect. Table 1 gives an example of computing the relative error $\delta\alpha$ in the "chain" method (α_{Bc}) for a parabolic-exponential model of the ionosphere ($z_0 = 180$ km, $z_m = 320$ km and $H_1 = 300$ km up to $z \leq 600$ km and $H_2 = 800$ km for $z \geq 600$ km, $b^2 = 0.1$) for one flight of the "Elektron-1" on February 25, 1961 over Kharkov (velocity components of the satellite V_R and V_β and the coordinates z_B , β_B are also shown on Table 1). It is easy to see that even for small angles of elevation of the given AES flight the precision of the "chain" method is still applicable.

Thus, the value of $\sigma\alpha$ in Table 1 was computed as the difference in

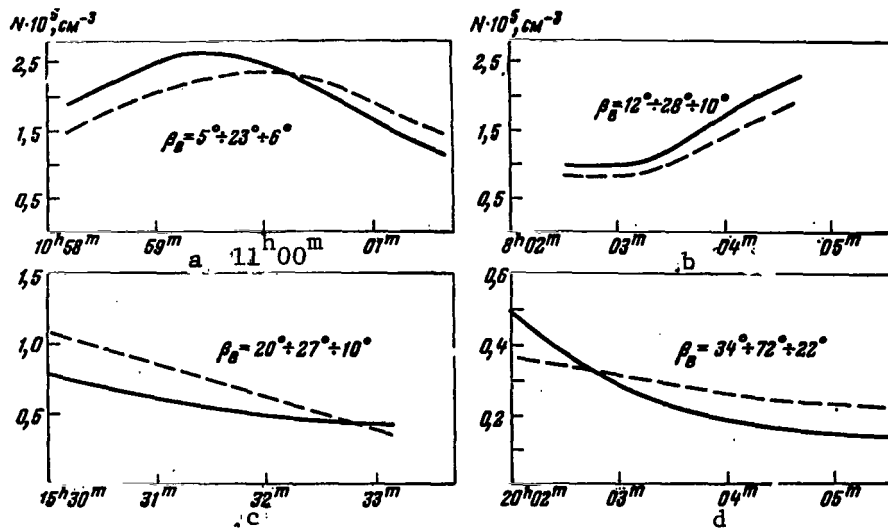


Figure 4. Dependence of N for the Given Model (Solid Line) and that Computed by the "Chain" Method (Broken Line) on Flight Time (Moscow) over Kharkov of the Satellite "Elektron-1".

- a. March 7, 1964, $z_B = 447 - 413 - 510$ km, model; b. March 11, 1964, $z_B = 626 - 480$ km; c. February 25, 1964, $z_B = 680 - 820$ km; d. February 6, 1964, $z_B = 1110 - 1420$ km.

values of α from the known model of N and computed by the "chain" method.

Under the experimental conditions we find the main distinction to be that the real model of the ionosphere is unknown and $\sigma\alpha$ is computed from the imprecise model obtained from the experiment. The question naturally arises as to how much this latter value $(\sigma\alpha_{Bce})^{(10)}$ differs from the real error.

Analysis showed that the errors do not differ strongly when they are not very high ($\approx 30\%$). This agrees with the convergence of the known model

/127

(10) $\sigma\alpha_{Bce}$ is the error in determining α_B , found as the difference in values of α_B , computed by the "chain" method and the corresponding imprecise method obtained in the experiment.

TABLE 1 *

(Moscow) Time of observation	5 ^h 31 ^m 30 ^s	50 ^s	32 ^m 00 ^s	10 ^s	40 ^s	50 ^s
z_B , km	795	823	837	851	895	910
β_B , deg	26,7	26,0	25,5	25,1	23,4	22,8
ϵ_B , deg	36,6	42,8	45,7	48,4	55,5	57,6
V_R , km·sec ⁻¹	3,38	4,04	4,33	4,60	5,29	5,48
V_β , km·sec ⁻¹	-0,84	-1,27	-1,46	-1,62	-1,99	-2,08
$-\alpha_B \cdot 10^3$ (model)	32,5	31,4	30,8	30,3	28,7	28,2
$-\alpha_B \cdot 10^3$ ("chain")	29,5	25,1	37,5	22,9	20,8	34,7
$\alpha_B \% = \alpha N_B, \%$	10	~20	22	25	27	12
α_B , exp %	12	18	21	23	26,5	11
$-I_C \cdot 10^3$	0,59	0,50	0,17	0,41	0,34	0,81

TABLE 2 *

Time of observation (Moscow)	24.7 1958 r.				8.6 1958 r.			
	20 ^h 32 ^m 40 ^s	33 ^m 00 ^s	30 ^s	50 ^s	14 ^h 35 ^m 40 ^s	36 ^m 00 ^s	30 ^s	37 ^m 00 ^s
Z_B , km	317	325	339	348	694	701	724	747
β_B , deg	21,16	20,43	18,19	16,29	39,13	44,29	52,06	55,55
ϵ_B , deg	326,46	338	353	0,1	289	281	264	241
$F_\Phi \cdot 10^3$, Hz	3,6	6,25	8,49	10	68	69	70,5	73
V_R , km ⁻¹ ·sec	-0,602	-2,27	-4,126	4,99	-3,99	-3,34	-2,07	-0,23
V_τ , km ⁻¹ ·sec	2,05	2,3	2,8	3,1	42	3,09	2,9	1,5
$\alpha_B b_{LB} \cdot 10^5$	4,75	4,85	5,0	5,15	6,3	6,0	5,4	4,8
$-I \cdot 10^3$	8,4	8,35	8,2	8,1	4,02	4,07	4,16	4,75
$b_{LB} \cdot 10^3$	16,9	5,7	8,1	14,6	42	47	55	60
$\frac{\Delta V_R \cdot 10^3}{V_R + \Delta V_R}$	-150	-35	-13	8	6,6	10	23	300
$\frac{\Delta (\alpha_B b_{LB})}{\alpha_B b_{LB}} \cdot 10^3$	1,96	1,89	1,79	1,72	3,5	6,8	4,3	2,8
$\frac{\Delta V_\tau}{V_\tau + \Delta V_\tau} \cdot 10^3$	48,5	53	53	47	18	33	12	49
$\frac{\Delta I}{I} \cdot 10^3$	5,9	6,0	6,1	6,2	5	7	5	5
$\alpha N_B, \%$	31,4	6,2	14,4	31,8	25	15	14	16

*Translator's Note. Commas represent decimal points.

of the iteration process in interpreting by the "chain" method when the accuracy is naturally satisfied in smoothing out the experimental model after interpretation. Computation of $\sigma\alpha_{Bce}$ must be carried out even for this smoothed out (preferably by computation on a computer) model.

Table 2 gives the data from computation of $\sigma\alpha_{Bce}$ (σN_B , %) [21] from the registrations of the Faraday effect from signals of the third AES for two flights over Kharkov; for small angles of elevation and altitudes (flight on July 24, 1958, $z_B = 312 - 358$ km) and higher (June 8, 1958, $z_B = 679 - 755$ km). Table 2 gives the values of the frequency $F_\phi = \phi_\phi/2\pi$, the coordinates (z_B , β_B and ϵ_B), the velocities (V_T , V_R) of the satellite and other values necessary for proving the conditions of applicability of the "chain" method [11, 16]. From such a method the registrations of the Faraday effect from the signals of the third AES at Kharkov were interpreted at a frequency of 20 MHz in summer (June, July) of 1958 and fall (September, October) of 1959 and, from 20 flights of the satellite in each season, the "summer" and "fall" vertical profiles N up to an altitude of approximately 1000 km [21] were plotted (Figure 5)⁽¹¹⁾. The lower part of the profiles was plotted from the data on the vertical probing. These profiles agree with the data obtained using other methods [24].

The basic results of determining N_B along a rocket's trajectory [3, 7, 8, 11, 12, 19, 23, 25, 46, 47] and the orbit of a satellite [3, 9 - 13, 19, 20, 26, 27] include the following:

(1) The first correct and qualitatively new data were obtained (1958) on the vertical profile N of the outer ionosphere from measurements of $\dot{\phi}$ using geophysics rockets; this is especially significant in that the erroneous data from [28] had been fairly widely accepted; in [28] the extent of the outer ionosphere was significantly less than the actual value;

(11) The computations on Figure 6, just as on Figures 1, 2, etc., have been made by V. A. Podnos.

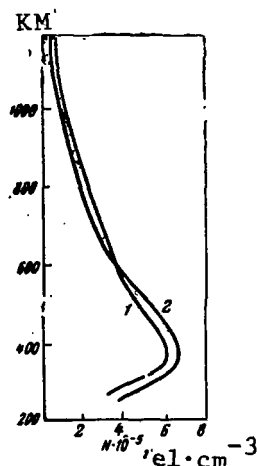


Figure 5. Average Vertical Profiles N , Obtained from the Faraday Effect of Signals from the Third Artificial Earth Satellite by the "Chain" Method and Vertical Probing at Kharkov.

1. Summer 1958; 2. Fall 1959.

(2) It was found that the outer ionosphere is "compressed" with transition from high to low solar activity;

(3) The fact of a stable nonmonotonic path of N_B was discovered experimentally along the inclined orbit of the AES above the F2 maximum; this has received no unequivocal interpretation as yet.

(4) It was established that the electron density at high altitudes (1500 - 2000 km):

(a) is fairly high ($\sim 10^4 \text{ el} \cdot \text{cm}^{-3}$) even at low solar activity;

(b) undergoes less pronounced diurnal and seasonal variations, the greater the altitude; and

(c) drops with altitude significantly more slowly than at altitudes of $\sim 350 - 400 \text{ km}$; i.e. at high altitudes the normalized altitude H of the outer ionosphere increases strongly, which is due mainly to variation in the ion composition (high predominance at high altitudes of light ions H^+) and also to the increase in plasma temperature.

These facts agree with the results obtained by the latest methods (probing the ionosphere from above the satellites [3, 26, 29]⁽¹²⁾ and data

(12) See the rocket data up to several thousand kilometers [46, 47].

from incoherent scattering of radio waves by the ionosphere [16, 30, 26]).

The most correct information on the total electron content (N_0 and N_{OL}) /128 can be obtained (and is widely used [3, 11, 15, 24, 31 - 33]) from measuring Φ or $\dot{\Phi}$ if we can eliminate the constants C_1 and C_2 in (1), (2) (for example, in the presence of uninterrupted registrations of Φ or $\dot{\Phi}$ including the moment when the radiator enters or leaves the ionosphere or including the moment of transit in the lower ionosphere with simultaneous vertical probing) or by the simultaneous registration of $\dot{\Phi}$ and $\ddot{\Phi}$. This latter follows from the fairly general expression obtained by differentiating (1), (2) with respect to τ (see, for example, [24, p. 138]):

$$\ddot{\Phi} = k_1 \ddot{b}_{\Delta L} + k_2 \ddot{b}_L \dot{\Phi},$$

where k_1, k_2 are known constants.

A number of other methods exist for excluding $C_{1,2}$ in (1), (2) [24, 13 - 15, 31, 32]. Computer computations using the method of least squares deserve mention [31 - 33]. N_{OL} can be converted into N_0 and \bar{b}_L can be determined quite correctly from formulas (2), (4) and (5) by using iterations [11] when necessary. It is easy to determine N by differentiation with respect to N_0 obtained as a function of z . Many publications exist for such measurements.

The total electron content can be obtained simply and quite reliably from the registrations of $\dot{\Phi}$ at two rather near frequencies. For example, such measurements have been carried out by us from data on the satellite "Elektron-3" [24]. The same thing can be done with data from the "Explorer XXII" [15, 21, 34, 47]. With this method, C_1 in (2) can be automatically dropped and any possible indeterminacy can be eliminated in the relative position of the antennas of the radiator and the receiver.

The most numerous, the simplest and apparently the least accurate mea-

measurements of N_{OL} (or N_0) were made under several conditions of registering $\dot{\Phi}_\phi$ from AES signals at one frequency⁽¹³⁾. The reliability of the measurements here was somewhat increased by using two (or three) crossed antennas and also by operating at two frequencies. The corresponding results of the investigations have been described quite well in the literature. The measurement errors may apparently reach 20 - 30%.

N_{OL} (N_0) and the refraction can be found approximately under certain conditions from $\dot{\Phi}_\phi$ and $\ddot{\Phi}_\phi$, from $\dot{\Phi}$, $\ddot{\Phi}$ or from $\dot{\Phi}_\phi$ and $\dot{\Phi}$ (see, for example, [34 - 36]). Essential in measuring the refraction is the fact that usually the horizontal gradients are not taken into account and this may lead to significant errors, especially in using satellites. In determining refraction using geophysical rockets, the gradients lying in the plane perpendicular to the plane of the beam exert no influence on the measurements, but those lying in the plane of the beam may be allowed for approximately in using both rockets and satellites [46, 47].

The vertical refraction $\Delta\beta$ and the phase lag ΔL , obtained [34] according to registrations of $\dot{\Phi}$ from signals from the "Elektron-1" at Kharkov, as a typical function of time (Moscow) and satellite coordinates (z_B and β_B) has a characteristic minimum which corresponds to the minimal distance of the satellite (Figure 6). Such a function agrees with theory. The value of $\Delta\beta$ and ΔL may reach (at a frequency of 20 MHz) the order of units of degrees and tens of kilometers, respectively.

Regular extended horizontal gradients of its parameters often exist in the ionosphere and these may be significant. The available data are inadequate (especially for the outer ionosphere). Interest has arisen in

/129

(13) We are tempted to use the "chain" method for obtaining N_B for the numerous registrations of $\dot{\Phi}_\phi$ accumulated for many years, although it is only roughly approximate.

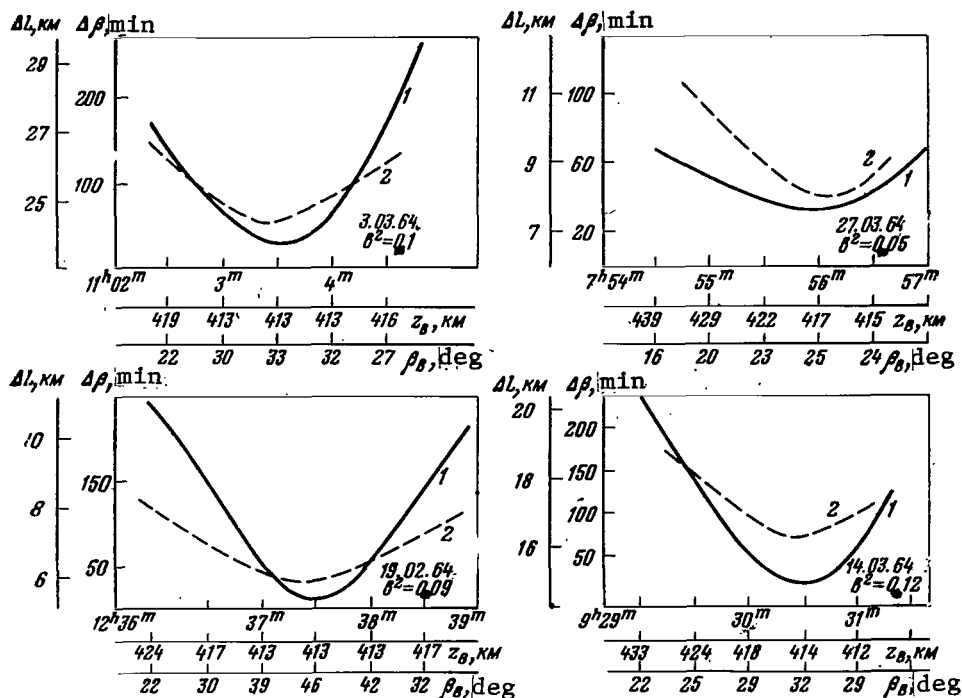


Figure 6. Vertical Ionospheric Refraction $\Delta\beta$ and Phase Lag ΔL of Signals from the "Elektron-1" as a Function of Time (Moscow) and Coordinates of the Satellite Based on Observations at a Frequency of 20 MHz at Kharkov.

1. ΔL ; 2. $\Delta\beta$

the measurement of these gradients [11 - 14, 23 - 25, 46, 47].

Measurements of these gradients can be accomplished not only by vertical probing by ionospheric stations from below and satellites from above, but also by the registrations of Φ or Φ_ϕ , as well as the combined registrations of Φ and Φ_ϕ in the presence of three dimensional equilibrium. In the event that geophysics rockets are used for this, the observation points must be spaced (for measurement of the total horizontal gradient the points must be angularly spaced in two horizontal directions [11, 23]; in measurements on board

satellites the spacing may be partially compensated by observations at one point for a sufficiently extended segment of an inclined satellite orbit [24]).

Using the data about the above-cited gradients we can obtain information on the regular variables of the ionosphere [16, 23, 27, 34, 36, 37]. Data on this are significant for ionospheric physics and for developing methods of ionospheric measurements (especially using $\dot{\phi}$ and $\dot{\phi}_0$).

The basic results of measuring the regular horizontal gradients of ionization and variables of the ionosphere are:

1. Horizontal gradients are obtained of the profiles of the entire ionospheric layer (including the outer ionosphere from observation of the signals from geophysics rockets at spaced points)⁽¹⁴⁾.

2. It was found that in first approximation the relative regular horizontal gradients of ionization γ_0 and γ , /130

$$\left(\gamma_0 = \frac{1}{N_0} \frac{dN_0}{ds}; \quad \gamma = \frac{1}{N} \frac{dN}{ds} \right)$$

where s is the horizontal coordinate) and especially the relative regular instabilities of ionization η_0 and η ,

$$\left(\eta_0 = \frac{1}{N_0} \frac{\partial N_0}{\partial t}; \quad \eta = \frac{1}{N} \frac{\partial N}{\partial t} \right)$$

are practically independent of altitude in the outer ionosphere and depend substantially on time of day as well as on season and solar activity.

(14) Apparently the first profiles were found in [46, 47] for the variables and the horizontal gradients of N_0 up to ~ 2500 km.

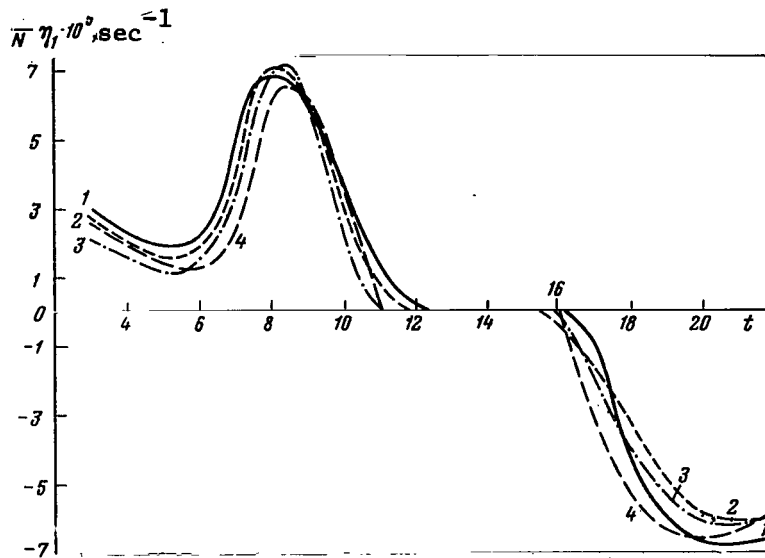


Figure 7. The Dependence of $\eta(\eta \cdot 10^5, \text{sec}^{-1}) = \frac{\partial N}{\partial t} N^{-1}$ on Time t of Day (Local) During the Period October - November, 1962 Based on Data from the Satellite "Alouette" in the Region $40 - 45^\circ \text{ N}$.

1. $z = 400 \text{ km}$; 2. $z = 600 \text{ km}$; 3. $z = 800 \text{ km}$; 4. $z = 1000 \text{ km}$.

Usually, other things being equal, with an increase in solar activity, these gradients are increased by several times or even by one order. For example, with transition from high to low solar activity the maximal value of $\delta N_0 / \delta t$ is decreased in order of magnitude from 10^9 to $10^8 \text{ el} \cdot \text{cm}^{-2} \cdot \text{sec}^{-1}$ [27, 37]⁽¹⁵⁾.

The instabilities η_0 and η have two extrema in diurnal variation: one immediately after sunrise and the second before sunset.

The characteristics of the variables N and N_0 are shown on Figures 7 - 9. The gradients γ and γ_0 behave like η and η_0 .

(15) Even from $\sim 10^{10}$ [47].

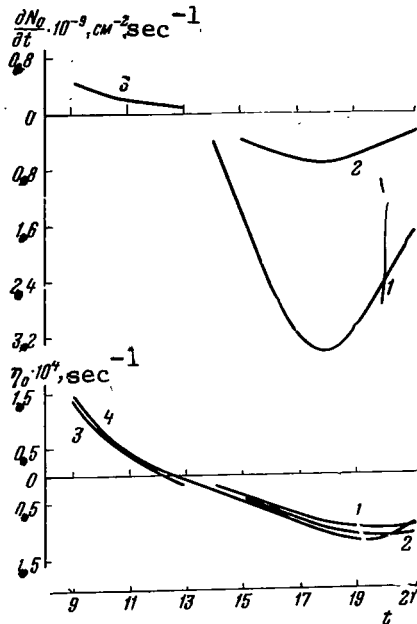


Figure 8. Dependence of $\frac{\partial N_0}{\partial t} \cdot 10^9 \text{ cm}^{-2} \text{ sec}^{-1}$ and $\eta_0 = \frac{\partial N_0}{\partial t} N_0^{-1} \cdot 10^4 \text{ sec}^{-1}$ on standard time of day t .

1. Third AES, February - March, 1959, $z = 1000 \text{ km}$; 2. "Elektron-1", February - March, 1964, $z = 1000 \text{ km}$;
3. "Elektron-1", February - March, 1964, $z = 415 \text{ km}$; 4. Vertical Probe, $z = z_{F2}$.

3. The relative regular gradients γ_0 and γ are of the same order, they are maximal at sunrise (they may reach tenths of a percent) and are directed at this time approximately along the line east-west ($\pm 7 - 8^\circ$); by day they are smaller by approximately an order and lie approximately in the meridional plane ($\pm 7 - 8^\circ$); at sunset they are also increased. In order of magnitude they may reach $\sim 10^{-2} \text{ km}^{-1}$.

4. The irregular component of instability (produced by the movement, onset, development and disappearance of random inhomogeneities) is significantly smaller than the regular component. It may be experimentally evaluated according to the registrations of $\dot{\Phi}$ from signals from the rockets at spaced points [23, 36].

The irregular components of $\dot{\Phi}$ and $\dot{\Phi}_\phi$, φ and Φ_ϕ permit determination of several "effective" dimensions d of the inhomogeneities and the relative intensities $\delta N/N$ of the electron density in them $\left(\frac{\delta \Phi}{\Phi} \approx \frac{\delta \Phi_\phi}{\Phi_\phi} \approx \frac{\delta N}{N} \right)$, and consequently, plotting of the respective spectra of the irregular effects and inhomogeneities [3, 10 - 13, 17, 38, 39] as well as their statistical characteristics [46, 47].

Most complete are the investigations of inhomogeneities by spacing the observation points.

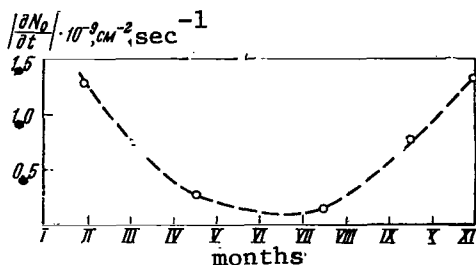


Figure 9. Seasonal Dependence of $\frac{\partial N_0}{\partial t} \cdot 10^{-9} \text{ cm}^{-2} \cdot \text{sec}^{-1}$ Based on Data From the Satellite "Vanguard - 1" in the Period April 1959 - February, 1960, $z = 1000 \text{ km}$.

We may also find useful in interpreting the irregular (and the regular) components $\dot{\Phi}$ and $\dot{\Phi}_{\Phi}$ the concept of $\dot{\Phi}$ and $\dot{\Phi}_{\Phi}$ as gradients N_{0L} along the satellite's orbit [12, 39]:

$$\dot{\Phi} \sim V \frac{dN_{0L}}{dl}; \quad \dot{\Phi}_{\Phi} \sim V \frac{dN'_{0L}}{dl}$$

where V is the velocity of the satellite, N_{0L} is obtained from N_{0L} by substituting ab_L for the function α in (3).

Below we give the basic results of analyzing the spectra of the irregular effects and inhomogeneities.

1. A tendency is observed to the formation of two⁽¹⁶⁾ structures of large ionospheric inhomogeneities (Figure 10): (a) a kind of "quasi-undulation" of the basic thickness of the ionosphere (in its illuminated part) [12, 39]; (b) random cloud structure (in the unilluminated ionosphere /132 and in the transition period).

2. Two stable maxima are observed for the dimensions of the large inhomogeneities: 15 - 30 km at any time and 150 - 200 km during the day. The spectra of the inhomogeneities are expanded with transition from night to day⁽¹⁷⁾. Apparently the diurnal variations in the dimensions are more sub-

(16) These facts agree also with the data from the radioastronomical [40] and correlation [41] measurements of large inhomogeneities.

(17) See also [47] for certain information on the statistical characteristics, including the correlation functions of the irregular effects and inhomogeneities.

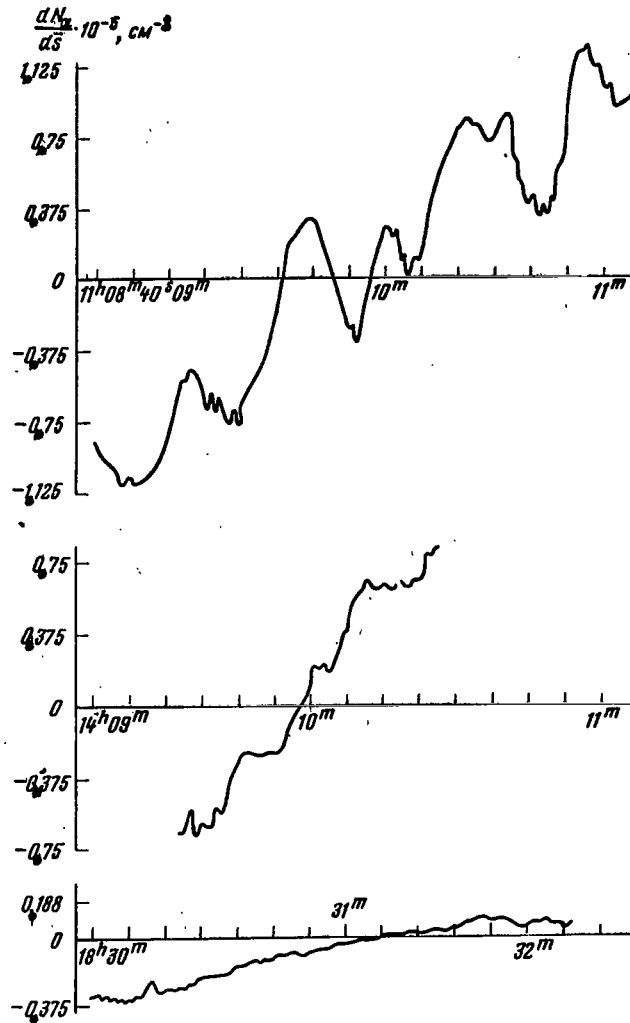


Figure 10. Quasiundulating and Cloud Structure of the Ionosphere (dN_{OL}/ds is the Gradient Along the Path of the Beam of the Total Electron Content Between the Satellite and the Observation Point) at Different Moments in Time (February, 1964).

stantial than the seasonal variations and are caused by variation in solar activity; the correlation between dimensions of the inhomogeneities and the fluctuations in electron density $\frac{\delta N}{N}$ (or $\frac{\delta \Phi}{\Phi} \sim \frac{\delta N}{N}$) remain high up to values of $d \lesssim 100$ km; when $d > 100$ km this correlation is diminished.

/133

3. Small inhomogeneities ($d \approx 1$ km) predominate at night and in the vicinity of the maximum N in the F2 region.

Comparisons and prospects of the methods of ionospheric measurements on registering the Faraday and Doppler effects at coherent frequencies:

(1) The method of the Faraday effect is the simplest and cheapest, but also the least accurate mainly due to inaccuracy in the information on the geomagnetic field and also due to the difficulties of processing and interpretation; the method of the Doppler effect at coherent frequencies is more accurate but requires special receivers and coherent radiation from the object in space; interpretation and processing in the first case is more complex than in the second;

(2) The combined use of both methods, by increasing the information, leads apparently to a decrease in accuracy (in comparison with the accuracy of the method of coherent frequencies);

(3) Observations of the effects at the site of the vertical rocket launch permit determining the vertical profile of the ionosphere with a high degree of accuracy. Observations of the signals from satellites and rockets with oblique propagation of radio waves permit measuring N_B more roughly but make it possible to measure a number of other effects and parameters (total electron content N_{0L} and N_0 , the gradients γ_0 and γ , inhomogeneities, refraction, etc.).

Therefore it is feasible to carry out simultaneously combined measure-

ments using geophysical rockets at the launching site and at spaced points, combined measurements using satellites and rockets, and especially in conjunction with such promising methods as vertical probing from above with satellites and the method of incoherent scattering of radio waves in the ionosphere.

For a more precise measurement of the "fine" structure of the vertical profiles N of the ionosphere (and especially in the "troughs" between the E and F and between the F1 and F2 layers) the best method in the future will be apparently the method of coherent radio waves emitted by geophysical rockets and registered in the vicinity of the launch⁽¹⁸⁾.

The so-called "geostatic" satellites using the Doppler effect for coherent frequencies, the Faraday effect and also group delay are convenient, for obtaining the time dependences $N_0(t)$ and in particular the instabilities of the ionosphere ($\partial N_0 / \partial t$).

In measurements by any of the latest methods it is always desirable to have a simultaneous vertical probe of the ionosphere.

METHODS BASED ON MEASURING REFRACTION AND LAG

Methods, based on measuring refraction. Based on measurement of the angles of incidence of the signals from satellites or rockets (either from natural emitters or re-emitters of radiowaves) whose coordinates are known or are measured by other methods with sufficient accuracy, we can also measure the ionospheric parameters and primarily N_0 (see, for example [42]) with acceptable accuracy.

(18) As well as the method of "incoherent" scattering of radio waves by the ionosphere, which is examined in the next article. An example of the combined measurements by different radiosphysics methods is shown in [46].

A peculiarity of the refraction methods is that they are effective at rather small angles β_B . At the same time the methods based on the Doppler and Faraday effects give an acceptable accuracy for rather large β_B . Consequently, these and other methods mutually complement each other. However the accuracy of the refraction methods is usually low.

The method of the so-called "radio rising" and "radio setting" is based /134 on measuring refraction at the zero angle of elevation of the beam. It was first proposed and used by Ya. L. Al'pert in the first measurements of the outer ionosphere using satellites (the first AES, 1957) for an approximate determination of the parameters for the a priori given model of the ionosphere [43]⁽¹⁹⁾. The horizontal ionization gradients were not taken into account. New results have been obtained which properly characterize the considerable extent of the ionosphere and agree with other measurements. The method has more than historical significance. It can be used also in the future in the simplest observations of mass, especially in the simultaneous use of radiation at two frequencies (it permits allowing for tropospheric refractions, facilitates exclusion of the cases of a complex propagation path, etc.). With a slight complication of the experiment, an approximate accounting of the horizontal gradients of N is also possible.

Method based on measuring group lag. In addition to the well-known and important use of this method for vertical probing of the ionosphere from the Earth and from above from satellites, the method permits determining N_0 with a high degree of accuracy in the general case where n depends on three coordinates and t , using two or more modulation signals. Here it is not completely necessary that one of the frequencies be very high; it is sufficient only that both frequencies exceed the critical frequency of the ionosphere by several times.

(19) As is done usually in all methods in which the initial measured value is some kind of integral effect.

Among the most interesting data on the outer ionosphere obtained by probing from above from satellites, we should mention the information on the relationship between the ionospheric profiles and geographic coordinates, and the discovery in particular of deep troughs at the levels $N = \text{const}$ because of the unusual previously unknown horizontal gradients in a limited latitude region in the large layer of the outer ionosphere [3, 29], and also the discovery of resonance phenomena at the natural frequencies of the plasma. The described method, along with the method of incoherent scattering, is the most promising for investigating N of the outer ionosphere. We can hope that the wide-spread usage of these methods must in the immediate future introduce significant clarity into the physics of this region.

Of the other radiophysical methods of investigating circumterrestrial plasma, we must mention the radioastronomical methods (see, for example, [40, 44, 45]), the use of whistling atmospherics and low-frequency waves in general [3, 43], the methods of the impedance probe [12] and others.

REFERENCES

/135

1. Browne, I. C. et al. Proc. Phys. Soc., No. 69, 1956, p. 901.
2. Evans, J. V. Proc. Phys. Soc., No. 69, 1956, p. 953; see also; J. Atm. Terr. Phys., No. 11, 1957, p. 259.
3. Sb: Raspredeleniye elektronnoy kontsentratsii v ionosfere i ekzosfere (In: Distribution of Electron Concentration in the Ionosphere and Exosphere). Translated from English, Edited by K. I. Gringauz, Mir Press, 1964.
4. Sb: Noveyshiye issledovaniya rasprostraneniya radiovoln' (In: Latest Research in the Propagation of Radio waves), State Publishing House of Technical and Theoretical Literature (Gostekhizdat), 1945.
5. Seddon, J. C. J. Geophys. Res., No. 59, 1954, p. 463.
6. Jackson, J. E. J. Geophys. Res., No. 59, 1954, p. 377.
7. Gringauz, K. I. Dokl. AN SSSR, No. 120, 1958, p. 1234.
8. Gringauz, K. I., and V. A. Rudakov et al. SB: Iskusstvennyye sputniki Zemli, (In: Artificial Earth Satellites), No. 6, 1961, pp. 33, 48.
9. Al'pert, Ya. L. Uspekhi fizicheskikh nauk (UFN), No. 64, 1958, p. 3, No. 71, 1960, p. 364
10. Al'pert, Ya. L. Geomagnetizm i aeronomiya, No. 4, 1964, p. 479.
11. Misyura, V. A. et al. Kosmicheskiye issledovaniya, Vol. 3, No. 4, 1965, pp. 595, 604.
12. Sb: Issledovaniya kosmicheskogo prostranstva (In: Research in Outer Space), Mir Press, 1965.
13. Mityakova, E. Ye., N. A. Mityakov and V. O. Rapoport. Izv. VUZov. Radiofizika, Vol. 3, No. 6, 1960.
14. Mityakov, N. A. and E. Ye. Mityakova. Geomagnetizm i aeronomiya, Vol. 3, No. 5, 1963.
15. Schmlovsky, K. N. and D. Felske. Gerlands Beitrage zur Geophysik, Vol. 74, No. 6, 1965, p. 451.
16. Misyura, V. A., G. K. Solodovnikov and V. M. Migunov. Kosmicheskiye issledovaniya, Vol. 5, No. 1, 1967, p. 82.

17. Al'pert, Ya. L. Geomagnetizm i aeronomiya, Vol. 3, No. 1, 1963, p. 10.
18. Gringauz, K. I., Yu. A. Kravtsov, V. A. Rudakov and S. M. Rytov. Geomagnetizm i aeronomiya, Vol. 6, No. 3, 1966.
19. Misyura, V. A., G. K. Solodovnikov, Ye. B. Krokhmal'nikov and V. M. Migunov. Sb: Issledovaniya kosmicheskogo prostranstva (In: Research in Outer Space). Mir Press, 1965, p. 138.
20. Misyura, V. A., G. K. Solodovnikov and V. M. Migunov. Geomagnetizm i aeronomiya, Vol. 6, No. 5, 1966, p. 852.
21. Misyura, V. A., G. K. Solodovnikov, V. M. Migunov and Ye. B. Krokhmal'nikov. Sb: Ionosfernyye issledovaniya (In: Ionospheric Research), Nauka Press, No. 21, In Press.
22. Misyura, V. A., Yu. G. Yerokhin, Ye. B. Krokhmal'nikov, G. N. Zinchenko, V. I. Ivanov, A. S. Firsakov, A. N. Gridin and G. A. Biryukov. Sb: Ionosfernyye issledovaniya (In: Ionospheric Research), Nauka Press, No. 20. In Press.
23. Misyura, V. A., Ye. B. Krokhmal'nikov, G. N. Zinchenko, A. S. Firsakov and S. M. Slutsker. Geomagnetizm i aeronomiya. In Press.
24. Misyura, V. A., G. K. Solodovnikov and V. M. Migunov. Geomagnetizm i aeronomiya, Vol. 7, No. 2, 1967, p. 284.
25. Rudakov, V. A. Kosmicheskiye issledovaniya, Vol. 2, No. 6, 1964, p. 946.
26. Al'pert, Ya. L. UFN., Vol. 90, No. 3, 1966, p. 405.
27. Otchet po teme, "Luch", (Report on the Subject, Beam) Kharkov University, 1966.
28. Berning, W. W. J. Meteorol., Vol. 8, No. 3, 1961. p. 175.
29. Kneht, R. W. and T. E. Van Zandt. Nature, Vol. 197, No. 14, 1963.
30. Misyura, V. A. et al. In: p. 136*.
31. Shmelovskiy, K. Kh. In: p. 84**
32. Burges, B. Radio Astronomical and Satellites Studies of the Atmosphere, Proc. of the Corfu Summer School, Amsterdam, 1963.

* Translator's note: The material will be found on page 223 of the English text.

** Translator's note: The material will be found on page 137 of the English text.

33. de Mendonca, F. Radio Astronomical and Satellites Studies of the Atmosphere. Proc. of the Corfu Summer School, Amsterdam, 1963.
34. Misyura, V. A., G. K. Solodovnikov, V. M. Migunov and G. A. Biryukov. Geomagnetizm i aeronomiya, Vol. 9, No. 3, 1969, p. 445.
35. Al'pert, Ya. L., V. B. Belyanskiy and N. A. Mityokov. Geomagnetizm i aeronomiya. Vol. 3, No. 1, 1963, p. 10.
36. Misyura, V. A., Ye. B. Krokhamal'nikov, G. N. Zinchenko, G. A. Biryukov, A. N. Gridin and A. S. Firsakov. Geomagnetizm i aeronomiya. In Press.
37. Misyura, V. A., V. M. Migunov and G. K. Solodovnikov. Geomagnetizm i aeronomiya, Vol. 6, No. 5, 1966, p. 931.
38. Yerukhimov, Ye. M. Geomagnetizm i aeronomiya, Vol. 2, No. 4, 1962.
39. Misyura, V. A., G. K. Solodovnikov and V. M. Migunov. Geomagnetizm i aeronomiya, Vol. 4, No. 6, 1964, p. 1124.
40. Kokurin, Yu. L. et al. Radiotekhnika i elektronika, No. 5, 1961.
41. Sb: Issledovaniya neodnorodnostey v ionosfere (In: Research on Inhomogeneities in the Ionosphere), Press of the Academy of Sciences, USSR, No. 4, 1960.
42. Titheridge, G. E. J. Atm. Terr. Phys. No. 26, 1964, p. 159.
43. Al'pert, Ya. L. et al. UFN, Vol. 65, No. 2, 1958, p. 161.
44. Bailey, D. K. Terrestr. Mag., No. 54, 1948, p. 41.
45. Smith, F. G. J. Atm. Phys. No. 2, 1952, p. 350.
46. Misyura, V. A. Geomagnetizm i aeronomiya, Vol. 9, No. 3, 1969.
47. IX Vsesoyuzn. konf. po raspr. radiovoln. (Ninth All-Union Conference on the Propagation of Radio waves), Authors' Abstract of Reports, Part 2, Kharkov, 1969, pp. 47, 51, 84, 55.

IONOSPHERIC MEASUREMENTS USING THE METHOD OF INCOHERENT SCATTERING OF RADIO WAVES BY THE IONOSPHERE

V. A. Misyura, G. N. Tkachev,
V. Ya. Bludov and Yu. G. Yerokhin

ABSTRACT. In principle, the incoherent-scattering method makes it possible to take regular measurements of ionospheric parameters in half-space around the observation point at distances of up to a few radii of the Earth.

In addition to measuring the electron density, this method can also be applied to measuring the temperature of ions (T_i) and electrons (T_e) and ion composition.

MAIN POINTS OF THE METHOD

The methods employed for investigating the outer ionosphere using /136
radio waves propagating from rockets and satellites, just as other methods (probe and radioastronomical, vertical probing, lunar radar, etc.) may have a number of disadvantages such as limitations in the number of measurable parameters, irregularity in the measurements, indeterminacy in the location of the region to which the measurements pertain, or, on the other hand, localization of this region (for example, measuring N only along the orbit of the emitters, only from one side of the ionosphere [above or below], or measurement only of the total electron content up to the trajectory of the object), etc. At the same time it is important to obtain N regularly as a function of three instantaneous coordinates throughout the entire ionosphere (outer and lower) and also to increase the number of measurable parameters (T_e , T_i , ion composition, etc.).

There is a new method for investigating the ionosphere, based on the so-called "incoherent" scattering of radio waves by the ionosphere, that is free to a significant degree from these disadvantages and which supplements the previous methods. In particular, this method apparently permits, in theory, obtaining regular measurements of the ionospheric parameters in the half-space around the observation point out to a distance of several earth radii [1]. In addition to the electron density N , it is possible to measure T_e , T_i , T_e/T_i as well as the ion composition of the ionosphere. The new prospects of this method have created considerable interest among scientific circles.

The basis of this method is scattering by the ionosphere of radio signals whose frequency significantly exceeds the maximal plasma frequency of the ionosphere:

$$\omega_{pl \max} = \sqrt{\frac{e^2 N_{\max}}{\epsilon_0 m}},$$

where e , m are the charge and mass of the electron; ϵ_0 is the dielectric constant in a vacuum in the practical system of units; N_{\max} is the maximal value of N . The initial measurements are the intensity P_s and the spectrum σ_ω of scattering, which depend on the parameters of the plasma.

In 1958 Gordon first [1] noted that in probing the ionosphere by modern high-potential USW-range radar, it is possible to record signals scattered by the free electrons of the ionosphere.

/137

The phenomenon of electromagnetic wave scattering by free electrons (Thomson-type scattering) has been known for some time in physics. Assuming the fluctuation phases of the free electrons to be random and equally probable, Gordon suggested that the scattering by electrons will be "incoherent" and consequently the powers dissipated by the individual electrons must be combined and independent of the frequency ω_0 . The total scattering intensity of

the irradiated volume V of the ionosphere must therefore be proportional to the number of electrons in this volume, and consequently, it must be proportional to the product of V times the value of the mean electron concentration N in this volume and be independent of the frequency of emission ω_0 .

When pulse radars are used, the volume V is determined (Figure 1 a) by the width of the radiation pattern of the radar antenna and by the duration of the emitted pulse τ . The extent of ΔR along the radar beam R of the scattering volume V , and consequently, the resolving power of the measurements of N along R will obviously be equal to $\Delta R = 1/2 c\tau$, where c is the speed of light in a vacuum ($\omega_0 \gg \omega_{pl,max}$ and therefore with a high degree of accuracy the group velocity of the signal in the ionosphere is equal to c). The mean distance R to the volume V is defined as $R = 1/2 c\Delta t$, where Δt is the interval of time between emission of the probe pulse and the arrival of the scattered volume V of emission. Usually $R \gg \Delta R$ and $V \simeq R^2 \Delta R \Omega$, where Ω is the solid angle of the radiation pattern of the antenna.

In view of the fact that the power scattered by the volume V , when it is irradiated by one pulse, is quite small, it is technically possible to increase the energy of the scattered signal received by summing the scattering energies of a large number of pulses (many thousands), using modern storage circuits. Because of the pulsed operation of the radar it is possible also, for the irradiation to distinguish successively different regions of the ionosphere V along the beam and to determine the varying distance R to these regions from measurements of Δt by what is called strobing. Thus we can find the N profile along the radar beam.

We can distinguish the scattering volume V and determine the distance R to it also with continuous emission (so-called bistatic equipment, the advantages of which we shall discuss below). For this (Figure 1 b) we space the antennas of the transmitting and receiving equipment. Then

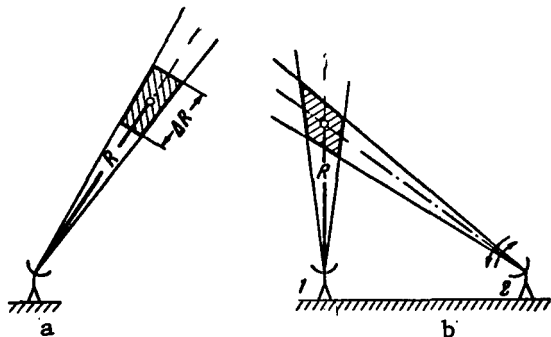


Figure 1. Shaping of the Scattering Volume V (Shades Area).

a. Using Pulse Radar; b. Continuous Radiation (Bistatic Equipment);
1. Transmitting Equipment; 2. Receiving Equipment With Scanning of Angle of Elevation (Depicted by the Arrows).

V is the volume of the mutual overlapping of the radiation pattern of both antennas. If we shift ("scan") the radiation pattern of the receiving antenna along the angle of elevation, then the volume V will be shifted along the vertical (of course another variation is also possible, i.e. shift of V along the slope).

As far as the spectrum of the /138

scattered radiation is concerned, in Gordon's opinion, it must then differ from the irradiation spectrum by the Doppler frequency shifts ω due to the chaotic thermal velocities of the electrons v_e , which determine the electron temperature T_e . Consequently T_e can be determined from the width of

the scattering spectrum $(\omega \sim \omega_0 v_e \sim \omega_0 \sqrt{T_e})^{(1)}$.

Since fluctuations arise in the electron density ΔN because of the thermal movement of the electrons we can then interpret the scattering of radio waves as scattering on these fluctuations. For the following discussion let us introduce the concepts used in physics (see, for example, [1, 2]):

$$\sigma_e = \frac{1}{2} r_e^2 \sin^2 \theta \quad (1)$$

(1) Since on the average in the ionosphere $v_e \approx 10^5 \text{ m} \cdot \text{sec}^{-1}$, then for the frequency $f_0 = \omega_0 / 2\pi = 40 \text{ MHz}$, we would expect the width of the scattering spectrum to be $\approx 100 \text{ kHz}$.

is the effective scattering cross section of a single electron, i.e. the ratio of the amount of scattered power per unit of the solid angle in a given direction to the density of the energy flux incident on the electron, where $r_e = e^2/mc^2$ is the classical radius of the electron, θ is the angle between the vector E of the incident wave and the direction of the scattered radiation. In particular, in σ_e for backscattering of an electron, $r_e^2 = 8 \cdot 10^{-30} \text{ m}^2$. Analogously we introduce the effective cross section σ of the system of scatterers or the total (integral) scattering cross section and the spectral or differential scattering cross section $\sigma(\omega_0 \pm \omega)$ or σ_ω , i.e., the effective scattering cross section per unit of spectral width of the scattered radiation, mutually related in the usual manner:

$$\sigma = \int_{-\infty}^{+\infty} \sigma(\omega) d\omega. \quad (2)$$

A relationship, obtained by a number of authors (see, for example, [3], p. 68, [4, 5, 6]), exists between σ_ω for the volume V and the fluctuations ΔN of electrons in this volume:

$$\sigma_\omega = 0.5V\sigma_e |\overline{\Delta N(\mathbf{q}, \omega)}|^2 \quad (3)$$

where \mathbf{q} is the wave vector equal to $\mathbf{k}_{\text{inc}} - \mathbf{k}_{\text{refl}}$; $|\overline{\Delta N(\mathbf{q}, \omega)}|^2$ is the mean square value of the modulus of the Fourier-transform for the fluctuations $\Delta N(\mathbf{r}, t)$ in electron concentration.

As mentioned, Gordon assumed [1] that the ionospheric electrons scatter the incident radio waves incoherently. The total scattering cross section of the free electrons σ per unit volume V in computing (2) will be

$$\sigma = \sigma_e N, \quad (4)$$

i.e. it agrees with the Thomson formula. By definition

$$P_{\bullet} \sim \sigma V. \quad (4')$$

The presence of ions, whose influence on the electron motium was not taken into account by Gordon, makes $\Delta N(q, \omega)$ dependent on the movement of the ions because of the existence in the plasma of a self-consistent Coulomb interaction between electrons and ions. This leads to another (in addition to the mean free path)^{*(2)} characteristic dimension, i.e., the Debye radius of the electrons:

$$d = \sqrt{\frac{k v_0 T_e}{N_e}} = \frac{v_e}{\sqrt{2} \omega_{p1}} \quad (5)$$

where k is the Boltzmann constant, v_e is the average thermal velocity of the /139 electrons. The scattering of electrons in the general case of an arbitrary relationship between λ and d will no longer be purely incoherent. The influence of ions on the excited motion of the electrons is manifested all the stronger, and consequently, the deviation of the scattering from Thomson scattering by free electrons will be all the greater as the following inequality is satisfied more strongly,

$$\lambda \gg d, \quad (6)$$

and vice versa when $\lambda \ll d$, formula (4) is again found to be valid (see, for example [2]), i.e. the influence of the ions on the scattering of radio waves is not manifested. It is clear that in this latter case many λ are packed within the limits of d , and the movement of the electrons on an interval equal to λ may be assumed uniform, i.e. independent of the ion movement.

The first experiments conducted by Bowles in 1958 [7] showed that the

(2) In the rationalized system of mks units.

scattering intensity is less than that predicted by Gordon by approximately two times (when $T_e = T_i$), and the spectrum is substantially (by an order or more) narrower. The reason for this latter, as Bowles correctly assumed [8] in his qualitative theory, involves the influence of Coulomb interaction between the electrons and the ions⁽³⁾ which Gordon did not take into account. Subsequent, including stricter, theories of incoherent scattering [5, 6, 8 - 10] took this fact into account and were found to be in agreement with experiment.

In Reference [8] Bowles studied the scattering of radio waves in an electron gas introduced into a viscous medium consisting of positive ions. The density of the ions was assumed to be variable, and relatively slowly fluctuating (in comparison with the more rapid fluctuations of the electron density) due to the thermal velocity of the ions. Accordingly the electrostatic field of the ions also fluctuated slowly. It influenced the fast fluctuations in electron density and caused it to fluctuate like ions, i.e. more slowly. Then the scattering intensity was determined as previously by scattering on electrons⁽⁴⁾, and the spectrum was determined by the thermal velocities of the ions, which are naturally less than the thermal velocities of the free electrons. This also led to a narrowing of the scattering spectrum.

In the present qualitative and simplified examination of the concept of the incoherent scattering method, the more complex actual picture of the phenomenon

(3) Condition (6) was reliably satisfied experimentally [7, 8], since $\lambda = 7.3$ m, and d varies from fractions to tens of centimeters between F2 and the magnetosphere.

(4) The ion scattering power is obviously much less than the electron and can be completely ignored (for ions of atoms of oxygen O^+ , of hydrogen H^+ and helium He^+ and an electron of radius r , it is respectively equal to: $9.6 \cdot 10^{-20}$; $1.54 \cdot 10^{-18}$; $3.84 \cdot 10^{-19}$; $2.82 \cdot 10^{-15}$ m).

associated with the effect which the temperature imbalance of ions and electrons ($T_e > T_i$), the multiple-component nature of the plasma, the geomagnetic field, collisions, the nonmonochromaticity of radar emission etc., have on incoherent scattering was not taken into account. These problems will be covered in the sections concerned with the initial quantitative data for the method taken from the modern theory of incoherent scattering and also in sections dealing with the method of processing and interpreting experimental data. For the present let us confine ourselves to mentioning that under the influence of the magnetic field, temperature imbalance and the multiple-component nature of the plasma, this latter appears to be a complex system with many degrees of freedom in which the increasing number of types of waves, fluctuations and resonances must be reflected in the phenomenon of radio wave scattering, thus complicating its utilization in the method, on the one hand, and increasing the useful information on the parameters of the ionospheric plasma and the physical processes in it, on the other. In particular, a large number of characteristic dimensions are found (gyroradii of various sorts of ions and electrons, their mean free path, the radii of correlation of the fluctuations and their density, the Debye radius, etc.) whose relationship with the wavelength of the radar emission should theoretically affect the intensity ($P_s \sim \sigma$) and the spectra σ_ω of the scattered radiation. However in a strict examination it was found (see below) that the magnetic field may influence the shape of σ_ω , but when $T_e = T_i$ it can in no way influence P_s . The influence of the presence of several sorts of ions, and especially the temperature imbalance, is more complex and usually substantial. The collisions may have significance in the lower ionosphere.

INITIAL RESULTS OF THE THEORY

Let us cite the basic results of the modern quantitative theory of electromagnetic wave scattering by fluctuations in electron concentration (see also [13, 18, 43]).

To simplify the analysis let us look at two typical modifications: (1) The plasma is isothermal ($T_e = T_i$) and the constant magnetic field is taken into account; and (2) The plasma is partially nonisothermal ($T_e \neq T_i$ but the temperatures of the different ions are identical), and the magnetic field may be taken into account or (for simplicity) not taken into account. Such an approach, without limiting the generality, permits establishing the most fundamental relationships for scattering intensity ($P_s \sim \sigma$) and spectra σ_ω of scattering as functions of: (1) d, λ and the gyroradii R of the ions (R^i) and the electron (R^e) in the first version; and (2) d, λ and T_e/T_i in the second; it also permits evaluating the influence of ion composition of P_s and σ_ω .

The case of isothermal plasma in allowing for a constant magnetic field. The basic assumptions of the qualitative theory [8] are given above. In subsequent qualitative theories for $T_e = T_i$ [6 - 10], similar [8] models of plasma were used that consist of electrons and ions. The problem was solved both by ignoring and by allowing for the magnetic field, which was assumed constant, as is near to actual conditions that exist in the irradiated volume of the ionosphere. With a strict examination it was found that allowing for the magnetic field does not affect the intensity of the scattered radiation⁽⁵⁾, but under certain conditions may influence the shape of its spectrum [6 - 10]. To compute the spectrum of the scattering intensity we used the generalized Nyquist theorem which in application to plasma is valid when $T_e = T_i$ ⁽⁶⁾ (though this does not always occur in the ionosphere). The cross section σ_ω obtained in these papers is quite complex and is expressed through the effective tensor

(5) When $T_e \gg T_i$ the value of P_s already depends on the magnetic field [39, 40].

(6) A nonisothermal plasma ($T_e \neq T_i$) may be assumed to be in quasi-equilibrium (because of the significantly slower exchange of energy between electrons and ions than between particles of one sort) and consequently we can use the Nyquist theorem (on the influences of collisions; see [38, 44]).

of plasma conductivity which contains the product of three tensors, each of the elements of which is in turn a complex function of a number of parameters.

Let us give the basic relationships and results of their analysis by following these papers.

As we know, to obtain in explicit form the expressions for σ and σ_ω we must compute $|\Delta N(\mathbf{q}, \omega)|^2$. For this, in the studied case $T_e = T_i = T$, we can use the generalized Nyquist theorem which confirms that if the system of particles is influenced by the generalized force F which produces in the volume V the particle flux y , then the mean square of the modulus of the i^{th} component of the Fourier transform for the fluctuation in flux is equal to

$$|\Delta y_i(\mathbf{q}, \omega)|^2 = \frac{2kT}{\pi V} \operatorname{Re} \{Y_{ii}(\mathbf{q}, \omega)\}, \quad (7)$$

i.e. it is proportional to the real part (Re) of the conductivity tensor of the particles Y . In application to this problem assuming in such case that the externally applied force is small and influences only the electrons (the other assumptions will be examined below), when $T_e = T_i$, by introducing the effective conductivity tensor of the plasma Y' , we can write (6):

$$|\Delta N(\mathbf{q}, \omega)|^2 = \frac{2kT}{\pi V \omega^2} \operatorname{Re} \{q Y' q\}$$

or by directing the z -axis of the rectangular coordinate system along \mathbf{q} and taking (3) into account, we obtain

$$\sigma_\omega = \sigma_e \frac{kT q^2}{\pi \omega^2} \operatorname{Re} \{Y'_{zz}\},$$

where the effective conductivity tensor of the plasma Y'_{zz} is related to the tensors of the electron Y^e and ion Y^i conductivity by the expression

$$Y'_{zz} = \left[\left(Y^i - \frac{D}{c^2} \right) \left(Y^e + Y^i - \frac{D}{c^2} \right)^{-1} Y^e \right]_{zz},$$

where

$$D = \frac{ie^2}{4\pi\omega} \left[\left(q^2 - \frac{\omega^2}{c^2} \right) I - qq \right],$$

and I is the unit tensor. If, for convenience, we introduce the dimensionless tensor y and the matrix g for the expressions

$$Y_{ij} = \frac{\bar{N}\omega}{kTq^2} y_{ij}; \quad D_{ij} = \frac{\bar{N}\omega}{kTq^2} g_{ij},$$

we ultimately find

$$\sigma_{\omega} = \bar{N} \sigma_e \operatorname{Re} \left\{ \frac{y'_{zz}}{\pi\omega} \right\}, \quad (8)$$

where

$$y'_{zz} = [(y^i - g)(y^e + y^i - g)^{-1} y^e]_{zz}, \quad (9)$$

$$\bar{N} = \bar{N}^i = \bar{N}^e.$$

Thus, the problem of finding the effective scattering cross section is reduced to finding the tensors of the electron and ion conductivity. It can be solved by two methods: the orbital method -- by integrating the equations of motion of the particles, and by solving the kinetic Boltzmann equation. Although the first method is physically obvious, the second is mathematically more strict.

The rather complex expression (9) for the tensor of the effective conductivity y'_{zz} , and consequently expression (8) for σ_{ω} in the specific case of inverse scattering under the condition

$$\left(\frac{\omega_0}{\omega_{p1}^e} \right)^2 \gg \left(\frac{m^e}{m^i} \right)^{1/2} \sec \chi \quad (10)$$

may be significantly simplified and written in the form

$$\sigma_{\omega} = \frac{\bar{N}\sigma_e}{\pi\omega} \operatorname{Re} \left\{ \frac{Y_{zz}^i + jdq^2}{Y_{zz}^i + Y_{zz}^e + jdq^2} \right\}, \quad (11)$$

where

$$Y_{zz} = j + \theta \int_0^{\infty} \exp \left\{ -j\theta t - \frac{\sin^2 \chi}{\varphi^2} \sin^2 \frac{\varphi t}{2} - \frac{t^2 \cos^2 \chi}{4} \right\} dt;$$

$$\theta = \frac{\omega}{q} \left(\frac{m}{2kT} \right)^{1/2}; \quad \varphi = \frac{\Omega}{q} \left(\frac{m}{2kT} \right)^{1/2} = \frac{1}{qR}; \quad \Omega = \frac{eB}{m\omega};$$

Ω , R are the gyrofrequency and gyroradius of the charged particles; B is the magnetic field strength (inductance); ϕ , θ are the normalized gyrofrequency and Doppler frequency

$$\left(\varphi \sim \frac{\Omega}{q} \sim \frac{\Omega}{\omega_0}; \theta \sim \frac{\omega}{\omega_0} \right);$$

d is the Debye radius; ω_0 is the effective frequency; χ is the acute angle between the vectors $\mathbf{q} = \mathbf{k}_{\text{inc}} = \mathbf{k}_{\text{refl}}$ and the magnetic field strength \mathbf{B} .

For electrons and ions the expressions for Y_{zz} , ϕ , ψ , m , Ω and R must have the superscripts i and e . Condition (10) is satisfied, for example, for protons when

$$f_0 = \frac{\omega_0}{2\pi} = 50 \text{ MHz} \quad \text{and} \quad f_{p1}^{(e)} = \frac{\omega_{p1}^e}{2\pi} = 10 \text{ MHz} \quad \text{for} \quad 0 \leq \chi \leq 89^\circ.4.$$

Expression (11) permits simplifying, analyzing and plotting the respective curves, which are found to be different for different relationships between $\lambda' = \lambda/4\pi$, the gyroradii R^e and R^i and d and R^i . Accordingly we can distinguish five characteristic cases: (1) $\lambda' \ll R^e \ll R^i$; (2) $\lambda' \approx R \ll R^i$; (3) $R^e \ll \lambda' \ll R^i$; (4) $R^e \ll \lambda' \approx R^i$; and (5) $R \ll R^i \ll \lambda'$. Illustrations of the computations are shown on Figures 2

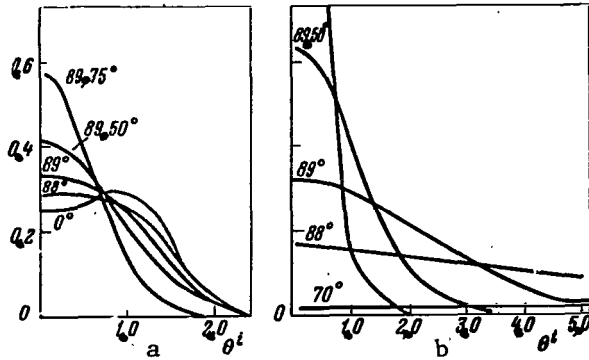


Figure 2. The Spectrum $\sigma_{\omega} \frac{V_{\pi}}{N r_e^2}$ (Ordinate Axis) for 0^+ when $T_e = T_i$, $R^e \ll \lambda \ll R^i$ as a Function of $\theta^i = \frac{\omega}{q} \sqrt{\frac{m_i}{2kT}} = \sqrt{\frac{m_i}{m_e}} \theta^e = 1720^\circ$ (for 0^+).

a. $\lambda' > d (\lambda > d)$; b. $\lambda' < d$ for Various χ .

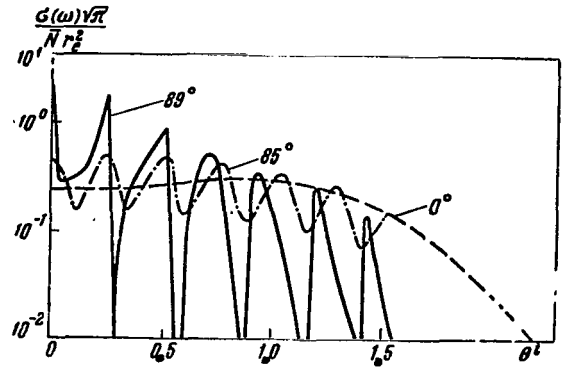


Figure 3. Scattering Spectra $\sigma_{\omega} \frac{V_n}{N r_e^2}$ for 0^+ when $T_e \ll T_i = T$, $R^e \approx \lambda' \approx R^i$ as a Function of $\theta^i = 1720^\circ$ with Various χ for $\lambda \gg d$.

and 3. The normalized Doppler frequency $\theta^i = \frac{\omega}{q} \left(\frac{m_i}{2kT} \right)^{1/2}$ is plotted along the abscissa; $-\frac{V_{\pi} \sigma_{\omega}}{N r_e^2}$, is plotted along the ordinate; χ is the parameter given on the curves.

Let us mention that R^e and R^i in a real ionosphere vary⁽⁷⁾ with altitude just as d varies. Cases (3) and (4) most often are valid in fact.

The spectra σ_{ω} in Case (3) depend substantially on the degree of closeness of the angle χ to $\pi/2$ and are different when $d/\lambda' \geq 1$; for $\lambda' > d$ (Figure 2 a) for small angles χ the spectra σ_{ω} are double-humped, wide and flat. Physically the second hump corresponds to scattering by ion-accountical /143

(7) In the vicinity of the F2 maximum at middle latitudes, R^e and R^i for atomic ions of 0^+ , H^+ and He^+ are on the order of 10 - 1, 1000 - 300, 300 - 100 and 500 - 200 cm, respectively.

waves having a resonance character. As we shall see below this effect appears more clearly in the absence of a temperature balance ($T_e \neq T_i$) in the plasma. With the approach of $\chi \rightarrow \pi/2$ the spectra become single-humped, are narrowed and become higher; when $\lambda' < d$ (Figure 2 b) the spectra σ_ω for any χ are single-humped; when $\chi \rightarrow \pi/2$ they are sharply narrowed and extend upward.

In Case (4) when $\lambda' < d$ the spectra σ_ω are the same as in Case (3); when $\lambda' > d$ and with sufficient nearness of $\chi \rightarrow \pi/2$, for σ_ω the appearance of maxima are characteristic (Figure 3) near values of the frequency that are multiples of the gyrofrequency of the ions and electrons⁽⁸⁾. With a decrease in χ these maxima are shifted, decreased and disappear altogether. Physically the "bursts" σ_ω , at frequencies multiple to the gyrofrequencies of the ions, are associated with scattering by ion-cyclotron waves having a resonance character.

As far as the other cases are concerned we can mention the following. In Case (1) when $\lambda \ll R^{e,i}$, equivalent to the vanishingly small magnetic field, σ_ω does not depend on the angle χ , and when $\lambda' < d$ the spectrum σ_ω will be determined by the thermal velocities of the electrons. In Case (2) λ is comparable with R^e ; therefore, the spectrum has maxima at the harmonics of the gyrofrequency of the electrons ω_H^e . When $\lambda > d$, these maxima are slightly shifted and when $\lambda \gg d$ narrow maxima appear in the spectrum at the harmonics ω_H^e , but they are several orders smaller than in the case of $\lambda \ll d$. Case (5) is similar to Case (3), i.e., the spectrum is narrowed with increase in χ from 0 to $\pi/2$.

Scattering of electromagnetic waves by fluctuations in the electron density of a nonisothermal plasma. In the real ionosphere, often $T_e > T_i$ and this may be substantially manifested in the intensities and the spectra of

(8) Since $\theta' \sim \theta^e \sqrt{m_i/m_e}$.

scattered radio waves. On the one hand, the method of incoherent scattering caused the processing and interpretation of the measurement results to be complicated, but on the other hand new possibilities are opened for obtaining supplemental information on the parameters of the plasma and processes taking place in it.

The theory of incoherent scattering when $T_e \neq T_i$ has been developed in recent years by a number of authors [5, 11, 12]. Basically we shall follow Fejer [4, 5]. He made his study both by allowing for the magnetic field and without. He took into account the presence of several sorts of ions. In the theory a number of other assumptions were also made: (1) the ionized gas is quasineutral and the ionization is total; (2) the forces which act on the electrons are small, the nonlinear effects are not taken into account, and the external field acts only on the electrons; (3) of the external fields only the constant magnetic field can act on the gas; (4) the electrostatic field is a Coulomb field of electrons and ions; (5) the velocity distribution of the particles may deviate from the Maxwellian only because of Coulomb forces; (6) the frequency of the incident wave exceeds the plasma frequency and the gyrofrequency significantly, as well as the frequencies of collisions of all the particles contained in the ionized gas; (7) the collisions between particles can be ignored; and (8) the fluctuations in electron concentration are quasistationary relative to the frequency of the incident wave. /144

All these assumptions (and especially those from the fifth to the eighth) in the real ionosphere are usually satisfied. Let us confine ourselves only to certain comments.

Although the total ionization part of the first condition is exact, and is not satisfied nevertheless, the frequency of the incident wave significantly exceeds the frequency of collisions of the electrons with other particles, including neutral particles, so that the presence of these latter plays no

role. We should perhaps make corresponding evaluations for the lower regions of the ionosphere (D and E). We can not eliminate the possibility that the collisions which increase the "viscosity" of the medium will lead to a slight narrowing of the spectrum σ_ω , and also to a smearing of the different resonance "bursts" in σ_ω (including the gyrofrequencies).

Although the condition of quasineutrality for the earth's ionosphere apparently is satisfied, in the literature, however, there are other indications [13, 14] that at altitudes of 20 - 160 thousand km the electron energy may exceed the ion energy by approximately 100 - 1000 eV. If we attribute this to a disruption in the quasineutrality of the plasma, then this may lead to such a strong electric field (with a strength of $E_0 \sim (1 - 4) \cdot 10^{-2}$ V/cm) that we can not eliminate the possibility that it will influence the spectra σ_ω . If the method is used for measurements at these altitudes, then this must be taken into account.

As far as the second condition is concerned, apparently we must have corresponding evaluations, for example for such a possible situation when one and the same volume of the ionosphere is simultaneously probed by two powerful radars.

The third assumption is reduced under ionospheric conditions to neglecting the force that acts on the electrons from the side of the Earth's electric field. The evaluations showed that the force of the geomagnetic field exceeds this electric field by several orders (~ 4).

Although in the earth's ionosphere in the absence of Coulomb forces the assumption as to a Maxwellian velocity distribution of the particles is satisfied, for the theory under study this is not necessary. We may assume other velocity distributions for the particles which will lead to other formulas for σ_ω .

The heating of the electrons by the probing wave or by emission from another radar may apparently be one of the reasons for disruption in the Maxwellian distribution. The possibility of ignoring the "heating" can be easily figured based on the known (see, for example, [15]) condition for ignoring this:

$$E_i \ll E_p \quad (12)$$

where E_0 is the strength of the irradiating field and

$$E_p = \sqrt{\frac{3mk}{e^2} T \delta (\omega_0^2 + \nu_0^2)}$$

is the strength of the "plasma" field; ν_0 is the effective number of electron collisions in the equilibrium plasma; δ is the amount of energy transmitted by the electron during the collision. The results of evaluating the quantities E_i and E_p in the regions D, E, and F⁽⁹⁾ of the ionosphere for various strengths of emission are illustrated in Table 1. /145

TABLE 1

Region of Ionosphere	$\omega_0 \cdot 10^{-3}, \text{ sec}^{-1}$	$E_p \cdot 10^{-2}, \text{ mV/m}$	$10^{-2} E_0, \text{ mV/m}$		
			1 Mw	5 Mw	10 Mw
D	1	32	1.5	3.4	4.8
	10	32			
E	1	27	1	2.2	3
	10	27			
F	1	19	0.3	0.7	1
	10	190			

(9) The parameters of these regions are taken in the limits of the usual values ($\nu_0 = 10^7, 7 \cdot 10^5$ and 10^3 sec^{-1} , $z_0 = 60, 90, 300 \text{ km}$, $T = 300, 200, 2000^\circ \text{ K}$ for the D, E, F regions, respectively).

Although from Table 1, it follows that condition (12) is satisfied, we can however not eliminate the possibility in a weak field ($E_i < E_p$) that nonlinear effects may take place which, on the strength of their specific nature, may be distinguished in measurements by the method of incoherent scattering [16] and in particular may expand the possibilities of the method.

According to Fejer [5] with the above assumptions, the Fourier transform S_j of the fluctuations in concentration of particles of the j^{th} sort consists of two components

$$S_j = S_{rj} + S_{fj}, \quad (13)$$

where S_{rj} is the component of S_j which is determined by the known method of electron fluctuations in the absence of Coulomb interaction between particles; S_{fj} is the component of S_j that is determined by the presence of Coulomb forces (fluctuations in charge density $e \sum_j Z_j S_j$ directly produce the fluctuating electric field which in turn produces fluctuations in density S_{fj}). Existence of a proportionality was assumed between fluctuations S_{fj} and the charge density

$$S_{fj} = \xi_j \sum_j Z_j S_j,$$

where Z_j is the relative charge of the particle of j^{th} sort (for the electron $j = 1$, $Z_1 = -1$); ξ_j is the coefficient of proportionality.

To compute S_{fj} by solving the kinetic equation we determined the deviation $\Delta f(v)$ of the velocity distribution function $f(v)$ for electrons from the Maxwellian distribution produced by the fluctuating electric field of the plasma E , which is associated with the charge density in the usual manner

$$\epsilon_0 \operatorname{div} E = e \sum_j Z_j S_j.$$

By integrating $\Delta f(v)$ over the space of the velocities we determined the value of S_{fj} , and consequently also σ_ω .

The final expression for σ_ω may be written in the form

/146

$$\frac{\sqrt{\pi}}{\sigma_e} \sigma_\omega = A^2 \Omega_1^{-1} N_1 Q_1 + B^2 \sum_{j=2}^n \Omega_j^{-1} N_j Q_j, \quad (14)$$

where

$$A = \left| \frac{1 - \sum_{j=1}^n Z_j \xi_j}{1 - \sum_{j=1}^n Z_j \xi_j} \right|; \quad B = \left| \frac{\xi_1}{1 - \sum_{j=1}^n Z_j \xi_j} \right|;$$

$$Q_j = \exp(-\omega^2 \Omega_j^{-2}); \quad \Omega_j = q \sqrt{\frac{2kT_j}{m_j}};$$

$$\xi_j = Z_j d_j^{-1} q^{-1} (2\omega \Omega_j^{-1} Q_j \int_0^{\omega \Omega_j^{-1}} \exp y^2 dy + i \sqrt{\pi} \omega \Omega_j^{-1} Q_j - 1);$$

ω is the deviation of the frequency in the scattering spectrum from the frequency ω_0 of the primary radiation; σ_e is the effective scattering cross section of the free electron;

$$d_j = C_1 \sqrt{\frac{T_j}{N_j}} = \frac{v_j}{\sqrt{2} \omega_{pe,j}};$$

d_j, T_j, m_j, Z_m are the Debye radius, the kinetic temperature, the mass and relative charge (relative to the unit charge; for the electron $j = 1, Z_1 = -1$ and for a singly ionized positive ion of any sort $Z_j = 1$); $C_1 = \sqrt{\frac{k\epsilon_0}{e^2}}$ is a constant; ϵ_0 is the dielectric constant of the vacuum, the index "1" pertains to the electron, $q = |\mathbf{k}_{\text{inc}} - \mathbf{k}_{\text{refl}}| = \frac{4\pi}{\lambda} \sin \frac{\theta}{2}$, k is the Boltzmann constant, n is the number of sorts of charged particles in the plasma. The values in formula (14) are expressed in a system of mks units.

Formula (14) is also the solution to the problem formulated without taking the magnetic field into account. The value of σ_ω determines the scattering energy per unit of density of energy of the incident wave, per unit of the solid angle, per unit of the scattering volume and per unit of spectral width of the stray radiation. The integral scattering cross section σ and consequently the strength of the stray radiation P_s as well, is determined in the usual manner from σ_ω , i.e., using formulas (2) and (3).

If we vary the ion composition and temperature of the charged particles and use (14), we can obtain all the diverse spectra σ_ω for the multicomponent plasma in the presence and absence of a temperature balance.

Analysis of formula (14) shows that the scattering spectrum σ_ω consists of two parts: a wide high-frequency electron part (the first term), where $\omega \sim qv_e$ (v_e is the mean thermal velocity of the electrons) and a narrow low-frequency ion part [the other terms in (14)]⁽¹⁰⁾, where $\omega \sim qv_i$ ($v_i \ll v_e$). The intensity σ_ω of the electron part is everywhere significantly smaller than the ion part.

In the electron part of the spectrum σ_ω there exists a maximum (plasma "peak") which corresponds to the plasma frequency $\omega_{pl,e}$ of the electrons. It becomes significant when $\lambda' \sim d$, narrows with increase in λ' and when $\lambda' \gg d$ precisely corresponds to $\omega_{pl,e}$. In the presence of a magnetic field it is shifted slightly and is found at the hybrid frequencies [13] /147

$$\omega_1 = \omega_{pl,e} - \frac{\Omega_e^2 \cos^2 \chi}{2\omega_{pl,e}^2} \text{ and } \omega_2 = \Omega_e \cos \chi,$$

where Ω_e is the gyrofrequency of the electrons. It is assumed that $\omega_{pl,e} \gg \Omega_e$.

For illustration the following dependence is shown on Figure 4

$$\frac{\sqrt{\pi}}{Nr_e^2} \sigma_\omega \text{ on } \theta^4 = \frac{\omega}{q} \sqrt{\frac{m_i}{2kT_i}}$$

(10) We can assume that this narrow component of the spectrum σ_ω arises, during scattering by coherent fluctuations ΔN in the form of damped acoustical waves, which occur as part of the thermal fluctuations in the plasma.

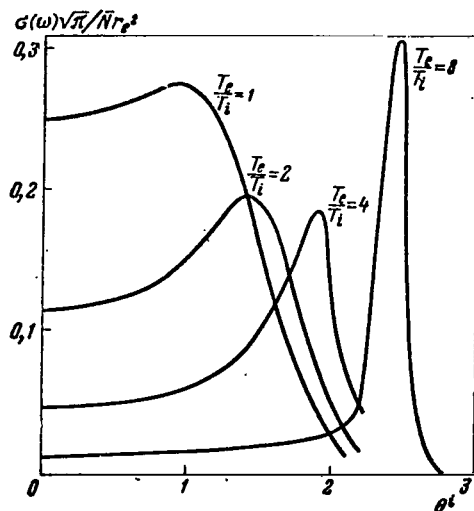


Figure 4. Dependence of Scattering Spectra on frequency parameter $\sigma_\omega \frac{\sqrt{\pi}}{N r_e^2}$ $\theta^1 = \frac{\omega}{q} \sqrt{\frac{m_i}{2kT_i}}$ when $\lambda \gg d$ for various $\frac{T_e}{T_i} \geq 1$ when $H = 0$.

($\lambda \gg d$) is found to be proportional to $m_i^{-1/2} \sqrt{T_i}$, and the increase γ of this maximum above the value σ_ω when $\omega = 0$ is a function of τ_0 , which is sensitive to change in the ratio $\tau_0 = T_e/T_i$. This shows the theoretical possibility of determining T_e and T_i separately from the spectrum σ_ω if m_i of the two-component plasma is known. The normalized spectra are not very sensitive to change in the sort of ions (change in m_i) in a two-component plasma and the relationship between ions of known composition.

Figure 5 shows from Reference [5] the change in the spectra σ_ω with variation in the relationship between components of a known sort of three-component plasma (electron and ions of atomic oxygen O^+ and hydrogen H^+)

(11) This value of ω corresponds to the velocity of the longitudinal ion-acoustical waves.

for different values of the ratio $\tau_0 = T_e/T_i$ as a parameter for the practically significant case $\lambda' > d$ ($\lambda \gg d$). The plasma here is two-component and contains only one sort of ions (O^+). Most characteristic in this case is the above-mentioned presence of a maximum when

$$\theta^1 = \sqrt{\frac{T_e}{T_i}} \quad \left(\omega = q \sqrt{\frac{2kT_i}{m_i}} \sqrt{\frac{T_e}{T_i}} \right) \quad (11)$$

which is more clearly expressed the greater τ_0 . Physically it corresponds to scattering by ion-acoustical waves having a resonance character. Landau damping for these waves is small when T_e significantly exceeds T_i . The spectral width in this case

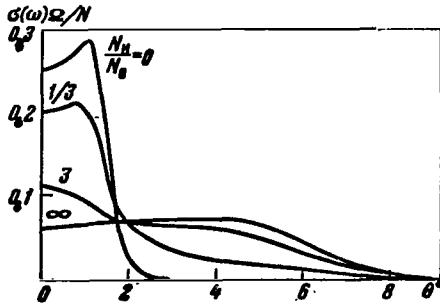


Figure 5. Spectrum σ_ω of a Three-Component Plasma (H^+ and O^+ Ions) for Various Relationships N_H/N_0 Between Them.

when $T_e = T_i = T$ and $\lambda \gg d$. Along the abscissa is plotted the value

$$\theta^0 = \frac{\omega}{q} \sqrt{\frac{m_0^+}{2kT}}, \text{ and along the ordi-}$$

$$\text{nate } \frac{\sigma_\omega N}{\Omega_0} = \frac{\sigma_0 N}{q} \sqrt{\frac{m_0^+}{2kT}}, N = N_H + N_0.$$

(the index "0" refers to O^+ and the index "H" to H^+), for the parameter of the curves we chose the ratio N_H/N_0 of ion concentrations. On the figure, the expansion of the spectra can be clearly traced with increase in N_H/N_0 .

In the case of a four-component plasma, containing three sorts of ions (for example, O^+ , H^+ and He^+), the spectra are quite diverse and differ strongly from the cases of two- and three-component plasma [17]. Their computation is practically possible only by using electronic computers. An example of such a family of spectra is shown on Figure 6 in the form of a triangular diagram; each family of spectra corresponds to one value of the ratio $\tau_0 = T_e/T_i$ (on the figure $\tau_0 = 2$) as a parameter. The second parameter is the relationship between components. This parameter distinguishes the curves of one family: at the apex of the triangular diagram are the degenerate spectra containing 100% ions of one sort (different at each apex); along the sides of the triangle the spectra contain two sorts of ions and inside the triangle are three sorts /149 of ions, the relationship between which clearly follows from the geometry of the diagram. Each curve of the spectral family is the dependence of $\frac{\sigma_\omega}{\sigma_0}$ on $\theta^0 = \frac{\omega}{q} \sqrt{\frac{m_e}{2kT_e}}$ with fixed parameters (composition of the mixture and T_e/T_i).

It is obvious that, with approach of τ_0 to unity, the difference in the spectra of a given family, other things being equal, is decreased, and with increase in τ_0 it is increased.

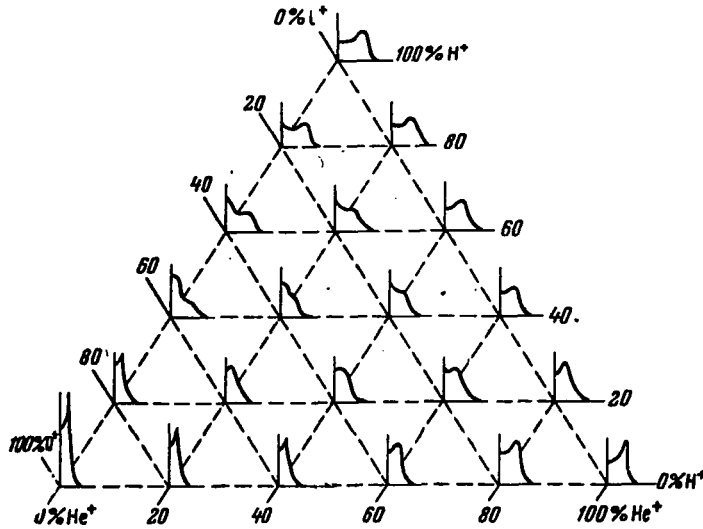


Figure 6. Spectra $\frac{\sigma_{\omega}}{\sigma_0}$ of Mixtures O^+ , He^+ and H^+ When $T_e = 2T_i$; $i = 2, 3, 4$ as a Function of $\theta^* = \frac{\omega}{q} \sqrt{\frac{m_e}{2kT_e}}$.

In the work of Fejer [5] computation of σ_{ω} when $T_e/T_i \neq 1$ is carried out as shown above also by allowing for the constant magnetic field. Results are obtained analogous to that described above. It is characteristic that it is possible to find resonance "peaks" in σ_{ω} at frequencies equal to (or near) the gyrofrequencies of ions and electrons and their harmonics.

As far as the integral scattering cross section σ is concerned, and consequently the scattering intensity P_s as well, as noted above, the magnetic field does not influence them at all [5], as long as τ_0 is not too high⁽¹²⁾.

The results from other research [9, 10, 12, etc.], in spite of the different approaches to solving the problem, are similar to the results of [5], but in practice are less feasible.

(12) When $\tau_0 \gtrsim 10$ the magnetic field already affects σ significantly [11, 18].

It should be mentioned that it is characteristic of the contemporary state of the method that we have as its basis a theory which confirms the experiment, as we shall show below. The theory of incoherent scattering may basically be assumed to be complete although there are unresolved questions especially in the method of processing and the physical interpretation of the observation results. It is natural that the comparatively fast (within a few years following publication of [1, 7]) development of a satisfactory theory is to a certain extent the result of the high level of contemporary knowledge of plasma physics and kinetic theory in general; here Soviet scientists [2, 15, 18, etc.] have made a considerable contribution.

TECHNICAL MEANS, METHOD OF MEASUREMENTS AND PROCESSING

In order to give some idea as to the technical means used in ionospheric research involving the method of incoherent scattering, Table 2 gives data apparently about all the information that has been published at the present time (see [3, 7, 8, 19 - 25]).

As mentioned, for processing the data on scattered radiation, a storage element is necessary. In earlier research [7, 8] these were analog integrators. Later they were replaced by digital integrators. In modern research it is usually necessary to process the registrations of P_s and σ_ω on an electronic computer for the purpose of obtaining temperatures and ion composition of the ionosphere. Therefore, it is natural that we tend to use them for storage as well.

The electron concentration N is determined either by measuring the scattering intensity P_s or by measuring the angle of rotation Φ_ϕ of the polarization plane of the scattered radiation due to the Faraday effect⁽¹³⁾.

(13) It is also possible to measure N from the "bursts" on σ_ω at frequencies ω , equal to $\omega_{pl,e}$ if we have a set of narrow-band receivers tuned to the frequencies of $\omega_0 + \omega_{pl,e}$ for the various expected values of $\omega_{pl,e}$.

TABLE 2. PARAMETERS OF RADARS FOR IONOSPHERIC MEASUREMENTS
USING THE METHOD OF INCOHERENT RADIO WAVE SCATTERING

No.	Location (Country)	Frequency, MHz	Power MW	Antenna Dimension, m	Duration of Impulse, μ s
1	Illinois (USA) 40° N, 90° W	41	1-6	116x140	3-150
2	Millstone-Hill (USA) 43° N, 71° W	440	1,2-2,2	Ø25	250,500
3	Same	440	3	Ø70	—
4	Same	1295	5	Ø25	—
5	Trinidad 11° N, 62° W	425	2	Ø25	800
6	Cajamarca (Peru) 12° S, 78° W	50	1-8	290x290	100— 30 000 000
7	Arecibo (Puerto-Rico) 19° N, 67° W	430	2,5	Ø300	2-10 000
8	Same	40	—	—	—
9	Nancy (France) 45° N, 2° W	935	0,075	100x20 - transm. 200x35, 200x40 receiv.	continuous
10	Prince Albert (Canada) 52° N, 106° W	435	2	Ø25	—
11	Palo Alto (Califor- nia, USA)	400	0.5 (ave.)	Ø30	—
12	Malvern Hill (England) 51° N, 2° W]	400	10	Ø42	—
13	Thetford (England)	300	0,1	Two 25	130
14	Scotland	400	0,2	Ø13	—
15	Stanford (USA)	50, 80, 1200	—	—	—

TABLE 2. PARAMETERS OF RADARS FOR IONOSPHERIC MEASUREMENTS
USING THE METHOD OF INCOHERENT RADIOWAVE SCATTERING (Cont'd)

No.	Location (Country)	Noise Factor (-)	Polarization	Message Frequency, sec	Time of Measurement, years
1	Illinois (USA) 40° N, 90° W	2	Linear	25-100	1958-1961
2	Millstone-Hill (USA) 43° N, 71° W	~2	Circular	50	1960-1961
3	Same	—	—	—	—
4	Same	—	—	—	—
5	Trinidad 11° N, 62° W	~3	Linear Orthogonal	25, 32	1960-1962
6	Cajamarca (Peru) 12° S, 78° W	~1,5	Circular	var	C 1962
7	Arecibo (Puerto-Rico) 19° N, 67° W	~1,5	Circular	var	—
8	Same	—	—	—	—
9	Nancy (France) 45° N, 2° W	—	—	—	C 1965
10	Prince Albert (Canada) 52° N, 106° W	—	—	—	—
11	Palo Alto (California, USA)	—	—	—	—
12	Malvern (England) 51° N, 2° W]	—	—	—	—
13	Thetford (England)	~2	Linear	48,8	1962
14	Scotland	—	—	—	1960
15	Stanford (USA)	—	—	—	1960

TABLE 2. PARAMETERS OF RADARS FOR IONOSPHERIC MEASUREMENTS
USING THE METHOD OF INCOHERENT RADIOWAVE SCATTERING (Cont'd)

No.	Location (Country)	Organization	Authors	Where Parameters Publ.	Comments
1	Illinois (USA) 40° N, 90° W	NBS USA	Bowles	[3, 7, 8]	
2	Millstone-Hill (USA) 43° N, 71° W	Lincoln Lab.	Pineo, Kraft, Brisco	[12, 19]	
3	Same	Same	Evans	[20]	
4	Same	Same	Evans	[20]	
5	Trinidad 11° N, 62° W	USAF	Millman, Pineo	[21, 26, 27]	
6	Cajamarca (Peru) 12° S, 78° W	NBS USA & Geo- physics Insti- tute, Peru	Farley Bowles	[22, 23]	
7	Arecibo (Puerto Rico) 19° N, 67° W	Cambridge Res. Cen., USAF	Gordon	[20, 22]	
8	Same		Gordon	[20]	
9	Nancy (France) 45° N, 2° W	National Res. Center	Carry Petit Waldtey	[22, 28]	receiving antenna 300 km from transmitter
10	Prince Albert (Canada) 52° N, 106° W	—	Maynard	[20, 29]	
11	Palo Alto (Califor- nia, USA)	—	Eshleman	[20]	
12	Malvern (England) 51° N, 2° W]	Brit. Radar Dept.	Watkins	[3, 30]	
13	Thetford (England)	Roy. Radar Ad.	Watkins	[3, 30]	
14	Scotland	Stanford Res. Institute	Eshleman	[24]	
15	Stanford (USA)	Same	—	[22]	

The original expression, relating P_s and N which is the basis of formula (14), may [taking (14), (2) and (4')] into account] be represented for a two-component plasma (electrons and one sort of ions) in the following form [3 - 5, 20, 23, 31]:

$$\frac{P_s}{P_{se}} = 1 - \frac{1}{1+D} + \frac{1}{(1+D)(1+D+T_e/T_i)}, \quad (15) \quad \underline{/151}$$

where $P_{se} = \frac{\xi N(R)}{R^2}$ is the scattering intensity in the case of free electrons ($D \rightarrow \infty$); P_s is the actually measured scattering intensity from the volume V ; $N(R)$ is the mean electron concentration in the volume V ; R is the mean distance to the scattering volume; ξ is a factor determined by the radar:

$$D = d^2 (\lambda')^{-2}, \quad \lambda' = \frac{\lambda}{4\pi}, \quad (16)$$

d is the Debye radius of the electron.

Analogous to (15), but more awkward, relationships may be written also for a plasma having more than two components. The first two terms in (15) correspond to the electron high-frequency component (EC) and the third term corresponds to the ion low-frequency component (IC) in P_s/P_{se} ⁽¹⁴⁾. The relationship between them depends on D (on the relationship between λ and d); particular (maximal and intermediate) values of P_s/P_{se} are shown on Table 3.

(14) This division does not at all mean that scattering by ions makes a significant contribution to the scattering intensity P_s . The term "ion component" of P_s means only the degree to which the ions affect the movement of the electrons and consequently only the spectra σ_ω (so, when $\lambda \gg d$, the fluctuations ΔN which take place on an interval equal to λ are determined by the thermal velocities v_i of the ions and the spectrum $\omega \sim v_i$; when $\lambda \ll d$ the influence of the field of ions on the movement of the electrons in the interval λ can be ignored and $\omega \sim v_e$).

TABLE 3

Relationship Between λ and d	EC - First Two Terms in (15)	IC - Third Term in (15)
$\lambda \gg d$	0	$\frac{1}{1 + T_e/T_i}$
$\lambda \ll d$	1	0
$\lambda = 4\pi d$	$\frac{1}{2}$	$\frac{1}{2(2 + T_e/T_i)}$

Since under experimental conditions the condition $\lambda \gg d$ is often satisfied, the effective formula in this case will obviously have the form

$$P_s = \frac{\xi N(R)}{R^2(1 + T_e/T_i)} \quad (17)$$

The dependence of P_s on ion mass is weak and can usually be ignored [17]. A number of authors [7, 23, 28, 31, 36, 38, 43, 44] have used formula (17) in their interpretations.

However we must bear in mind that at sufficiently high altitudes ($z > 1000$ km), in the range of 300 - 3000 MHz, condition (6) may cease to be satisfied and in the processing the general formula (15) must now be used. The processing in this case is complicated, since one other unknown parameter d appears. Naturally we can give it in some manner and then refine the results using the method of iterations.

The dependence of P_s/P_{se} on D and T_e/T_i in the general case (15) is shown graphically on Figure 7.

From (17) it follows that for determining N it is necessary to have available data on $\tau_0 = T_e/T_i$ and vice versa, in the presence of

/152

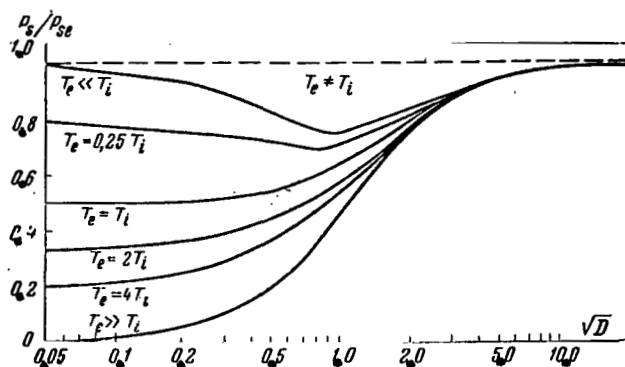


Figure 7. Dependence of the Scattering Intensity, Relative to its Value for Free Electrons, on the Relationship Between

λ and $d\left(\sqrt{D} = \frac{4\pi d}{\lambda}\right)$ for Various Values

$$\text{of } \tau_0 = \tau_e / \tau_i.$$

cases we can simply set $\tau_0 = 1$. For example, this may be done at night at all altitudes⁽¹⁶⁾, by day for altitudes of $z \gtrsim 400 - 500$ km and always at sufficiently high altitudes⁽¹⁷⁾. However, in the morning up to altitudes of ~ 400 km, τ_0 differs significantly from unity [25] and the maximal error in determining N because of this (if we set $\tau_0 = 1$) can at this time reach $\sim 100\%$ at altitudes of $200 - 400$ km. Since the data on the dependence of τ_0 on time and altitude are still scarce, we must then either accept the errors which arise or measure τ_0 .

(15) For example, from the Faraday effect for scattered signals or from the "burst" in σ_ω at the plasma frequency of electrons, using the method of coherent frequencies or by using the Faraday effect for signals from rockets and satellites [33], vertical probing of the ionosphere from above, below, etc.

(16) Apparently it is more correct to say $\tau_0 \approx 1.1 - 1.2$ [20, 24, 25, 28], but this does not notably affect the business at hand.

(17) The upper limit of this altitude has not been yet established. Apparently it is ≥ 500 km and depends on the time of day, season, solar activity and geographic coordinates.

simultaneous measurements of the N profile by other independent methods⁽¹⁵⁾ we can determine τ_0 . The distance R , as already noted, can be easily determined from the lag Δt of the reflected signal with respect to the emitted signal, and the coefficient ξ can be computed from the known characteristics of the radar or determined experimentally from vertical probing or by using satellites [32].

The basic difficulty in determining N using (17) involves lack of knowledge of τ_0 . In a number of

The electron concentration at sufficient wavelength is determined also in the experiments on incoherent scattering from measurements of the Faraday rotation Φ_ϕ of the polarization plane of the scattered radiation, by using the known formula

$$\Phi_\phi = \frac{\text{const}}{\omega_0^2} \int_0^R b_L(\rho) N(\rho) d\rho.$$

Since the shift in the volume V occurs along R, which coincides with the intergration path, then by differentiating this latter expression with respect to R, we find

$$N(R) = \frac{1}{b_L(R)} \frac{d\Phi_\phi(R)}{dR}, \quad \text{/153}$$

where b_L is determined (see, for example, [33]) from the data on the geomagnetic field along R.

Measurement of the angle Φ_ϕ at sufficient wavelengths may be done in the usual manner, for example, from the number of fadings of the scattered signal during reception on one or two plane-polarized antenna arrays.

It is interesting to look at the method of measuring $\Phi_\phi(R)$ and consequently $N(R)$ as well in [34]. Two pulses are emitted simultaneously with circular polarization in opposite direction of rotation. As a result of porcessing the individually received signals of both polarizations, we can obtain values of $P_s \sin \Phi_\phi$ and $P_s \cos \Phi_\phi$ and consequently R_s and Φ_ϕ individually as well.

When necessary, from the measurements of Φ_ϕ we can introduce corrections for influence of the Faraday effect on the measurements using the method of

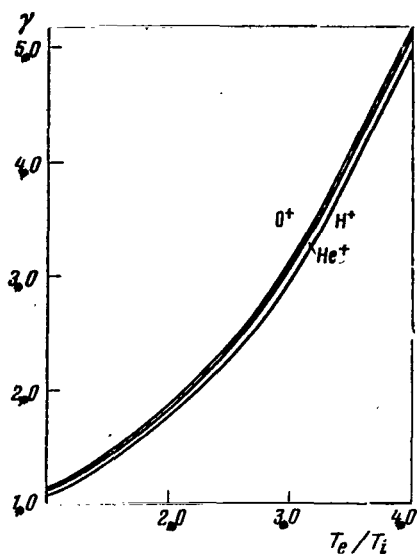


Figure 8. Excess $\gamma = \frac{\sigma_{\omega m}}{\sigma_0}$ of the Maximum $\sigma_{\omega m}$ of the Spectrum σ_m Over its Value σ_0 (σ_m when $\omega = 0$) as a function of $\tau_0 = T_e/T_i$ when $\lambda \gg d$ for Ions O^+ , H^+ and He^+ .

incoherent scattering. The influence of Φ_ϕ on P_s in using antennas with linear polarization leads, when sufficient wavelengths are used, to a decrease in P_s by two times and to the appearance of oscillations in the dependence of P_s on R with sufficient shortening of λ .

Determination of τ_0 can be done as mentioned above from the spectra σ_ω such as that in Figure 4. Figure 8 [6] shows for illustration the dependence of $\gamma = \frac{\sigma_{\omega m}}{\sigma_0}$ on τ_0 for O^+ , He^+ and H^+ ions when $\lambda \gg d$ for a monoionic plasma ($\sigma_{\omega m}$ is the maximal value of σ_ω when $\omega = \omega_m$). We can see the sharp dependence of γ on τ_0 and the weak sensitivity ($\leq 10\%$) γ of a monoionic plasma to the sort of ions.

The width ω of the spectrum $\Delta\omega$ [sic] of the scattered signal when $p \ll \gamma$ is determined basically by the ion mass m_i , the temperature and magnitude of τ_0 . Thus with a known (given) m_i , by measuring τ_0 and $\Delta\omega$ we can determine the temperatures T_e and T_i .

Thus we arrive at the conclusion:

(1) if we know the sort of ions then from the measured relationship between λ , the intensity P_s and the width $\Delta\omega$ of the scattering spectrum σ_ω we can determine N , T_e , T_i ;

(2) without measuring the spectral width it is theoretically impossible to measure the absolute values of the temperatures T_e and T_i ⁽¹⁸⁾ only by the method of incoherent scattering, but we can measure only the ratio τ_0 .

The case of a monoionic upper ionosphere in practice is valid usually /154 at altitudes of $z \sim 300 - 400$ km (O^+) and $z \geq 1000$ km (H^+).

The problem of analyzing the spectra σ_ω in the presence of several sorts of ions (the sorts of ions are known, but the relationship between them is unknown; for example, for $z \sim 600 - 700$ km we have ions of O^+ and H^+) is substantially more complicated [17]. This is involved with the above-mentioned (Figures 5, 6) complication and diversity of the spectral shapes. However special processing on electronic computers permits, even with three sorts of ions (for example, O^+ , H^+ and He^+ at an altitude of $z \sim 600 - 800$ km) when $\lambda \gg d$ selecting a spectrum which most nearly approximates the experimental one, and determining thus τ_0 , T_i , T_e and the ion composition of the ionosphere (see, for example, [17, 20, 31]).

In particular for two known sorts of ions, the resultant new unknown relationship between the ions may be compensated in the presence of a sufficiently detailed spectral shape by the value of the slope of the spectrum in its middle part relative to the sensitivity to change in the relationship between ions. We can also use the slope of the spectrum at its "nose" [17] which is only slightly sensitive to the influence of signal nonmonochromaticity.

Further problems in analyzing the spectra may be introduced by the

(18) In the event that P_s can be measured simultaneously at two frequencies when $\lambda_1 \gg d$ and $\lambda_2 \approx d$, we can theoretically measure d as well and consequently measure T_e and T_i separately. Without knowing ξ in (17), from P_s we can determine τ_0 up to $\sim \sqrt{N^2}$ and N from the ionograms containing the E region.

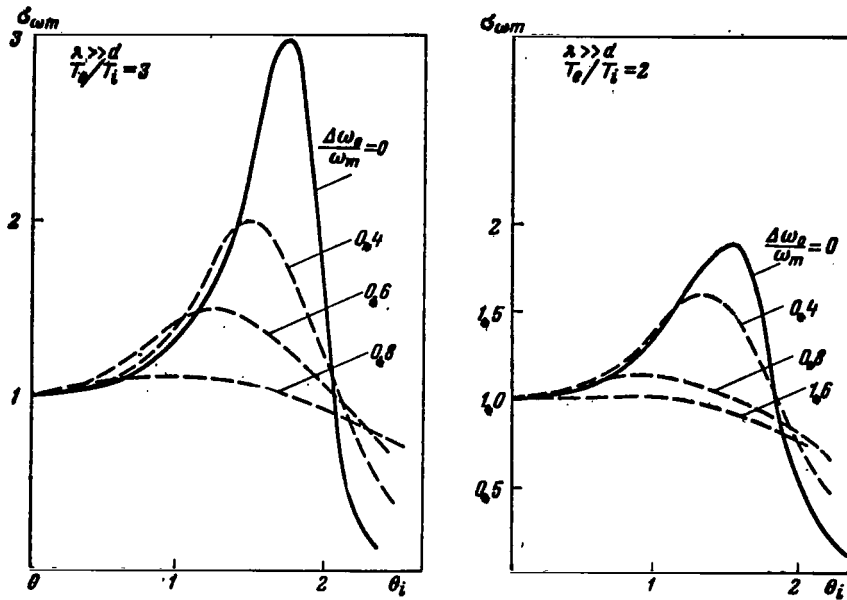


Figure 9. Influence of the Spectral Width of the Signal $\Delta\omega_0$, $(\Delta\omega_0/\omega_m)$ on the Distortion of the Spectral Shape σ_ω (The Solid Line for $\Delta\omega_0 = 0$ and the Broken Line for $\frac{\Delta\omega_0}{\omega_m} \neq 0$).

signal nonmonochromaticity of the radar, thus leading to a distortion in the spectra σ_ω and to further errors in determining the ion composition and temperatures. Figure 9 shows the influence of the finiteness of the spectral width of the signal $\Delta\omega_0$ on the spectrum σ_ω . With a small value of $\Delta\omega_0/\omega_m$ (ω_m is the value of ω at which σ_ω for $\Delta\omega_0 = 0$ reaches the maximum σ_{ω_m}) a deformation takes place in the spectrum σ_ω (reduction and displacement of the maxima). For sufficiently large $\Delta\omega_0/\omega_m$ the maxima σ_ω may disappear altogether. The width $\Delta\omega$ of this spectrum σ_ω with increase in $\Delta\omega_0$ is decreased less than is measured at the lower level σ_ω .

The effect of the probing signal on spectral measurements, if we know its width $\Delta\omega_0$, may apparently be taken into account if this influence is not too high [44]. To decrease it we can make the probing pulses longer, but this will lead to a deterioration in the resolution of R in the measurements /155

since the length ΔR of the volume V is increased (see Figure 1 a). The use of bistatic equipment (see Figure 1 b) is intended to remove these disadvantages in pulse radars.

These discussions pertained to the case when $\lambda \gg d$. However, for sufficiently high altitudes in the range of 300 - 3000 MHz, this condition may be satisfied poorly or not at all and then the processing is complicated since we must use the more complex formula (15) to determine N . Here we can use the method of trial and error assuming first that $\lambda/d \rightarrow \infty$ (for large values of λ/d) or by taking (for any of the not very large values of λ/d) the expected value of d (from that expected under the experimental conditions of N and T_e) and then successively refine d and N . Considerably greater problems arise in this case in analyzing the spectra for obtaining the ion composition and temperatures [17]. For the ionosphere with ions of one sort these problems are still surmountable, but for the ionosphere containing ions of several sorts these problems, when $d \sim \lambda$ or $d > \lambda$ in using the existing methods, may possibly be insurmountable. This significant fact must be taken into account in selecting an effective radar frequency for purposes of incoherent scattering⁽¹⁹⁾.

Thus, the facts which may be valid in the real ionosphere (i.e. the presence of ions of several sorts, the temperature imbalance of ions and electrons, collisions, variability and inhomogeneity of the atmosphere) theoretically and practically complicate analysis of the measurements utilizing the method of incoherent scattering.

The processing and refinement of special computer methods for analyzing the spectra σ_ω and P_s , as well as for obtaining the autocorrelation function

(19) Additional complications arise when the method of incoherent scattering is used to study the fine structure of the lower ionosphere, gradients, variables and random inhomogeneities [38, 43]

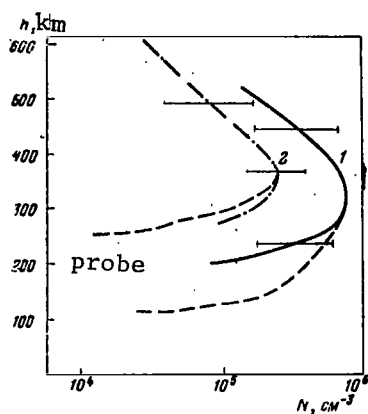


Figure 10. Profiles N, Obtained in April, 1966, by the Method of Incoherent Scattering.

1. By Day; 2. By Night and Vertical Probing (Broken Line) at Middle Latitudes of the Soviet Union.

of the scattered signal and the spectra themselves as the Fourier-transforms of this latter, have become apparently quite necessary for the effective utilization of the great potentialities of this method especially in determining ion composition.

BASIC RESULTS. COMPARISON OF EXPERIMENT AND THEORY

1. Examples of the N profiles which we obtained [36, 44] using the simplest method of processing are shown on Figures 10 and 12. The processing was carried out using expres-

sion (17). We assume $\tau_0 = T_e/T_i = \text{const} \neq 1$. The P_s profiles for transition to N were calibrated from vertical probing. The nocturnal profiles obtained by the method of incoherent scattering and by probing agree within the limits of allowable error, thus apparently indicating that $T_e \simeq T_i$ and permitting determination of the parameter ξ . The daylight profiles diverge significantly and show that with decrease in altitude z from the value $z_{F2m} \simeq 300$ km to $z \simeq 200$ km the ratio τ_0 is sharply (by several times) lowered in comparison with its maximal value near the F2 maximum. Therefore in this region of altitudes $T_e > T_i$. If we assume ξ to be the same during the day as at night, we can determine the absolute value of T_e/T_i from vertical probing at the F2 maximum and below; we found that at sunrise $\tau_0 = 4 \pm 1$ at an altitude of $z \lesssim z_{F2m}$.

The storage element which we used in the beginning is described in [36]. Its basis is the scheme used in radar probes of Venus [37], but with a substantially different comparison scheme.

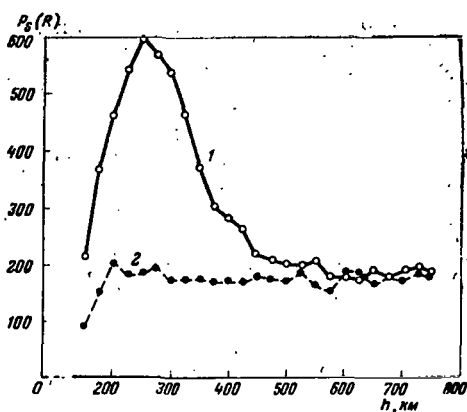


Figure 11. Profiles of the Measurements of $P_s(R)$ (Including the Internal Noises) in Relative Units (1) and of Internal Noises During Operation of the Dummy Antenna (2) on November 1, 1966.

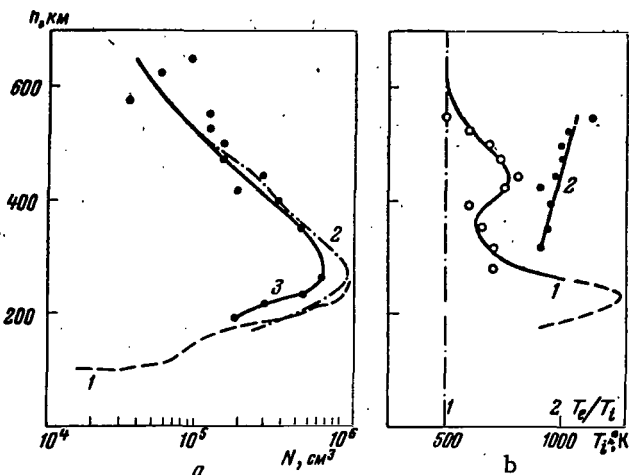


Figure 12. Profiles Obtained on November 1, 1966.

a. N Profiles; 1. Probe; 2 and 3. Incoherent Scattering Without Correction for the Variable τ_0 and With Correction, Respectively; b. τ and T_i Profiles; 1. τ , Obtained from σ_ω in Comparison with the N Profile (Curve 1 on Figure a); 2. T_i Profiles.

Further storage, just as processing, was carried out using an electronic computer. Correction for change in temperature with altitude was introduced from the measurement of the spectra σ_ω of the autocorrelation function of the /156 scattered signals, and below the F2 maximum, from vertical probing. Examples obtained using such a storage element of the P_s , N , τ_0 and T_i profiles are illustrated on Figures 11 and 12. Figure 11 shows the function $P_s(R)$ including also the power of the internal noises of the receiver which can be eliminated by measuring it during operation of the equipment on a dummy antenna. From N , τ_0 and T_i profiles (Figure 12) it is clear that the temperature imbalance τ_0 of the plasma during this time extends to an altitude of ~ 600 km, is nonmonotonic with respect to altitude and maximal below z_m F2 (here $T_i \simeq 875^\circ\text{K}$ and $T_e \simeq 2200^\circ\text{K}$).

2. There exist a number of new and significant data on the outer

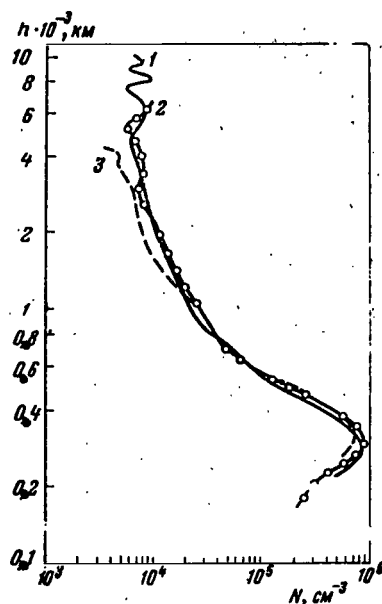


Figure 13. Vertical N Profiles in Cajamarca

1. February 1, 1965, at 15^h24^m;
2. February 2, 1965, at 15^h44^m;
3. February 3, at 15^h38^m (Local Time).

$z \gtrsim 1200 - 2000$ km), this being associated with the change first of all in the ion composition (from O^+ for $z \gtrsim 300 - 400$ km up to H^+ for $z \geq 1200 - 2000$ km).

In particular at an altitude of $z \sim 3000$ km the value $N \lesssim 10^4$ el·cm⁻³; for $z \gtrsim 5000 - 10,000$ km the value of N is on the order of several units times 10^3 el·cm⁻³, which agrees with the data from the satellite and other measurements [33, 13].

Regular measurements of the N profiles permit plotting altitude-time

(and lower) ionosphere. The most valuable results were obtained in Cajamarca, Millstone-Hill, Arecibo, Malvern and in Nancy, respectively, under the direction of Bowles and Farley [31, 34], Evans [25, 39, 40], Gordon [20, 41], Watkins [30] and the group of Carry, Petit and Waldteyfil [28] (see Table 2).

(1) In the vertical N profiles up to ten thousand kilometers (Figure 13 [20]) on Figure 18 we can see a sharp slow-down in the drop in the size of N with altitude when $z > 1000 - 1500$ km in comparison with the region directly over the F2 maximum. This represents an increase in the normalized altitude H of the outer ionosphere from a value on the order of hundreds of kilometers (for $z \gtrsim 300 - 500$ km) up to a value of several thousand kilometers (for

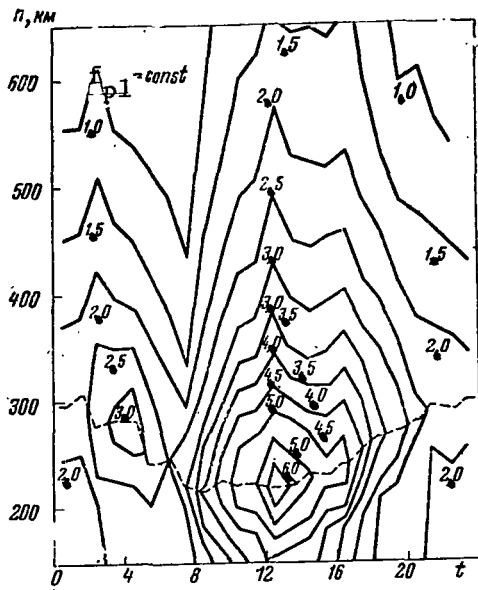


Figure 14. Altitude-Diurnal Dependence of the Plasma Frequency f_{p1} MHz at Millstone in January, 1964, as a Function of Local Time; $f_{p1} = \text{const}$ (Solid Lines), Altitude of the F2 Maximum (z_{F2m}) (Broken Line).

(diurnal and seasonal) distributions of N (see, for example, [20, 34]) near the equator and at middle northern latitudes of the western hemisphere (Figure 14) [38, 43].

Characteristic and natural are the daytime elevations and the predawn troughs of the level $f_{p1} = \text{const}$ throughout the entire ionosphere accompanied by a decrease in the altitude of the F2 maximum and an increase toward the nighttime hours. Seasonal variations are observed in the behavior of the curves (see, for example, [20, 31, 38, 43]).

At altitudes of $\sim 5000 - 10,000$ km in individual measurements (Figure 13) irregularities are observed in the variation of N with altitude of a quasiundulating shape, the altitude thickness of which is thousands of kilometers. Their nature is still not clear [20].

Wave irregularities are observed throughout the entire ionosphere⁽²⁰⁾. Attempts have been made to interpret them as gravity waves which set in due to difference in the temperatures of the cold lower ionosphere and the heated lower part of the magnetosphere [20].

(20) Apparently these are the phenomena which were observed previously in the measurements employing the method of coherent frequencies on board satellites [33].

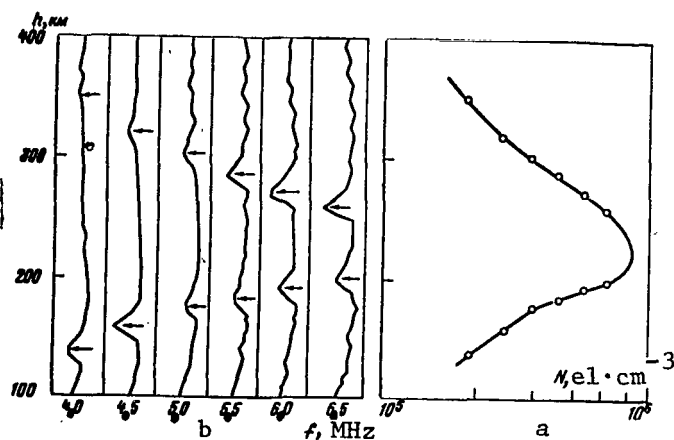


Figure 15. Vertical N Profile, Obtained from Registration of Resonance "Bursts" in the Spectra σ_ω at Plasma Frequencies of Electrons (a) and Registration of the Bursts Themselves as a Function of the Frequency Control of Narrow-Band Receivers (b).

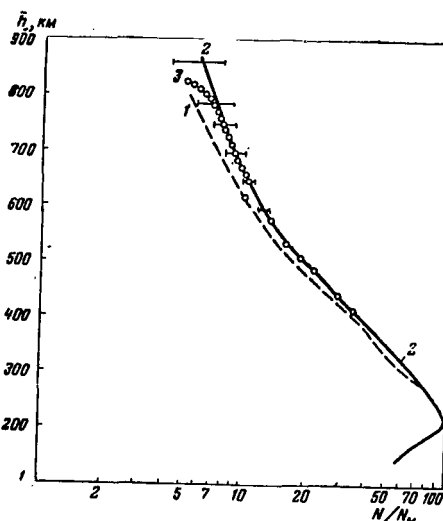


Figure 16. N Profiles, Obtained Simultaneously by Different Methods:
1. Incoherent Scattering; 2. Coherent Frequencies of Signals From Rockets (Jackson); 3. Probe Measurements.

The first successful attempts will obviously be interesting in registering, according to theory, the peaks in the spectra σ_ω at the plasma frequencies of the electrons $\omega_{p1,e}$ of the ionosphere and to plot from them the vertical N profiles (Figure 15). For this, narrow-band receivers were used tuned to a number of frequencies $\omega_0 + \omega_{p1,e}$ [11, 18, 20, 24, 42].

The question of measurement accuracy using the method of incoherent scattering, just as using other methods [33] of the N profiles (and other parameters of the ionosphere), is of considerable interest. Figure 16 shows visibly the unique results [41] (see also [38]) of the simultaneous measurement of such type using independent methods: incoherent scattering, coherent frequencies (Jackson's method) of signals from geophysical rockets and the probe method, characterizing the relative accuracy of the measurements. An astonishingly good agreement is observed for the profiles obtained.

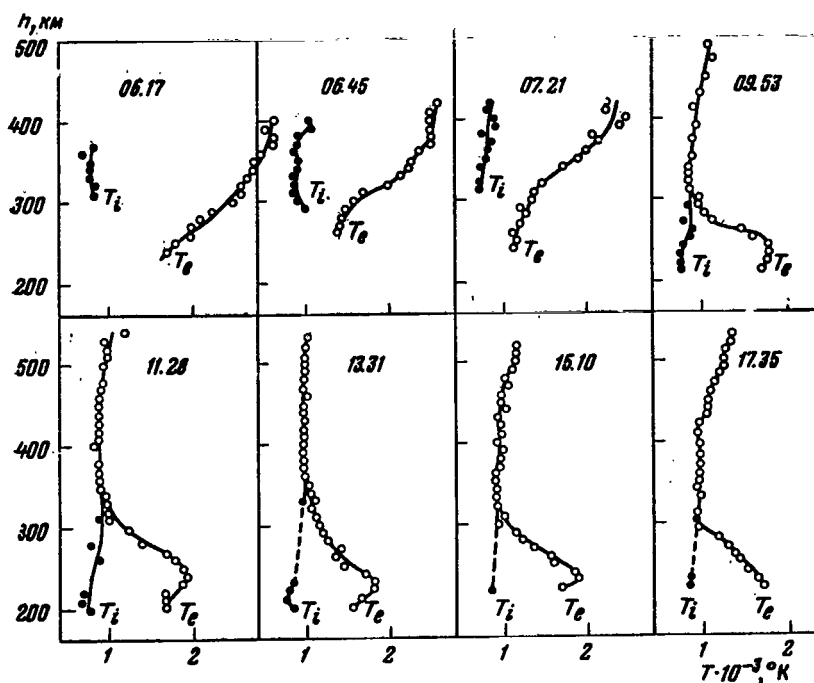


Figure 17. T_e and T_i Vertical Profiles Obtained in Cajamarca December 16, 1965, at Various (Local) Times of Day. Sunrise and Sunset at $h \approx 300$ km, respectively at $\sim 5^{\text{h}}30^{\text{m}}$ and 19^{h} [25].

(2) Altitude T_e , T_i (or τ_0) profiles were obtained, as well as ion composition, up to altitudes of $\sim 700 - 1200$ km for different times of day and seasons (Figures 17, 18) [3, 20, 24, 25, 34, 38, 42] and the altitude-time diurnal and seasonal dependences of these values following from them (Figures 19 - 22).

/159

A very important result of this type of measurement, using the method of incoherent scattering, is the reliable establishment (or confirmation) of the most fundamental fact that a temperature imbalance is possible between electrons and ions in the ionosphere ($T_e > T_i$).

In the diurnal variation of the temperatures we find to be characteristic

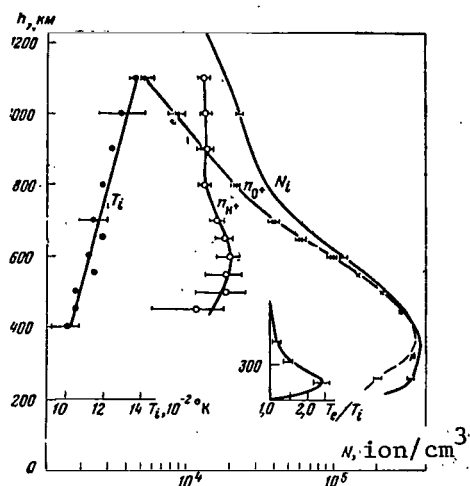


Figure 18. Vertical Temperature Profiles $T_i (^{\circ}\text{K} \cdot 10^{-2})$, $\tau_0 = T_e/T_i$ and Ion Density (n_{0+} , n_{H+} , $N_i = n_{0+} + n_{H+}$) in Cajamarca, July 23, 1964, $14^{\text{h}}12^{\text{m}} - 15^{\text{h}}14^{\text{m}}$ [31].

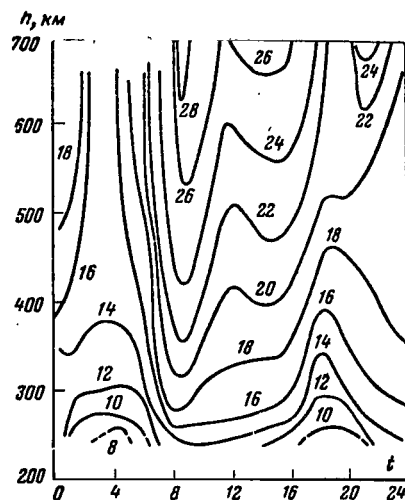


Figure 19. Altitude-Diurnal Mean-Monthly (November, 1963) Dependence $T_i \cdot 10^{-2} ^{\circ}\text{K}$ at Millstone, Local Time of Day [20].

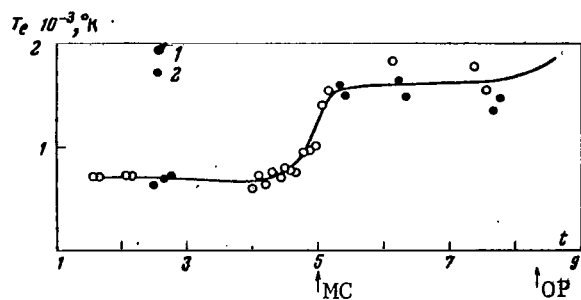


Figure 20. Diurnal Dependence $T_e (^{\circ}\text{K} \cdot 10^{-3})$ [26] at Nancy, January, 26, 1966, at Altitudes of:

1. 275 and 2. 300 km; Local Time; "MC" and "OP" Refer to Sunrise at the Magnetosconjugate Point and at the Observation Points, Respectively.

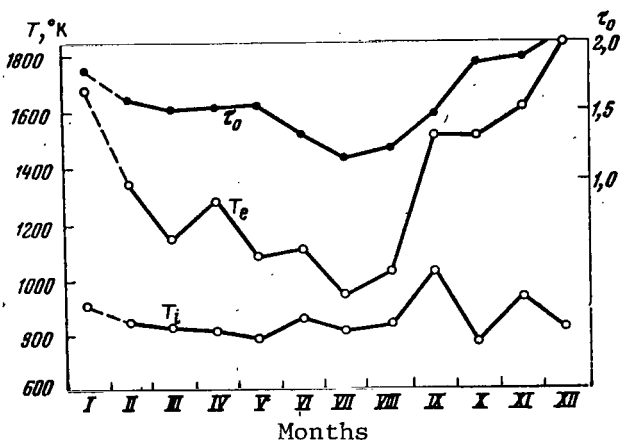


Figure 21. Seasonal Dependence of T_e , T_i and $\tau_0 = T_e/T_i$ at Millstone [23] At an Altitude of $z = 350$ km During the Night For the Period from February 1, 1963, to January, 1964.

a sharp increase in τ_0 (up to 2 - 5) in the morning during sunrise at altitudes of $\sim 250 - 300$ km.

Thus, in the behavior of τ_0 with altitude the following characteristics are observed:

(a) at altitudes $\gtrsim 400 - 500$ km during the day as a rule $T_e = T_i$ with the exception of the morning hours;

(b) during the day τ_0 reaches a maximum equal to 2 - 4 at an altitude of $\sim 250 - 300$ km;

(c) at altitudes of 100 - 130 km $\tau_0 = 1$ which disagrees with the rocket measurements and consequently requires further experimental proof.

In several experiments an interesting fact was discovered [26], i.e. there is a substantial increase in $\tau_0 = 2 - 3$ hours prior to sunrise (Figure 20) and attempts have been made to explain this by heating of the ionosphere by photoelectrons, forming at the magnetoconjugate points illuminated by the sun, where sunrise takes place 2 - 3 hours earlier than at the observation point.

A new and unexpected result [25, 28] is that during the night the ratio of temperatures τ_0 in all seasons slightly (at middle latitudes up to ~ 0.2) exceeds unity (Figure 21), thus indicating the presence apparently of an unknown source for heating the electrons. Suggestions have been made that this /161 may take place because of the transfer of energy from the cooled protonosphere of the lower ionosphere and the maintenance in it of $\tau_0 = T_e/T_i \sim 1.1 - 1.2$. It should be mentioned that in several experiments (for example, Cajamarca during the night $T_e/T_i = 1$ at all altitudes.

The altitude-time dependences for T_e and T_i (Figures 17, 19) basically agree with the data from other measurements [25].

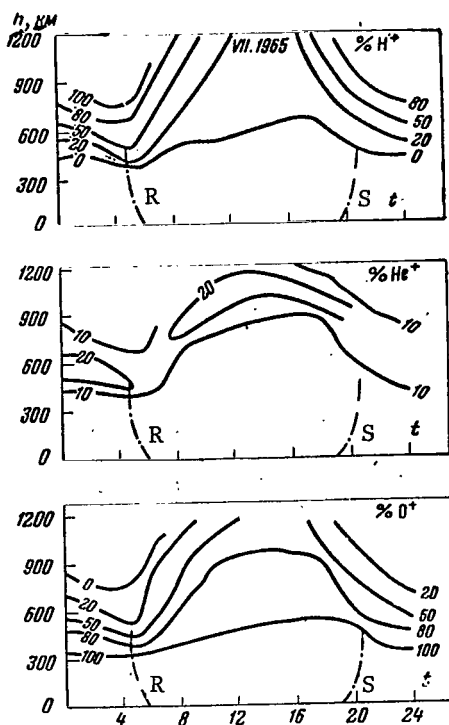


Figure 22. Altitude-Diurnal Mean-Monthly (July, 1965) Dependence of the Percent Content of O^+ , H^+ , He^+ at Arecibo [18]. The Solid Lines Represent the Levels of the Constant Percent Content; the Broken Lines Represent the Time of Sunrise "R" and Sunset "S" as a Function of z , Local Time.

Typical altitude-diurnal dependences (mean monthly, Figure 22) illustrate the possibilities of modern equipment employing incoherent scattering [20, 34] for obtaining systematic data on ion composition of the upper ionosphere. Figure 18 gives some idea about the complex of information obtained during one measurement in the form of graphs prepared for the profiles of temperatures and concentrations of electrons and ions on an electron computer.

The observed altitude-time dependences of the ion composition (O^+ , H^+ , He^+) of the outer ionosphere (Figure 22) are a sufficiently reliable confirmation of the presence of ions of helium He^+ in the ionosphere and were first detected using the satellites "Kosmos-2" and "Explorer VIII"; until quite recently it was assumed that their existence was only slightly probable because of the high ioniza-

tion potential of He (24.6 V). The observed maximal amount of He^+ ($\sim 20\%$) was localized in a relatively narrow range of altitudes ($\sim 600 - 1000$ km) and was subject to diurnal and seasonal variations.

As far as the theoretically possible sharp resonances in σ_ω at the gyrofrequencies of the ions are concerned, only quite recently has any discussion appeared [20] concerning the fact that such resonances were registered at the equatorial station (Cajamarca, Peru) at high altitudes (in

the H^+ region), where the collisions of electrons are rare and it is possible to keep the beam perpendicular to the lines of the geomagnetic field, which is necessary for this. At low altitudes, even when the beam was perpendicular, no resonance was observed possibly because of the influence of collisions [43].

In conclusion we can state that the basic characteristics of the phenomenon of incoherent scattering predicted by theory are confirmed in experiment.

The method of incoherent scattering revealed great potentialities for investigating the ionosphere below and above the chief maximum (up to the transition region in interplanetary space). As yet these potentialities are not being developed and used fully. Along with finding the most significant parameters of the ionosphere: complete regular vertical (and inclined) profiles of N , T_e , T_i , ΔL , N_0 , N_{OL} and the ion composition and the respective /162 altitude-time (diurnal, seasonal and solar activity phases) dependences of these parameters, it is interesting to have data on the irregular large-scale (in time and coordinates) variations in these parameters, the motion and evolutions in time, and the regular horizontal gradients, etc. [35, 36, 38, 44, 43].

In particular, in using multibeam radar stations with a high resolution for t and coordinates, in the space of the narrow beams we can not eliminate the possibility that a spatial-time correlation function and electron density of the large inhomogeneities of the ionosphere can be obtained as well as the horizontal gradients of the vertical profiles of N , N_i , T_e , T_i , N_0 and ion composition. It is particularly feasible to simultaneously use equipment operating at different frequencies ($\lambda \gtrsim d$) with a vertical and sloping path of the beam.

It is also important to make simultaneous complex measurements using

several independent methods including incoherent scattering [38, 43].

The prospects are very tempting for carrying out these simultaneous measurements in a number of geophysics rockets, spaced at various distances in latitude and longitude, and for investigating the latitude and longitude as well as the altitude correlations between the results of these measurements throughout the entire ionosphere.

REFERENCES

1. Gordon, W. E. Proc. IRE, Vol. 46, No. 11, 1958, p. 1824. (See also [3], p. 11).
2. Landau, L. D. and Ye. M. Lifshits. Teoriya polya (Field Theory), State Publishing House of Literature on Physics and Mathematics, (Fizmatgiz), 1960.
3. Incoherent Scattering of Radio waves, Translated from English, Edited by V. A. Rudakov, Mir Press, 1965.
4. Fejer, J. A. Canad. J. Phys., Vol. 38, No. 8, 1960, p. 1114. (See also Translation No. 535, State Committee of the Council of Ministers, USSR, for Radio Electronics, GKRE).
5. Fejer, J. A. Canad. J. Phys., Vol. 39, No. 5, 1961, p. 716. (See also Translation No. 537, GKRE).
6. Renau, J., H. Commins and W. Flood. J. Geophys. Res., No. 66, 1961, p. 2703. (See also [3], p. 123).
7. Bowles, K. L. Phys. Rev. Lett., No. 1, 1958, p. 454.
8. Bowles, K. L. J. Res. Nat. Bureau Standards, Vol. 65D, No. 1, 1961. (See also [3], p. 27).
9. Dougherty, J. P., and D. T. Farley. Proc. Roy. Soc., No. A259, 1960, p. 77.
10. Farley, D. T., J. P. Dougherty and D. Barron. Proc. Roy. Soc., No. A263, 1961, p. 238. (See also [3], p. 123).
11. Farley, D. T. J. Geophys. Res., Vol. 71, No. 17, 1966, p. 4091.
12. Pineo, V. C., L. G. Kraft and H. W. Briscos. J. Geophys. Res., No. 65, 1960, p. 2629.
13. Al'pert, Ya. L. Uspekhi Fizicheskikh Nauk (UFN) Vol. 90, No. 3, 1966, p. 405.
14. Sagalyn, R. C. and M. Smiddy. Preprint, 1960.
15. Ginzburg, V. L. Rasprostraneniye elektromagnitnykh voln v plazme (Propagation of Electromagnetic Waves in Plasma), Fizmatgiz, 1960.

16. Otchet po nauchno-issledovatel'skoy rabote "Luch" za 1966 g. (Report on Scientific Research Work "Beam" for 1966), Kharkov State University, 1966.
17. Moorcroft, D. R. J. Geophys. Res., No. 69, 1964, p. 955. (See also [3], p. 175).
18. Misyura, V. A., G. N. Tkachev, V. Ya. Bludov and Yu. G. Yerokhin. Sb: Ionosfernyye issledovaniya (Collection: Ionospheric Research), Nauka Press, No. 21. In Press.
19. Pineo, V. C. and D. P. Hyvek. J. Geophys. Res., Vol. 67, No. 13, 1962, p. 5119.
20. Gordon, W. E. Abstract for Commission III and IV, Munich, September, 1966.
21. Pineo, V. C. and D. P. Hyvek. J. Geophys. Res., Vol. 68, No. 9, 1963, pp. 2695-2706.
22. Distribution of Electron Concentration in the Ionosphere and Exosphere, Translated from English, Edited by K. I. Gringauz, Mir Press, 1964.
23. Bowles, K. L. Space Res., No. 3, 1962, pp. 253-264. (See also [12], p. 159.)
24. Electron Density Profiles in the Ionosphere and Exosphere, Amsterdam, 1966.
25. Evans, J. V. The Temperature of Neutral and Charged Particles in the Ionosphere and Magnetosphere, Inter-Union Symposium on Solar-Terrestrial Physics, Belgrade, 1966.
26. Millman, G. H. J. Atmos. Terr. Phys., Vol. 27, No. 4, 1965, p. 586.
27. Millman, G. H., V. C. Pineo and D. P. Hyvek. J. Geophys. Res., Vol. 69, No. 19, 1964, p. 4501.
28. Carry, H., M. Petit and P. Waldteyfil. Inter-Union Symposium on Solar-Terrestrial Physics, Belgrade, 1966.
29. Maynard, L. A. and E. D. Du Charmé. Canad. J. Phys., No. 43, 1965, p. 11.
30. Watkins, C. D. and H. K. Sutcliffe. Research at RRE Brit. Commun. and Electron., No. 11, 1963, p. 848.
31. Bowles, K. L. Space Res., No. 3, 1963, p. 253.
32. Bowles, K. L., G. R. Ochs and J. L. Green. Radio Propagation, No. 66D, 1962, p. 395.

33. Misyura, V. A. This Collection, p. 120*.
34. Farley, D. T. and K. L. Bowles. NBS Report 8489, 1964.
35. Misyura, V. A., G. N. Tkachev, Yu. G. Yerokhin, V. I. Ivanov, N. I. Nisnevich, N. M. Borodin and V. Ya. Bludov. Sb: Ionosfernyye issledovaniya (In: Ionospheric Research), Nauka Press, No. 20, In Press.
36. Misyura, V. A., G. N. Takachev, Yu. G. Yerokhin and V. I. Ivanov. Geomagnetizm i aeronomiya, No. 7, 1967, p. 12.
37. Morozov, V. A. and Z. G. Trunova. Radiotekhnika i elektronika, Vol. 7, No. 11, 1962.
38. Misyura, V. A., G. N. Tkachev, Yu. G. Yerokhin, V. I. Novozhilov, V. Ya. Bludov, N. I. Nisnevich and N. I. Moshnyakov. Sb: Kosmicheskiye issledovaniya (Collection: Space Research), Vol. 6, No. 5, 1968, p. 726.
39. Evans, J. V. J. Geophys. Res., Vol. 70, No. 17, 1965, p. 4365.
40. Evans, J. V. J. Geophys. Res., Vol. 70, No. 11, 1965, p. 2726.
41. Gordon, W. E. IEEE Transact. on Antennas and Propag., Vol. 12, No. 7, 1964, pp. 872-876.
42. Electron Concentration in the Ionosphere and Exosphere, Translated from English, Edited by K. I. Gringauz, Mir Press, 1966.
43. Misyura, V. A. et al. IX Vsesoyuzn. konf. po rasp. radiovoln. (IX All-Union Conference on Propagation of Radio Waves), Authors, Abstracts of Reports, Kharkov, Part 1, pp. 61, 65; Part 2, p. 84.
44. Misyura, V. A. et al. Geomagnetizm i aeronomiya, Vol. 9, No. 1, 1969, p. 75.

*Translator's Note: This material will be found on p. 195 of English text.

Translated for National Aeronautics and Space Administration under Contract No. NASw-2035 by SCITRAN, P. O. Box 5456, Santa Barbara, California, 93103.

★ U. S. GOVERNMENT PRINTING OFFICE : 1972 720-390/319



032 001 C1 U 13 711217 S00903DS
DEPT OF THE AIR FORCE
AF WEAPONS LAB (AFSC)
TECH LIBRARY/WLOL/
ATTN: E LOU BOWMAN, CHIEF
KIRTLAND AFB NM 87117

POSTMASTER: If Undeliverable (Section 158
Postal Manual) Do Not Return

"The aeronautical and space activities of the United States shall be conducted so as to contribute . . . to the expansion of human knowledge of phenomena in the atmosphere and space. The Administration shall provide for the widest practicable and appropriate dissemination of information concerning its activities and the results thereof."

—NATIONAL AERONAUTICS AND SPACE ACT OF 1958

NASA SCIENTIFIC AND TECHNICAL PUBLICATIONS

TECHNICAL REPORTS: Scientific and technical information considered important, complete, and a lasting contribution to existing knowledge.

TECHNICAL NOTES: Information less broad in scope but nevertheless of importance as a contribution to existing knowledge.

TECHNICAL MEMORANDUMS: Information receiving limited distribution because of preliminary data, security classification, or other reasons.

CONTRACTOR REPORTS: Scientific and technical information generated under a NASA contract or grant and considered an important contribution to existing knowledge.

TECHNICAL TRANSLATIONS: Information published in a foreign language considered to merit NASA distribution in English.

SPECIAL PUBLICATIONS: Information derived from or of value to NASA activities. Publications include conference proceedings, monographs, data compilations, handbooks, sourcebooks, and special bibliographies.

TECHNOLOGY UTILIZATION PUBLICATIONS: Information on technology used by NASA that may be of particular interest in commercial and other non-aerospace applications. Publications include *Tech Briefs*, Technology Utilization Reports and Technology Surveys.

Details on the availability of these publications may be obtained from:

SCIENTIFIC AND TECHNICAL INFORMATION OFFICE

NATIONAL AERONAUTICS AND SPACE ADMINISTRATION

Washington, D.C. 20546